ABSTRACT

Title of Document: NOR-SECO-CUCURBITURILS

Wei-Hao Huang, Ph.D, 2008

Directed By: Professor, Lyle Isaacs, Department of Biochemistry and Chemistry

With rapid growth in molecular recognition and self-assembly in recent years, α–, β–, and γ-cyclodextrins, as a platform for molecular recognition have been widely applied as molecular containers in water. In particular, cyclodextrins have been extensively used in industrial applications, such as drug delivery, cosmetics, and analytical chemistry (mainly chromatography). We, and others, believe that the cucurbit[n]uril family of molecular containers have the potential to supplant the cyclodextrins as platform of choice for molecular recognition in aqueous solution.

Even though the one-pot synthesis of CB[n] under strongly acidic aqueous condition can be easily performed on multi-kilogram scale, the separation of the various CB[n] (n = 5, 6, 7, 8, 10) is challenging and time consuming. This disseration focuses on the mechanism of CB[n] formation with the expectation that would allow the tailor-made synthesis of specific CB[n] and suggest versatile routes to new CB[n]-

type compounds that might display exciting new properties like chirality, chiral recognition, and allostery.

Herein, the condensation of glycoluril with less than two equivalents of formaldehyde delivers a reaction mixture that contains glycoluril oligomers (dimer, trimer, tetramer, pentamer and hexamer) and CB[n] compounds that lack one or more methylene bridges known as nor-seco-cucurbit[n]urils (*ns*-CB[n]). We studied the ability of double cavity host bis-*ns*-CB[10] to undergo size dependent homotropic allostery, (±)-bis-*ns*-CB[6] to undergo diastereoselective recognition toward amino acids and amino alcohols in water, and the transformation of *ns*-CB[6] to a CB[6] derivative which contains the folding of long chain alkanediammonium ions in water. A comprehensive mechanistic scheme is proposed that accounts for the observed formation of dimer – hexamer and *ns*-CB[n]. Overall, the experiments establish that a step-growth cyclo-oligomerization process operates during CB[n] formation.

NOR-SECO-CUCURBITURILS

By

Wei-Hao Huang

Dissertation submitted to the Faculty of the Graduate School of the
University of Maryland, College Park, in partial fulfillment
of the requirements for the degree of
Doctor of Philosophy
2008

Advisory Committee:
Associate Professor Lyle Isaacs, Chair
Professor Philip DeShong
Professor Jeffery Davis
Assistant Professor Andrei Vedernikov
Associate Professor Srinivasa Raghavan, Dean's Representative

Dedication

To my parents,
my parents-in-law,
my wife, Yen-Chuan Liu,
my daughter, Angela Huang.

Acknowledgements

I am grateful to thank Professor Lyle Isaacs for his help and guidance throughout my research and dissertation.

I would like to thank all faculty and staff in Chemistry Department to guide me moving forward.

I would like to thank Department of Chemistry and Biochemistry to provide me a great opportunity to pursue my Ph.D. in Maryland.

I would like to thank Ann Wylie Dissertation Fellowship for supporting me to finish my dissertation.

Table of Contents

List of Tables

Chapter 2

List of Figures

Chapter 1

Chapter 2

Chapter 3

Chapter 4

Chapter 5

List of Schemes

Chapter 1

Chapter 2

Chapter 3

Chapter 4

Chapter 5

I. Chapter 1: Cucurbit[n]uril (Huang, W.-H.; Liu, S.; Isaacs, L. *Cucurbit[n]urils*, Diederich, F.; Stang, P. J.; Tykwinski, R. R. Ed; In *Modern Supramolecular Chemistry,* Wiley-VCH, 2008, ch. 4, pp. 113-142.)

1.1 Introduction.

This chapter focuses on the synthetic and supramolecular chemistry of the cucurbit[n]uril (CB[n]) family of macrocycles. Isaacs and co-workers' research in this area which began in 1998 at the University of Maryland has been largely driven by their efforts to understand the mechanism of CB[n] formation. This Chapter is, therefore, organized around that theme sprinkled with subsequently developed applications of the CB[n] family which validate our initial goal of understanding the mechanism of formation of the CB[n] family.

1.2 Synthesis and Structure of Cucurbit[6]uril and Decamethylcucurbit[5]uril. The cucurbituril story begins in 1905 when Behrend published the condensation of glycoluril (**I-1a**) with 2 equivalents of formaldehyde (Scheme 1) under aqueous acidic conditions (HCl, 100 ˚C).[1] The substance formed during this reaction – referred to as Behrend's polymer in the literature – was insoluble in all common solvents but could be recrystallized from hot H_2SO_4 which yielded a well defined substance. Although Behrend was not able to structurally characterize this substance he did demonstrate that it forms complexes with a wide variety of species including $KMnO_4$, $AgNO_3$, and methylene blue. It was not until 1981 that Mock reported that the product of Behrend's reaction was the macrocyclic hexameric cucurbit[6]uril comprising 6 equivalents of glycoluril and 12 equivalents of formaldehyde.[2] During the course of this remarkable reaction, six rings and 24

bonds are formed with complete control over the disposition of the glycoluril methine C-H groups which point outward from the central cavity. It would be nearly 10 years later that Stoddart reported that the condensation of dimethylglycoluril (**I-1b**) with formaldehyde (2 equivalents) under similar conditions yielded the first cucurbituril derivative – macrocyclic pentameric $Me_{10}CB[5]$ (Scheme 1).[3] These two early members of the cucurbit[n]uril family provided us, and several other groups, with numerous questions:[4-6] 1) What is the scope of glycolurils that can be used in the CB[n] forming reaction?, 2) Why does the CB[n] forming reaction deliver hexameric CB[6] but pentameric $Me_{10}CB[5]$?, 3) What factors are responsible for the remarkably high yield (82%) obtained for CB[6]?, 4) What is the mechanism of CB[n] formation?

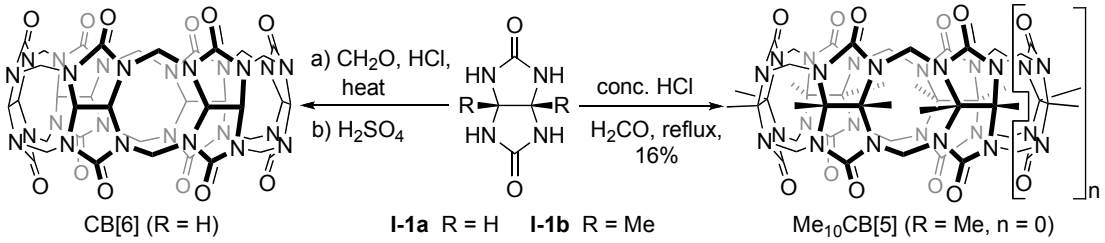

Scheme 1. Synthesis of CB[6] and $Me_{10}CB[5]$.

1.3 Molecular Recognition Properties of Cucurbit[6]uril. Throughout the 1980's Mock published a series of pioneering papers that demonstrated that CB[6] has remarkable abilities as a molecular container in aqueous solution.[2,7-9] For example, Mock showed that pentanediamine (**I-2**) and hexanediamine (**I-3**) bind to CB[6] as their ammonium salts with values of $K_a > 10^6$ M^{-1} in 40% aq. HCO_2H. Even more remarkable was the fact that compounds with shorter or longer spacer

groups between the ammonium centers (e.g. butanediamine **I-4** or heptanediamine **I-5**) bind significantly more weakly ($K_a \approx 10^4 - 10^5$ M^{-1}). This high affinity and selectivity can be ascribed to the juxtaposition of three distinct binding regions: 1) two symmetry equivalent ureidyl–carbonyl lined portal which have a pronounced negative electrostatic potential which interact with cations (e.g. H^+, M^+, or RNH_3^+) by ion-dipole interactions and/or hydrogen bonds, and 2) a central hydrophobic cavity which has a gently negative electrostatic potential which preferentially interacts with hydrophobic guests (Scheme 2). The high selectivity observed for **I-2** and **I-3** over **I-4** and **I-5** is due to the good match between the $H_3N{\bullet\bullet\bullet}NH_3$ separation on the guest and the C=O•••O=C separation on the host. CB[6] is also quite selective based on size and shape. For example, CB[6] binds nicely to *p*-methylaniline (**I-6**) but completely rejects the meta-isomer (**I-7**). Similarly, CB[6] readily encapsulates **I-8** which has a volume of 86 $Å^3$ but rejects the similarly sized **I-9** (89 $Å^3$). Lastly, polyammonium species like spermine (**I-10**) achieve very high affinity in their binding with CB[6] ($K_a = 1.3 \times 10^7$ M^{-1}).[8] These high affinity and highly selective binding events were utilized by Mock to achieve a 10^4-fold rate enhancement of a dipolar cycloaddition within the cavity[10] and in the construction of a molecular shuttle based on changes in pH.[11] These examples convinced us that the supramolecular chemistry of CB[6], its derivatives, and it analogues would be especially well suited for the preparation of molecular machines and biomimetic systems. In 1998, therefore, we embarked on a journey to understand the mechanism of CB[6] formation since we were confident that would lead to the preparation of new members of the cucurbituril family with exciting new properties.

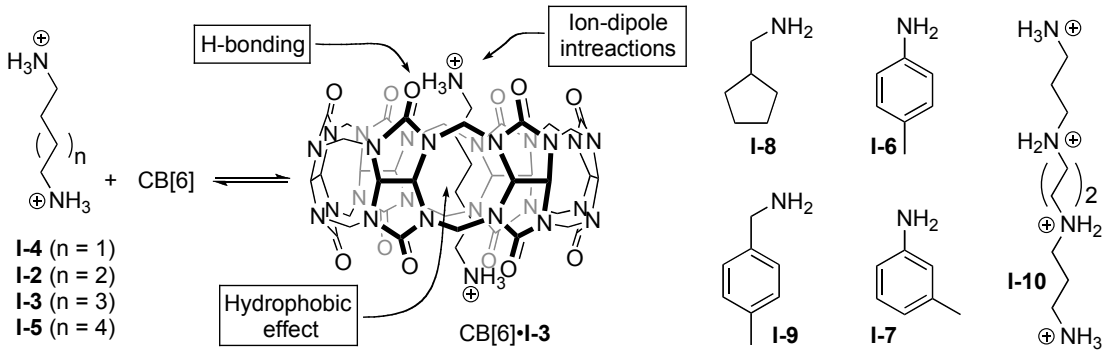

Scheme 2. Molecular recognition properties of CB[6].

1.4 New Members of the Cucurbit[n]uril Family. This section describes the preparation of CB[n] homologues (n = 5, 7, 8, 10). We begin the discussion with a mechanistic hypothesis for CB[n] formation advanced by the Day and Isaacs groups.[5,12]

1.5 Proposed Mechanism of Cucurbit[n]uril Formation. Although the CB[n] forming reaction is remarkably complex, we sketched out a rough mechanism in 1998 and supplemented it along the way as new information became available.[4,5,13,14] Scheme 3 depicts our current understanding of the mechanism of CB[n] formation. Initially, glycoluril (**I-1a**) reacts with formaldehyde to yield methylene bridged glycoluril dimers (**I-11**C and **I-11**S). These two compounds are diastereomers that differ in the relative orientation of the H-atoms on the convex face of the molecule. In CB[6], however, all of the methine C-H groups project outward from the center of the macrocycle similar to **I-11**C. Key questions that we wished to address, therefore, were: 1) Are compounds with **I-11**S-type stereochemistry formed?, 2) Are **I-11**S and

I-11C in equilibrium with each other?, and 3) What is the mechanism of the **I-11**S to **I-11**C interconversion? These methylene bridged glycoluril dimers can then undergo further oligomerization to yield methylene bridged glycoluril oligomers (e.g. trimer – decamer) as a mixture of S-shaped and C-shaped diastereomers (**I-12**). This mixture of oligomers has been referred to in the literature as Behrend's polymer. The mixture of oligomers can then undergo S- to C-shaped isomerization, perhaps under the influence of a templating group to yield the all C-shaped oligomer (**I-13**). The ends of oligomer **I-13** then react with one another to enter the CB[n] manifold as a mixture of CB[n] (n = 5, 6, 7, 8, 10). Through product resubmission experiments, Anthony Day demonstrated that CB[8] undergoes ring contraction to yield CB[5] – CB[7] whereas the smaller CB[n] homologues (CB[5] – CB[7]) are stable to the reaction conditions.[12]

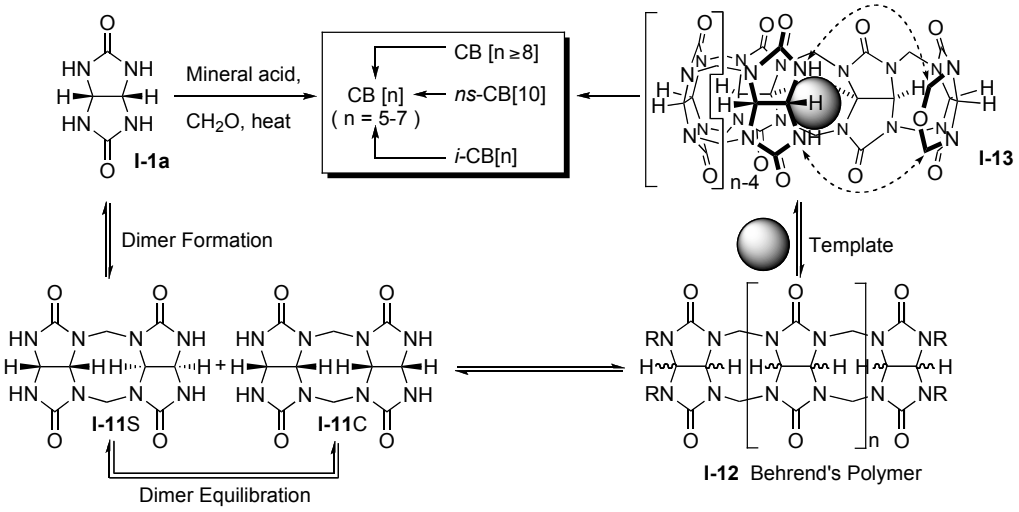

Scheme 3. Proposed mechanism of CB[n] formation.

1.6 Synthesis and Structure of Cucurbit[n]uril Homologues (n = 5, 7, 8, 10).

The isolation of CB[n] homologues (CB[5], CB[7], and CB[8]) by the groups of Kim and Day around the turn of the millennium represented a major breakthrough in the cucurbituril field.[12,15] Figure 1 shows top views of CB[5] – CB[8] (drawn to scale) which illustrate the circular shape of the cavity and the gradual progression to larger cavity volumes.[15,16] In particular, the larger homologues CB[7] (279 Å^3) and CB[8] (479 Å^3) with their larger cavities which parallel those of β- and γ-cyclodextrin promise to greatly expand the range of applications to which CB[n] can be applied.

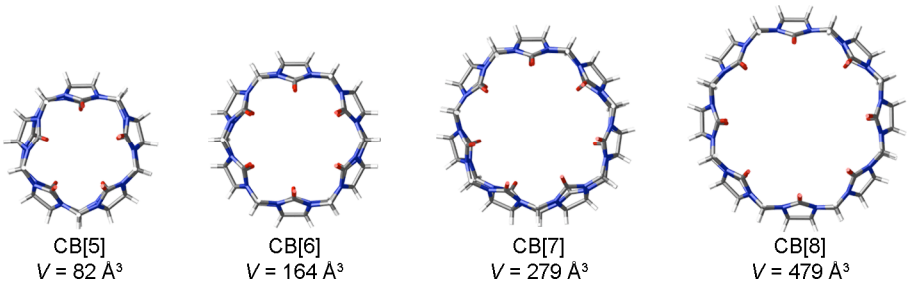

Figure 1. Molecular models of CB[5] – CB[8] and their calculated cavity volumes.

1.6.1 Reaction Conducted Under Milder Conditions. To access the unknown cucurbituril homologues, Kim and Day performed the CB[n] forming reactions under milder conditions (100 ˚C, conc. HCl; 75 ˚C, 9M H_2SO_4).[12,15] Although CB[6] is still the major component of the reaction mixture, the CB[n] homologues (CB[5], CB[7], and CB[8]) can be readily isolated on the 10 – 100 g scale by straightforward – but time consuming – washing and recrystallization procedures that are detailed in Section 1.17.

1.6.2 CB[5] Can be Released from CB[10]•CB[5] to Yield Free Cucurbit[10]uril. In addition to CB[5] – CB[8], Day and co-workers were also able to isolate CB[10] as its CB[10]•CB[5] complex (Scheme 4).[12,17] Day and co-workers also demonstrated that added ^{13}C-labeled CB[5] undergoes chemical exchange with unlabeled CB[5] in the CB[10]•CB[5] complex. This observation suggested that it should be possible to remove CB[5] and isolate free CB[10] in its uncomplexed form. From our 1 kilogram scale CB[n] forming reaction (Section 1.17) we were lucky enough to isolate a significant quantity of CB[10]•CB[5] and decided to try and remove CB[5]. We discovered that some of the guests commonly used (e.g. **I-14** – **I-18**) to complex to the larger CB[n] (n = 7, 8) are capable of partially displacing CB[5] from the CB[10]•CB[5] complex. Unfortunately, in many cases, all of the components (CB[5], excess guest, and CB[10]•guest) remained in solution which complicated the isolation of the CB[10]•guest complex. Luckily, we discovered that addition of excess guest **I-19** to CB[10]•CB[5] results in the formation of the soluble CB[10]•**I-19**$_2$ complex and precipitation of the (CB[5]•**I-19**)$_n$ supramolecular polymer (Scheme 4). The pure CB[10]•**I-19**$_2$ complex is isolated by filtration and rotary evaporation. Removal of the less strongly bound second equivalent of **I-19** occurs readily by washing with MeOH which yields CB[10]•**I-19**. The final equivalent of **I-19** can be removed by heating with acetic anhydride which transforms the ammonium groups into acetamides followed by washing (DMSO, MeOH, H_2O). Uncomplexed CB[10] has a cavity volume of approximately 870 Å^3 and is poorly soluble in water and mildly acidic solution. Luckily, its complexes have good solubility in D_2O which allowed us to study its molecular recognition properties (Section 1.7.5).

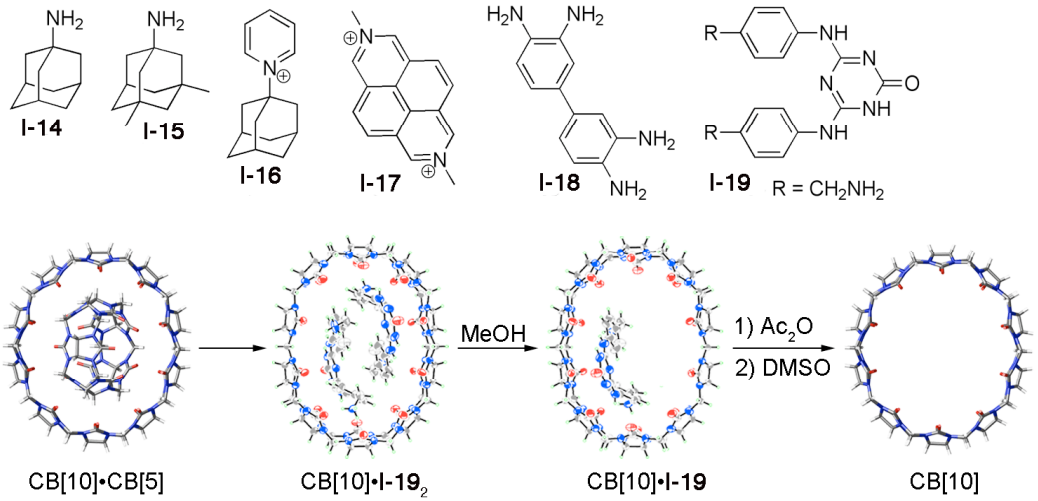

Scheme 4. Sequence used to remove CB[5] from CB[10]•CB[5]. The structures of CB[10]•CB[5][17] and CB[10]•**I-19**$_2$[18] are based on the x-ray crystal structures whereas those for CB[10]•**I-19** and CB[10] are purely schematic representations.

1.7 Applications of Members of the Cucurbit[n]uril Family. The early work of Mock on the recognition properties of CB[6] established that this macrocycle was amongst the tightest binding and most selective synthetic hosts in aqueous solution.[2,7-9] Subsequent work from our group demonstrated that the high affinity and selectivity translates to *individual* host-guest complexes of CB[7] and CB[8]. Even more impressively, the selectivity of a single guest toward CB[6], CB[7], and CB[8] can be remarkably large (> 10^4).[19] These, and related observations,[20,21] suggested to us and others that CB[n] would function as smart components in a variety of applications that are described in this section.

1.7.1 Preparation of Molecular Switches. Compounds that function as molecular switches exist in two stable forms and can be reversibly switched between those two

forms by application of a given stimulus (e.g. pH change, electrochemistry, photochemistry, or chemical). A particularly interesting molecular switch based on the triaminofluorene compound **I-20** was reported by Kim in 2000 (Scheme 5).[22] When CB[6] is added to **I-20** in pH 1.0 solution, rotaxane CB[6]•**I-20** is formed where the CB[6] bead resides on the longer hexylene spacer in order to maximize both ion-dipole interactions and hydrophobic binding. In this form, the anilinium N-atom is protonated and the fluorene chromophore is highly fluorescent. When the pH is raised (8.0), however, the anilinium N-atom is deprotonated and the CB[6] macrocycle slides over to the butylene spacer to maintain two ion-dipole interactions while sacrificing some hydrophobic driving force. In this new complex (CB[6]•**I-21**), the aniline N-atom is conjugated to the fluorene ring and the complex has a violet color; the N-atom also quenches the fluorescence output of the system. Upon lowering the pH, the CB[6] bead again switches back to the original location. Thus, CB[6] acts as a pH controlled molecular switch with both UV/Vis and fluorescent output.

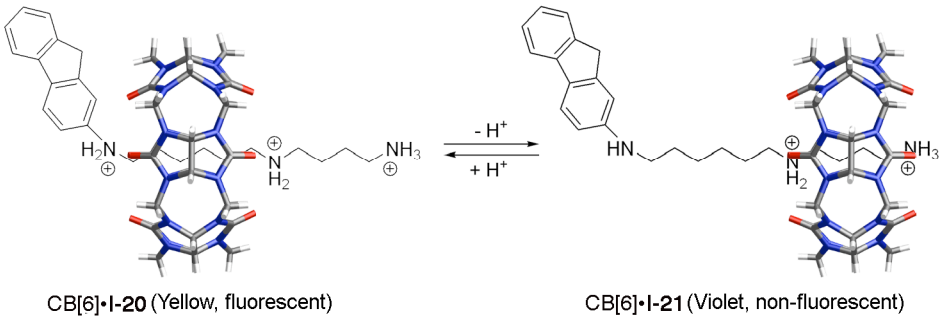

Scheme 5. A pH responsive molecular switch that signals by color and fluorescence changes.

1.7.2 Self-Assembled Dendrimers. The ability of members of the CB[n] family to bind tightly to their guests has been used by the groups of Kaifer[23,24] and Kim[25] to modify the properties of dendrons containing guests at their focal points and to bring two or more dendrons together to create a self-assembled dendrimer. For example, Kaifer synthesized 1st, 2nd, and 3rd generation Newkome-type dendrons **I-22a** – **I-22d** containing viologen units at the focal point (Scheme 6).[23] UV/Vis titrations allowed Kaifer to demonstrate that the association constant for the formation of the binary complex CB[8]•**I-22** decreases as the generation of the dendrimer increases. The electrochemical behavior was even more interesting. Upon a two-electron reduction the viologen is transformed from its dicationic to its monocationic form which subsequently induces dimerization inside CB[8] yielding ternary complex CB[8]•**I-22**$_2$ as evidenced by changes in the UV/Vis spectrum. The dramatic change in size of the ternary complex was also determined by measurement of its diffusion constant by pulsed field gradient NMR techniques. No dimerization is observed in the absence of CB[8]. This lovely example demonstrates proof-of-concept for redox-switchable dendrimer self-assembly.

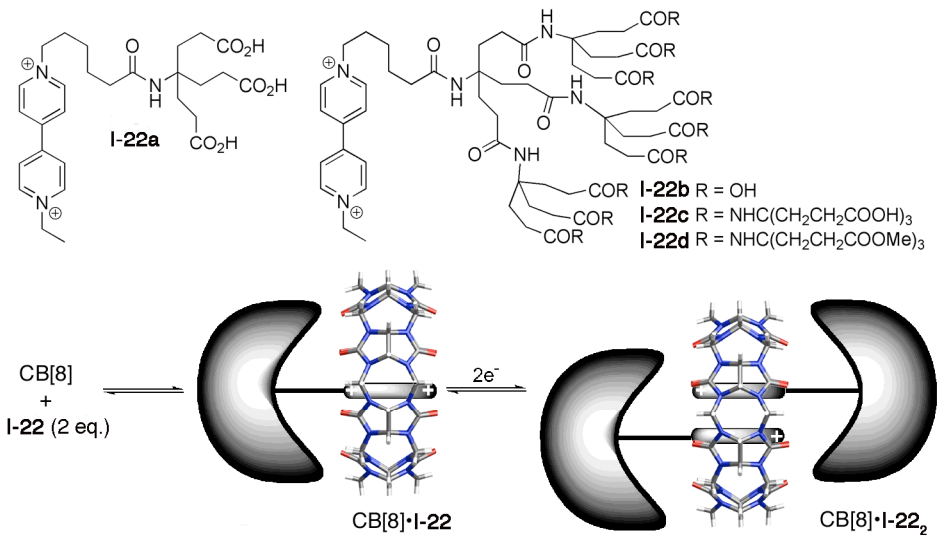

Scheme 6. Electrochemical control of dendrimer assembly.

1.7.3 Preparation of Molecular Machines. The Kim group has capitalized on the ability of CB[8] to simultaneously bind two aromatic rings in the construction of a variety of molecular machines.[26,27] A recent and particularly elegant example is the construction of a molecular loop lock (Scheme 7).[27] They found that the interaction of CB[8] with **I-23**$^{3+}$ leads to the folded conformation of CB[8]•**I-23**$^{3+}$ (Scheme 7) which benefits from intramolecular charge transfer interaction between the electron rich naphthalene and electron poor viologen units. The addition of 1 equivalent of methylviologen (**I-24**$^{2+}$) does not result in a change in conformation of CB[8]•**I-23**$^{3+}$ presumably because **I-24**$^{2+}$ binds less strongly than the intramolecularly held viologen unit. Very interestingly, however, upon reduction of the solution of the mixture of CB[8]•**I-23**$^{3+}$ and **I-24**$^{2+}$ with $Na_2S_2O_4$, the equilibrium shifts toward the unfolded ternary complex CB[8]•**I-23**$^{2+}$•**I-24**$^{+}$. This ternary complex benefits from the enhanced π-π interactions as evidenced by the appearance of new bands at 368, 550, and 890 nm in the UV/Vis spectrum of the viologen radical-cation dimer. The system

is fully reversible between the CB[8]•**I-23**$^{2+}$•**I-24**$^{+}$ and CB[8]•**I-23**$^{3+}$ states by exposing the system to molecular oxygen (O_2). This system may be regarded as a safeguarded molecular loop lock in that it requires not only the addition of **I-24**$^{2+}$, but also the application of a redox stimulus ($Na_2S_2O_4$ or O_2) to open or close the lock.

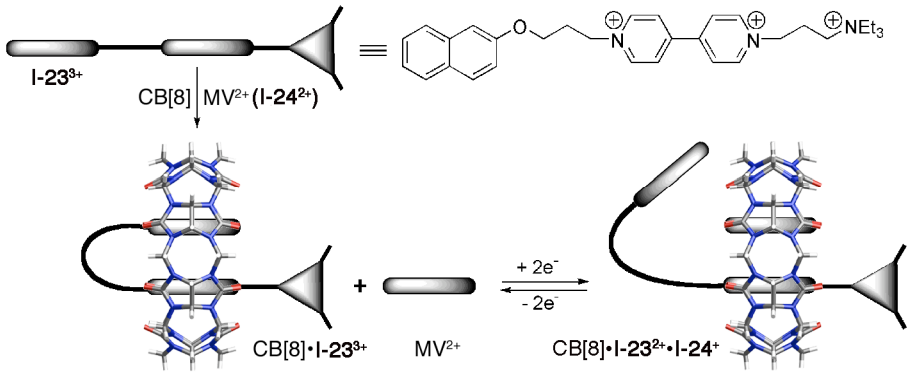

Scheme 7. A molecular loop lock that responds to chemical and redox stimuli.

1.7.4 Preparation of Complex Self-Sorting Systems. Mock has shown that CB[6] undergoes tight and selective binding with cationic guest molecules in aqueous solution.[8] Our investigations of complex (e.g. 12-component) self-sorting mixtures which utilized CB[6] and CB[8] as components suggested that the binding strengths (K_a) and selectivities might be even higher than previously appreciated.[20] To provide quantitative evidence for this hunch, we measured the binding constants for CB[6], CB[7], and CB[8] toward a variety of guests by ^{1}H NMR competition experiments.[19] We found that values of K_a ranged between 10^2 – 10^{12} M^{-1} and moreover that selectivities could be exceedingly large (> 10^3) in response to small structural changes. For example, CB[8] binds **I-19** 3250-fold tighter than CB[7] and induces a folding process at the same time (Scheme 8). Similarly, CB[7] binds **I-14** 5150-fold

tighter than CB[8] due to an excellent size, shape, and electrostatic match between host and guest.

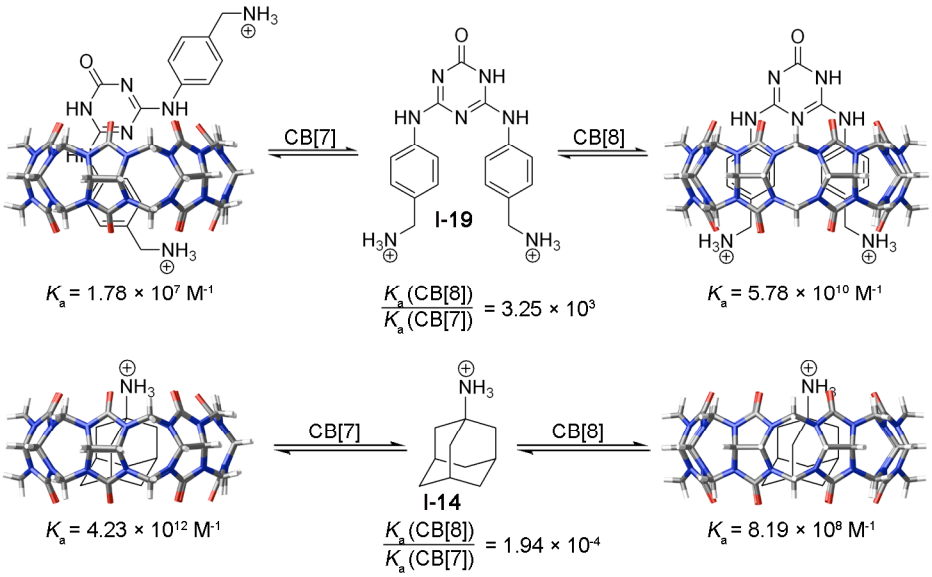

Scheme 8. High selectivity binding within CB[n].

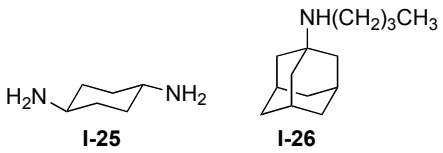

I-25 **I-26**

In addition to the high affinity and selectivity, members of the CB[n] family can exhibit unusual dynamics of complex association and dissociation.[9,21,28] We used the high binding affinities, high selectivities, and unusual dynamics to construct a system that undergoes well defined transitions from free components, to one set of aggregates under kinetic control, to a second set of aggregates under thermodynamic control (Scheme 9). For example, when a solution of CB[6] and CB[7] is mixed with a second solution containing guests **I-25** and **I-26** the components initially associate

to form CB[6]•**I-26** and CB[7]•**I-25**. In this process, **I-25** undergoes fast kinetically controlled association with CB[7] in preference to CB[6] to form CB[7]•**I-25**. Subsequently, **I-26** – which we refer to as a two-faced guest since it contains two binding epitopes – uses its slimmer alkylammonium binding epitope to associate with CB[6]. This kinetically controlled self-sorting state comprising CB[6]•**I-26** and CB[7]•**I-25** slowly transforms over the course of 56 days into the thermodynamic self-sorting state comprising CB[6]•**I-25** and CB[7]•**I-26**.

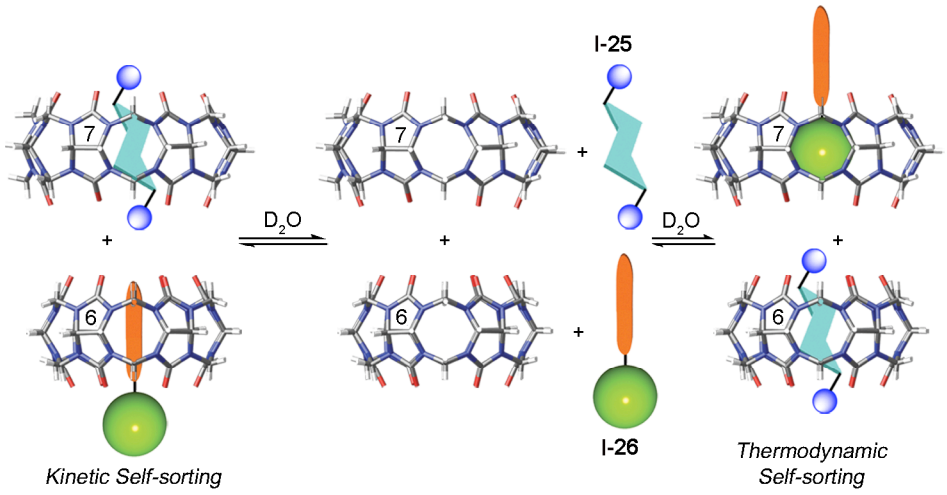

Scheme 9. Kinetic versus thermodynamic self-sorting using two-faced guests.

1.7.5 Allosteric Control of the Conformation of a Calix[4]arene Inside CB[10].

After we synthesized CB[10] we wanted to investigate its abilities as a host molecule. We found that CB[10] forms host-guest complexes with many of the guests typically used with the smaller members of the CB[n] family (e.g. alkyl and arylamines, adamantanes, viologens, and ferrocene derivatives like **I-14** – **I-19**).

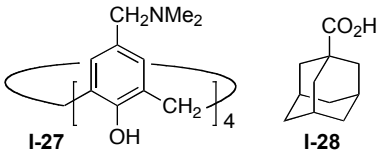

We discovered that CB[10] was also capable of forming a complex with cationic calix[4]arene **I-27** which itself usually functions as a host molecule in aqueous solution (Scheme 10).[18] Interestingly, when **I-27** goes inside CB[10] we observed two sets of resonances that were in slow exchange on the NMR time-scale. The major set of resonances corresponds to the CB[10]•1,3-*alt*-**I-27** conformer whereas the minor set of resonances corresponds to a dynamic equilibrium between CB[10]•1,2-*alt*-**I-27**, CB[10]•*partial cone*-**I-27**, and CB[10]•*cone*-**I-27** conformations. Scheme 10 shows the MMFF calculated geometry of the CB[10]•1,3-*alt*-**I-27** conformation which shows a good match between the circular shape of 1,3-*alt*-**I-27** and the cavity of CB[10]. We wondered whether it would be possible to stabilize one of the other three conformers of the macromolecular CB[10]•**I-27** complex by the addition of a guest molecule. After some experimentation, we found that adamantane carboxylic acid **I-28** is capable of shifting the equilibrium toward the CB[10]•*cone*-**I-27•I-28** complex. In this ternary complex, the calixarene **I-27** assumes the *cone*-**I-27** conformation in order to maximize non-covalent interactions with **I-28**. The *cone*-**I-27•I-28** complex in turn binds within CB[10]; in the MMFF computed conformation of CB[10]•*cone*-**I-27•I-28** we once again see a good match between the overall size, shape, and electrostatic complementarity between the cone-**I-27•I-28** complex and the cavity of CB[10]. To complete the cycle of allosteric control of conformation within CB[10], we added CB[7] which binds tightly to **I-28**

forming CB[7]•**I-28** which switches the conformation of calix[4]arene **I-27** back to the original mixture of CB[10]•**I-27** conformers. This result demonstrates that CB[10] has great potential in controlling the conformation of non-natural macromolecular complexes.

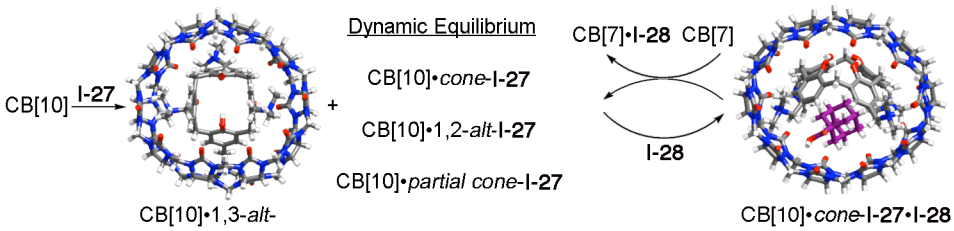

Scheme 10. Allosteric control of the macromolecular conformation inside CB[10].

1.7.6 As a Carrier of Anti-Cancer Agents. One of the potential uses of any molecular container compound is in the formulation of active pharmaceutical agents. Accordingly, the groups of Kim[29] and Day[30] have demonstrated the ability of CB[7] and CB[8] to modify the properties of Pt-based anti-cancer agents (Scheme 11). For example, Kim's group reported that CB[7] forms a 1:1 complex with oxaliplatin (CB[7]•**I-29**). They found that encapsulation of the drug within CB[7] results in a dramatic increase in its lifetime (e.g. 6 hours *versus* > 1 year). Furthermore, CB[7]•**I-29** shows markedly decreased reactivity toward L-methionine as a protein model relative to its reactivity toward guanosine as a DNA model. This result suggests that encapsulation of **I-29** within CB[7] may reduce unwanted side effects caused by protein binding of the drug.

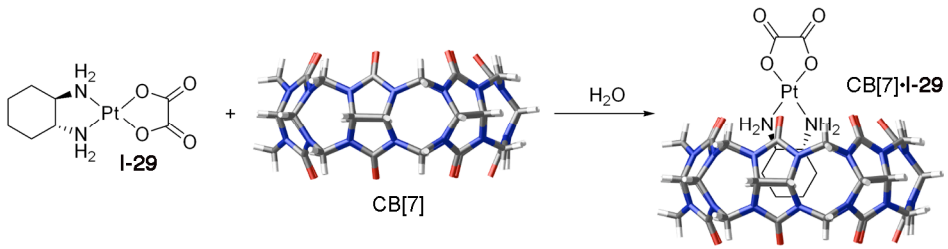

Scheme 11. Complexation of oxaliplatin **I-29** within CB[7].

1.8 Experimental Support for the Proposed Mechanism of CB[n] Formation.

Although none of the applications of the CB[n] family described in Section 1.7 of this Chapter were known in 1998 when the Isaacs' group began their work in the area they provide post-facto support for our assertion that a firm knowledge of the mechanism of CB[n] formation would be important. This section describes our work with S- and C-shaped methylene bridged glycoluril dimers that gave us insights into the early steps in the mechanism of CB[n] formation.

1.8.1 S-shaped and C-Shaped Methylene Bridged Glycoluril Dimers. The high level of complexity of the CB[n] forming reaction lead us to choose to study S-shaped and C-shaped methylene bridged glycoluril dimers (**I-11**C and **I-11**S, Scheme 3) initially. This section details the lessons learned from those model studies.

1.8.2 Synthesis of Methylene Bridged Glycoluril Dimers. Although we wanted to study methylene bridged glycoluril dimers **I-11**C and **I-11**S, we were mindful of the fact that the presence of four free ureidyl NH groups and the absence of solubilizing groups on the convex face of the glycoluril skeleton might lead to poor

solubility characteristics. Thus, in accord with the precedent of the Nolte and Rebek groups, we decided to target compounds whose NH-groups were "protected" by *o*-xylylene groups and that contain solubilizing substituents on their convex face.[31] Although we have investigated this reaction in detail, the bare essence of the process is presented in Scheme 12. In brief, we discovered three pathways to methylene bridged glycoluril dimers that each occur in refluxing dichloroethane containing *p*-toluenesulfonic acid with azeotropic removal of water. The first method involves the homodimerization of glycoluril NH-compounds (e.g. **I-30**) with CH_2O and delivers both **I-31**C and **I-31**S. The second involves the homodimerization of glycoluril cyclic ethers (e.g. **I-32**) that occurs with formal extrusion of formaldehyde and selectively delivers **I-33**C (**I-33**S not detected). The third involves heterodimerization of a glycoluril NH-compound (e.g. (±)-**I-34**) with a glycoluril cyclic ether (e.g. **I-35**) which delivers a mixture of (±)-**I-36**C and (±)-**I-36**S. In this example of heterodimerization, the unsymmetrical substitution on the aromatic ring renders (±)-**I-34** and (±)-**I-36**C and (±)-**I-36**S chiral and racemic. All three reactions occur in good to high yield and generally deliver the C-shaped diastereomers selectively. All three reactions are tolerant of substitution on the convex face of the glycoluril units (e.g. R = Ph, $(CH_2)_4$, CO_2Et, CO_2H, imide) and substitution on the *o*-xylylene rings (e.g. OMe, CH_3, Br, NO_2, and F). Interestingly, the heterodimerization reaction allows the selective preparation of C-shaped methylene bridged glycoluril dimers (e.g. **I-34**C) containing differentially functionalized aromatic rings. These three methods not only allowed us to prepare a wide variety of methylene bridged glycoluril dimers for studies of self-assembly, they also suggested methods for the

tailor-made synthesis of partially substituted CB[n] from appropriate glycoluril building blocks (Section 1.9).

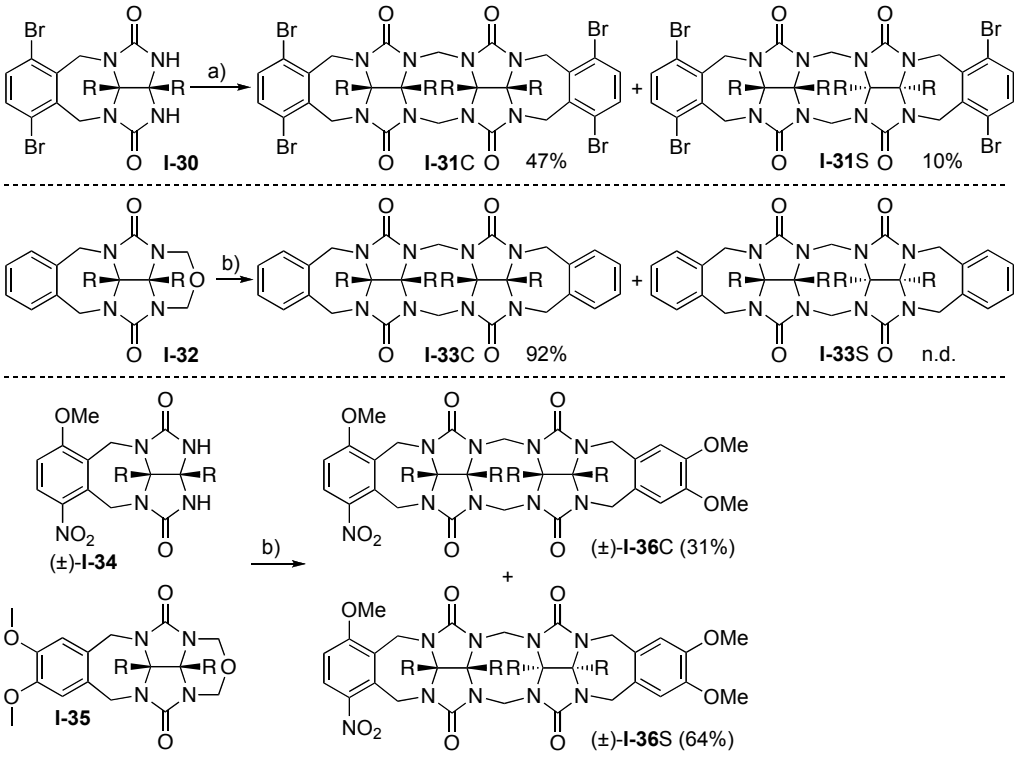

Scheme 12. Synthesis of S- and C-shaped methylene bridged glycoluril dimers. R = CO_2Et. Conditions: a) PTSA, $(CH_2O)_n$, $ClCH_2CH_2Cl$, reflux; b) PTSA, $ClCH_2CH_2Cl$, reflux.

1.8.3 S- to C-Shaped Isomerization of Methylene Bridged Glycoluril Dimers.

In our synthesis of methylene bridged glycoluril dimers (Section 1.8.2) we were somewhat surprised that only very small amounts of the S-shaped diastereomers were observed in most cases. To determine whether this diastereoselectivity is due to thermodynamic or kinetic preferences we isolated diastereomerically pure samples of six C-shaped and S-shaped compounds and separately resubmitted them to the

reaction conditions. Scheme 13 shows the separate isomerization of **I-37**C and **I-37**S. We found that both the C-shaped and S-shaped forms deliver an equilibrium mixture of S-and C-shaped forms in which the C-shaped form predominates (≈ 95:5) for a variety of compounds. This result established that the C-shaped form is thermodynamically more stable than the S-shaped form by ≈ 2 kcal mol^{-1} which provides a rationale for the high yield observed in the formation of CB[6] which presumably required all C-shaped oligomers. To delve deeper into the origin of this thermodynamic preference we performed the equilibration of **I-37**C and **I-37**S in a variety of solvents (e.g. $CHCl_3$, CCl_4, C_6F_6, THF, CH_3CN, $ClCH_2CH_2Cl$, CH_3NO_2, $MeOCH_2CH_2OMe$). The C-shaped to S-shaped ratio remains high (> 90:10) across this series which indicates that solvation is not a key factor determining the thermodynamic preference for the C-shaped form. We also ruled out the possibility that PTSA acts as a template by selectively engaging in π-π interactions with the cavity of the C-shaped form. Currently, we believe that the C-shaped form is more stable due to the conformational preference of the newly formed 8-membered ring for the crown-conformation.[32]

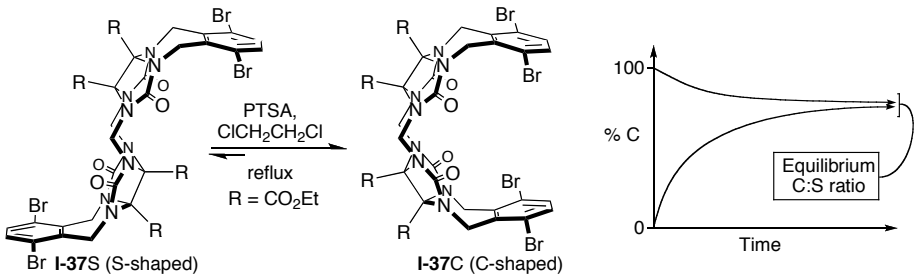

Scheme 13. Equilibration of **I-37**C and **I-37**S.

1.8.4 Mechanism of S- to C-Shaped Isomerization. The selective heterodimerization of glycoluril NH-compounds and glycoluril cyclic ethers (Section 1.8.2) and the general preference for the C-shaped diastereomers suggested that the mechanism of S-shaped to C-shaped equilibrium might proceed by an intramolecular rather than an intermolecular process under anhydrous acidic conditions (e.g. PTSA, $ClCH_2CH_2Cl$, reflux). To test this hypothesis, we designed a "double-labeling" experiment that utilized (±)-**I-38** and **I-39** (Scheme 14). In the equilibration of chiral but racemic (±)-**I-38**S, for example, one might expect to obtain either (±)-**I-38**C or **I-39**, or potentially a mixture of both.[5] Similarly, the equilibration of **I-39**S might deliver either (±)-**I-38**C or **I-39**, or both. In the experiment, we observed that (±)-**I-38**S cleanly delivered the chiral but racemic (±)-**I-38**C whereas the achiral meso compound **I-39**S cleanly delivered the achiral meso compound **I-39**C. This result indicates that the transformation of S- to C-shaped methylene bridged glycoluril dimers is an *intramolecular process* under *anhydrous acidic conditions* that proceeds via retention of configuration of the two glycoluril "halves". Scheme 14 also shows a proposed mechanism that tracks the position of the labels (green dots). Initially, **I-40** undergoes protonation and ring opening to yield iminium ion **I-41**. Iminium ion **I-41** can undergo ring closure by nucleophilic attack of the glycoluril N-atom to yield spirocyclic intermediate **I-42** which can fragment in the opposite direction to yield iminium ion **I-43**. Subsequent ring closure of **I-43** followed by deprotonation gives **I-44** which rationalizes the experimental results.

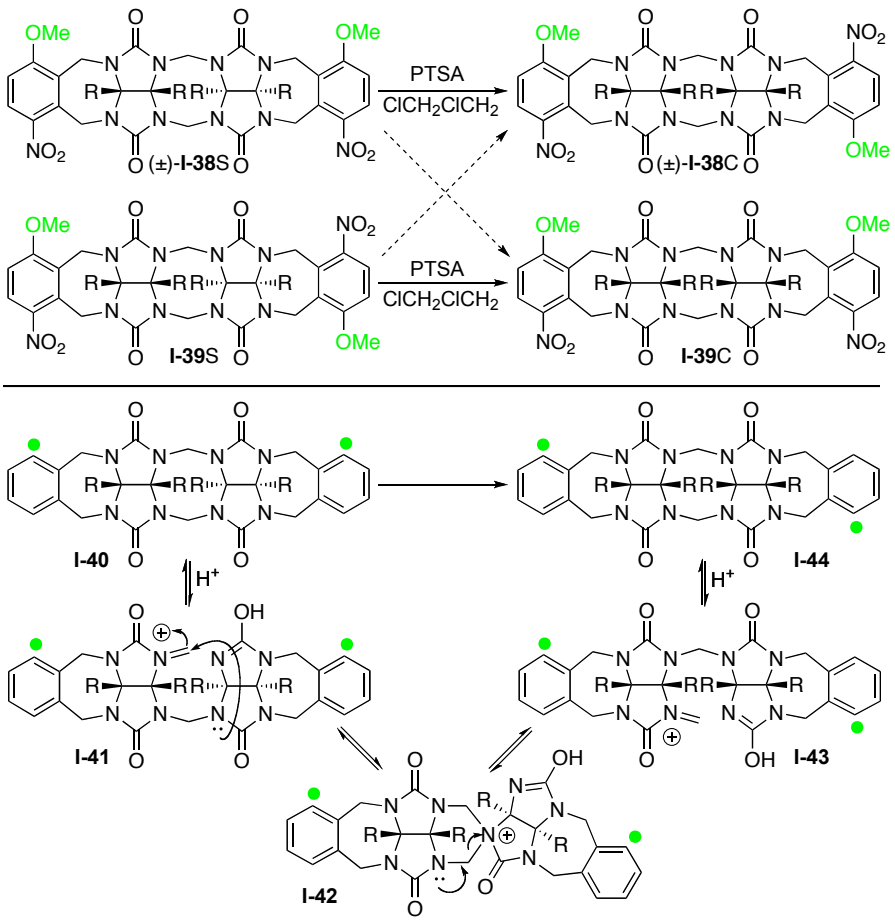

Scheme 14. Mechanism of diastereoselective intramolecular isomerization of S- to C-shaped compounds.

1.8.5 Implications for the Synthesis of Cucurbit[n]uril Analogues and Derivatives. The results presented in Sections 1.8.2 – 1.8.4 provide a number of insights into the mechanism of CB[n] formation. For example, the isolation of the S-shaped diastereomers provides strong evidence that both **I-11**S and **I-11**C form in the initial stages of the CB[n] forming reaction. The observed strong preference for the C-shaped diastereomers (> 90:10) provides a rationale for the high yield obtained in the synthesis of CB[6].[33] A simple calculation suggests that in a worst case scenario 53% (0.9^6) of the linear glycoluril hexamers would exist as the all C-shaped

diastereomer required to form CB[6]. In addition, the intramolecular nature of the S-shaped to C-shaped equilibration suggested that the length of the growing methylene bridged glycoluril oligomer chain (**I-13**, Scheme 3) determines the size (e.g. n) of the CB[n] formed. When considered together with highly selective heterodimerization reactions the results further suggest that the pattern of substituents on the surface of the growing methylene bridged glycoluril oligomer will be preserved in the CB[n] derivatives formed. As a specific example, we predicted that heating a combination of **I-1a** and bis(cyclic ether) **I-45a** under anhydrous acidic conditions (e.g. PTSA or $MeSO_3H$) would deliver the hexa-substituted CB[6] derivative **I-46a** (Scheme 15).[5] Although this reaction did not yield the desired product in practice, the predictions made above were subsequently borne out in the synthesis of CB[n] analogues and derivatives described below (Sections 1.9 and 1.10).

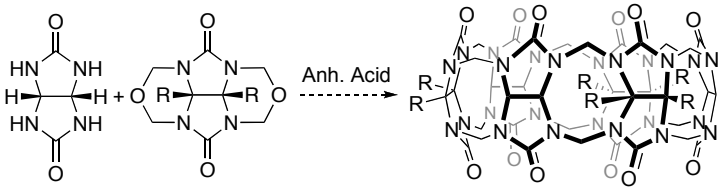

Scheme 15. Predicted synthesis of CB[n] derivatives.

1.9 Building Block Approach to Cucurbit[n]uril Analogues. We hypothesized that the reaction depicted in Scheme 16 did not proceed smoothly in practice because the CO_2Et-groups on the convex face of the glycoluril reduce its reactivity (sterically and electronically) relative to the unsubstituted glycoluril **I-1a**. To circumvent this issue we decided to search for a glycoluril analogue that might participate efficiently

in heterodimerization reactions with compounds like **I-45** to yield CB[n] analogues. With a little bit of luck we discovered that phthalhydrazides are superior nucleophiles – presumably due to the α-effect – that undergo selective heterodimerization with glycoluril cyclic ethers under anhydrous acidic conditions.[34-36] Specifically, bis(phthalhydrazide) **I-47** was found to undergo separate macrocyclization with dimeric **I-48** and trimeric **I-49** to yield CB[n] analogues (**I-50** and (±)-**I-51**) in remarkably high yield which incorporate the UV/Vis, fluorescent, and electrochemically active bis(phthalhydrazide) walls. The carboxylic acid version of **I-50** can be used as a fluorescent sensor in aqueous solution.[36] Compound (±)-**I-51** was particularly intriguing to us since the presence of two free ureidyl NH-groups and the twisted connection between the tips of the two glycoluril trimer building blocks **I-49** imparts C_2-symmetry to the macrocycle which renders (±)-**I-51** chiral and racemic. Compound (±)-**I-51** is the only chiral member of the CB[n] family.

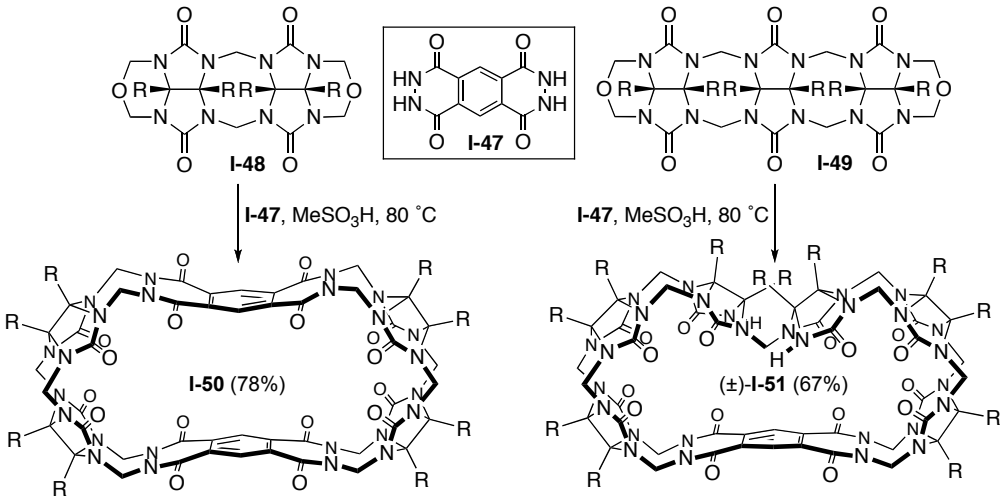

Scheme 16. Synthesis of CB[n] analogues. R = CO_2Et.

1.10 Building Block Approach to Cucurbit[n]uril Derivatives. Concurrently with the synthesis of the CB[n] analogues, the groups of Day and Tao were also pursuing a building block approach toward CB[n] derivatives.[37,38] For example, Day was able to isolate Me_6CB[6] (**I-46b**) from the reaction of **I-1a** and **I-45b** using aqueous acidic reaction conditions (Scheme 15). An elegant example of a building block approach toward CB[n] derivatives was realized by reacting the unsubstituted methylene bridged glycoluril dimer **I-52** with cyclic ether **I-45b** which delivered the tetra-substituted CB[6] derivative Me_4CB[6] in 30% yield (Scheme 17). Quite interestingly, Me_4CB[6] has an ellipsoidal shape which binds aromatic rings with a common orientation of the long axes of both host and guest.[38]

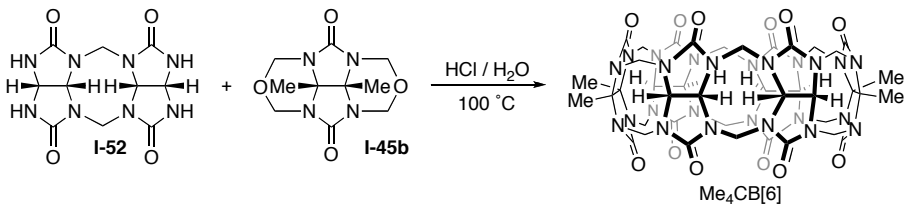

Scheme 17. Synthesis of Me_4CB[6].

1.11 Identification and Isolation of Inverted Cucurbit[n]urils (n = 6, 7). The preferred – but not exclusive – formation of C-shaped methylene bridged glycoluril dimers provided a rationale for the observed high yields in CB[n] forming reactions. Conversely, those same experiments can also be interpreted as suggesting the possibility of diastereomeric CB[n]. Such diastereomeric CB[n] in which one or more pairs of glycoluril H-atoms point into the central CB[n] cavity are referred to as inverted CB[n] (*i*-CB[n]). The first members of the *i*-CB[n] family were discovered

by the groups of Isaacs and Kim and investigated jointly (Scheme 18).[13] *i*-CB[6] and *i*-CB[7] are formed in small amounts in the CB[n] forming reaction and can be detected in the ^{1}H NMR spectrum of the mixture by diagnostic resonances for the inverted H-atoms (≈ 5 ppm, *vide infra*). Pure *i*-CB[6] and *i*-CB[7] could be isolated in low yield (2.0 and 0.4%) by a combination of fractional recrystallization and gel permeation chromatography. Scheme 18 also shows the x-ray crystal structures of *i*-CB[6] and *i*-CB[7] and their electrostatic potential energy surfaces. The consequences of the inverted glycoluril ring are reduced cavity volumes, flattened ellipsoidal shaped cavities, more positive intra-cavity electrostatic potentials, and more open C=O lined portals. In accord with these considerations, *i*-CB[6] and *i*-CB[7] preferentially bind ellipsoidal and electrostatically negative aromatic guests like *p*-xylylene diamine **I-53** and ferrocene derivative **I-54**. Overall, the inverted glycoluril modulates the guest binding affinity and rates of dissociation in a way that might be useful in the creation of function CB[n] based systems.

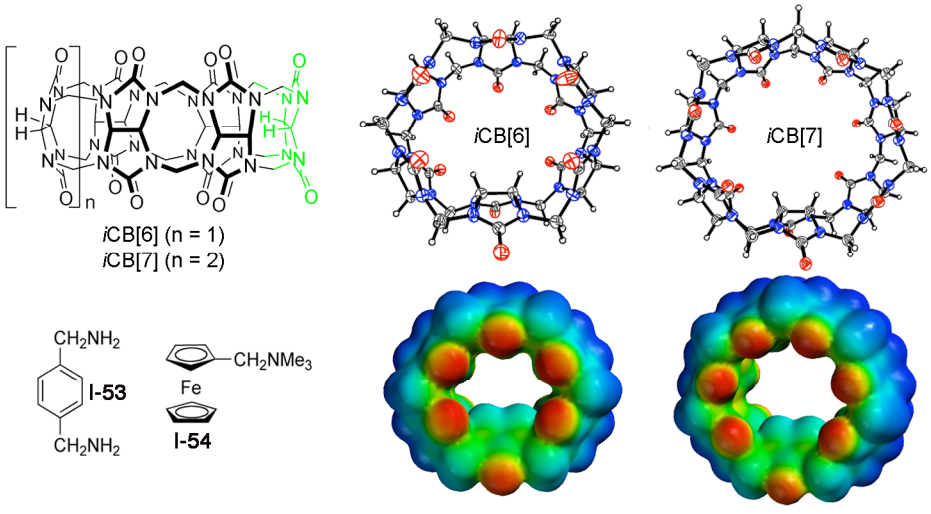

Scheme 18. Chemical structures, x-ray crystal structures, and electrostatic potential maps for *i*-CB[6] and *i*-CB[7].

1.12 Direct Functionalization of Cucurbit[n]urils. One of the major challenges in CB[n] chemistry is the poor solubility of CB[n] in neutral water and far worse solubility in organic solution. A potential solution to this problem that has been pursued by several groups involves the preparation of CB[n] derivatives or analogues that contain solubility enhancing functional groups on the convex face of the macrocycle. That strategy is easier to propose than to execute in practice, and the sections above detailed some of the challenges of using glycoluril derivatives in CB[n] forming reactions. Perhaps the most onerous issue to be addressed in such a route is the modification of the separation scheme for each new CB[n] derivative. An alternative approach to the preparation of CB[n] derivatives is the direct functionalization of purified unfunctionalized CB[n].

1.12.1 Perhydroxylation and Further Derivatization of CB[5] – CB[8]. Kim and co-workers addressed a major issue in CB[n] chemistry with their discovery of a method for their direct functionalization.[39] They found that heating CB[5], CB[6], CB[7], or CB[8] with $K_2S_2O_8$ in water results in the perhydroxylation of CB[n] (n = 5 – 8) yielding $(HO)_{2n}$CB[n] in modest to low yield (Scheme 19). Furthermore, the $(HO)_{2n}$CB[n] have excellent solubility in DMSO and DMF which allows for subsequent functionalization. For example, $(HO)_{2n}$CB[n] (n = 5, 6) undergo reaction with NaH and allyl bromide in DMSO to yield $(H_2C{=}CHCH_2O)_{2n}$CB[n] in good yields. $(H_2C{=}CHCH_2O)_{2n}$CB[n] (n = 5, 6) undergo photochemical addition of thiols (e.g. $CH_3(CH_2)_7SH$ or $CH_3[O(CH_2)_2]_3SH$) to yield the highly lipophilic $\{CH_3(CH_2)_7S(CH_2)_3\}_{2n}$CB[n] and $\{CH_3[O(CH_2)_2]_3S(CH_2)_3\}_{2n}$CB[n].

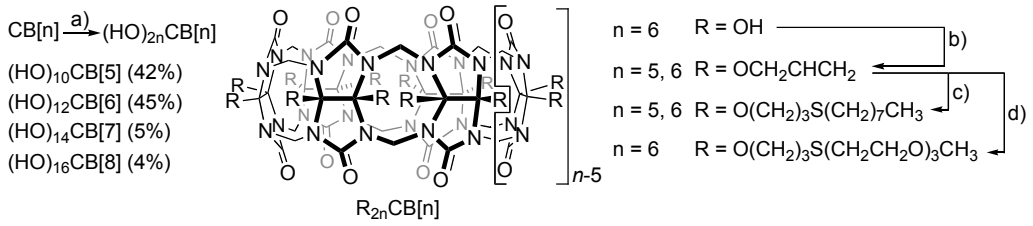

Scheme 19. Direct functionalization of CB[n]. Conditions: a) $K_2S_2O_8$, H_2O, 85 ˚C; b) NaH, DMSO, allyl bromide; c) $CH_3(CH_2)_7SH$, hν; d) PEG-thiol, hν.

1.13 Multivalent Binding of Sugar Decorated Vesicles to Lectins. The study of vesicles is an area of wide interest due largely to their potential use in areas as drug and gene delivery, biomimetic systems, and in the preparation of nanostructured materials. Kim's group discovered that the amphiphilic CB[6] derivative $\{CH_3[O(CH_2)_2]_3S(CH_2)_3\}_{2n}$CB[6] formed vesicles of 170 ± 50 nm diameter as evidenced by transmission electron microscopy (**I-55**, Scheme 20).[40] When the vesicles were prepared in a solution containing sulforhodamine G and purified by gel permeation chromatography, the vesicles showed bright fluorescence which demonstrates their low permeability. The efficient non-covalent derivatization of the exterior of vesicles **I-55** is possible simply by the addition of the spermine-fluorescein conjugate **I-56** to yield **I-55•I-56**$_n$. Conjugate **I-56** is bound strongly to the cavities of the CB[6] derivatives on the surface of the vesicles by the hydrophobic effect and ion-dipole interactions as evidenced by ^{1}H NMR and confocal microscopy. This vesicle scaffold can also be used for the multivalent display of α-mannose groups tagged with a spermine tail. These α-mannose derived vesicles are capable of aggregating concanavalin A due to biospecific interactions between the sugar and the

lectin. The potential for the introduction of multiple tags onto a single vesicle suggests a route toward the targeted delivery of pharmaceutical agents.

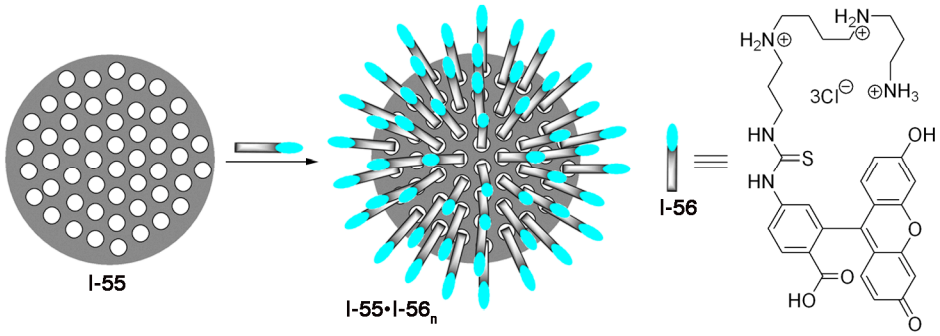

Scheme 20. Decoration of supramolecular vesicles with fluorescent labels.

1.14 Cucurbit[n]uril Based Artificial Ion Channels. One of the major issues that faced the development of applications of the CB[n] family – that has partially faded with Kim's direct functionalization route – is poor solubility in organic solution. To improve the solubility in organic solution and in lipid membranes Kim and co-workers attached long alkyl chains to the outside of CB[5] and CB[6] as described above.[39] Kim and co-workers found that $\{CH_3(CH_2)_7S(CH_2)_3\}_{2n}CB[n]$ (n = 5, 6) could be incorporated into large unilamellar vesicles (LUV's) comprising egg yolk L-α-phosphatidyl-choline (EYPC), cholesterol, and dicetyl phosphate (Scheme 21).[41] The flux of protons and alkali metal cations across the membrane could be quantified by following the fluorescence intensity (I_{460} / I_{403}) of 8-hydroxypyrene-1,3,6,-trisulfonate (HPTS) which functions as a pH sensitive dye. Interestingly, the order of transport activity across LUVs containing $\{CH_3(CH_2)_7S(CH_2)_3\}_{2n}CB[n]$ was $Li^+ > Cs^+ \approx Rb^+ > K^+ > Na^+$ which is opposite to the binding affinity of CB[6] toward

alkali metal cations. Somewhat surprisingly, planar bilayer conductance measurements show that the ion transport occurs by a channel rather than a carrier mechanism. The ion-channel properties of $\{CH_3(CH_2)_7S(CH_2)_3\}_{12}CB[6]$ could be switched off by the addition of acetylcholine ($Me_3NCH_2CH_2OAc$, **I-57**) which binds in the cavity of the CB[6] derivative. The CB[6] derivative $\{CH_3(CH_2)_7S(CH_2)_3\}_{2n}CB[n]$ permits remarkably fast transport of Cs^+ across the membrane (≈ 5 pA; ≈ 3×10^7 ions s^{-1}) which is comparable to that observed for gramicidin. By using synthetic chemistry to tailor the structure and solubility of CB[n] and its derivatives, it is possible to expand the range of applications to which the CB[n] family can be applied!

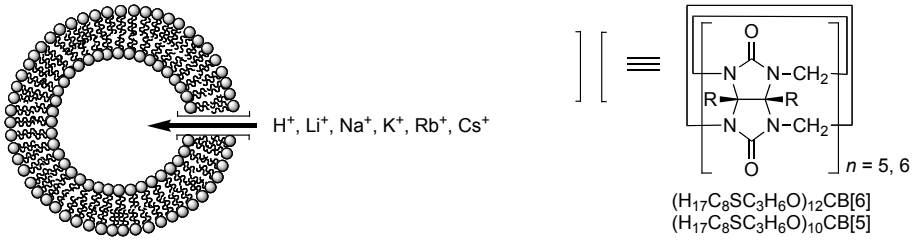

Scheme 21. Preparation of artificial ion-channels with CB[5] and CB[6] derivatives.

1.15 Experimental Procedures. This experimental section describes several key procedures encountered during the synthesis of members of the CB[n] family.

1.16 Synthesis of Glycolurils. An excellent review by Petersen describes the preparation of numerous glycolurils.[42] In general, the formation of glycolurils occurs by the condensation between urea and its derivatives with 1,2-diketones under acidic

conditions. Two specific examples are presented below which use either aqueous or anhydrous acidic conditions.

Synthesis of Glycoluril ***I-1a***. A modification of the literature procedure was used.[33] To a solution of urea (600 g, 10 mol) in water (1 L) was added a 40% aq. solution of glyoxal (500 g, 3.445 mol) and conc. HCl (86 mL). The resulting solution was heated at ≈ 85 – 90 ˚C until a heavy precipitate has formed. The reaction mixture is allowed to cool to room temperature and filtered. The filter cake is washed with copious amounts of water (2 L) followed by acetone to remove residual water. The resulting white solid is dried under high vacuum (397.5 g, 81%). ^{1}H NMR (DMSO, 400 MHz): 7.11 (s, 4H), 5.20 (s, 2H).

Synthesis of Glycoluril ***I-1b***. A modification of the literature procedures was used.[43] A mixture of benzil (21.0 g, 0.10 mol) and urea (12.1 g, 0.20 mol) in benzene (380 mL) was treated with TFA (20 mL) which results in a homogenous mixture. The reaction mixture is then heated at reflux with azeotropic removal of water for overnight. After cooling to room temperature, the white precipitate is isolated by filtration, washed with EtOH, and dried on high vacuum yielding **I-1b** as a white solid (22.8 g, 78%). ^{1}H NMR (DMSO, 400 MHz): 7.70 (s, 4H), 7.05 - 6.95 (m, 10H).

1.17 Synthesis and Separation of Cucurbit[n]urils. Although the synthesis and separation procedures given below may appear straightforward there are numerous details which do effect the outcome of the CB[n] forming reaction (e.g. rate

of stirring, physical state and degree of physical mixing of the starting materials, homogeneity of the solution, etc.) and the efficiency of the separation procedure (e.g. HCl content in the crude solid). Therefore, each of the major laboratories involved in CB[n] chemistry has developed their own modifications of the basic procedures published by Day and Kim.[12,15] We present here the procedures used by our group at the University of Maryland.

Synthesis of CB[n] and i-CB[n]. Powdered glycoluril (795 g, 5.59 mol) and powdered paraformaldehyde (354 g, 11.20 mol) were mixed thoroughly. An ice-cold concentrated HCl solution (1130 mL) was added gradually while stirring with a large glass rod. After the addition of ≈ 100 mL, stirring was no longer possible as the reactants were transformed into a brick like material. At this point the reaction becomes highly exothermic. The heterogenous mixture was gradually heated to 80 ˚C over 2.5 h and maintained at that temperature for an additional 2.5 hours at which point all of the solid had dissolved. The homogenous red solution was heated to 100 ˚C for 14 hours. After cooling to room temperature, the purification process was begun.

Monitoring of the Separation Process. It is possible to monitor the purification process by ^{1}H NMR using 20% DCl as the solvent. In this solvent CB[5] – CB[8] and CB[10]•CB[5] and *i*-CB[6] show diagnostic resonances for the high field diastereotopic CH_2-group (4.5 – 4.1 ppm). Figure 3 shows a representative ^{1}H NMR spectrum of the crude CB[n] forming reaction mixture.

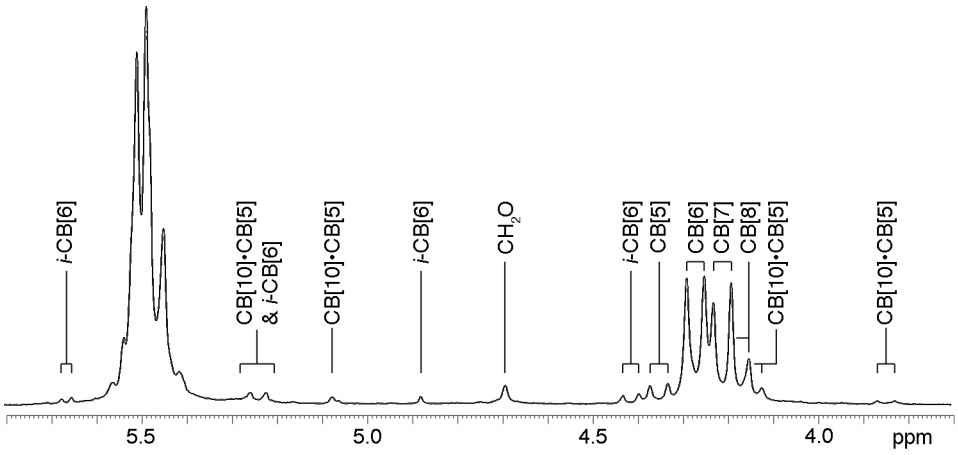

Figure 2. ^{1}H NMR spectrum (400 MHz, 20% DCl, RT) of the crude CB[n] reaction mixture.

Purification of CB[5], CB[6], CB[7], CB[8], CB[10]•CB[5] and i-CB[6]. The reaction mixture which contains a large amount of solid was evaporated to a minimum volume (≈ 600 mL). This slurry was poured into water (2.5 L). The solid was collected by filtration (Crop 1 contains CB[6], CB[7], CB[8], some *i*-CB[6], and some CB[10]•CB[5]). The filtrate was evaporated to about 600 mL and then slowly poured into a mixture of MeOH (3 L) and water (200 mL) with vigorous stirring. After stirring overnight, the precipitate was isolated by filtration (Crop 2 contains mainly CB[7] and CB[5] and smaller amounts of CB[6]).

Subsequent purification. The separation of each component (CB[5], CB[6], CB[7], CB[8], CB[10]•CB[5], and *i*-CB[6]) from Crop 1 and Crop 2 took advantage of their differential solubility in HCl solutions of different concentration. For example, CB[5] and CB[7] have moderate solubility in water but other CB[n] are nearly

insoluble in pure water. The crude solids were stirred in a beaker with large volumes of water (2 L) repeatedly to isolate a solution consisting of mainly CB[5] and CB[7]. After concentration to 200 mL, the solution is poured into MeOH (1.5 L) and the solid isolated by filtration. Separation of CB[5] from CB[7] is based on its moderate solubility (about 33 mg/mL) in 50% aqueous MeOH solution (v/v). The solubility of CB[7] is less than 4 mg/mL in this solution. Accordingly, the solid mixture of CB[5] and CB[7] was repeatedly stirred in a large beaker with 50% aq. MeOH to dissolve the CB[5] and leave the CB[7] as a solid. The solution of CB[5] is concentrated (not to dryness) which yields crystalline CB[5] (8% overall yield). Diffusion of acetone into an aqueous solution of CB[7] is used to obtain CB[7] as a crystalline solid (25% overall yield). The solid material from which CB[5] and CB[7] has been removed is subsequently processed to yield CB[6], *i*-CB[6], CB[8], and CB[10]•CB[5]. In 3 M HCl, CB[6], *i*-CB[6], and CB[10]•CB[5] have appreciable solubility whereas CB[8] is substantially less soluble. By stirring the crude mixture of CB[6], CB[8], CB[5]@CB[10], and introverted CB[6], with 3 M HCl in a large beaker it is possible to isolate CB[8] as an insoluble solid. CB[8] can then be recrystallized from warm conc. HCl to yield a crystalline solid (10% overall yield). The solution of CB[6], *i*-CB[6], and CB[10]•CB[5] in 3 M HCl is concentrated by rotary evaporation resulting in precipitation of CB[6]. The CB[n] remaining in solution are precipitated by pouring the aq. soln. into MeOH. The solid obtained which still contains CB[6], *i*-CB[6], and CB[10]•CB[5] can be separated by repeated fractional crystallization from different concentration HCl solutions. For example, CB[10]•CB[5] can be obtained by crystallization of the mixture from conc. HCl (2% overall yield). In samples that

contain a large amount of *i*-CB[6], the CB[6] impurity can be removed by dissolving the mixture in 20% HCl, adding the calculated amount of hexanediamine and diluting 10-fold with water. *i*-CB[6] is obtained as an insoluble precipitate (2% overall yield). CB[6] is obtained from multiple fractions and can be recrystallized from concentrated HCl (50% overall yield). The synthesis and purification procedure described above takes approximately 6 weeks.

1.18 Summary and Conclusions. The first synthesis of CB[6] by Behrend in 1905, its structural elucidation by Mock and co-workers in 1981, and subsequent studies by Mock and co-workers throughout the 1980's demonstrated the high potential of CB[6] in studies of molecular recognition in aqueous acidic solution. The field has taken rapid steps forward since 2000 with the discovery of the CB[n] homologues CB[5], CB[7], CB[8] by the groups of Kim and Day whose cavity volumes span and exceed those available with α-, b-, and γ-cyclodextrin. For example, the smaller CB[5] readily encapsulates gases[44] whereas the larger CB[n] homologues encapsulate species with high biological and chemical potential (e.g. anticancer agents, dyes, peptides, viologens, ferrocenes).

When Isaacs and co-workers began their work in this area in 1998 they decided to tackle the issue of preparing CB[n] derivatives that contained solubilizing groups on the exterior of the macrocycle that would extend the range of applications to which CB[n] could be applied. This Chapter has described the mechanistic approach pursued by the Isaacs' group that initially targeted the preparation of methylene bridged glycoluril dimers as the fundamental building blocks of the CB[n]

family. These model studies allowed us to provide evidence for some of the key early steps in the CB[n] formation mechanism, namely: 1) the presence of both S- and C-shaped diastereomers, 2) the presence of a thermodynamic driving force in favor of the C-shaped form (≈ 2 kcal mol^{-1}), and 3) the intramolecular nature of the S- to C-shaped equilibrium under anhydrous acidic conditions. These observations lead us to propose a building block strategy toward the preparation of CB[n] compounds[4,5] which was subsequently demonstrated experimentally in the synthesis of CB[n] derivatives and analogues.[34,37,38] Kim's synthetic advance in developing the direct per-hydroxylation of CB[5] – CB[8] allowed his group to prepare a wide range of per-functionalized CB[5] and CB[6] derivatives and use them in new applications like synthetic ion-channels and supramolecular vesicles.[39-41]

More recently, in collaboration with Kim's group, we isolated inverted cucurbiturils (*i*-CB[6] and *i*-CB[7]) which are kinetic intermediates along the pathway toward CB[n] whose transformation into CB[5], CB[6], and CB[7] was demonstrated by product resubmission experiments.[13] These key experiments provided evidence on the fate of some of the final intermediates along the mechanistic pathway toward CB[n] and stimulated us to further probe the latter stages of the mechanism of CB[n] formation. Our key realization was that CB[n] forming reaction mixtures containing a deficiency of formaldehyde would be unable to proceed to completion and therefore deliver intermediates as final products. Based on this idea, we were able to isolate *ns*-CB[10] which is formally derived from CB[10] by the removal of two CH_2 groups with subsequent bond reorganization. *ns*-CB[10] has displays recognition properties

including that are reminiscent of biological systems including the stabilization of ternary complexes and homotropic allostery based on guest size.

If the CB[n] family is to supplant the cyclodextrins as the platform of choice for basic and applied studies of molecular recognition then a series further developments must take place many of which involve the development of new synthetic procedures. First, improved methods for the separation of crude CB[n] mixture on laboratory (e.g. up to 1 kg) to industrial (e.g. tons) scale must be developed. Alternatively, synthetic procedures that selectively target a specific CB[n] (e.g. CB[8] or CB[10]) would be tremendously valuable. Second, the development of high yielding methods of functionalizing pre-formed CB[n] – particularly for CB[7], CB[8], and CB[10] would have a dramatic impact on the field. Third, a deficiency of the CB[n] family relative to the cyclodextrins is that they are inherently achiral which renders chiral recognition inside CB[n] challenging. Our group and Inoue's group have recently shown that chiral recognition inside CB[n] can be achieved by "assembled enantioselection" where a chiral binary complex can be transformed into a diastereomerically enriched ternary complex by interaction with a chiral but racemic guest.[18,45] Fourth, to date a small number of studies have targeted the development of CB[n] for electronic applications.[46] Fifth, for applications involving humans (e.g. drug delivery, foodstuff additive, perfume additive, etc.) it will be necessary to demonstrate that CB[n] are not toxic and that they are properly excreted from the body. Given the high chemical stability of CB[n] it seems unlikely that CB[n] will be metabolized in vivo. Lastly, it seems likely that CB[n] will be equal or

superior in the numerous application areas that have been demonstrated for the cyclodextrins and much future work will be directed in this direction.

II. Chapter 2: Cucurbit[n]uril Formation Proceeds by Step-Growth Cyclo-oligomerization (Huang, W.-H.; Zavalij, P. Y.; Isaacs, L. *J. Am. Chem. Soc.* 2008, submitted.)

2.1 Introduction. In 1981 Mock reported that the condensation of glycoluril and formaldehyde delivers the cyclic hexameric macrocycle cucurbit[6]uril (CB[6]).[2,18-19,47-48] This remarkable reaction (Scheme 1) results in the formation of 24 new C-N bonds and six eight-membered rings all with complete control over the relative orientation of the glycoluril C-H atoms which point out of the cavity. During the 1980's Mock extensively studied the host-guest recognition behavior of CB[6] and found that CB[6] exhibits remarkably tight (K_a up to 10^8 M^{-1}) and selective binding toward organic ammonium ions in water.[8,11] Subsequent work by Mock showed that these binding characteristics could be used to catalyze a dipolar cycloaddition (click-chemistry) and to create one of the first examples of a molecular shuttle.[10,49] As supramolecular chemists, we were inspired by the outstanding recognition properties of CB[6] and hypothesized that if we could tailor the recognition properties of CB[6] by synthetic chemistry (e.g., the creation of cucurbit[n]uril homologues (CB[n]),[16,49] analogues, derivatives, or congeners) that we might be in the position to create contemporary molecular devices like chemical sensors, supramolecular catalysts, ion and molecular channels, and molecular machines (e.g. molecular shuttles). As physical organic chemists, we decided to target a thorough understanding of the mechanism of CB[n] formation with the expectation that such knowledge would enable the tailor-made synthesis of CB[n]-type receptors with new geometrical features and recognition properties.

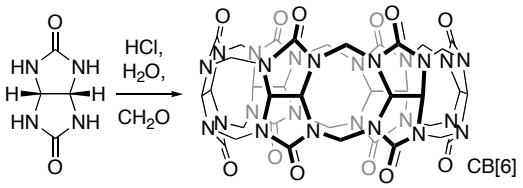

Scheme 1. Synthesis of CB[6].

Since I began my work on the mechanism of CB[n] formation upon arriving at the University of Maryland in 2003 there have been a number of developments in the CB[n] area that *post facto* validate our plan to enhance the range of applications to which the CB[n] family[49,50] can be applied by the creation of new CB[n]-type receptors. For example, the isolation of the cucurbit[n]uril homologues (n = 5, 6, 7, 8) by the groups of Kim and Day provided a series of macrocycles whose sizes (82, 164, 279, 479 $Å^3$) parallel those of α-, β-, and γ-cyclodextrins.[12,15] These new macrocycles, therefore, participate in a variety of interesting applications including supramolecular dye lasers,[51] novel drug delivery vehicles[29,30,52] as a mediator of organic reactions,[53] peptide recognition,[54] chemical sensors,[36,55] as components of complex self-sorting systems,[11,19-21] and in the development of molecular machines.[26,27,56] More recently, our group has reported the isolation of free CB[10] from its CB[10]•CB[5] complex and the ability of its 870 $Å^3$ cavity to promote folding, forced unfolding, and refolding of non-natural oligomers in water and as a host for metallo-porphyrins.[17,57] Most recently, in collaboration with Kimoom Kim's group, we have reported the isolation and recognition properties of diastereomeric CB[n] known as inverted-CB[n] (*i*-CB[n]) in which a single pair of methine C-H

groups point into the central cavity.[13,58] The formation of these new CB[n] under milder kinetically controlled conditions provide an existence proof for intermediates in the mechanism of CB[n] formation and have helped guide our mechanistic studies over the years.[5,6,13,34,35,58,59]

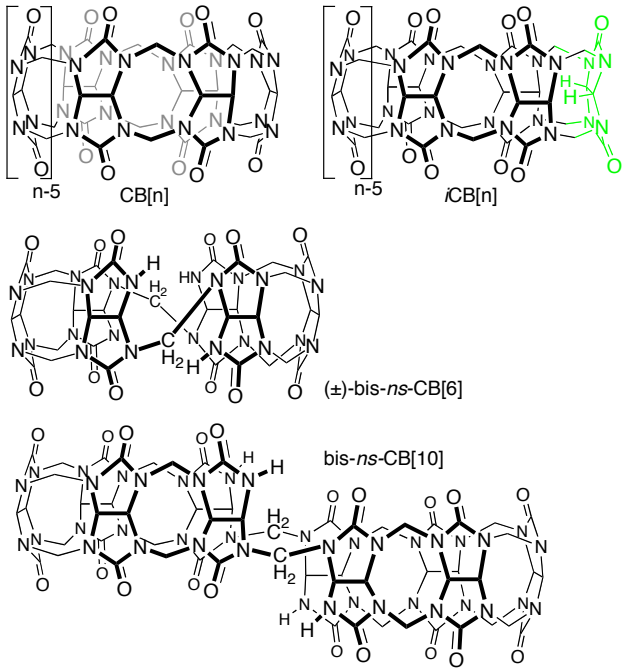

Scheme 2. Chemical structures of CB[n], *i*CB[n], bis-*ns*-CB[10], and (±)-bis-*ns*-CB[6].

2.2 Cyclic Oligomeric CB[n]. In this chapter we explore the consequences of our realization that the cyclo-oligomerization reaction of glycoluril and formaldehyde – tetra-functional and di-functional monomers, respectively – is in many ways related to a classical polymerization reaction. For example, classical polymerization reactions between two different multi-functional monomers only proceed to give high molecular weight material when there is a stoichiometric balance between the reactive groups of the two monomers.[60] When there is an excess of one of the

monomers, it acts as an end-capping group and shorter oligomers are obtained. Realizing that cyclic oligomeric CB[n] can be viewed as infinitely long oligomers raised the question in our mind of what would happen if we starved the CB[n] forming reaction of formaldehyde. Would new mechanistic intermediates in the formation of CB[n] be delivered as kinetically stable isolable materials? Our previous reports on the isolation, structural characterization, and recognition properties of bis-nor-seco-CB[10][14] and (±)-bis-nor-seco-CB[6] provide an answer in the affirmative and we describe our complete mechanistic study in detail here.

2.3 Results and Discussion. We begin this results and discussion section with a brief review of the state-of-the-art concerning the mechanism of CB[n] formation that sets the stage for a discussion of the results reported in this paper.

2.3.1 Previous Mechanistic Studies. Scheme 3 shows the fundamental steps of the mechanism of CB[n] formation that were previously presented by the groups of Isaacs and Day.[5,12] First, glycoluril **II-1** reacts with two equivalents of formaldehyde to potentially deliver a mixture of diastereomers (**II-2** and **II-2**S) that differ in the relative orientation of the pairs of methine C-H groups. It was further hypothesized that these dimers undergo further oligomerization via **II-3** – **II-8** to ultimately yield a substance known as Behrend's polymer. The length of the polymer chain and diastereomeric orientation of methine C-H groups in Behrend's polymer is ill-defined. At this stage, Behrend's polymer must undergo an isomerization reaction that converts its S-shaped to C-shaped subunits – potentially aided by templating

groups[61] – to create an oligomer (e.g. **II-9** or **II-10**) that is poised to undergo macrocyclization to enter the CB[n] family manifold by either end-to-end cyclization or back-biting mechanisms.

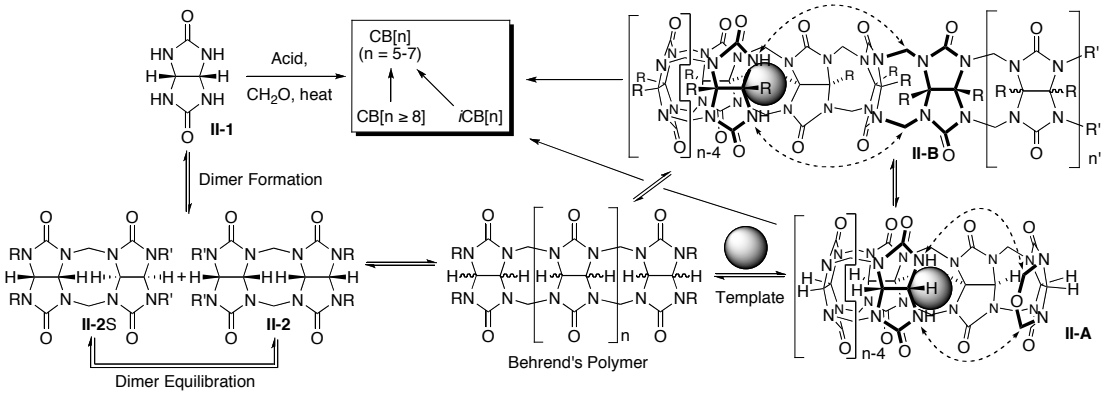

Scheme 3. Proposed mechanism of CB[n] formation.

Our group and the group of Anthony Day have been heavily involved in elucidating the mechanistic details of the CB[n] forming reaction.[5,12,35,61] Day's group has focused on the final steps of the mechanism of CB[n] formation and have examined the influence of numerous potential templating agents on the distribution of CB[n] obtained (e.g. ammonium ions and alkali metal ions).[62] Further transformations can occur inside the manifold of CB[n]-type receptors. For example, Day showed that heating CB[8] under the reaction conditions – where CB[5], CB[6], and CB[7] are stable – results in a partial ring contraction to deliver the smaller CB[n] homologues.[12] Similarly, we recently reported product resubmission experiments that show that *i*-CB[6] and *i*-CB[7] are converted into CB[n] which establishes that these diastereomeric CB[n] are kinetically controlled intermediates in the mechanism of CB[n] formation.[58]

Based on our realization that the methylene bridged glycoluril dimer substructure (bold in Chart 1) constituted the fundamental building block of the CB[n] family of macrocycles we initially studied derivatives of **II-2** and **II-2**S that contained solubilizing CO_2Et groups on their convex face and capping *o*-xylylene groups.[5,59] These model studies of the earliest steps of the mechanism of CB[n] formation (e.g. dimer formation and interconversion) allowed us to establish the high thermodynamic preference for the C-shaped forms ($\Delta\Delta G \approx 2$ kcal mol^{-1}), elucidate the intramolecular nature of the S-shaped to C-shaped interconversion, and to propose and validate the great potential of building block strategies in the formation of CB[n]-type receptors.[5,6,34,35,37,38,59] In combination, the results described above shed significant light on the earliest and latest steps of the mechanism of CB[n] formation. What was lacking was information about what goes on in the middle.

2.3.2 **Reaction Mixtures Deficient in Formaldehyde Deliver Glycoluril Oligomers II-2 – II-6 and Nor-seco-CB[n] as Isolable Species.** Based on the connections described above between a classical co-polymerization between multifunctional monomers and CB[n] formation we decided to conduct the condensation of glycoluril (**II-1**) with less than two equivalents of formaldehyde under aqueous acidic conditions (Scheme 4). From these reaction mixtures, we were able to isolate the series of glycoluril oligomers **II-2** – **II-6** by a combination of Dowex™ ion-exchange chromatography and recrystallization. We were able to establish the constitution of glycoluril oligomers **II-2** – **II-6** by mass spectrometry. Given the large number of potential diastereomers of these oligomers **II-2**, **II-3**, **II-4**,

II-5, **II-6** structural elucidation by ^{1}H NMR spectroscopy alone is challenging (Figure 1). Compounds **II-2** – **II-6** with all methine C-H groups on a single side of the molecule are C-shaped and C_{2v}-symmetric. Symmetry consideration dictate that dimer **II-2** show two doublets for the methine C-H groups (H_a and H_b) and two doublets for the diastereotopic CH_2-groups (H_c and H_d) as is observed experimentally. The ^{1}H NMR spectrum for trimer **II-3** consists of two doublets and one singlet for the glycoluril methine C-H groups (H_a, H_b, H_c) in addition to two doublets for the diastereotopic CH_2-groups. The ^{1}H NMR spectra for **II-4** – **II-6** are complicated in by spectral overlap in the methine CH region – although the number and relative intensity of the resonances for the diastereotopic CH_2-groups are in accord with symmetry considerations – and complete assignment was not possible on the basis of mass spectrometry and ^{1}H NMR spectroscopy alone.

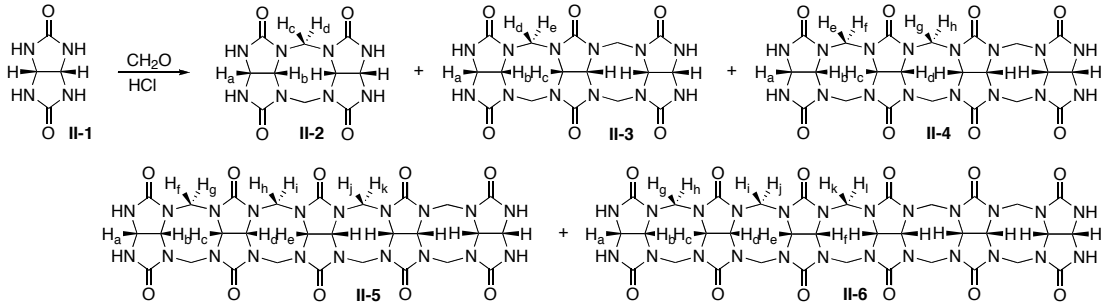

Scheme 4. Synthesis of C-shaped **II-2** – **II-6**.

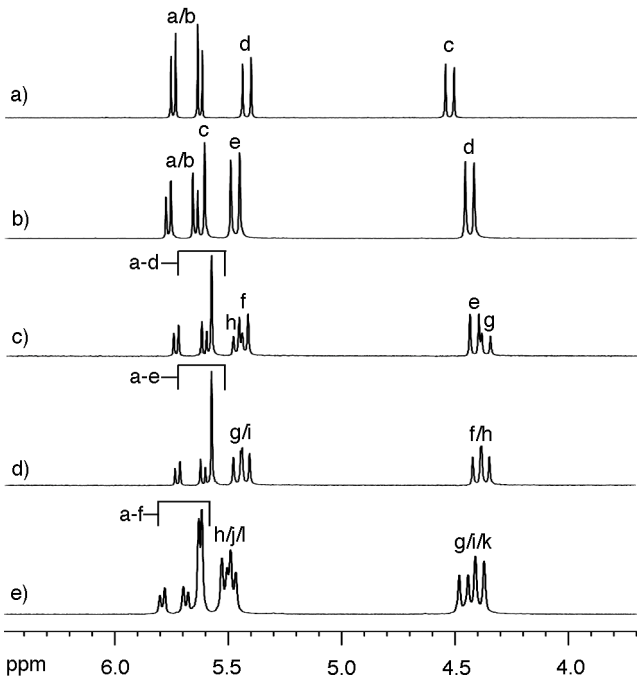

Figure 1. ^{1}H NMR spectra (400 MHz, 35% DCl) for: a) dimer **II-2**, b) trimer **II-3**, c) tetramer **II-4**, d) pentamer **II-5**, and e) hexamer **II-6**.

2.3.3 **X-ray Crystal Structures of II-2 – II-6.** Although we were quite confident in our assignment of the structures of the oligomers **II-2** – **II-6** based on spectroscopic techniques and previous model studies which indicated a significant thermodynamic preference for the C-shaped diastereomers we wanted to obtain final structural proof in the form of x-ray crystal structures. With some effort we were able to obtain single crystals of **II-2**, **II-3**, **II-4**, **II-5**, and **II-6** (Figure 2). The structures of **II-2** – **II-6** are striking for several reasons: 1) the anticipated C-shaped geometries are observed in all cases, 2) the curvature of **II-2** – **II-5** is mainly restricted to a single plane (e.g. out of plane twisting is not significant, and 3) the degree of curvature maps well onto that of CB[6] which is in accord with theoretical calculations which show that CB[6] is the least strained CB[n] on a per glycoluril basis.[50] Beyond the simple

connectivity of the molecular structures of **II-2** – **II-6** there are intriguing aspects of the solvation and packing of **II-2** – **II-6** in the crystal (Supporting Information). For example, compound **II-2** crystallizes (Figure 2a) as the CF_3CO_2H (TFA) solvate which segregates the molecules of **II-2** from one another by forming H-bonds to the ureidyl groups of **II-2**. Trimer **II-3** also crystallizes (Figure 2b) as the TFA solvate by H-bonding interactions with the ureidyl groups of **II-3**. In this case, however, multiple molecules of **II-3** segregate themselves into slabs in the ab-plane that are separated by solvating slabs of TFA molecules along the c-axis. The packing of tetramer **II-4** (Figure 2c) in the crystal is facilitated by the interaction of the center two ureidyl C=O groups of two equivalents of **II-4** forming a head-to-tail dimeric entity by ion-dipole interactions with Na^+. Interestingly, these dimers of **II-4** are further organized by NH•••O=C H-bonds between the tips of **II-4** and the C=O rim of another molecule of **II-4** to form a complex network motif (Appendices). The packing of pentamer **II-5** which begins to look like CB[5] is even more interesting. Each molecule of pentamer **II-5** contains one solvating molecule of TFA *within its cavity*. Furthermore, these molecules of **II-5** organize themselves into infinite 1-dimensional tapes along the a-axis by *four* H-bonds between the N-H tips of **II-5** with the ureidyl C=O of the adjacent equivalents of **II-5** (Appendices). Most interesting and relevant toward the mechanism of CB[n] formation is the packing observed in the crystal structure of **II-6**. Individual molecules of **II-6** are distorted from a symmetric CB[6]-like shape and exhibit a out-of-plane twist toward the tips of the molecule. Both features speak to the inherent flexibility of the growing glycoluril oligomer chains which is less apparent by examination of the macrocyclic CB[n]. Furthermore,

two molecules of **II-6** dimerize in the crystal driven by NH•••O H-bonds. Although glycoluril derived supramolecular structures[65] are well-known to undergo self-association in organic and aqueous solution by H-bonds or π-π interactions this is the first example that we are aware of that implicates self-association of water soluble CB[n] fragments. The implication is that self-association of glycoluril oligomers may be considered as a relevant side pathway during the CB[n] forming reaction.

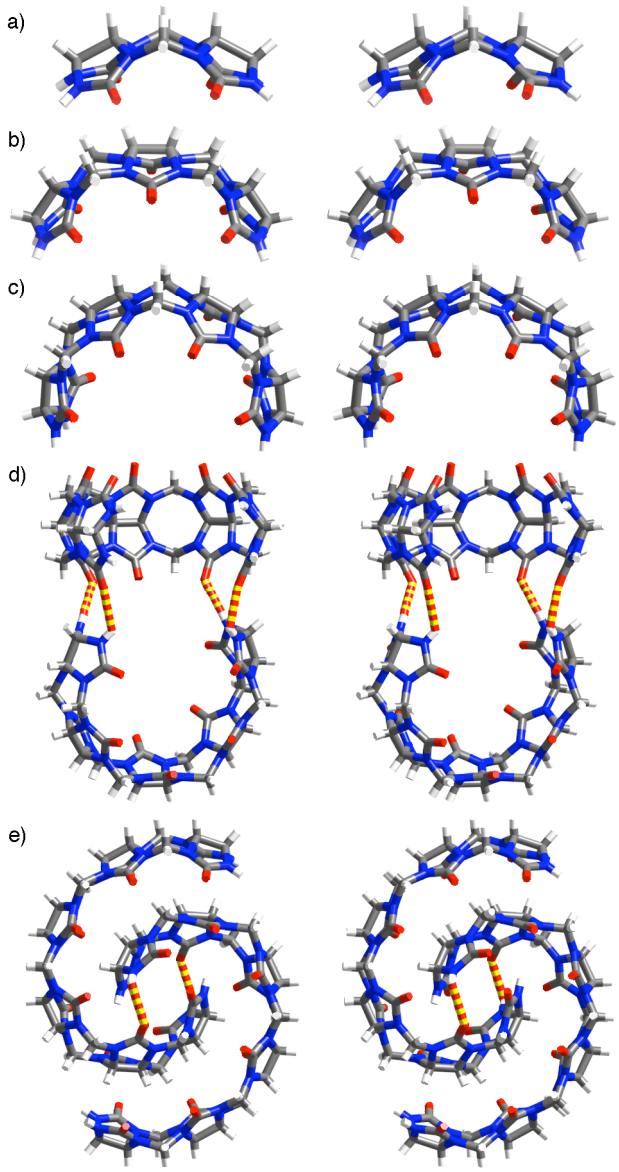

Figure 2. Cross-eyed stereoviews of the crystal structures of: a) **II-2**, b) **II-3**, c) **II-4**, d) **II-5**, and e) **II-6**. Solvating CF_3CO_2H and H_2O molecules have been removed for clarity. Color code: C, gray; H, white; N, blue; O, red; H-bonds, red-yellow striped.

2.4 Reaction Mixtures Deficient in Formaldehyde Also Deliver Nor-seco-CB[n] as Isolable Species. From similar reaction mixtures we have previously isolated bis-*ns*-CB[10], (±)-bis-*ns*-CB[6], and *ns*-CB[6].[14,63,64] Although the quantitation of the

amounts of each oligomer and nor-seco-CB[n] in a given reaction mixture has proved challenging due to extensive peak overlap in the ^{1}H NMR spectrum and losses that occur during Dowex™ ion exchange we have developed a guiding principle to maximize the yield of a given compound from condensations of glycoluril and formaldehyde that contain a deficiency of formaldehyde. This guideline is based on the theoretical ratio of glycoluril to formaldehyde in a given oligomer or *ns*-CB[n] (Table 1) and can be considered a consequence of Le Chatelier's principle. For example, dimer **II-2** is composed of two equivalents of glycoluril and two equivalents of formaldehyde and is best targeted with reaction mixtures containing a 1:1 ratio of the two starting materials. Similarly, the recently described *ns*-CB[n] (*ns*-CB[6], bis-*ns*-CB[10], and (±)-bis-*ns*-CB[6]) can be efficiently isolated from reaction mixtures comprising a 1:1.5 – 1:1.67 molar ratio of glycoluril:formaldehyde. This ratio is slightly lower than the calculated ratio since entry into the CB[n] manifold is an irreversible process that reduces overall yield and complicates product isolation. Lastly, the synthesis of CB[n] is known to be most efficient at a stoichiometric ratio of 1:2.[12]

Table 1. The molar ratio of glycoluril and formaldehyde units needed to construct CB[n], *i*-CB[n], *ns*-CB[n], and oligomers **II2 – II-6**.

Compound	Glycoluril	Formaldehyde
CB[n]	1	2
i-CB[n]	1	2
ns-CB[6]	1	1.84

bis-*ns*-CB[10]	1	1.80
(±)-bis-*ns*-CB[6]	1	1.67
II-6	1	1.67
II-5	1	1.60
II-4	1	1.50
II-3	1	1.33
II-2	1	1

2.5 Implications of the Isolation of II-2 – II-6, bis-ns-CB[10], (±)-bis-ns-CB[6], and ns-CB[6] Toward the Mechanism of CB[n] Formation. The isolation of glycoluril oligomers **II-2** – **II-6** and nor-seco-CB[n] allows us to add levels of detail to the mechanism of CB[n] formation that was not previously possible. Scheme 4 illustrates in detail our current level of understanding of the CB[n] formation process. The isolation of oligomers **II-2** – **II-6** from reaction mixtures comprising glycoluril and a deficiency of formaldehyde provides an existence proof for these structures as kinetically controlled intermediates in the formation of CB[n]. Accordingly, Scheme 5 shows the stepwise interconversion of glycoluril **II-1** into hexamer **II-6** by stepwise addition of monomer **II-1** (aqua arrows). Such a process where monomer is added stepwise is known in polymer chemistry as chain growth polymerization.[60] Although we have not isolated glycoluril heptamer or octamer (**II-7** and **II-8**) we depict them as highly likely mechanistic intermediates. As the oligomer lengthens from **II-1** to **II-8** the formation of undesired S-shaped diastereomers is likely. As depicted for **II-2**S

and **II-2** – and studied in detail in model systems by us[5,59] – an equilibration occurs that dramatically favors the C-shaped forms **II-3** – **II-8**. Once these oligomer chains have grown long enough (**II-5** – **II-8**) they may undergo direct *intramolecular* end-to-end cyclization by way of chiral hydroxymethylated intermediate (±)-**II-11**(n), *ns*-CB[n], and finally enter into the CB[n] manifold by addition of the final CH_2-group. This portion of Scheme 4 is in essence an enhanced version of Scheme 2 which accounts in detail for the presence of oligomers **II-3** – **II-6** and also takes into account the intermediacy of *ns*-CB[6].

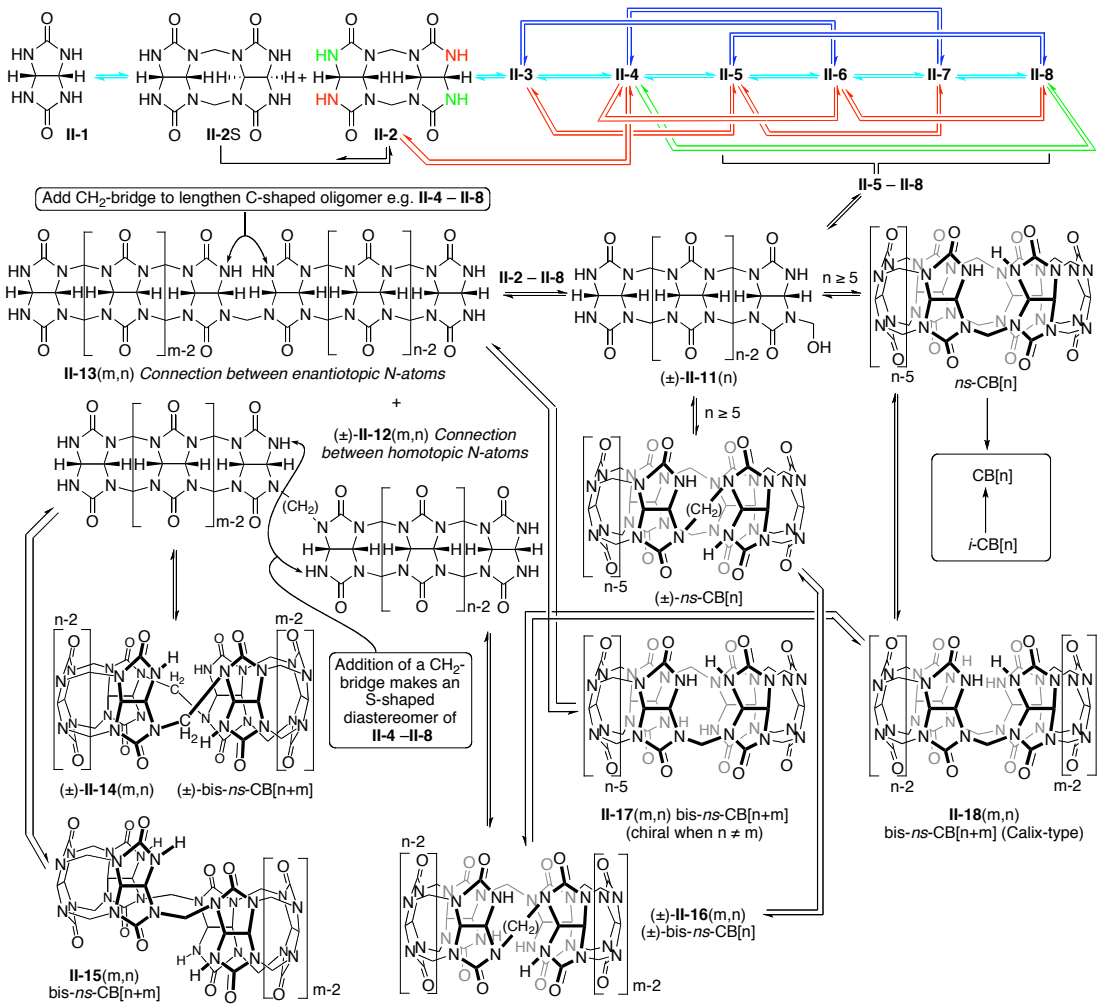

Scheme 5. Comprehensive mechanistic scheme for the formation of CB[n]. Color coding: chain growth, aqua arrows; step growth; red arrows (addition of **2**), blue arrows (addition of **3**); green arrows (addition of **4**).

The isolation of bis-*ns*-CB[10] and (±)-bis-*ns*-CB[6] – comprising two oligomer chains (e.g. **II-5** and **II-3**, respectively) linked by two CH_2-groups – alerted us to the potential operation of a second type of mechanistic pathway known as a *step-growth* process. In a step-growth process, the reaction between two oligomer chains is also possible. Consider, for example, intermediate (±)-**II-11**(n) (n ≤ 4)

which is too short to undergo direct *intramolecular* end-to-end cyclization. Intermediate (±)-**II-11**(n) is, therefore, forced to undergo intermolecular reaction with an oligomer of identical or different length. The sets of colored equilibrium arrows in Scheme 4 indicate the step-growth occurring by addition of dimer **II-2** (blue arrows), trimer **II-3** (red arrows), and tetramer **II-4** (green arrows) and two equivalents of formaldehyde to give longer C-shaped oligomers. Analysis of the intermediate stage of addition of one equivalent of formaldehyde is instructive. Despite the fact that **II-1** – **II-8** are achiral, their ureidyl NH groups are prochiral and pairs of NH groups are either homotopic (pairs of red or pairs of green NH groups in structure of **II-2**) or enantiotopic (pairs of red and green NH groups in structure of **II-2**). Connection of a pair of homotopic groups between two oligomers results in intermediate (±)-**II-12**(m,n) whereas connection of a pair of enantiotopic NH groups by means of a CH_2-bridge results in the formation of **II-13**(m,n).[66] Intermediates **II-13**(m,n) and (±)-**II-12**(m,n) may add a second CH_2-group in the middle of the molecule to form longer C-shaped oligomers **II-4** – **II-8** or diasteromeric oligomers with one S-shaped subunit, respectively. Alternatively, if intermediates (±)-**II-12**(m,n) and **II-13**(m,n) are long enough ($m + n \geq 5$) they may make a new N-CH_2-N bridge between the ends of the oligomer chain to deliver macrocyclic compounds In this manner, (±)-**II-12**(m,n) leads to (±)-**II-14**(m,n) and **II-15**(m,n) by connection of homotopic NH groups. The previously isolated (±)-bis-*ns*-CB[6] and bis-*ns*-CB[10] serve as examples of these types of macrocycles and provide strong evidence for the depicted mechanistic pathway. To provide even stronger evidence for this mechanistic scheme we performed product resubmission experiments with trimer **II-3** and pentamer **II-5**.

When trimer **II-3** was treated with 1 equivalent of formaldehyde in HCl we observed the formation of (±)-bis-*ns*-CB[6] by ^{1}H NMR at partial conversion.[63,67] When **II-5** was treated similarly, we observed and quantified the formation of CB[6] and bis-*ns*-CB[10] (0.39:1 ratio) by ^{1}H NMR spectroscopy of the crude reaction mixture. In combination, these results provide strong evidence for the operation of a step-growth cyclo-oligomerization reaction in the mechanism of CB[n] formation.

This mechanistic analysis that can be used to rationalize the formation of **II-2** – **II-8**, *ns*-CB[6], (±)-bis-*ns*-CB[6], and bis-*ns*-CB[10] can also be used to predict the structures of *ns*-CB[n] that have not yet been isolated.[68] For example, although (±)-**II-11**(n) may cyclize to yield *ns*-CB[n] by connection between enantiotopic NH groups it may also react to form (±)-*ns*-CB[n] by connection between enantiotopic NH groups. Similarly, either **II-13**(m,n) or (±)-**II-12**(m,n) may be transformed into (±)-**II-16**(m,n) by addition of an appropriate bridging group. Two additional bis-*ns*-CB[n] can be conceived by addition of a CH_2-bridge between enantiotopic NH groups of **II-13**(m,n) which delivers **II-17**(m,n) and **II-18**(m,n).[66] We are particularly intrigued by the geometrical features of **II-18**(m,n) which is reminiscent of the calixarenes with bridging at the lower rim and flexibility at the upper rim. We predict that **II-18**(m,n) will display quite interesting hybrid recognition and dynamic behavior.

2.5.1 ***Oligomer Resubmission Experiments.*** Although we viewed the evidence for the mechanistic scheme presented above as strong given the isolation of **II-2** – **II-6**,

bis-*ns*-CB[10], (±)-bis-*ns*-CB[6], and *ns*-CB[6] and previous mechanistic studies by us[5,6,34,35,37,38,59] and others[12,62,69] we wanted to obtain further evidence that applies directly to CB[n] formation rather than relying on evidence from *ns*-CB[n] formation. For this purpose we decided to perform product resubmission experiments between formaldehyde (2 equiv.) and oligomers **II-2** – **II-6** alone and in binary mixtures. We assess the outcome of these reactions by ^{1}H NMR spectroscopy of the crude reaction mixtures in 20% DCl in which CB[5], CB[6], CB[7], and CB[8] display separate easily integrated resonances (Table 2).[70]

2.5.2 Reactions Conducted Between Formaldehyde and II-1 – II-6. Initially, we conducted the separate reaction between formaldehyde (2 equiv.) and **II-1** – **II-6** (Table 2). The reaction of monomer alone (Table 2, entry 1) – which serves as our point of reference for the results described below – delivers a reaction mixture that contains mainly CB[5] (15%), CB[6] (53%), and CB[7] (30%); CB[8] content is low (2%). In contrast, use of dimer **II-2** and trimer **II-3** lead to reaction mixtures that contain higher percentages of CB[6] and diminished amounts of CB[5] and CB[7] (Table 2, entries 2 and 3). This result is in accord with the portion of our mechanistic scheme which is based on step-growth polymerization in that **II-2** would be expected to give enhanced yields of CB[n] where n is an even number (e.g. a multiple of 2) and **II-3** would be expected to give enhanced yields of CB[n] where n is a multiple of 3. As anticipated based on the step-growth cyclo-oligomerization model for CB[n] formation, the reaction of tetramer **II-4** was found to give a high yield of CB[8] (40%) and lesser amounts of CB[6] and CB[7] (Table 2, entry 4). The reactions of

pentamer **II-5** and hexamer **II-6** – the first oligomers capable of direct unimolecular macrocyclization – were particularly interesting (Table 2, entries 5 and 6). Pentamer **II-5** delivers mainly CB[5] (84%) and **II-6** delivers only CB[6] (100%) which indicates that these oligomers are pre-organized to undergo macrocyclization in preference to further oligomerization. In these reactions conducted under aqueous acidic conditions – with the use of purified oligomeric building blocks **II-2** – **II-6** – the operation of step-growth processes is *not exclusive* as can be seen for example in the reaction of **II-3** (Table 2, entry 3) which gives CB[5] and CB[7] as side products. This indicates that under the reaction conditions a given oligomer can undergo fragmentation processes (e.g. tetramer fragments to two dimers or to a trimer and monomer) to yield shorter oligomers which can then recombine to also give longer oligomers.[10] We have indicated this reversibility explicitly in Scheme 4.

2.5.3 Reactions Conducted Between Formaldehyde and Binary Combinations of Building Blocks II-1 – II-6. Although a complete analysis of the reactions conducted between formaldehyde (2 equivalents with respect to total building block concentration) and binary mixtures of building blocks **II-1** – **II-6** is not possible given the mixtures that are generally obtained from CB[n] forming reactions it is possible to tease out some information that we believe is significant (Table 2, entries 7 – 17). For example, combinations of oligomers **II-2** – **II-4** with monomer **II-1** increases the proportion of the first oligomer capable of macrocyclization – CB[5] – which is consistent with the increased importance of a chain-growth process when the amount of monomer is significant.[12,71] The results obtained with combinations of building

blocks intended to lead to CB[7] (**II-1** + **II-6**, **II-2** + **II-5**, and **II-3** + **II-4**; Table 2, entries 11, 14, 15) are interesting. Of these combinations, **II-1** + **II-6** delivers mainly CB[6], **II-2** + **II-5** delivers a significant portion of CB[5] due to competing cyclization of **5** along with CB[7] (35%), and **II-3** + **II-4** delivers a substantial amount of CB[6] presumably due to competing formation of CB[6] formed from two molecules of **II-3** along with CB[7] (42%). In combination, these reactions shed light on the reason why CB[6] is the dominant CB[n] formed under a variety of condition. Although there are a variety of pathways that lead to CB[6] in high relative yield (e.g. **II-6**, **II-1** + **II-5**, **II-2** + **II-4**, **II-3** + **II-3**) there are fewer pathways that lead to CB[7] (e.g. **II-2** + **II-5** and **II-3** + **II-4**) or CB[8] (only **II-4** + **II-4**) and those do so only in modest yield due to competing dimerization, cyclization, or fragmentation (e.g. tetramer to trimer and monomer) pathways. In this regard, the quantitative cyclization of **II-6** suggests that this cyclization (Table 2, compare entries 5 and 6) may be particularly favorable from a kinetic standpoint.

Table 2. The distribution of CB[n] obtained from reaction of **II-1** – **II-6** with formaldehyde (2 equivalents) alone and in combination.

Entry	Reactant(s)	CB[5]	CB[6]	CB[7]	CB[8]
1	**1**	15%	53%	30%	2%
2	**2**	12%	68%	17%	3%
3	**3**	8%	75%	17%	0%
4	**4**	5%	22%	33%	40%
5	**5**	84%	10%	6%	0%

6	**6**	0%	100%	0%	0%
7	**1** + **2**	14%	52%	31%	3%
8*	**1** + **3**	20%	43%	33%	4%
9	**1** + **4**	35%	44%	18%	3%
10	**1** + **5**	27%	67%	6%	0%
11	**1** + **6**	3%	90%	7%	0%
12	**2** + **3**	26%	41%	30%	3%
13	**2** + **4**	10%	53%	17%	7%
14	**2** + **5**	41%	24%	35%	0%
15	**3** + **4**	11%	42%	42%	5%
16	**3** + **5**	48%	36%	13%	3%
17	**4** + **5**	57%	21%	15%	7%

* A small amount (4%) of *i*-CB[6] was also detected in this reaction mixture.

2.6 ***Glycoluril Oligomers II-5 and II-6 Retain the Ability to Binding Ammonium Ions.*** Previously, Day's group has extensively studied the ability of organic and alkali metal cations to act as templates for a specific CB[n] during the CB[n] forming reaction from **II-1** and formaldehyde (2 equivalents).[61] The influence of such guests as templates is generally modest and the point in the mechanism of CB[n] formation that they influence remains unclear although Day hypothesizes that they exert their influence by forming oligomer•guest complexes that either promote or disfavor certain cyclization reactions. Given access to oligomers **II-2** – **II-6** we decided to test their ability to form complexes with representative guests. In accord with the recognized importance of ion-dipole interactions provided by a fully formed the

ureidyl C=O portals of CB[n] as an important driving force in the formation of CB[n] guest complexes,[50,63,70] we did not observe any evidence of binding between **II-2** – **II-4** and **II-19** or **II-20** in water. In contrast, we find that pentamer **II-5** and hexamer **II-6** begin to exhibit recognition properties characteristic of CB[n]. For example, **II-5** forms a complex with **II-19** that displays slow exchange on the chemical shift timescale. Evidence of binding between **II-5** and other guests (**II-21** – **II-24**) is apparent based on induced upfield shifts in the ^{1}H NMR spectrum although exchange is faster than the ^{1}H NMR chemical shift timescale. The recognition behavior of **II-6** is equally interesting (Figure 3). Hexamer **II-6** retains the ability to bind with common guests for CB[6] (e.g. **II-19** – **II-21** and **II-25**) and does so with slow exchange on the chemical shift timescale which is noteworthy given the acyclic nature of **II-6**. Other guests that are rejected by CB[6] (e.g. **II-23**, **II-24**, and **II-26**) are readily complexed by **II-6**. The ability to bind these guests – which are good guests for CB[7] (**II-23** and **II-26**) or even CB[8] (**II-24**) – indicates that hexamer **II-6** is quite flexible in solution and is able to expand its cavity and wrap itself around larger guests (e.g. **II-24**) in order to form complexes (Figure 4). One particularly interesting aspect shown in Figure 4 is that the NH tips of **II-6** are held apart from one another in a way that would disfavor direct cyclization to CB[6]. Overall, these results show that glycoluril oligomers **II-5** and **II-6** and by extension **II-7** and **II-8** are capable of binding guests typical of the CB[n] family. This suggests that the use of suitable templating groups that either promote or disfavor cyclization of a particular oligomer may be useful in directing the CB[n] forming reaction toward an enhanced yield of a single CB[n] compound.

Scheme 6. Guests for **II-5** and **II-6**.

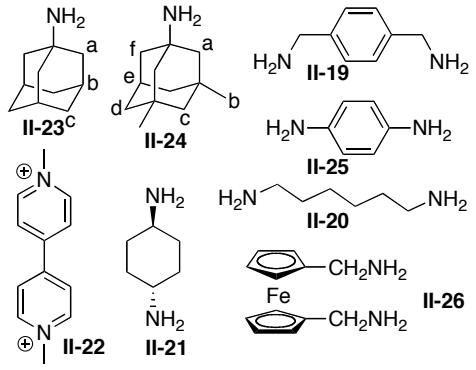

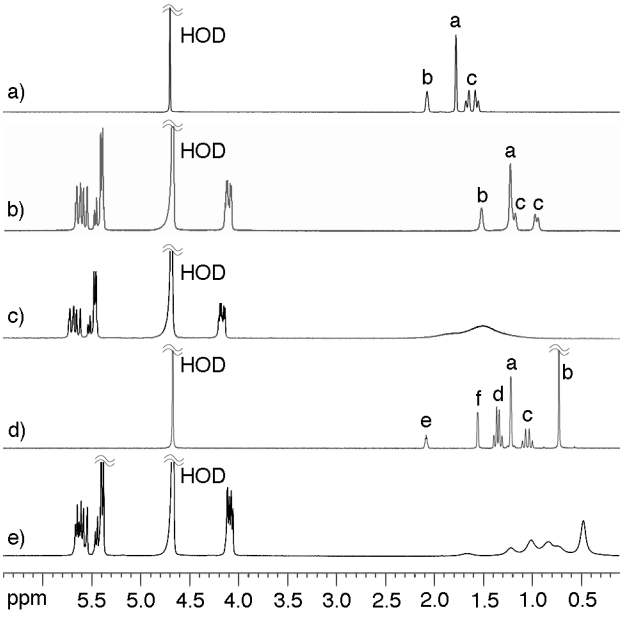

Figure 3. ^{1}H NMR spectra (400 MHz, D_2O, RT) for: a) **II-23**, b) **II-6•II-23**, c) a mixture of **II-6•II-23** and excess **II-23**, d) **II-24**, and e) **II-6•II-24**.

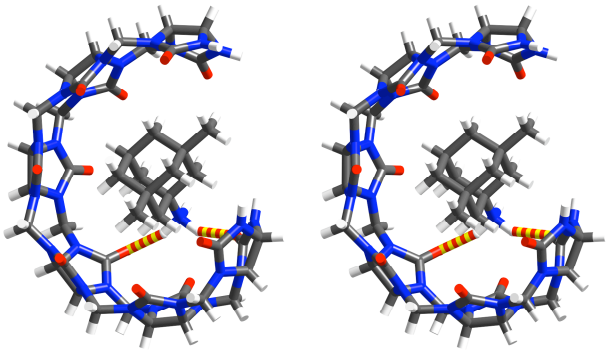

Figure 4. Cross-eyed stereoview of the MMFF minimized geometry of the **II-6•II-24** complex. Color code: C, grey; H, white; N, blue; O, red; H-bonds, red-yellow striped.

2.7 Conclusions. In summary, we have described the synthesis, purification, and solution and solid state characterization of methylene bridged glycoluril oligomers **II-2** – **II-6**. As expected based on previous model studies, glycoluril oligomers **II-2** – **II-6** possess the energetically favored all C-shaped geometry. The curvature of **II-2** – **II-5** maps well onto that exhibited by CB[6] which is calculated to be the least strained member of the CB[n] family. The packing of oligomers **II-4** – **II-6** in the crystal is dominated by C=O•••Na•••O=C and NH•••O=C interactions. Most interesting is the dimeric geometry of **II-6** in the crystal which demonstrates the inherent flexibility of the methylene bridged glycoluril oligomer chain and suggests that self-association should be considered as a side pathway in the mechanism of CB[n] formation. Based on the isolation of **II-2** – **II-6** and the previously isolated bis-*ns*-CB[10], (±)-bis-*ns*-CB[6], and *ns*-CB[6] we were able to formulate a detailed picture of the mechanism of CB[n] formation based on a step-growth cyclo-oligomerization process. To further support the step-growth mechanism we

performed product resubmission experiments between formaldehyde (2 equivalents) and oligomers **II-1** – **II-6** and binary combinations thereof and observed the effect on the ratio of CB[5] – CB[8] formed. Finally, we find that pentamer **II-5** and hexamer **II-6** – but not **II-2** – **II-4** retain the ability to bind organic ammonium ions (e.g. **II-19** – **II-26**) in water.

In conclusion, this study has painted a much more detailed picture of the mechanism of CB[n] formation – based on step-growth cyclo-oligomerization – than was previously possible. For example, this study allows us to rationalize the preferred formation of CB[6] in CB[n] forming reactions as a consequence of the multiplicity of pathways that leads to CB[6] relative to CB[7] or CB[8] and the pronounced kinetic tendency of **II-6** to undergo cyclization to CB[6] rather than oligomerization or fragmentation. The formulation of the mechanism of CB[n] formation as a step growth cyclo-oligomerization patway also allows us to predict the structures of different sized relatives of the previously isolated bis-*ns*-CB[10], (±)-bis-*ns*-CB[6], and *ns*-CB[6] and formulate the structures of classes of nor-seco-CB[n] that have not yet been isolated including (±)-*ns*-CB[6] and **II-17**(m,n) and **II-18**(m,n). We predict that **II-18**(m,n) will show particularly interesting recognition properties that blend the advantages of the CB[n] family of macrocycles with those of the calixarenes.

Of particular interest is the observation that **II-5** and **II-6** are capable of binding CB[6] sized guests (e.g. **II-19** and **II-20**) and can even expand their cavities

to associate with larger guests (e.g. **II-23** and **II-24**) typically bound within CB[7] or CB[8]. This result establishes a high level of flexibility of the growing methylene bridged glycoluril oligomer chain that suggests that the presence of suitable templating guests in the CB[n] forming reaction may be able to direct the reaction toward enhanced yield of a single sized CB[n]. This result also raises the prospect of using suitable guests to template the formation of larger *ns*-CB[n] ($n \geq 10$), *ns*-CB[n] containing multiple cavities and lacking more than two CH_2-groups,[14] and even the enantioselective synthesis of chiral *ns*-CB[n] (e.g. (±)-**II-14**(m,n), bis-*ns*-CB[n+m]). Given the wide range of applications to which CB[n] (e.g. sensing, molecular machines, drug delivery)[6] and its derivatives can be applied (e.g. polymer nanocapsules, affinity chromatography, and artificial ion-channels)[49,50] we expect that the ability to target tailor-made CB[n], CB[n] derivatives, and *ns*-CB[n] which is enabled by the mechanistic insights described herein will lead to new application areas that currently benefit from calixarene or cyclodextrin molecular containers.

2.8 Experimental Section. ***General Experimental Details.*** The guests used in this study were purchased from commercial suppliers and were used as their HCl salts. Dimer **II-2** was reported previously but no experimental details or characterization data are given.[38] The synthesis, characterization, and x-ray crystal structure of **II-3** (CCDC 647412) were previously reported by us.[63] Melting points were measured on a Meltemp apparatus in open capillary tubes and are uncorrected. IR spectra were recorded on Thermo Nicolet IR200 spectrometer and are reported in cm^{-1}. NMR spectra were measured on spectrometers operating at 400 and 500 MHz for ^1H and

100 or 125 MHz for ^{13}C. Mass spectrometry was performed using a VG 7070E magnetic sector instrument by fast atom bombardment (FAB) using the indicated matrix or on a JEOL AccuTOF electrospray instrument. Computational results were obtained using Spartan 02 running on a Macintosh personal computer.

2.8.1 Oligomers II-2 – II-6: A mixture of glycoluril (1.42 g, 9.99 mmol), paraformaldehyde (0.300 g, 9.99 mmol) and conc. HCl (4 mL) was heated at 50 ˚C for 18 hours. The precipitate was isolated by filtration, washed with MeOH and dried overnight at high vacuum to yield a crude white solid (577 mg) containing **II-2**. The soluble portion of the reaction mixture containing **II-2** – **II-6** was precipitated by the addition of MeOH followed by filtration and drying at high vacuum to yield a crude solid (952 mg). The white solid was recrystallized from TFA to yield **II-2** as a white solid (480 mg, 16%). Purification of the crude solid containing **II-2** – **II-6** was performed by column chromatography on Dowex 50WX2. A 5 cm diameter column was packed with Dowex 50WX2 resin to a height of 34 cm. The crude solid was dissolved in 88% HCOOH:0.2 M HCl (1:1, v:v) and loaded onto the column. The column was eluted using 88% HCOOH:0.2 M HCl (1:1, v:v). The oligomers come off the column in the following order **II-2**, **II-3**, **II-4**, **II-5**, and then **II-6**. The column fractions were individually concentrated by rotary evaporation and dried by high vacuum overnight. Purity was assessed by ^{1}H NMR and appropriate fractions were combined. The solids thus obtained were washed with MeOH to remove soluble impurities, dried overnight at high vacuum, and then recrystallized from TFA to yield: **II-3** (120 mg, 10%), **II-4** (30 mg, 3%), **II-5** (30 mg, 3%), and **II-6** (10 mg, 1%) as white solids. **Dimer II-2**: Mp: > 300 ˚C. IR (KBr, cm^{-1}): 3595s, 3205s, 3068s,

1696s, 1492s, 1466s, 1329s, 1234s, 1156s, 1109s, 958s, 884s, 801s, 707s, 680s, 640s. ^{1}H NMR (400 MHz, 35% DCl, RT): 5.73 (d, J = 8.8 Hz, 2H), 5.60 (d, J = 8.8 Hz, 2H), 5.37 (d, J = 16.0 Hz, 2H), 4.48 (d, J = 16.0 Hz, 2H). ^{13}C NMR (125 MHz, 35% DCl, RT, ext. dioxane reference): 159.4, 74.1, 62.2, 50.5. ES-MS: *m/z* 309 (100, $[M + H]^+$: ($[M + H]^+$, $C_{10}H_{12}N_8O_4$, calcd 308.10). X-ray crystal structure (from TFA). **Tetramer II-4**: Mp: > 300 ˚C. IR (KBr, cm^{-1}): 3405br, 1726s, 1472s, 1418s, 1379s, 1328s, 1295s, 1243s, 1199s, 1180s, 1127s, 969s, 802s. ^{1}H NMR (400 MHz, 35% DCl, RT, ext. dioxane reference): 5.74 (d, J = 8.6 Hz, 2H), 5.62 (d, J = 8.6 Hz, 2H), 5.60 (s, 4H), 5.49 (d, J = 14.8 Hz, 2H), 5.46 (d, J = 15.6 Hz, 4H), 4.42 (d, J = 15.6 Hz, 4H), 4.40 (d, J = 14.8 Hz, 2H). ^{13}C NMR (125 MHz, 35% DCl, RT): 159.3, 156.0, 74.1, 69.9, 69.8, 62.3, 51.1, 50.8. ES-MS: *m/z* 641 (100, $[M + H]^+$: ($[M + H]^+$, $C_{22}H_{24}N_{16}O_8$, calcd 640.2). X-ray crystal structure (from TFA). **Pentamer II-5**: Mp: > 300 ˚C. IR (KBr, cm^{-1}): 3399br, 1728s, 1471s, 1418s, 1377s, 1330s, 1295s, 1240s, 1222s, 1197s, 1181s, 968s, 804s. ^{1}H NMR (400 MHz, 35% DCl, RT, ext. dioxane reference): 5.73 (d, J = 8.6 Hz, 2H), 5.62 (d, J = 8.6 Hz, 2H), 5.58 (s, 6H), 5.46 (d, J = 14.8 Hz, 4H), 5.43 (d, J = 15.4 Hz, 4H), 4.41 (d, J = 15.4 Hz, 4H), 4.37 (d, J = 14.8 Hz, 4 H). ^{13}C NMR (125 MHz, 35% DCl, RT): 159.2, 155.8, 74.1, 69.8, 69.7, 62.2, 51.0, 50.8. (only 8 of the 10 expected resonances were observed). MS (ES): *m/z* 472 (100, [M + *p*-xylenediamine + 2H]$^{2+}$, *m/z* spacing = 0.5 confirmed for molecular ion). $C_{28}H_{30}N_{20}O_{10}$, X-ray crystal structure (from TFA). **Hexamer II-6**: Mp: > 300 ˚C. IR (KBr, cm^{-1}): 1717s, 1469s, 1422s, 1375s, 1325s, 1232s, 1190s, 1090s, 966s, 890s, 804s, 757s. ^{1}H NMR (400 MHz, 35% DCl, RT): 5.80 (d, J = 8.4 Hz, 2H), 5.69 (d, J = 8.4 Hz, 2H), 5.64 (s, 4H), 5.62 (s, 4H), 5.52 (d, J = 15.4 Hz, 6H), 5.49 (d, J = 15.4

Hz, 4H), 4.46 (d, J = 15.6 Hz, 4 H). 4.39 (d = 15.4 Hz, 6H). ^{13}C NMR (125 MHz, 35% DCl, RT, ext. dioxane reference): 159.4, 155.9, 74.4, 70.1, 70.0, 62.1, 51.4, 51.3, 51.1. (only 9 of the 12 expected resonances were observed). MS (ES): *m/z* 555 (100, [M + *p*-xylenediamine + 2H]$^{2+}$, *m/z* spacing = 0.5 confirmed for molecular ion). $C_{34}H_{36}N_{24}O_{12}$, X-ray crystal structure (from TFA).

2.8.2 ***General Procedures for Product Resubmission Experiments.*** Procedure A: A mixture of one glycoluril oligomer (**II-1**, **II-2**, **II-3**, **II-4**, **II-5**, or **II-6**, 5.0 mg) and paraformaldehyde (2.0 equivalents) was dissolved in 35% DCl (0.5 mL) and heated at 80 ºC for 18 hours. The resulting solution was precipitated by the addition of MeOH. The precipitate was isolated by centrifugation and dried overnight to yield a crude white solid. The content of CB[5], CB[6], CB[7], and CB[8] in the solid was determined by careful integration of the appropriate resonances in the ^{1}H NMR spectrum (20% DCl in D_2O). Procedure B: A equimolar mixture of two different glycoluril oligomers (**II-1**, **II-2**, **II-3**, **II-4**, **II-5**, or **II-6**, 7.5 mg total weight) and paraformaldehyde (2.0 equivalents) was dissolved in 35% DCl (0.5 mL) and heated at 80 ºC for 18 hours. The resulting solution was precipitated by the addition of MeOH. The precipitate was isolated by centrifugation and dried overnight to yield a crude white solid. The content of CB[5], CB[6], CB[7], and CB[8] in the solid was determined by careful integration of the appropriate resonances in the ^{1}H NMR spectrum (20% DCl in D_2O).

2.8.3 ***Synthesis of bis-ns-CB[10] from II-5.*** A mixture of **II-5** (30.0 mg, 0.037 mmol), paraformaldehyde (1.1 mg, 0.037 mmol), and conc. HCl (0.5 mL) was heated at 50 ºC overnight. The reaction mixture was pipetted into MeOH. The resulting precipitate was isolated by centrifugation and dried under high vacuum overnight to yield a crude solid (27 mg). The CB[6]:bis-*ns*-CB[10] ratio in this crude solid was

determined by ^{1}H NMR to be 0.39:1. Final purification was achieved by suspending the sample in an aqueous solution containing the calculated amount of hexanediammonium ion to complex the CB[6] impurity. The heterogenous mixture was then centrifuged and the solid obtained by decanting the supernatant. The solid was washed with several portions of water and dried at high vacuum overnight to yield bis-*ns*-CB[10] as a white solid (11 mg, 36%).

III. Chapter 3: Nor-Seco-Cucurbit[10]uril Exhibits Positive Homotropic Allosterism (Huang, W.-H.; Liu, S.; Zavalij, P. Y.; Isaacs, L. *J. Am. Chem. Soc.* 2006, *128*, 14744-14745.)

3.1 Introduction. Cucurbit[6]uril (CB[6]) – the prototypical member of the CB[n] family[16,49] – has outstanding recognition properties toward aliphatic and aromatic amines in aqueous solution.[2,73] In recent years, a homologous series of hosts (CB[n]: n = 5, 7, 8, 10)[12,15,17,18] has been isolated and investigated. These new CB[n] – with their increased cavity volumes – bind to a wide range of chemically and biologically important guests and therefore participate in a variety of interesting applications including fluorophore photostabilization,[74] gas binding,[75] chemical sensing,[14,36,76] supramolecular vesicles,[40] supramolecular dendrimers,[23] molecular machines,[26,27] and complex self-sorting systems.[19,20,77] Stimulated by the discovery of inverted CB[n] (n = 6, 7),[13] we postulated that other kinetically controlled structures might be formed as stable mechanistic intermediates[5] during CB[n] formation. We report the isolation and recognition properties of nor-seco-cucurbit[10]uril (*ns*-CB[10]) which results from formal extrusion of two CH_2 bridges from CB[10] along with bond reorganization.

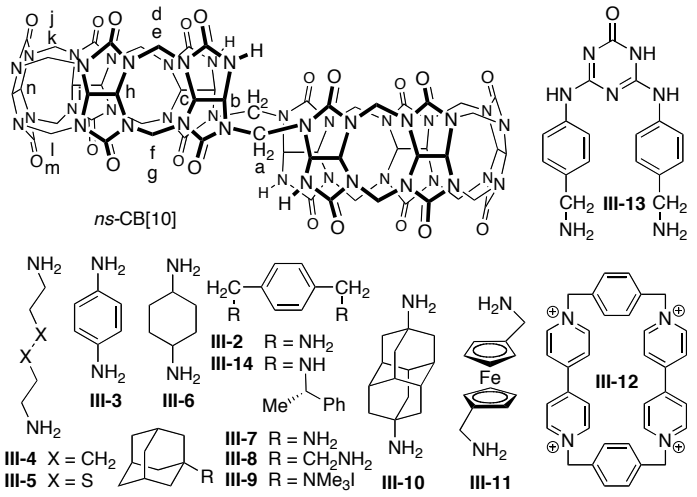

Scheme 1. Structure of *ns*-CB[10] and guests used in this study.

3.2 ^{1}H NMR spectra of free *ns*-CB[10]. We discovered that heating a mixture of glycoluril (**I-1a**) and paraformaldehyde at 50 ˚C in concentrated HCl delivers a reaction mixture that contains CB[n] and *ns*-CB[10] (Scheme 1). We isolated *ns*-CB[10] as a white solid in 15% yield by washing and recrystallization. The ^{1}H NMR spectra of free *ns*-CB[10] (Figure 1a) was not informative due to significant signal overlap although the resonance for the inwardly directed CH_2 bridge (H_a) appeared in a distinctive region of the spectrum. In contrast, the NMR spectra of *ns*-CB[10]•**III-2**$_2$ was relatively well dispersed which allowed unambiguous assignment of its structure by 2D NMR methods (Supporting Information). Of particular diagnostic utility are the resonances for H_a and H_n which appear as singlets due to the overall C_{2h}-symmetry of *ns*-CB[10]•**III-2**$_2$.

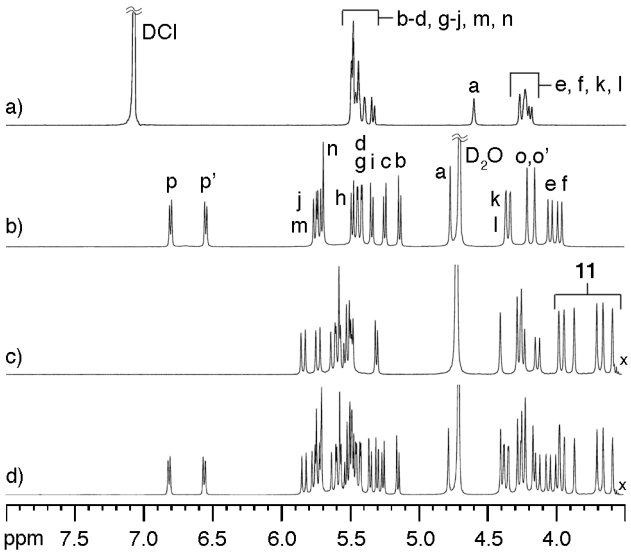

Figure 1. ^{1}H NMR spectra for: a) *ns*-CB[10] (400 MHz, 20% DCl), b) *ns*-CB[10]•**III-2**$_2$, c) *ns*-CB[10]•**III-11**$_2$, d) 2:2:2 mixture of *ns*-CB[10], **III-2**, and **III-11** (b-d: 500 MHz, D_2O). X = trace EtOH impurity.

3.3 X-Ray Crystals of *ns*-CB[10]. Fortunately, we obtained single crystals of *ns*-CB[10] as its *p*-phenylenediamine (**3**) complex (*ns*-CB[10]•**III-3**$_2$) which were suitable for x-ray structure determination (Figure 2). Several structural features are intriguing including: 1) the absence of two CH_2 bridges and the internal disposition of the two single CH_2 bridges, 2) two symmetry equivalent cavities and their lack of vertical registration, and 3) infinite guest filled channels defined by the stacking of *ns*-CB[10]•**III-3**$_2$ in the crystal (Supporting Information). Interestingly, the solvating H_2O molecules in the ureidyl carbonyl region of *ns*-CB[10]•**III-3**$_2$ act as bridges between guest NH and host C=O groups.

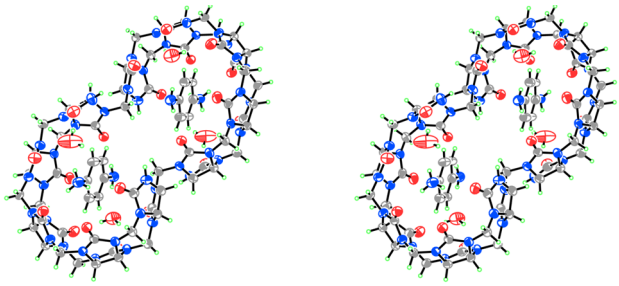

Figure 2. Cross-eyed stereoview of the crystal structure of *ns*-CB[10]•**III-3**$_2$. Solvating H_2O molecules have been removed for clarity. Color code: C, gray; H, green; N, blue; O, red.

3.4 Molecular Recognition Properties of Nor-Seco-Cucurbit[10]uril. After the structure of *ns*-CB[10] was elucidated, we investigated its recognition properties. The two cavities of *ns*-CB[10] are caparable in size to those of CB[6] and CB[7] and therefore bind guests commonly used with these hosts. For example, *ns*-CB[10] forms ternary (1:2) complexes with alkyl, cycloalkyl, aryl, and adamantyl amines (**III-2** – **III-10**) although some of these complexes display fast exchange on the NMR timescale. *ns*-CB[10] also binds some more chemically and biologically interesting species (Supporting Information) like dyes (e.g. coumarins, acridines, nile blue), amino acids (tryptophan, 4-aminophenylalanine, and arginine), and electrochemically active substances (ferrocenes (e.g. **III-11**) and viologens). More sizable guests (e.g. **III-12** and **III-13**) which are too large for the individual CB[6] – CB[7] sized cavities of *ns*-CB[10] instead form binary (1:1) complexes that fill both cavities simultaneously.

Several types of selectivity are observed within ternary complexes of *ns*-CB[10]. For example, when unsymmetrical guests are bound within *ns*-CB[10] three

diastereomers are possible (Figure 3: top-top, center-center, and top-center). For some guests a single diastereomer is observed (e.g. *ns*-CB[10]•**III-7**$_2$) which we tentatively assign the top-top conformation. In the top-top conformation, the NH_3^+ groups bind at the more flexible C=O portals which lack a CH_2-bridge. For other guests (e.g. **III-8**) all three conformations can be observed by ^{1}H NMR (Supporting Information).[78] A second type of selectivity is possible during the binding of chiral but racemic guests. For example, when a mixture of **III-14** and *ent*-**III-14** is offered to *ns*-CB[10], two homochiral forms (*ns*-CB[10]•**III-14**$_2$ and *ns*-CB[10]•*ent*-**III-14**$_2$) and one heterochiral form (*ns*-CB[10]•**III-14**•*ent*-**III-14**) are observed as a statistical mixture. Further studies are needed to understand the structural features that allow an efficient transmission of chiral information.

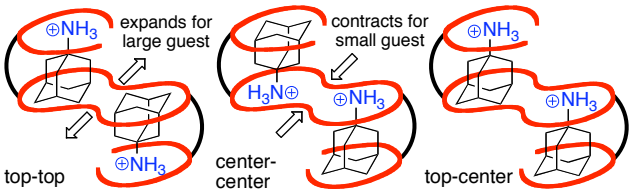

Figure 3. Three potential diastereomers of *ns*-CB[10]•**III-7**$_2$. The arrows illustrate the key CH_2•••CH_2 non-bonded distance that changes according to guest size.

3.5 Positive Homotropic Allosterism. Interestingly, during our binding studies we never observed the formation of binary complexes concomitant with ternary complexes, which establishes a sizable positive homotropic allosterism[14] in the system. To demonstrate its potential in allostery, we offered *ns*-CB[10] guest mixtures containing two (e.g. **III-2** and **III-11**, **III-5** and **III-7**, **III-2** and **III-5**, or **III-**

7 and **III-10**) different guests. When guests of quite different sizes are used (**III-2** and **III-11**, Figure 1b–d) allosteric control leads to a mixture of homomeric complexes (e.g. *ns*-CB[10]•**III-2**$_2$ and *ns*-CB[10]•**III-11**$_2$). In contrast, mixtures of similarly sized guests (e.g. **III-2** and **III-5** or **III-7** and **III-10**) result in mixtures of the homomeric and heteromeric ternary complexes. These results show that binding of the first guest to *ns*-CB[10] preorganizes the second cavity for binding of a *similarly sized guest*. Computational results suggest that the allosteric control is transmitted between binding sites in the putative 1:1 complex *via* the central $H_2C{\bullet\bullet\bullet}CH_2$ separation which varies systematically with the size of the guest (Figure 3 and Supporting Information).

3.6 Summary. In summary, we have reported the isolation of a new member of the CB[n] family – *ns*-CB[10] – which is both structurally and functionally intriguing. For example, *ns*-CB[10] retains much of the binding profile of CB[n] but also: 1) binds larger guests that are rejected by the corresponding CB[n] due to the less rigid, structurally more responsive *ns*-CB[10] cavity, 2) displays unusual top-center isomerism, and 3) displays positive homotropic allostery based on a guest size induced preorganization mechanism. As an intermediate in the formation of CB[n] with reactive NH groups, we believe that *ns*-CB[10] will enable straightforward access to CB[n] derivatives, surface immobilized CB[n], and CB[n] dimers.[38,80] The isolation of *ns*-CB[10] deepens our understanding of the mechanism of CB[n] formation and presages the formation of CB[n] hosts of even higher complexity. In combination, these results promise to broaden both the structural range of CB[n] that

can be accessed and the applications (e.g. biomimetic allosteric systems, supramolecular polymers, and covalent multivalent CB[n] scaffolds) to which CB[n] can be applied.

3.7 Synthesis of Nor-Seco-Cucurbit[10]uril.[14] A mixture of glycoluril (1.42 g, 9.99 mmol), paraformaldehyde (0.50 g, 16.69 mmol), and conc. HCl (4 mL) was heated at 50 ºC for 3 days. The resulting precipitate was separated by centrifugation to yield a crude solid (300 mg). The crude solid was dried on high vacuum for 10 min., washed with HCl:H_2O (1:1, v/v), washed with MeOH to remove HCl, and dried under high vacuum overnight to yield *ns*-CB[10] (238 mg, 0.145 mmol, 15%) as a white solid. ^{1}H NMR (400 MHz, 20% DCl): 5.47 (m, 28H), 5.40 (s, 4H), 5.33 (d, J = 4.0, 4H), 4.60 (s, 4H), 4.20 (m, 16H).

IV. Chapter 4: Chiral Recognition Inside a Chiral Cucurbituril

(Huang, W.-H.; Zavalij, P. Y.; Isaacs, L. *Angew. Chem. Int. Ed.* 2007, *46*, 7425-7427.)

4.1 Introduction. The supramolecular chemistry of the cucurbit[n]uril family[16,49] (CB[*n*]) of molecular containers has undergone rapid development in recent years including the development of a homologous series of CB[*n*] hosts (*n* = 5, 6, 7, 8, 10),[2,12,15,17,18] diastereomeric inverted CB[*n*],[13] and most recently bis-nor-seco-CB[10].[14] These new CB[*n*] compounds have cavity volumes (V = 82 – 870 Å^3) that span and exceed those available with α-, β-, and γ-cyclodextrin and are therefore capable of interacting with a wide range of chemically and biologically interesting guest species including gases, chromophores and fluorophores, anti-cancer agents, peptides, and neurotransmitters in water.[28,36,52,74,75,81] The extremely high affinity (K_a up to 10^{12} M^{-1}) and very high selectivity that are characteristic of CB[n] hosts[8,18,82] has been exploited in the creation of molecular machines, supramolecular vesicles, artificial ion channels, self-assembled dendrimers, and complex self-sorting systems.[20,21,23,27,39,30] Chiral recognition – a property readily achieved inside chiral cyclodextrins – has been challenging to reproduce using achiral CB[*n*].[18,83] In this paper, we report the isolation of a chiral nor-seco-cucurbituril – namely (±)-bis-*ns*-CB[6] – and demonstrate its ability to undergo enantio- and diastereoselective recognition inside its cavity.

4.2 Step-Growth Polymerization. The conversion of glycoluril (1 equiv.) and formaldehyde (2 equiv.) into CB[*n*][2,12,15,17,18] is a remarkably complex process involving the formation of 4*n* bonds and *n* rings with complete stereochemical control. Based on the hypothesis that the mechanism of CB[*n*] formation[5,12,34,60,61] involved step-growth polymerization we decided to starve the

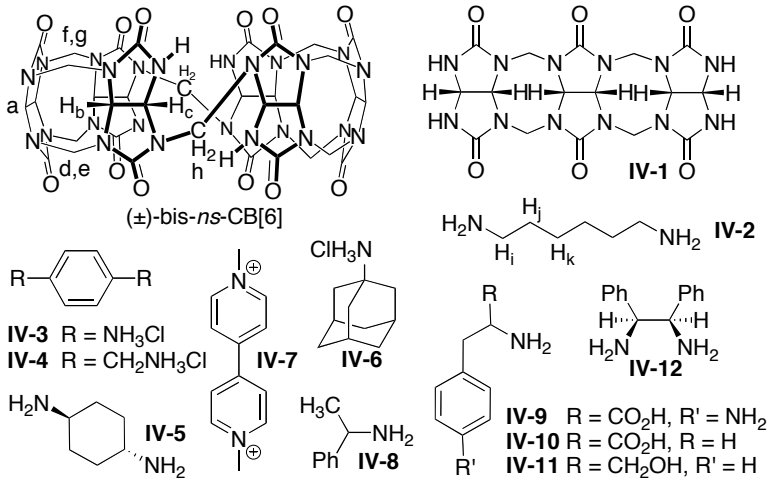

Scheme 1. Structure of compounds used in this study.

reaction of one of its monomers – formaldehyde – to access mechanistic intermediates *en route* to CB[*n*] that might display exciting recognition properties. From a reaction mixture consisting of glycoluril (1 equiv.) and paraformaldehyde (1.5 equiv.) in conc. HCl at 80 ˚C we isolated methylene bridged glycoluril trimer **IV-1** and (±)-bis-*ns*-CB[6] compound (Scheme 1). Fortunately, we were able to obtain x-ray crystal structures of **IV-1** and (±)-bis-*ns*-CB[6] (Figure 1) which conclusively established their structures.[84] A number of features of the structure of (±)-bis-*ns*-CB[6] deserve comment: 1) the exclusive connection between homotopic NH-groups of the two constituent glycoluril trimer fragments,[85] 2) the idealized presence of

three mutually perpendicular C_2-axes which leads to overall D_2-symmetry, and 3) the presence of intramolecular hydrogen bonds between the NH-groups and the C=O group on an adjacent glycoluril ring.

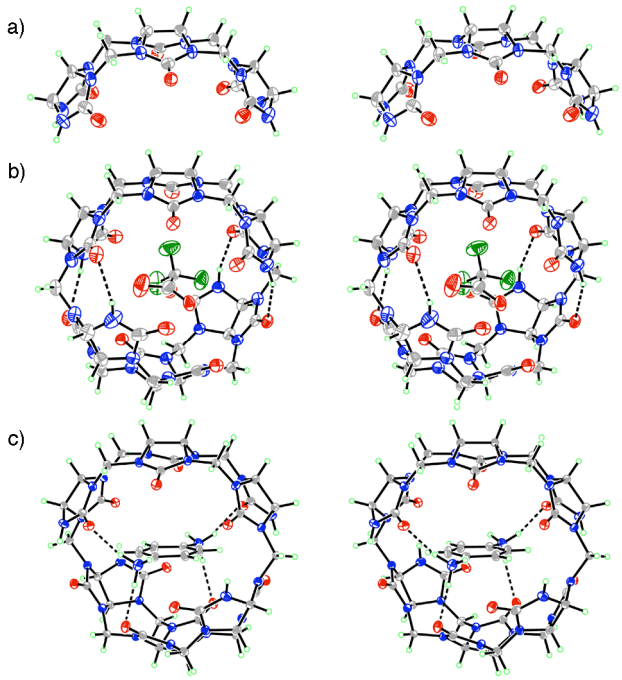

Figure 1. Cross-eyed stereoviews of the crystal structures of: a) **IV-1**, b) (±)-bis-*ns*-CB[6]•CF_3CO_2H, and c) (±)-bis-*ns*-CB[6]•**IV-3** with 30% probability ellipsoids. Solvating CF_3CO_2H and H_2O molecules have been removed for clarity.

4.3 The Affinity of (±)-bis-*ns*-CB[6]. After the structure of (±)-bis-*ns*-CB[6] was elucidated, we decided to study its abilities as a host in aqueous solution. We first sought to experimentally determine the effective cavity volume of (±)-bis-*ns*-CB[6] by ^{1}H NMR complexation experiments. Similar to CB[6] itself, we found that (±)-bis-*ns*-CB[6] forms inclusion complexes with **IV-2** – **IV-5** but not with the larger adamantane amine **IV-6** which binds with high affinity to CB[7] (Supporting

Information). Unlike CB[6], (±)-bis-*ns*-CB[6] does form an inclusion complex with methyl viologen (**IV-7**) which allows us to bracket the cavity volume as follows (CB[6] ≤ (±)-bis-*ns*-CB[6] < CB[7]). We next sought to measure the values of K_a for (±)-bis-*ns*-CB[6] toward guests **IV-2** – **IV-5** and **IV-7**. For this purpose, we performed a UV/Vis spectroscopic titration between (±)-bis-*ns*-CB[6] and **IV-3** (K_a = 2.5 × 10^3 M^{-1}, Figure 2). Taking advantage of the slow chemical exchange displayed by many (±)-bis-*ns*-CB[6] complexes we performed ^{1}H NMR competition experiments[6a,b] (Supporting Information) to determine the affinity of (±)-bis-*ns*-CB[6] toward **IV-2** (1.3 × 10^5 M^{-1}), **IV-4** (3.6 × 10^4 M^{-1}), **IV-5** (320 M^{-1}), and **IV-7** (9.9 × 10^3 M^{-1}).

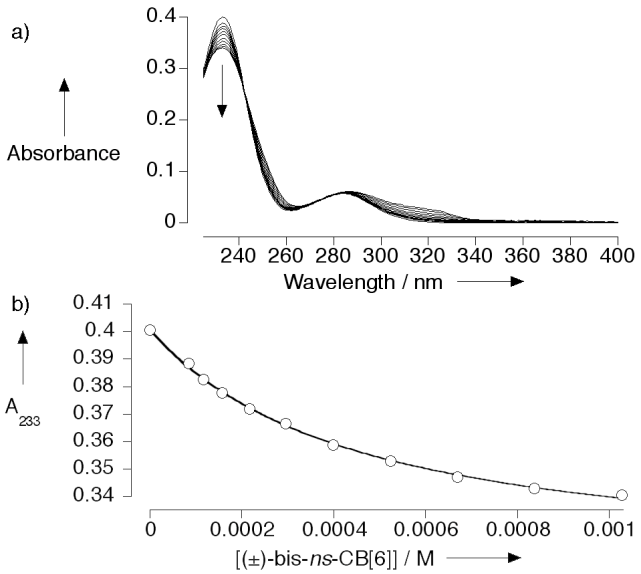

Figure 2. a) UV/Vis spectroscopic titration of **IV-3** (60 mM) with (±)-bis-*ns*-CB[6] (50 mM NaO_2CD_3 buffered D_2O, pD 4.74), b) plot of absorbance versus [(±)-bis-*ns*-CB[6]] used to obtain K_a.

4.4 Electrostatic Surface Potential Maps for Both CB[6] and (±)-bis-*ns*-CB[6]. To probe the origin of the differences in binding strength of (±)-bis-*ns*-CB[6] toward guests **IV-2** – **IV-7** relative to CB[6][8,18] we computed electrostatic surface potential maps for both CB[6] and (±)-bis-*ns*-CB[6] (Figure 3). The four intramolecular NH•••O H-bonds present in free (±)-bis-*ns*-CB[6] substantially narrow its carbonyl-lined portals and impart distinct electrostatic surface potentials to the three chemically non-equivalent C=O groups (L, -66; M, -77; H, -98 kcal mol^{-1}). For comparison, the electrostatic surface potential on the C=O groups of CB[6] cluster at ≈ -87 kcal mol^{-1}. Consequently, the flexibility of (±)-bis-*ns*-CB[6] and its shape complementarity toward flatter guests (e.g. **IV-4** and **IV-7**) results in higher affinity for these guests than can be obtained with CB[6]. Conversely, the affinity of **IV-2** toward (±)-bis-*ns*-CB[6] is 3400-fold lower than CB[6], presumably due to differences in the strength of ion-dipole interactions, the degree of aqueous solvation of the C=O portals, or both.

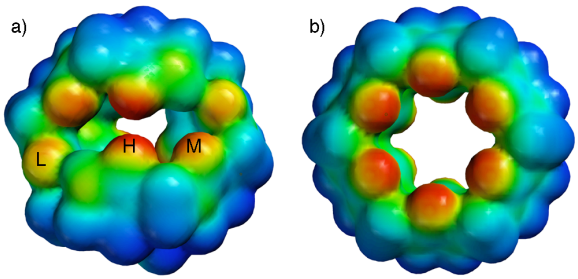

Figure 3. Electrostatic surface potential maps (red to blue: -90 to +31 kcal mol^{-1}) for: a) (±)-bis-*ns*-CB[6], and b) CB[6]. L, M, H = low, medium, high electrostatic surface potentials.

4.5 Chiral Recognition of (±)-bis-*ns*-CB[6]. Our first hint that (±)-bis-*ns*-CB[6] would display useful levels of chiral recognition toward racemic guests came in our ^{1}H NMR studies of the binding of (±)-bis-*ns*-CB[6] with achiral guest **IV-2**. Intriguingly, the ^{1}H NMR spectrum of (±)-bis-*ns*-CB[6]•**IV-2** (Figure 4a) displays a pair of resonances for the diastereotopic CH_2-group (H_i, $H_{i'}$) of guest **IV-2** which reflects the asymmetric magnetic environment within the chiral host-guest complex. Accordingly, we decided to investigate the ability of (±)-bis-*ns*-CB[6] to undergo diastereoselective complexation with guests containing one or more stereogenic centers. Although several chiral aliphatic amines bind to (±)-bis-*ns*-CB[6], they do so with fast exchange on the chemical shift timescale which precludes observation and quantitation of the degree of diastereoselectivity within (±)-bis-*ns*-CB[6] (Supporting Information). We turned, therefore, to guests **IV-8** – **IV-12** which contain aromatic rings that exhibit slower kinetics of exchange. Figure 4b shows the ^{1}H NMR spectrum recorded for a mixture of (±)-bis-*ns*-CB[6] and excess (+)-**IV-8** which shows resonances for a 50:50 mixture of diastereomers (+)-bis-*ns*-CB[6]•(+)-**IV-8** and (-)-bis-*ns*-CB[6]•(+)-**IV-8**. When (±)-bis-*ns*-CB[6] is combined with excess (±)-**IV-8**, however, a moderately diastereoselective process leads to a 72:28 ratio of the diastereomers (Figure 4c).[86] Further studies revealed that (±)-bis-*ns*-CB[6] displays moderate to very good levels of diastereoselectivity toward amino acids **IV-9** (77:23) and **IV-10** (88:12) and amino alcohol **IV-11** (76:24). Interestingly, (±)-bis-*ns*-CB[6] is even able to distinguish between the enantiotopic groups of *meso*-compound **IV-12** (74:26).[87]

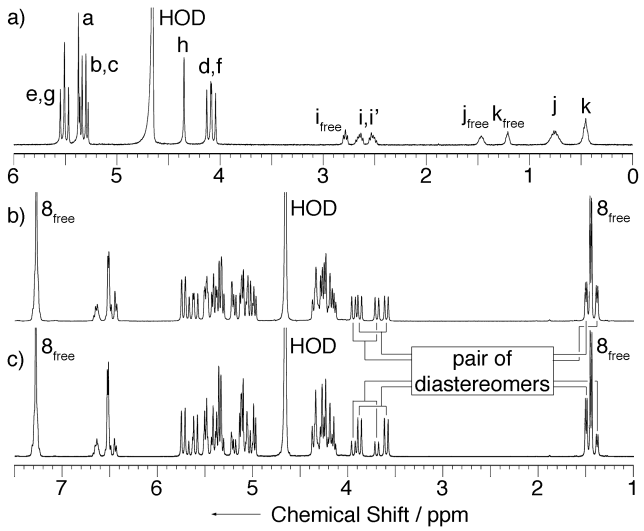

Figure 4. ^{1}H NMR spectra (400 MHz, D_2O) for: a) (±)-bis-*ns*-CB[6]•**IV-2**, b) a mixture of (±)-bis-*ns*-CB[6] and excess (+)-**IV-8**, c) a mixture of (±)-bis-*ns*-CB[6] and excess (±)-**IV-8**.

4.6 Summary. In summary, we have reported the isolation of a new member of the CB[*n*] family – (±)-bis-*ns*-CB[6] – which is formally prepared by condensation of two equivalents of methylene bridged glycoluril trimer **IV-1** with two equivalents of CH_2O by the exclusive connection between homotopic glycoluril NH-groups.[88] The isolation of (±)-bis-*ns*-CB[6] – in combination with bis-*ns*-CB[10][14] – deepens our understanding of the mechanism of CB[*n*] formation[5,12,34,60,61] by establishing the operation of a step-growth polymerization in this reaction. (±)-Bis-*ns*-CB[6] undergoes moderately diastereoselective complexation (up to 88:12) with chiral amines including amino acids and amino alcohols as well as *meso*-diamine **IV-12**. Larger (±)-bis-*ns*-CB[*n*] (n = 7, 8, 10) and N-functionalized derivatives can be readily envisioned and are expected to display even higher enantioselectivity.[89] Access to (±)-bis-*ns*-CB[6] and other chiral nor-seco-cucurbit[*n*]urils promises to dramatically

broaden the scope of the applications to which the achiral members of the CB[*n*] family have already been applied[16,49,83] by enabling the creation of enantioselective molecular devices.

V. Chapter 5: Nor-Seco-Cucurbit[6]uril Functions as an Aldehyde Cucurbituril Synthon (Huang, W.-H.; Zavalij, P. Y.; Isaacs, L. *Angew. Chem. Int. Ed.* 2008, submitted.)

5.1 Introduction. The supramolecular chemistry of the cucurbit[*n*]uril family[16,49] (CB[*n*]) of molecular containers has undergone rapid development in recent years due to availabilty of a homologous series of molecular containers (*n* = 5, 6, 7, 8, 10)[2,12,15,17,18] with high binding affinity and high selectivity toward cationic species in aqueous solution. These unfunctionalized CB[*n*] may be employed in a variety of intriguing applications including molecular machines, sensors, drug delivery, and the controlled release of gases.[27,52,75,81,90] In order to tailor the recognition properties toward specific applications – including supramolecular vesicles, artificial ion channels, sensors, and protein immobilization – several groups have pursued the preparation of CB[*n*] derivatives by direct functionalization[39,91-93] and building block strategies.[34,36-38] In this chapter we continue to develop an alternate approach toward novel CB[*n*]-type compounds based on CB[*n*] compounds lacking one or more bridging CH_2-groups known as nor-seco-cucurbiturils.[14,63] In this chapter we report the isolation of *ns*-CB[6] (**V-1**), its chemical reactivity toward aldehydes, and the unique recognition properties of the top-bottom desymmetrized *ns*-CB[6] and **V-2** toward guests **V-3** – **V-20**.

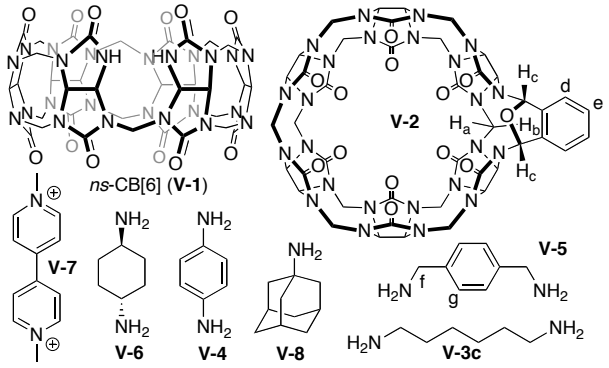

Scheme 1. Structure of compounds used in this study.

5.2 Isolation and ^{1}H NMR spectrum of *ns*-CB[6]. From a reaction mixture comprising glycoluril (1 equiv.) and paraformaldehyde (1.67 equiv.) in conc. HCl at 50 ˚C we have now isolated *ns*-CB[6] (**V-1**). Although the ^{1}H NMR spectrum of **V-1** was uninformative (Figure 1a), its mass spectrum and the ^{1}H NMR spectrum of *ns*-CB[6]•**V-5** (Figure 1b) allowed us to conclusively determine its molecular formula and overall C_s-symmetry. To provide further proof of structure we allowed *ns*-CB[6] to react with *o*-phthalaldehyde under acidic conditions and obtained **V-2** in 57% yield after recrystallization.[(94)] Although the ^{1}H NMR spectrum of **V-2** and its **V-2•V-5** complex (Figure 1c-1d) allowed us to elucidate its structure, final proof of structure was obtained in the form of an X-ray crystal structure (Figure 2).[(95)] Several aspects of the ^{1}H NMR spectra and X-ray crystal structure are noteworthy: 1) the resonance for H_b is significantly upfield shifted due to its proximity to the face of the bridging aromatic ring, 2) the resonance for H_c appears at 6.6-6.7 ppm due to the combined deshielding effect of the bridging N-CH-O-CH-N and *o*-xylylene groups, 3) the presence of the new N-CH-O-CH-N bridge results in distinct upper and lower C=O lined rims of different diameter, and 4) the expansion at the upper rim, imposed by

the bridging *o*-xylylene group results in a pinching at the lower rim which promotes its solid state structure via C=O•••K^+•••O=C interactions (Figure 2b).

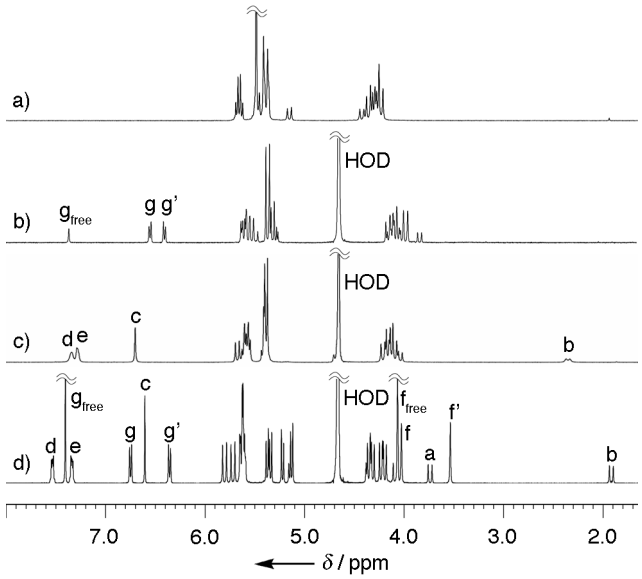

Figure 1. ^{1}H NMR spectra (400 MHz, D_2O, RT) recorded for: a) *ns*-CB[6] (20% DCl / D_2O), b) a mixture of *ns*-CB[6] and excess **V-5**, c) **V-2**, and d) a mixture of **V-2** and excess **V-5**, (D_2O).

5.3 Binding Properties of *ns*-CB[6]. Once the structures of *ns*-CB[6] and **V-2** had been established we decided to investigate their recognition behavior toward symmetrical diamines of increasing size (**V-3c** – **V-8**) to determine their effective cavity volumes. We found that both *ns*-CB[6] and **V-2** form inclusion complexes with **V-3c** – **V-7** but not with **V-8**. These experiments allow us to bracket the cavity volumes of *ns*-CB[6] and **V-2** between CB[6] (164 $Å^3$) and CB[7] (279 $Å^3$). Apparently, the expansion of the upper rim of **V-2** does not increase the cavity volume of **V-2** enough to allow complexation of the best guests for CB[7] (e.g. **V-8**).

Complexation of symmetric guests like **V-3c** – **V-7** within hosts like *ns*-CB[6] and **V-2** with different upper and lower rims leads to reduction in guest symmetry upon complexation that is readily observed by ^{1}H NMR (e.g. Figure 1d, H_g, $H_{g'}$).

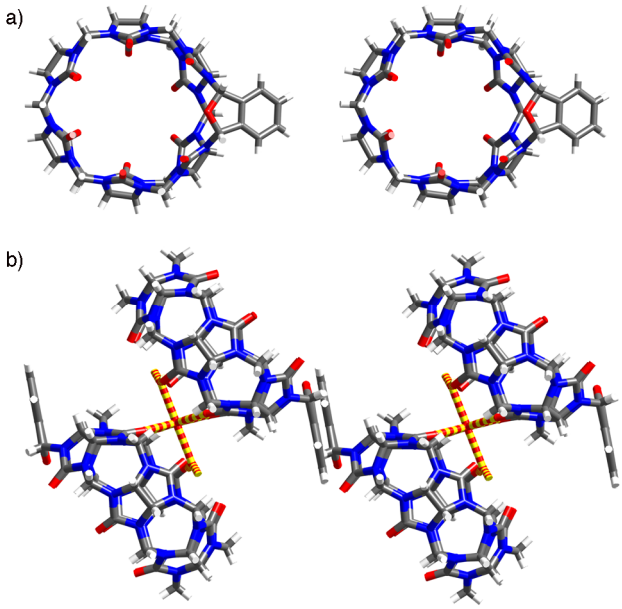

Figure 2. a) Cross-eyed stereoview of **V-2**, and b) illustration of the packing of **V-2** in the crystal by C=O•••K^+•••O=C interactions. Color code: C, grey; H, white; N, blue; O, red; O•••K^+ interactions, red-yellow striped. Solvating CF_3CO_2H and H_2O molecules have been removed for clarity.

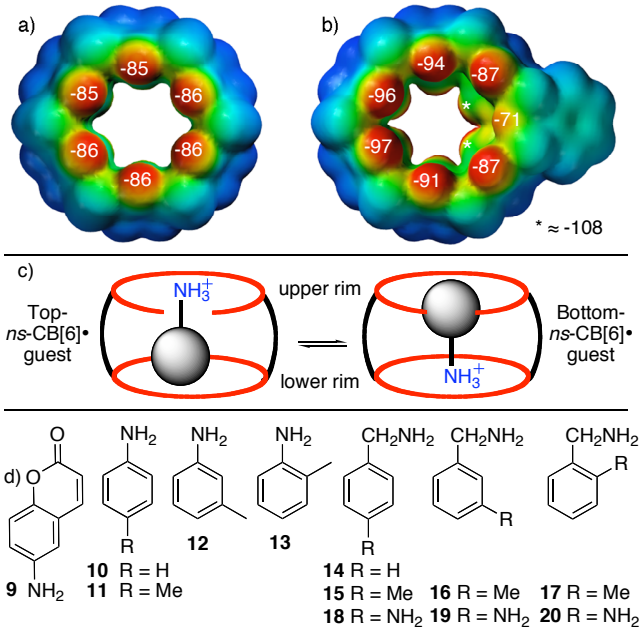

Figure 3. Electrostatic surface potential maps for: a) CB[6] and b) **V-2**. The red to blue color range spans -85 to +35 kcal mol^{-1}. c) Illustration of the two diastereomeric complexes possible with *ns*-CB[6] and **V-2**, and d) structures of guests for *ns*-CB[6].

5.4 Electrostatic Surface Potential (ESP) Map for CB[6] and *ns*-CB[6]. Compared to the electrostatic surface potential (ESP) map for CB[6] which has two equivalent ureidyl C=O portals the ESP maps for *ns*-CB[6] (Supporting Information) and **V-2** (Figure 3b) are unsymmetrical. The upper rim of *ns*-CB[6] and the lower rim of **V-2** are significantly more negative. Given the fact that *ns*-CB[6] and **V-2** possess two different ureidyl C=O lined portals and that electrostatic potential at CB[*n*] portals is known to influence binding strength[49,72] we wondered whether the complexation of unsymmetrical amines and diamines (e.g. **V-9** – **V-20**) would favor one of the two conceivable diastereomers (Figure 3c; e.g. top-*ns*-CB[6]•guest *versus*

bottom-*ns*-CB[6]•guest). Initially we prepared the complexes between *ns*-CB[6] and **V-9** and observed a single diastereomer by ^{1}H NMR (Supporting Information).[96] Encouraged by this result, we decided to investigate the three series of guests (**V-10** – **V-13**, **V-14** – **V-17**, **V-18** – **V-20**) where Me and NH_3^+ groups are moved around the aromatic rings of aniline and benzylamine. For the *ns*-CB[6]•**V-10** (67:33) and *ns*-CB[6]•**V-11** (76:24) complexes we observed two sets of resonances that we assign to a mixture of top- and bottom-diastereomers. Apparently, electrostatic effects alone are insufficient to completely control top-bottom diastereoselectivity. We next investigated the *meta*-substituted complex *ns*-CB[6]•**V-12**, which exists as a single diastereomer. The *meta*-substitution in **V-12** (and **V-9**) does not allow strong ion-dipole interactions without imposing steric interactions between the CH_3-group and the wall of the *ns*-CB[6] cavity in one of the diastereomers.[97] Similar trends in top-bottom selectivity are seen for the benzylamine series (**V-14** – **V-17**). The complexes between *ortho*-substituted compounds **V-13**, **V-17**, and **V-20** and *ns*-CB[6] all exhibit fast exchange kinetics which precludes a determination of the ratio of diastereomers in this series. Overall, we find that diastereoselective recognition inside *ns*-CB[6] can be achieved by combination of electrostatic and steric effects.

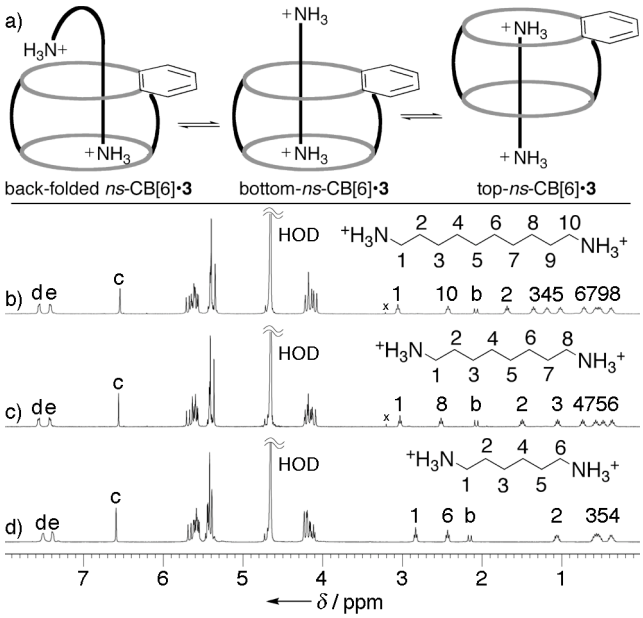

Figure 4. a) Illustration of three possible diastereomers for *ns*-CB[6]•**V-3**, and ^{1}H NMR spectra (400 MHz, D_2O) for a mixture of **V-2** and b) **V-3g**, c) **V-3e**, d) **V-3c**. (x = trace MeOH).

5.5 Controlling Diastereoselectivity for V-2. We discovered an intriguing method of controlling diastereoselectivity for host **V-2** during our study of the complexes between **V-2** and the series of 1,*n*-alkanediammonium ions (**V-3a** – **V-3i**, *n* = 4, 5, 6, 7, 8, 9, 10, 11, 12). For example, the ^{1}H NMR spectra for the **V-2•V-3c**, **V-2•V-3e**, and **V-2•V-3g** complexes (Figure 4) display a single set of resonances that correspond to a single diastereomer. Intriguingly, the symmetry equivalent CH_2-groups of the 1,*n*-alkanediamine become non-equivalent in the complex and display *n*-resonances in their ^{1}H NMR spectra which reflect the asymmetric magnetic environment in the host-guest complex. Of particular interest are the resonances for the CH_2-groups adjacent to the $^{+}NH_3$ groups (1 & 6, 1 & 8, and 1 & 10) that become widely separated

(0.4 – 0.7 ppm) upon binding with one CH_2 downfield and one CH_2 upfield related to the free diammonium ion. The well-defined shielding region inside the cavity of CB[*n*]-type receptors and the deshielding region just outside the ureidyl C=O portals[97,98] allowed us to formulate the back-folding that characterizes the geometry of the longer **V-2**•alkanediammonium ion (**V-3f** – **V-3i**) complexes (Figure 4a).[99,100] The pattern of the magnitude of complexation induced changes in chemical shift for the internal CH_2-groups are also consistent with the presence of this back-folded conformation. We conclude that the upper rim of **V-2** – in contrast to the lower rim – is wide enough to simultaneously permit the extension of the alkyl chain and allow ion-dipole interaction of a back-folded NH_3^+ group which drives the back-folding process. We were fortunate to obtain single crystals of **V-2**•**V-3f** and solve its x-ray structure (Figure 5).[8] As predicted based on the ^{1}H NMR studies, **V-2**•**V-3f** exhibits a back-folded geometry in the crystal that benefits from the hydrophobic effect and ion-dipole interactions and H-bonds at both ureidyl C=O lined portals. Interestingly, the NH_3^+ group at the lower rim forms ion-dipole interactions / H-bonds with the C=O groups below the bridging *o*-xylylene group which have the highest ESP (Figure 3b).

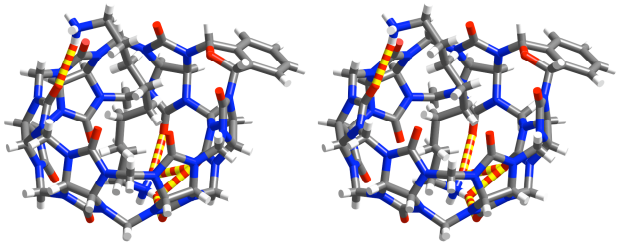

Figure 5. Cross-eyed stereoview of the structure of **V-2**•**V-3f** in the crystal. Color code: C, grey; H, white; N, blue; O, red; H-bonds, red-yellow striped.

5.6 Summary. In summary, we have reported the isolation of *ns*-CB[6] which is formally related to CB[6] by the removal of a single CH_2-group. *ns*-CB[6] functions as an aldehyde reactive cucurbituril synthon which allowed us to prepare CB[6]-derivative **V-2**. Both *ns*-CB[6] and **V-2** undergo top-bottom diastereoselective recognition processes toward ammonium and diammonium ions in water. Most intriguing is the ability of **V-2** to induce back-folding in the longer diammonium ions (e.g. **V-3f** – **V-3i**). Beyond these recognition properties, the availability of *ns*-CB[6] – the first aldehyde reactive CB[*n*] synthon – has potentially widespread impact. For example, *ns*-CB[6] can undergo reaction with di-, tri-, and oligo-aldehydes to deliver discrete well defined CB[*n*] dimers, trimers and oligomers as well as CB[*n*] derivatized surfaces, polymers, and separation materials. As such, we expect *ns*-CB[6] and its CB[*n*] derivatives to impact a range of application areas[4] including bio-chips, affinity chromatography, and drug delivery.

Appendices

Chapter 2: Cucurbit[n]uril Formation Proceeds by Step-Growth Cyclo-oligomerization – Supporting Information

*Wei-Hao Huang, Peter Y. Zavalij, and Lyle Isaacs**

Department of Chemistry and Biochemistry, University of Maryland College Park, MD 20742

Table of Contents

Pages

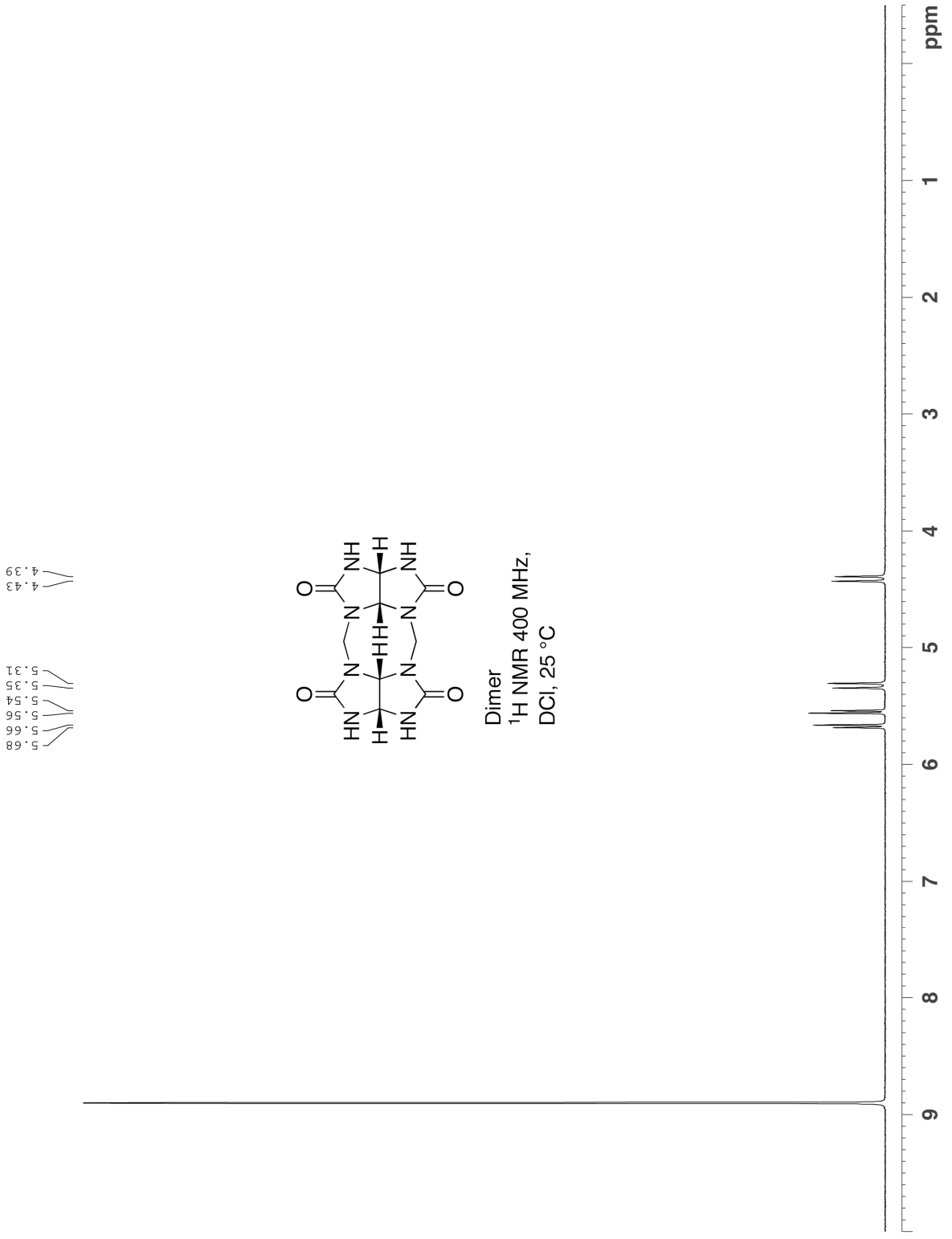

Figure S1. ^{1}H NMR spectrum recorded for dimer (400 MHz, 35% DCl, 25 ºC).

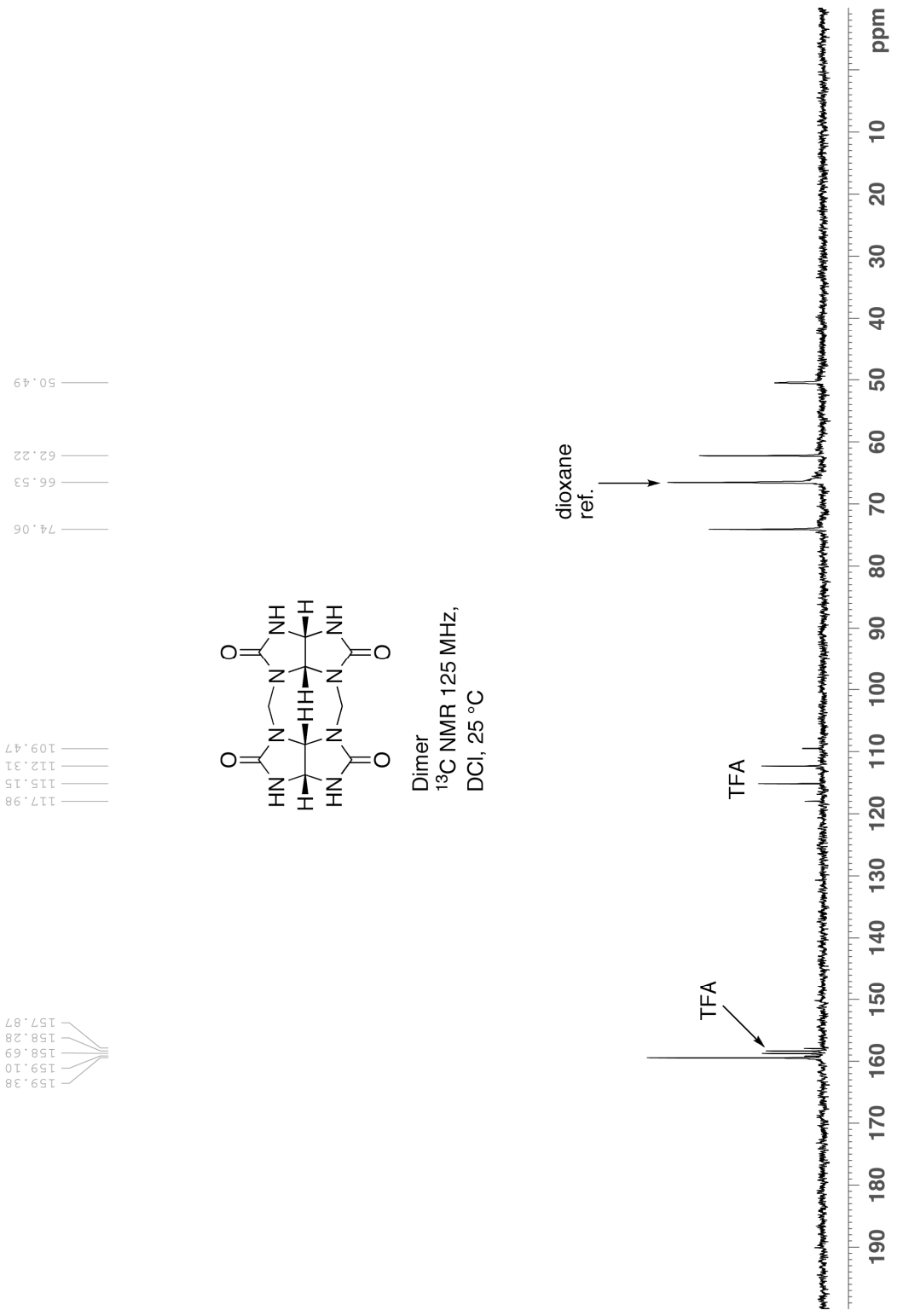

Figure S2. ^{13}C NMR spectrum recorded for dimer (125 MHz, 35% DCl, 25 ºC).

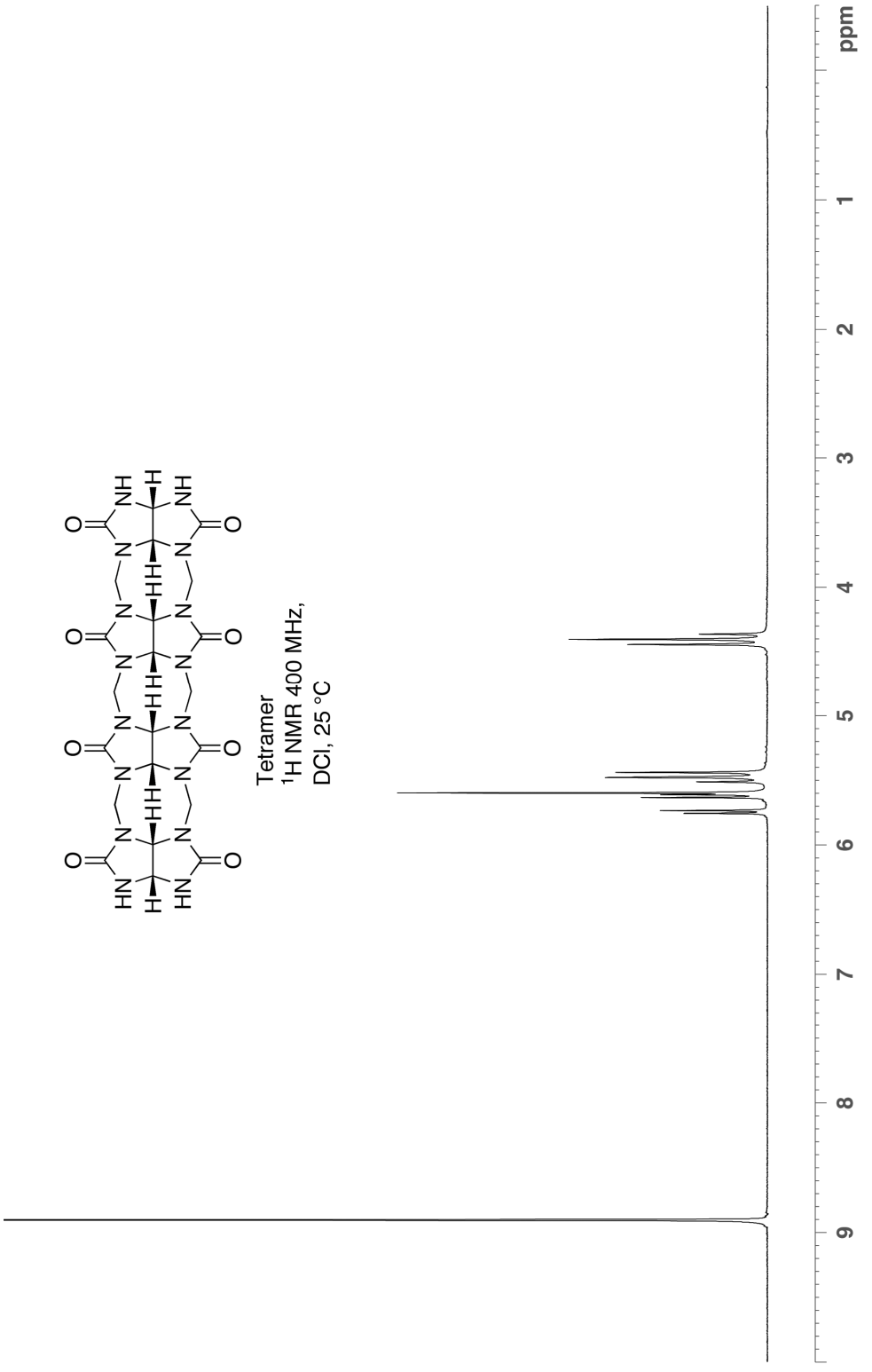

Figure S3. ^{1}H NMR spectrum recorded for tetramer (400 MHz, 35% DCl, 25 ºC).

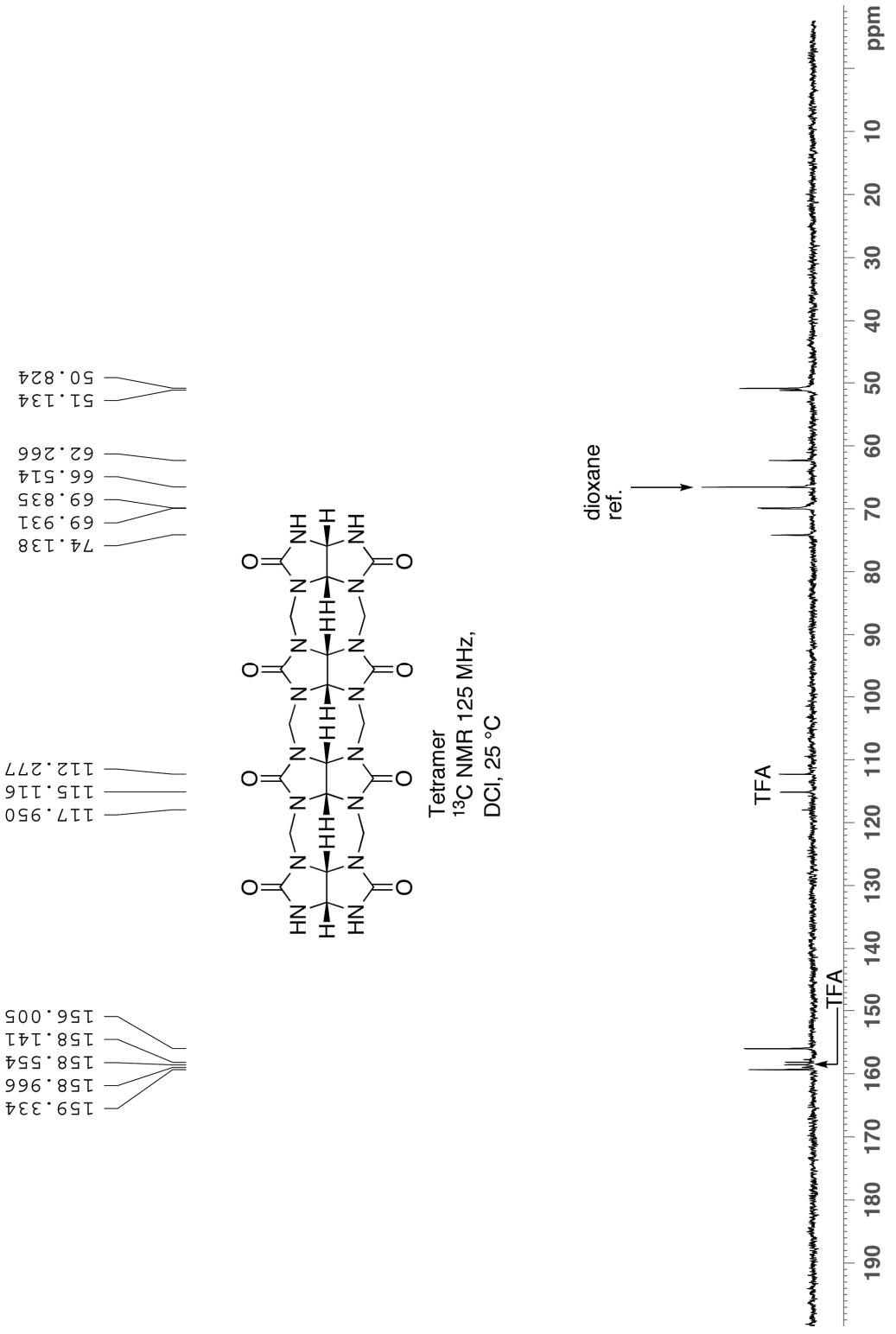

Figure S4. ^{13}C NMR spectrum recorded for tetramer (125 MHz, 35% DCl, 25 ºC).

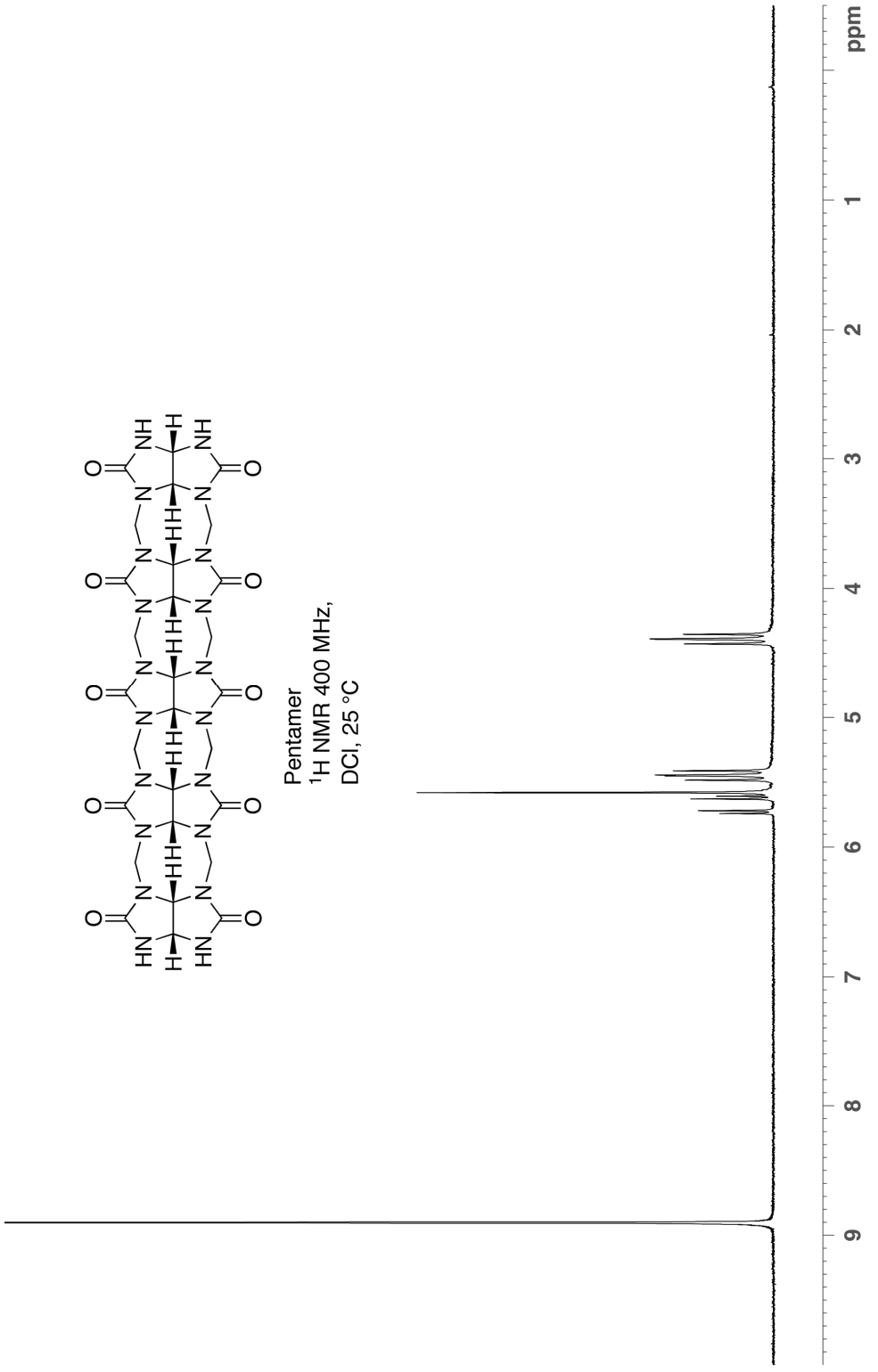

Figure S5. ^{1}H NMR spectrum recorded for pentamer (400 MHz, 35% DCl, 25 ºC).

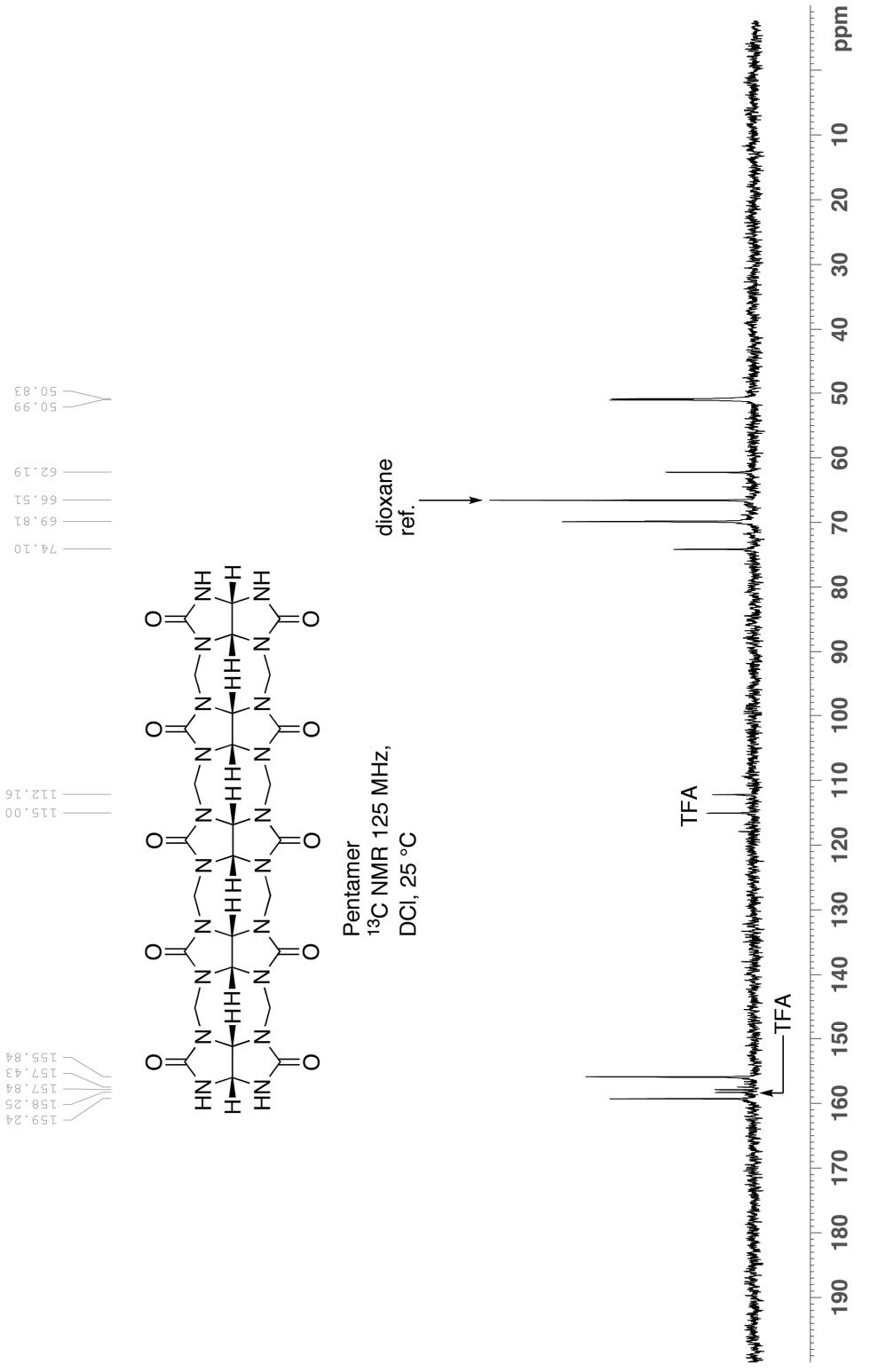

Figure S6. ^{13}C NMR spectrum recorded for pentamer (125 MHz, 35% DCl, 25 ºC).

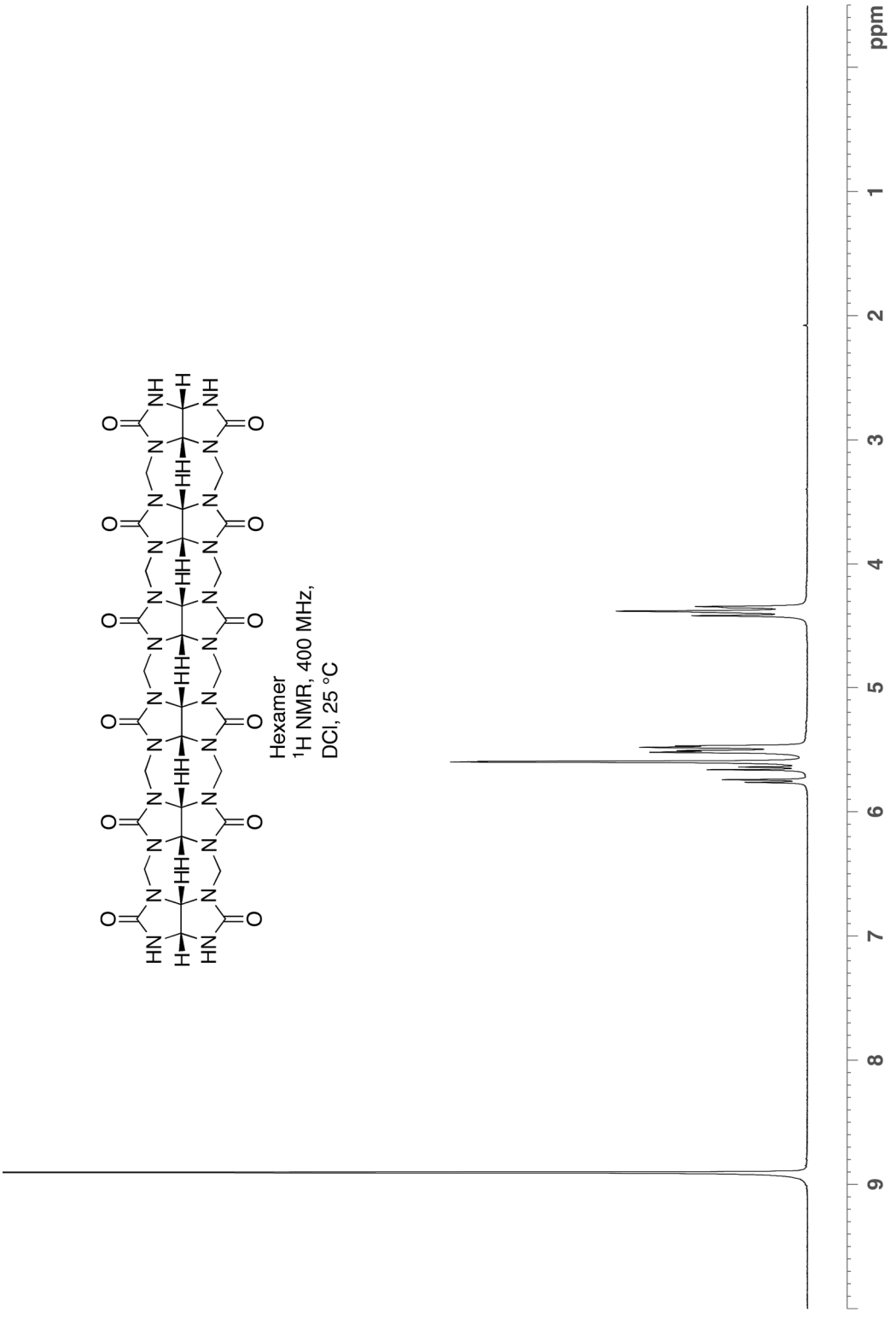

Figure S7. ^{1}H NMR spectrum recorded for hexamer (400 MHz, 35% DCl, 25 ºC).

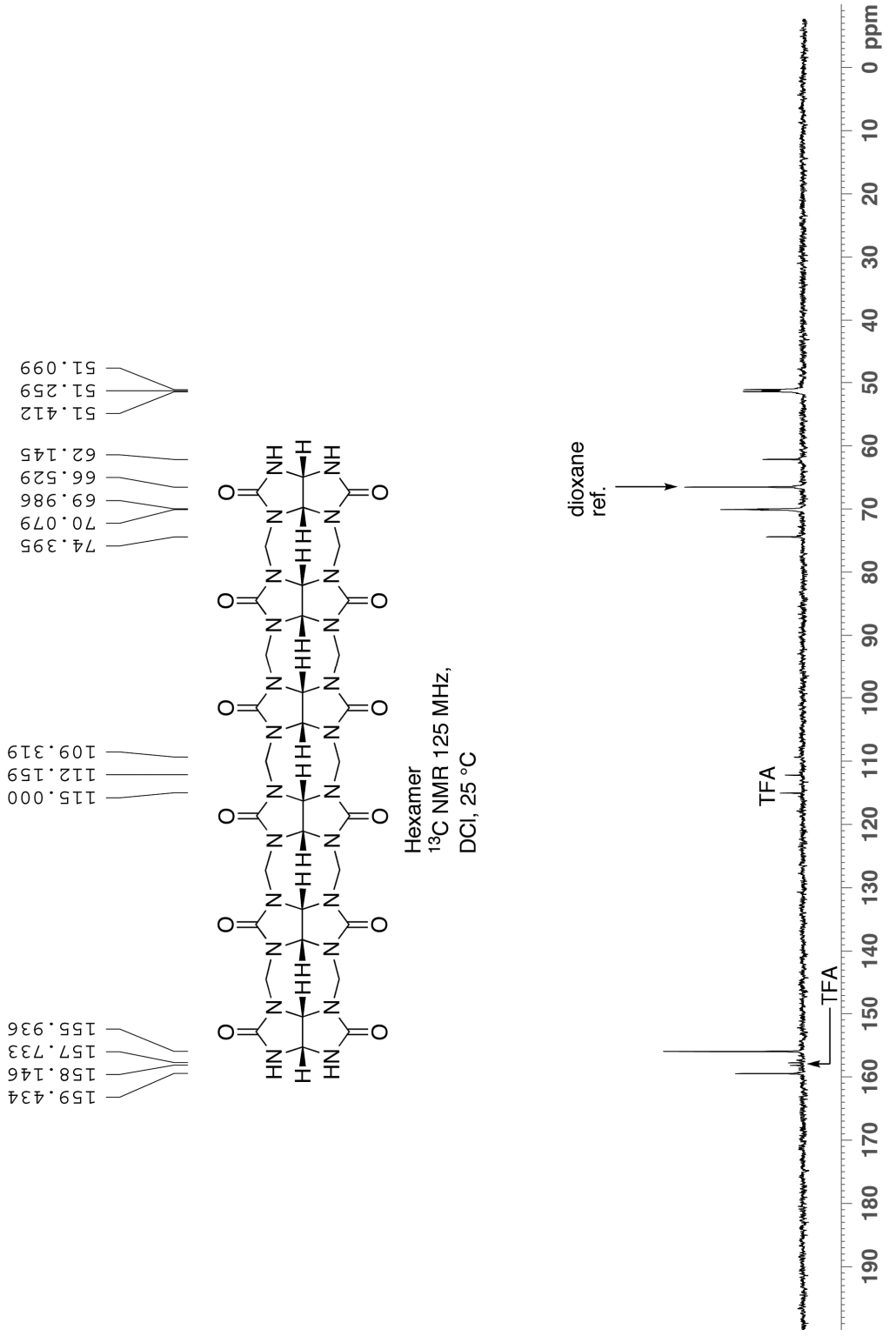

Figure S8. ^{13}C NMR spectrum recorded for hexamer (125 MHz, 35% DCl, 25 ºC).

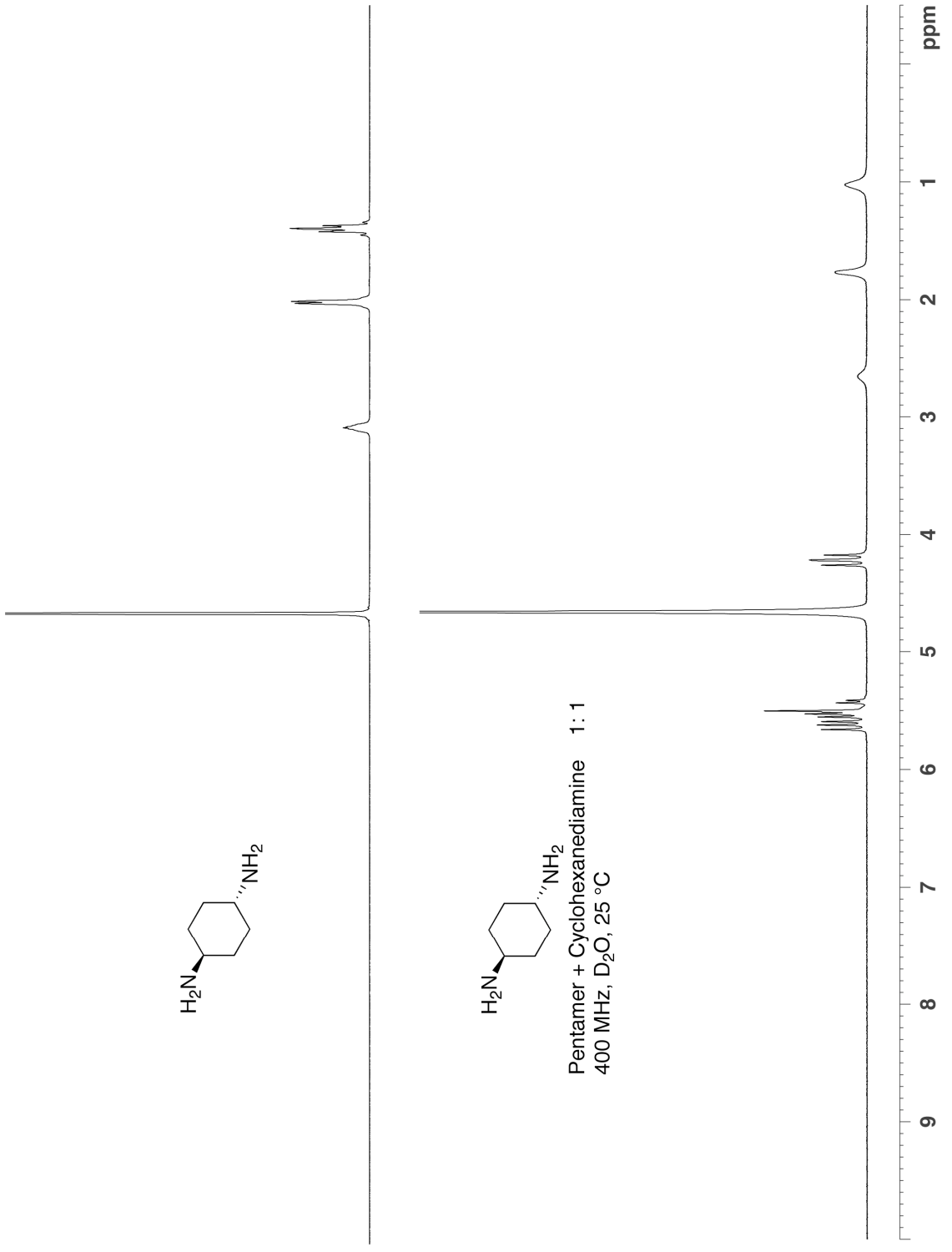

Figure S9. ^{1}H NMR spectra recorded for cyclohexanediamine and its complex with **5** (400 MHz, D_2O, 25 ºC).

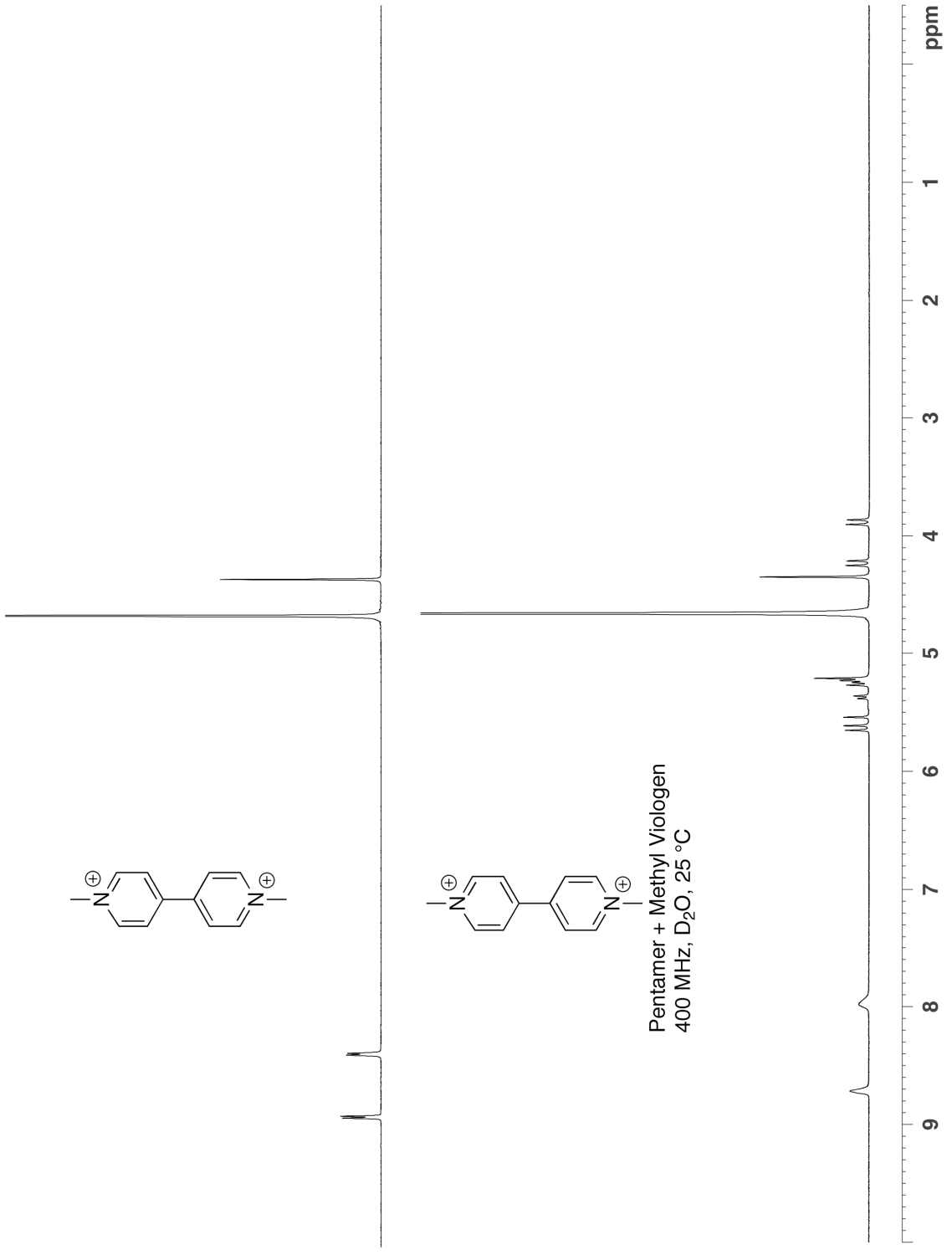

Figure S9. ^{1}H NMR spectra recorded for methyl viologen and its complex with **5** (400 MHz, D_2O, 25 ºC).

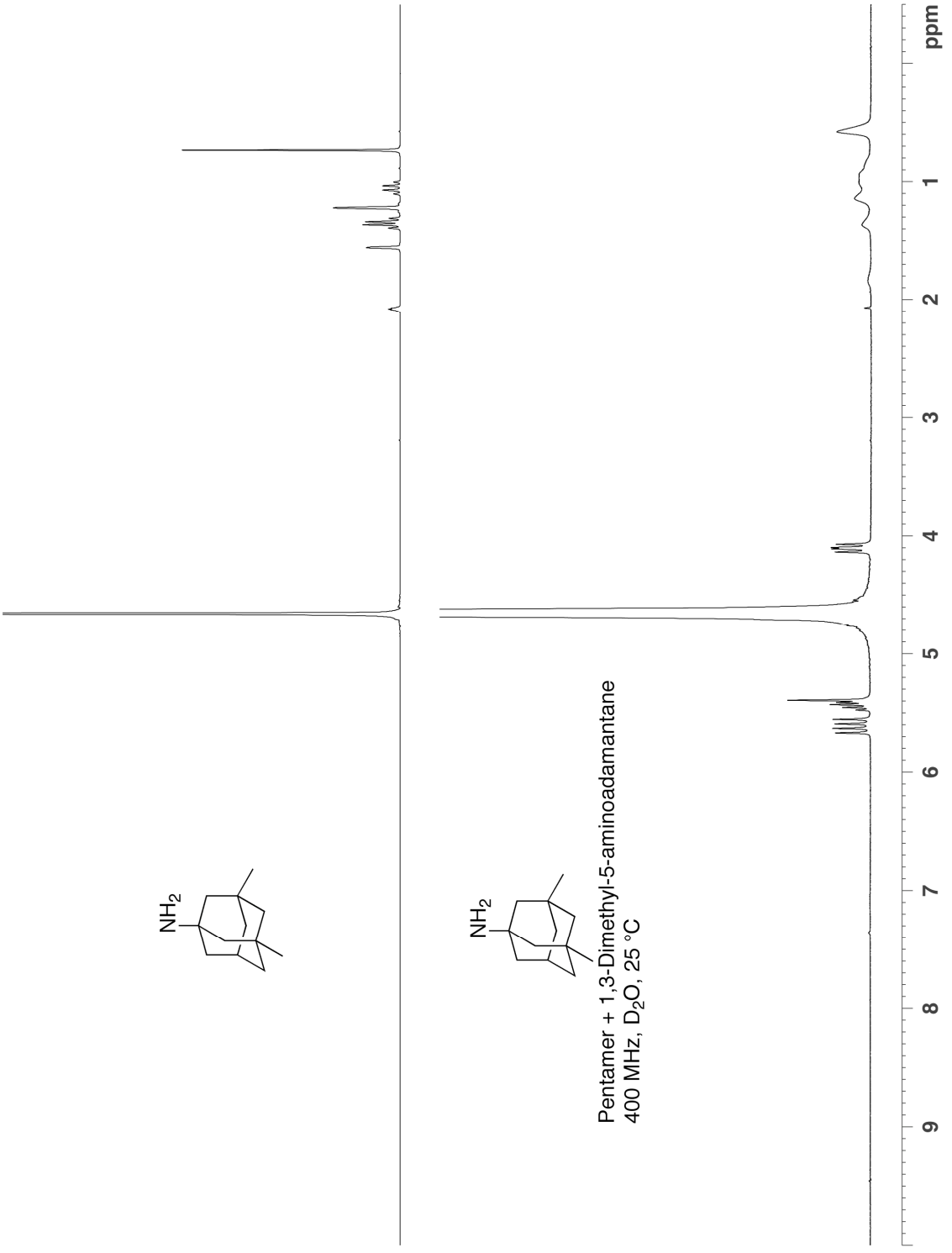

Figure S9. ^{1}H NMR spectra recorded for 1,3-Dimethyl-5-aminoadamantane and its complex with **5** (400 MHz, D_2O, 25 ºC).

Figure S9. ^{1}H NMR spectra recorded for 1-aminoadamantane and its complex with **5** (400 MHz, D_2O, 25 ºC).

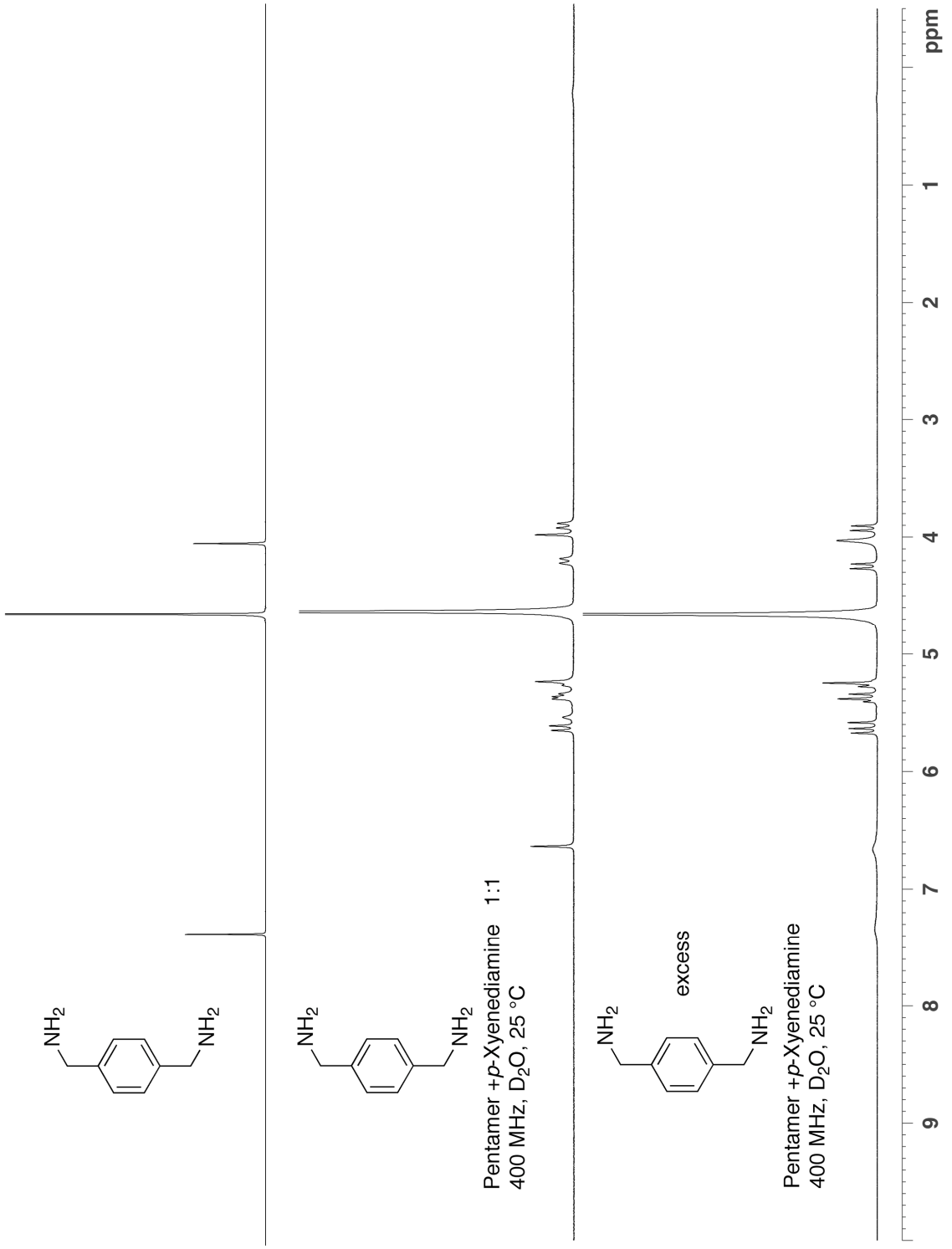

Figure S9. ^{1}H NMR spectra recorded for *p*-xylenediamineand its complex with **5** (400 MHz, D_2O, 25 ºC).

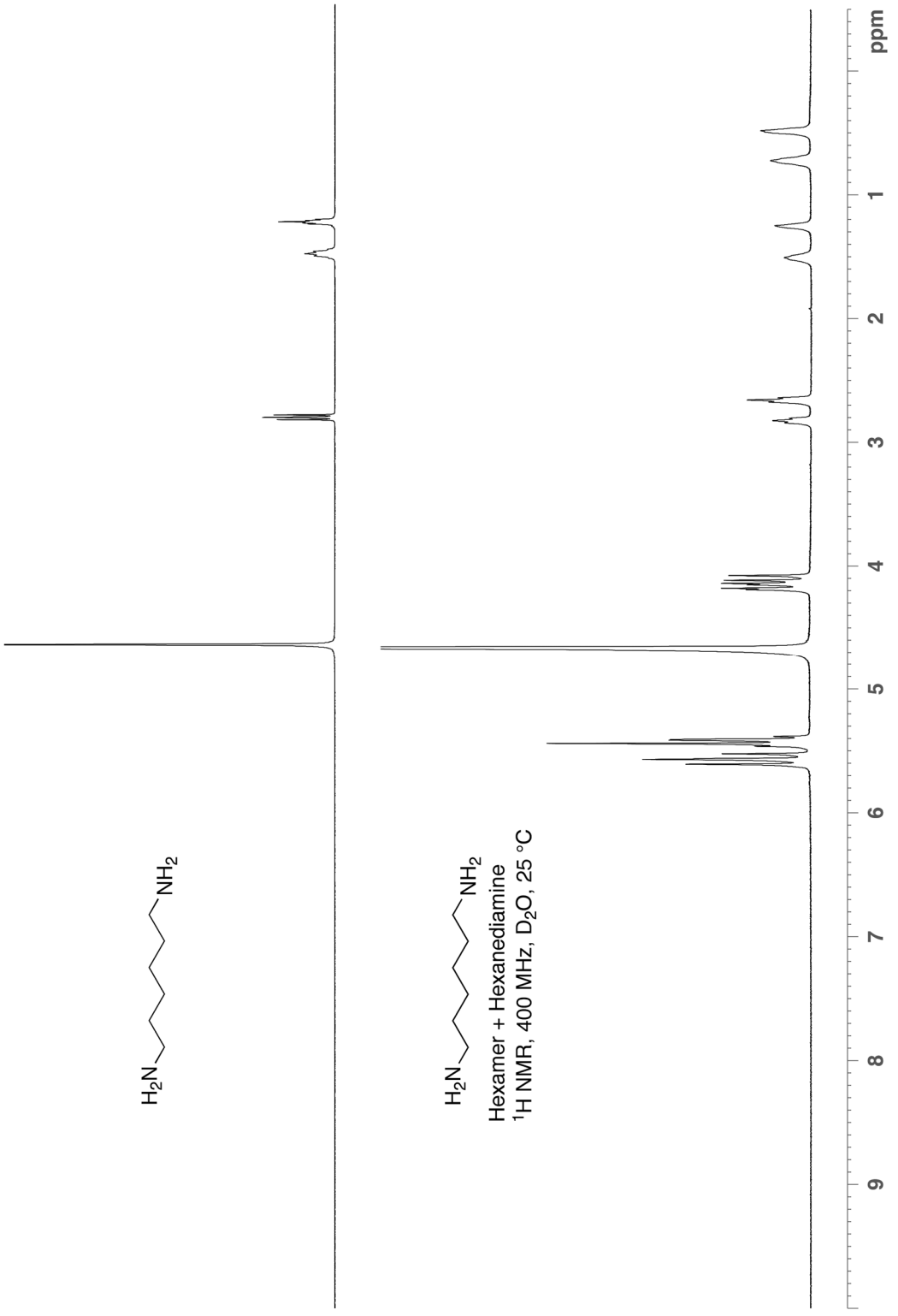

Figure S9. ^{1}H NMR spectra recorded for hexanediamine and its complex with **6** (400 MHz, D_2O, 25 ºC).

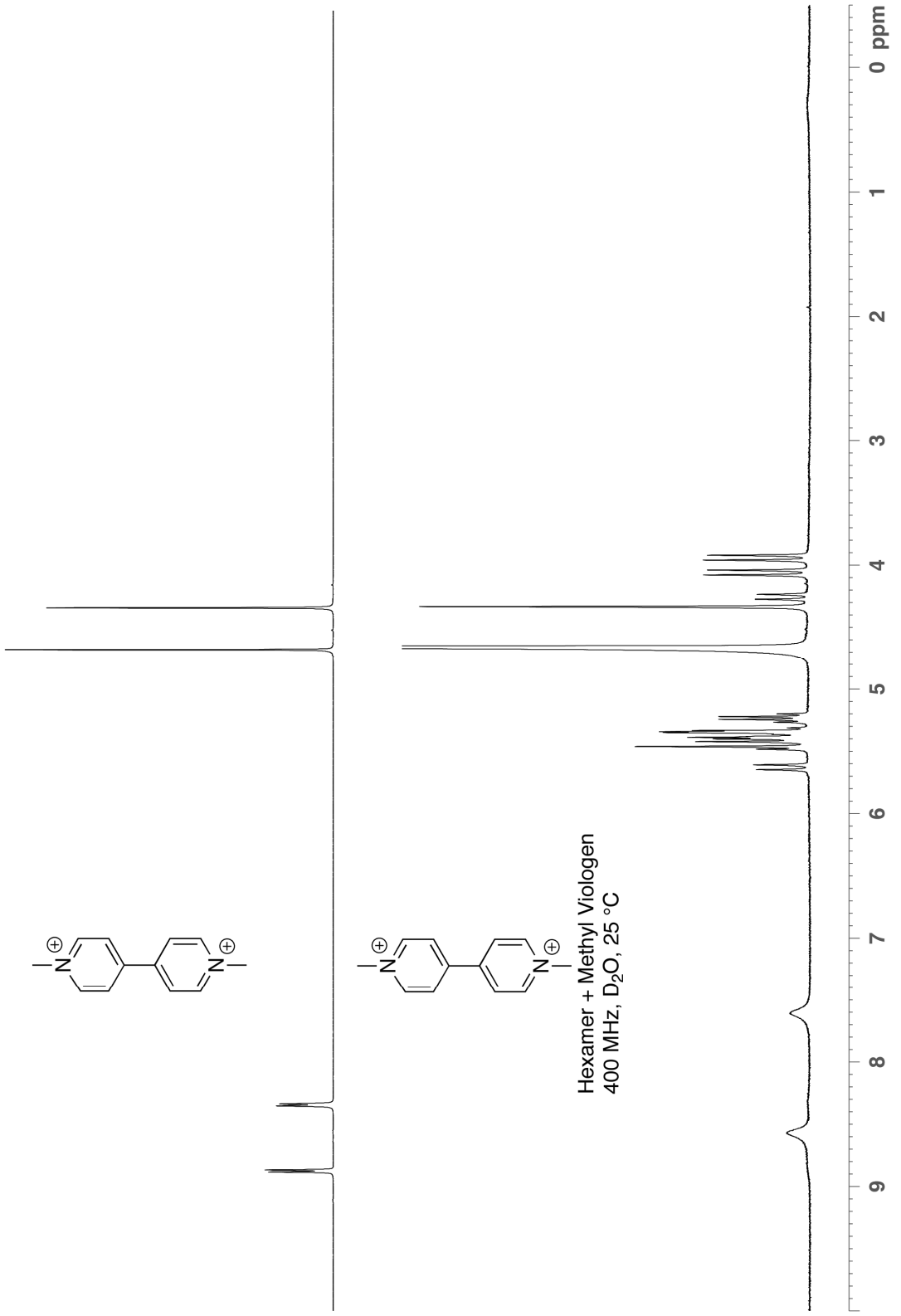

Figure S10. ^{1}H NMR spectra recorded for methyl viologen and its complex with **6** (400 MHz, D_2O, 25 ºC).

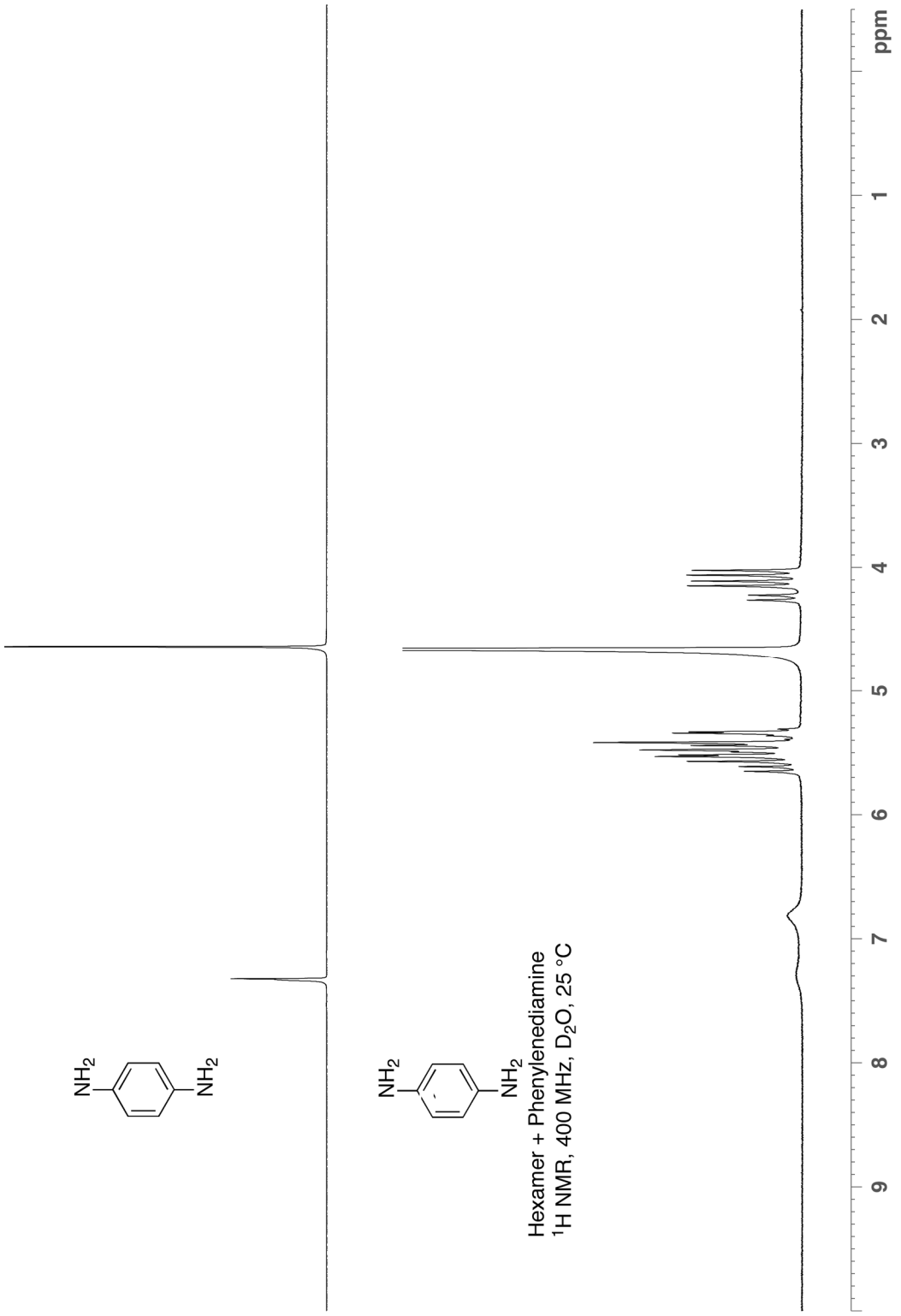

Figure S11. ^{1}H NMR spectra recorded for phenylenediamine and its complex with **6** (400 MHz, D_2O, 25 ºC).

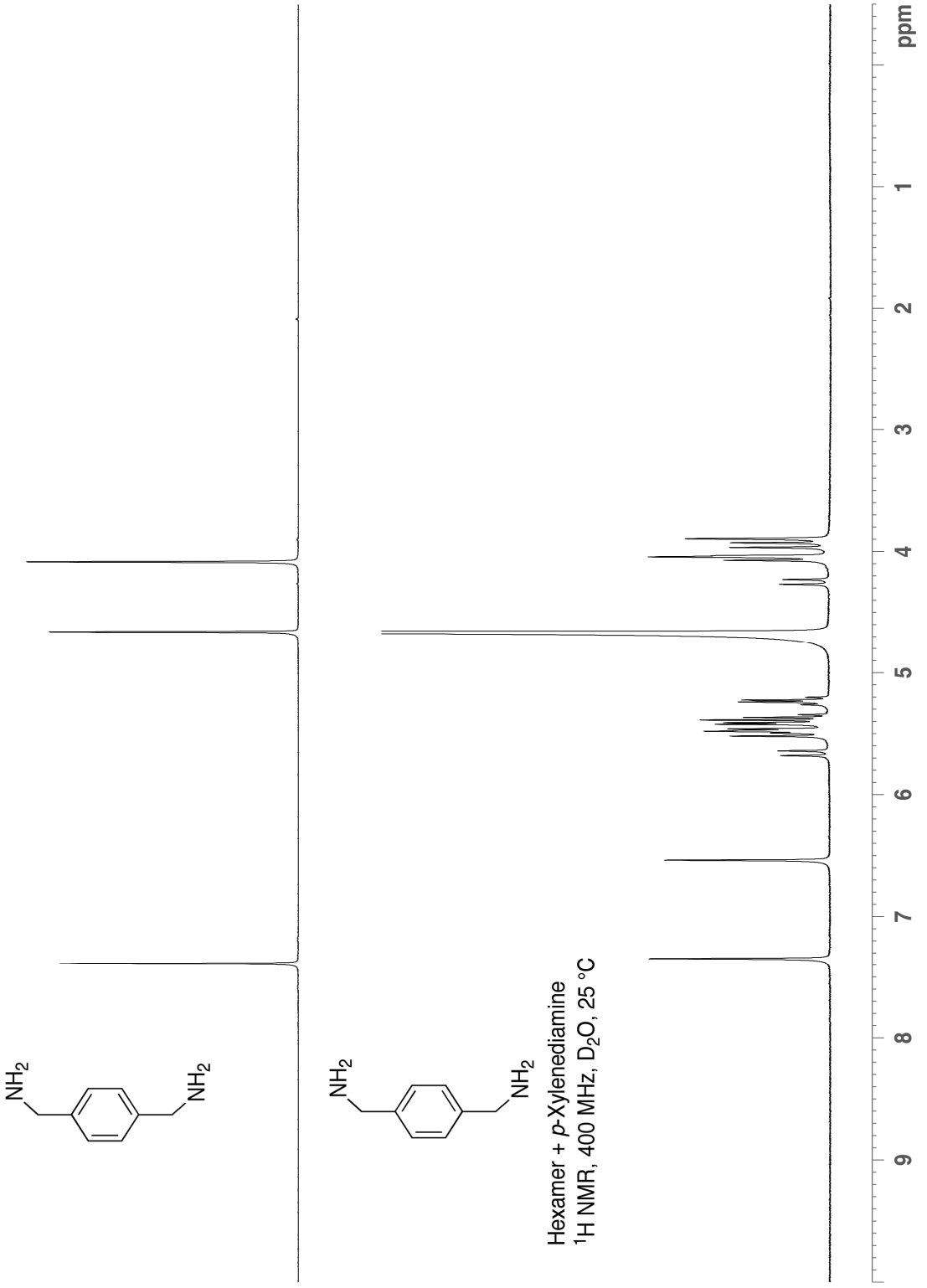

Figure S12. ^{1}H NMR spectra recorded for the *p*-xylenediamine and its complex with **6** (400 MHz, D_2O, 25 ºC).

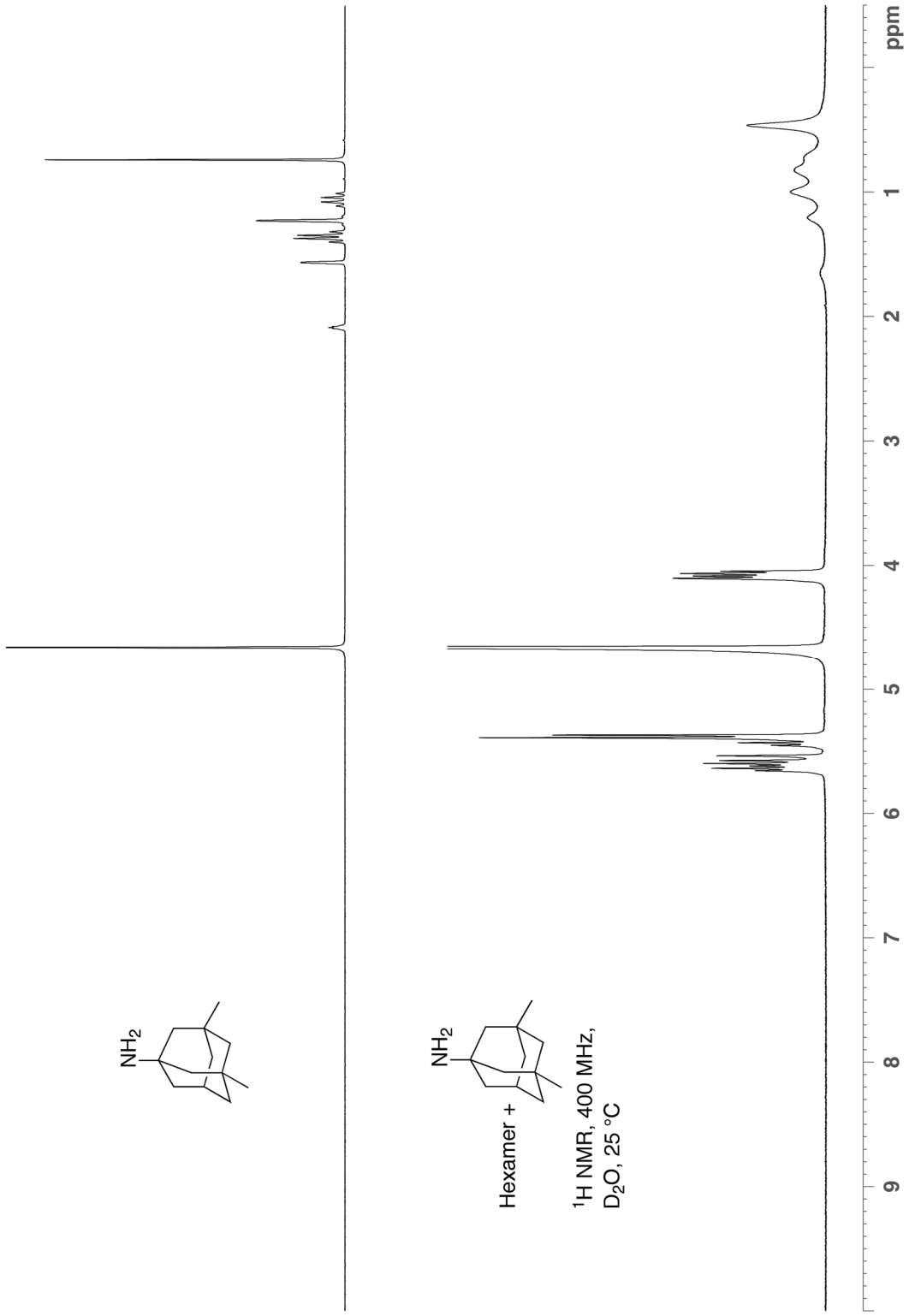

Figure S13. ^{1}H NMR spectra for 1,3-dimethyl-5-aminoadamantane and its mixture with **6** (400 MHz, D_2O, 25 ºC).

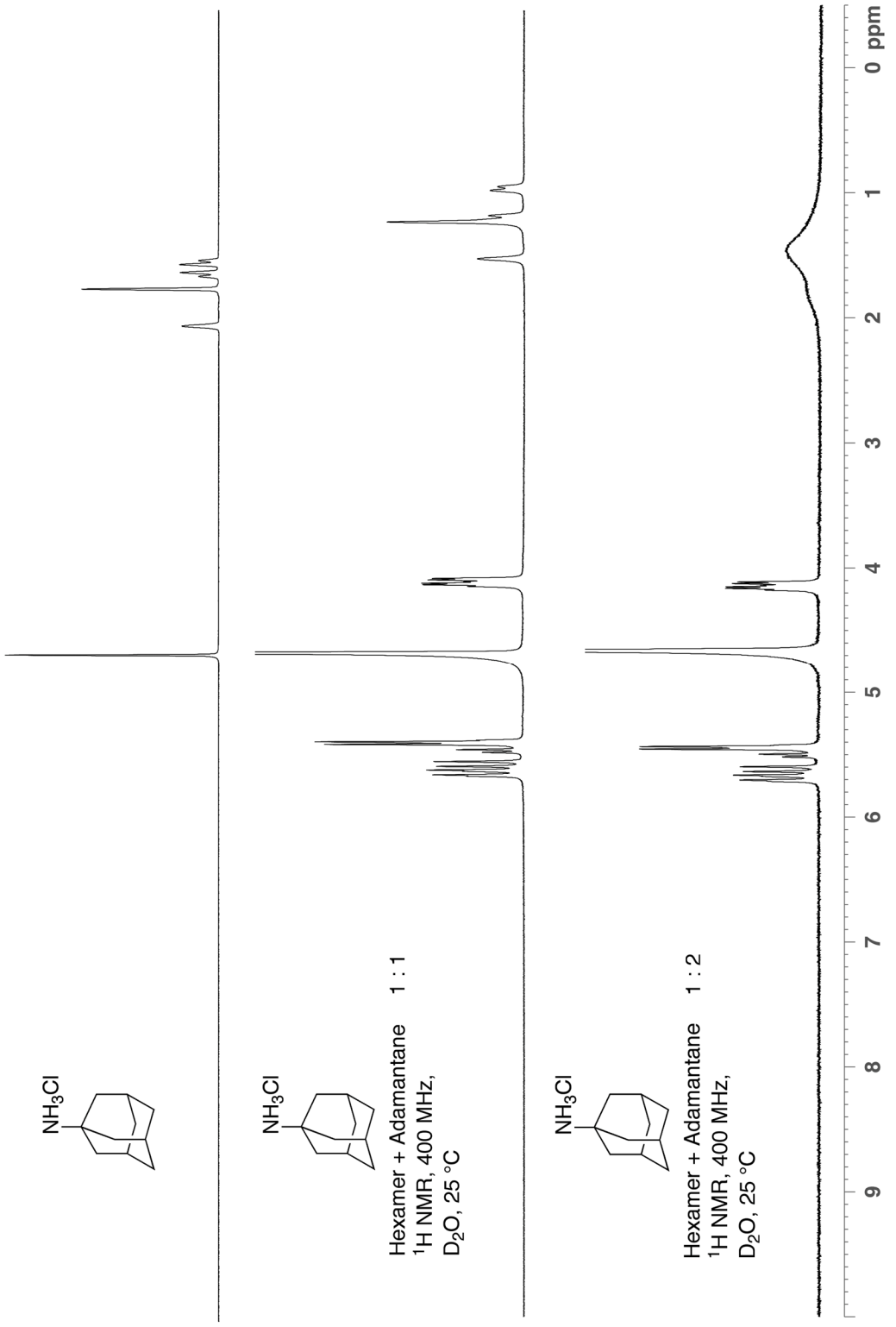

Figure S14. ^{1}H NMR spectra recorded for 1-aminoadamantane and its complex with **6** at 1:1 and 1:2 stoichiometries (400 MHz, D_2O, 25 ºC).

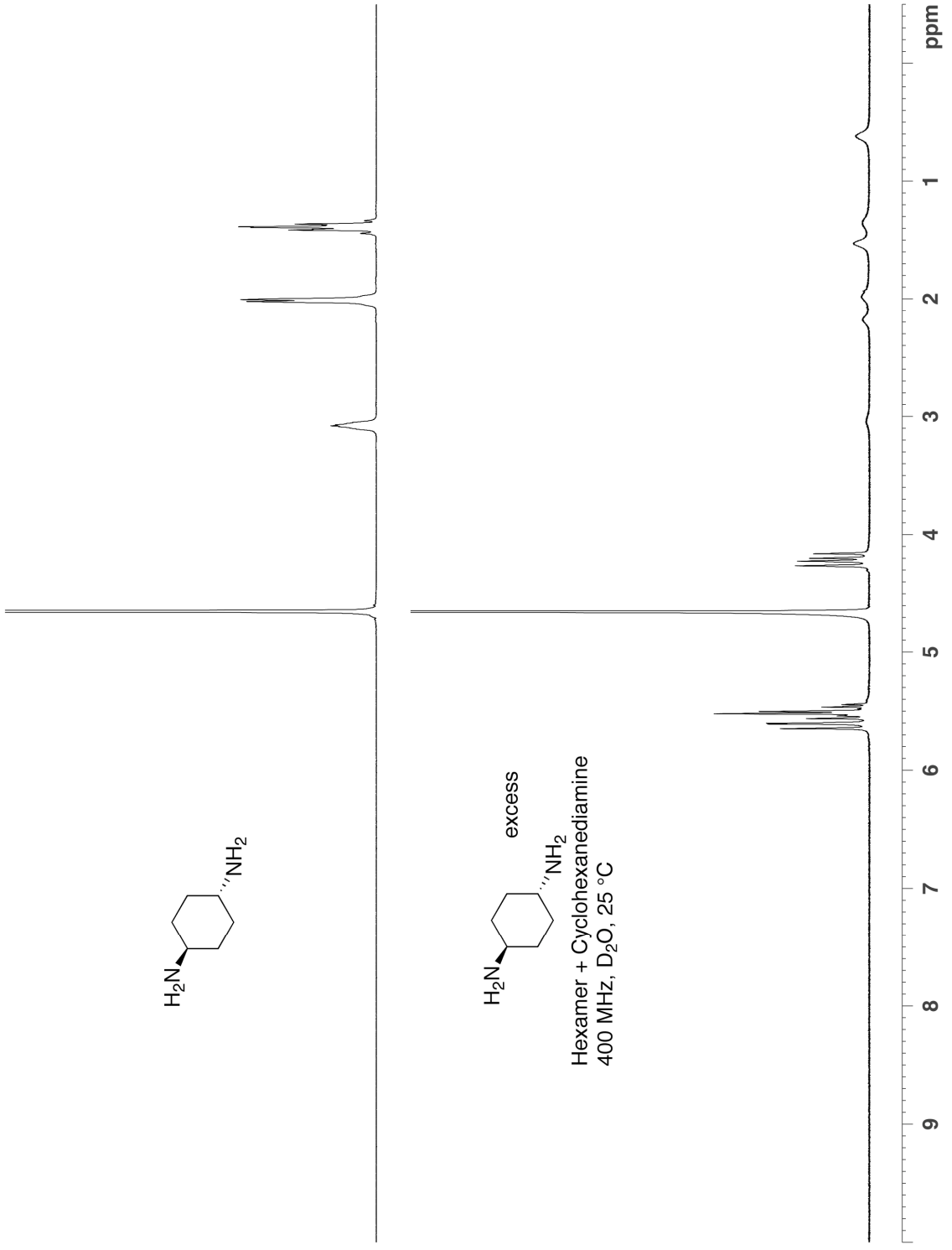

Figure S15. ^{1}H NMR spectra recorded for the cyclohexanediamine and its complex with **6** (400 MHz, D_2O, 25 ºC).

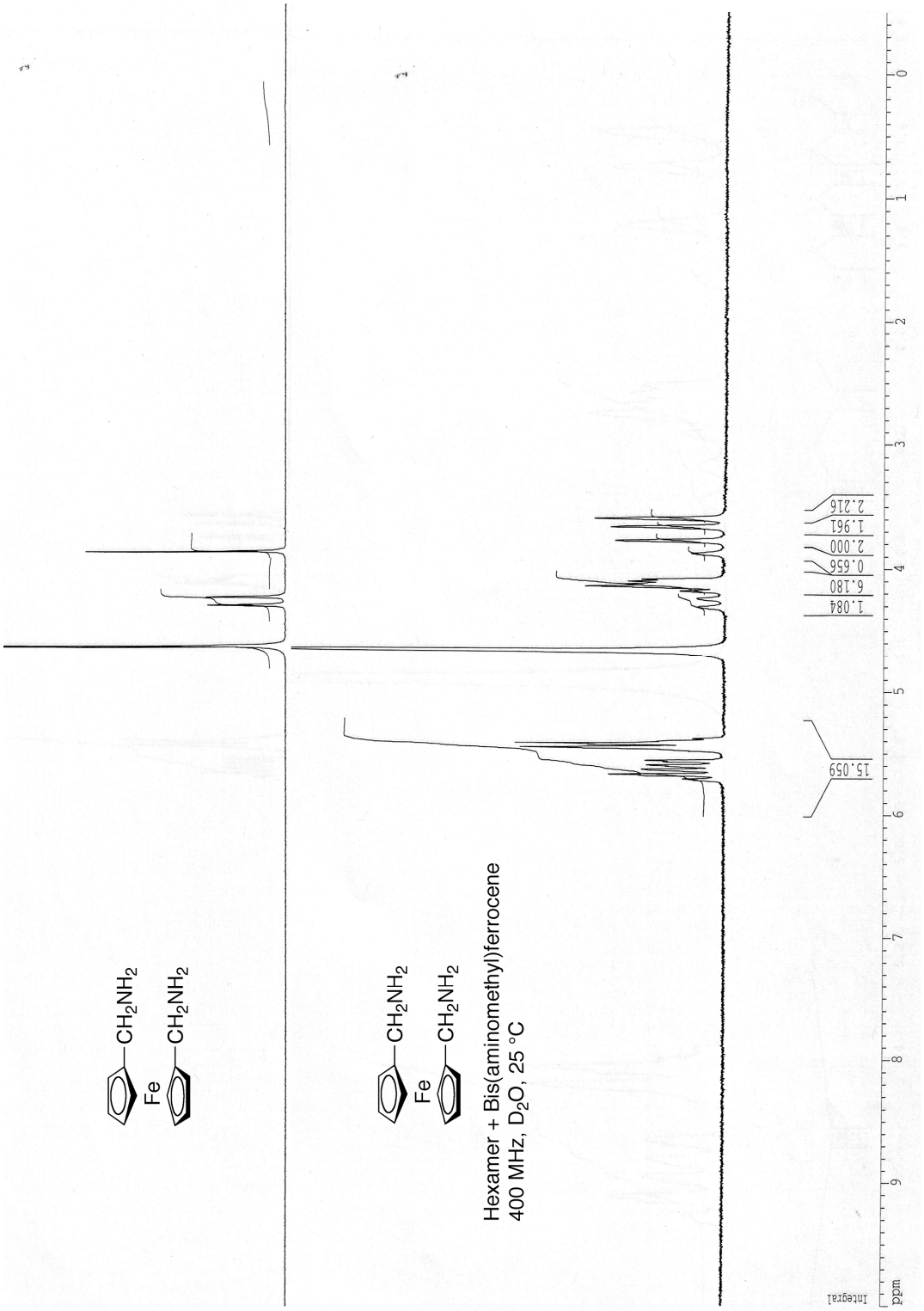

Figure S16. ^{1}H NMR spectra recorded for the bis(aminomethyl)ferrocene and its complex with **6** (400 MHz, D_2O, 25 ºC).

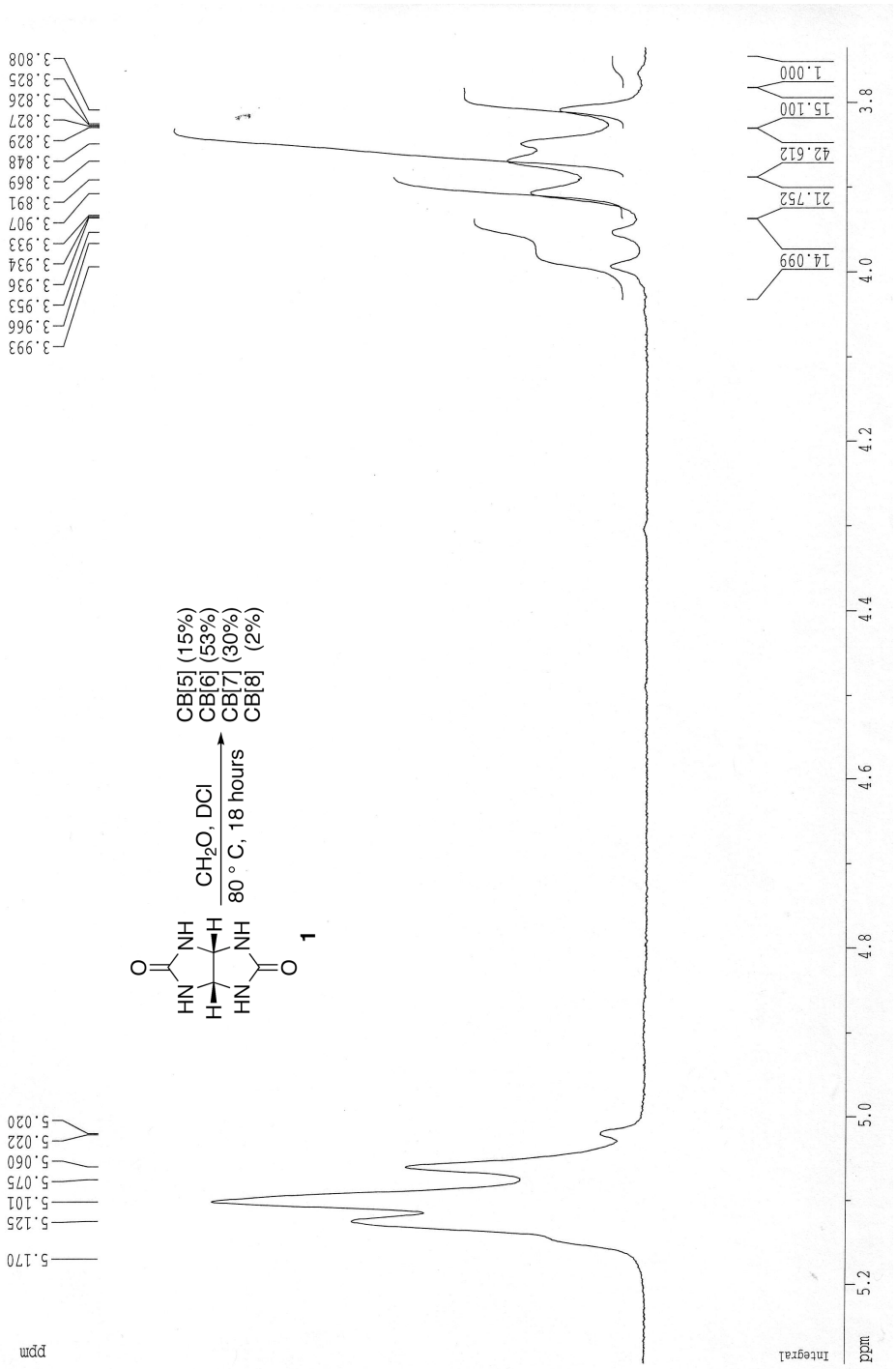

Figure S17. ^{1}H NMR spectra recorded for the reaction mixture composed of **1** and paraformaldehyde (2 eq.) upon conversion to CB[5], CB[6], CB[7], and CB[8] (400 MHz, 20% DCl / D_2O, RT).

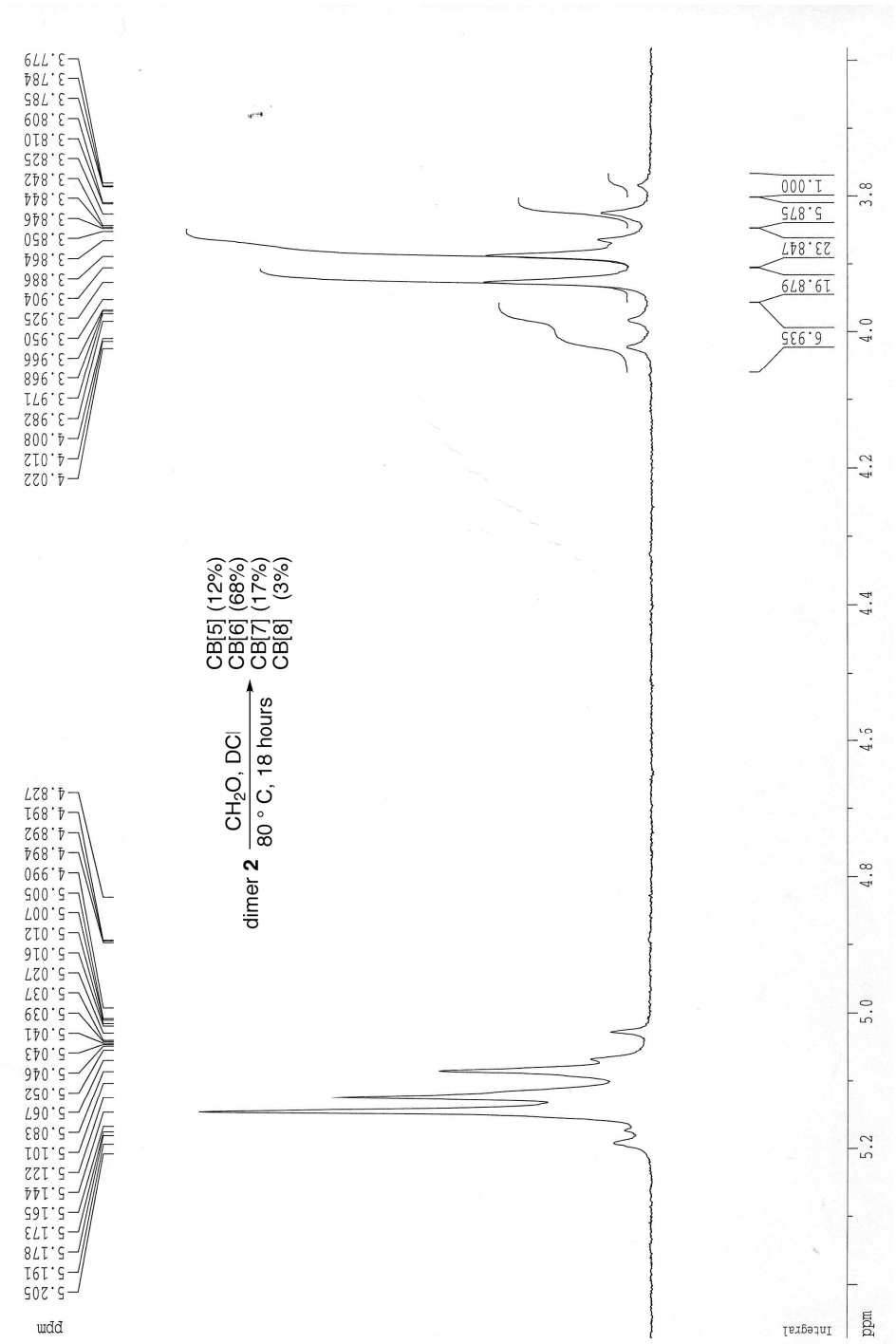

Figure S18. ^{1}H NMR spectra recorded for the reaction mixture composed of **2** and paraformaldehyde (2 eq.) upon conversion to CB[5], CB[6], CB[7], and CB[8] (400 MHz, 20% DCl / D_2O, RT).

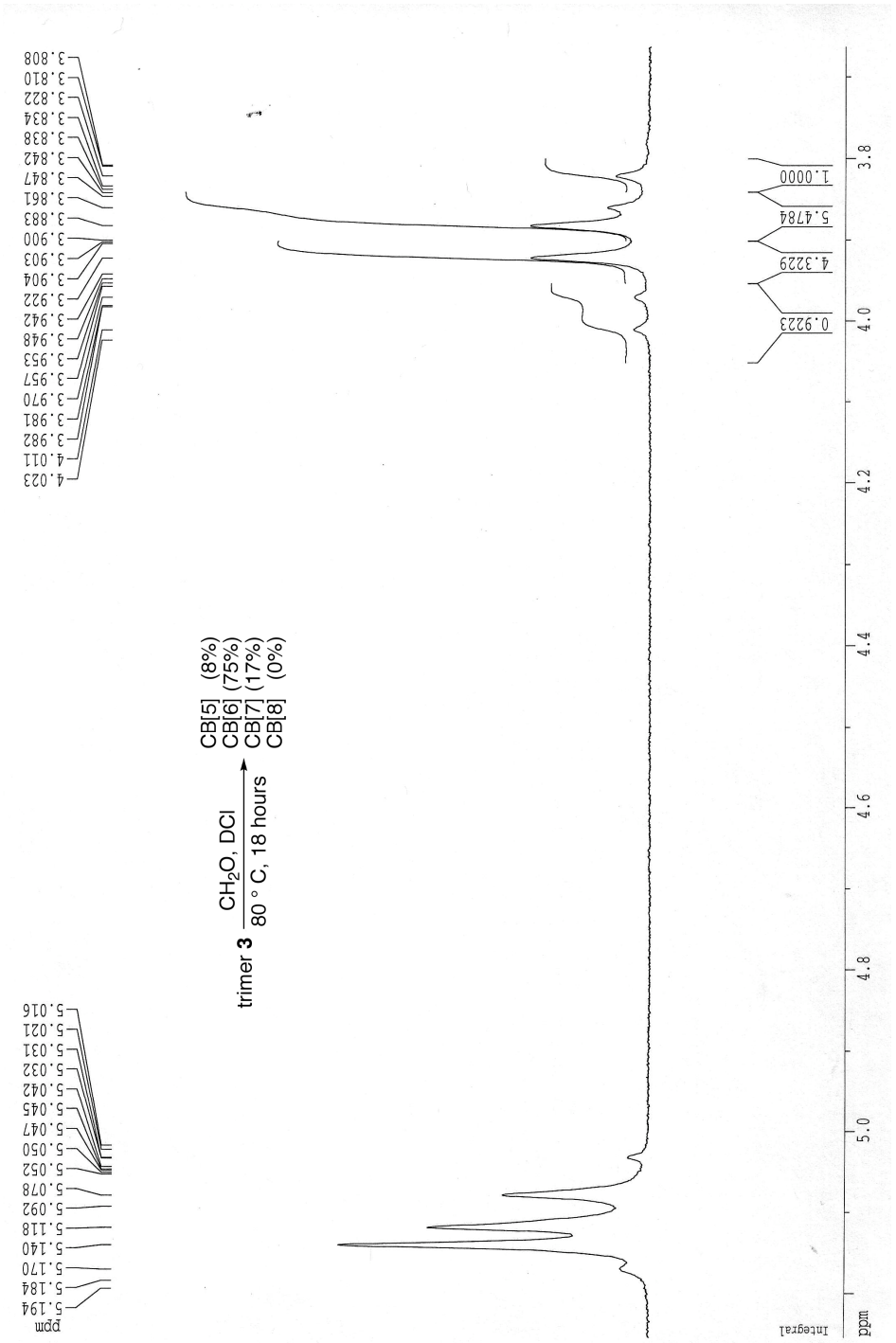

Figure S19. ^{1}H NMR spectra recorded for the reaction mixture composed of **3** and paraformaldehyde (2 eq.) upon conversion to CB[5], CB[6], CB[7], and CB[8] (400 MHz, 20% DCl / D_2O, RT).

Figure S20. ^{1}H NMR spectra recorded for the reaction mixture composed of **4** and paraformaldehyde (2 eq.) upon conversion to CB[5], CB[6], CB[7], and CB[8] (400 MHz, 20% DCl / D_2O, RT).

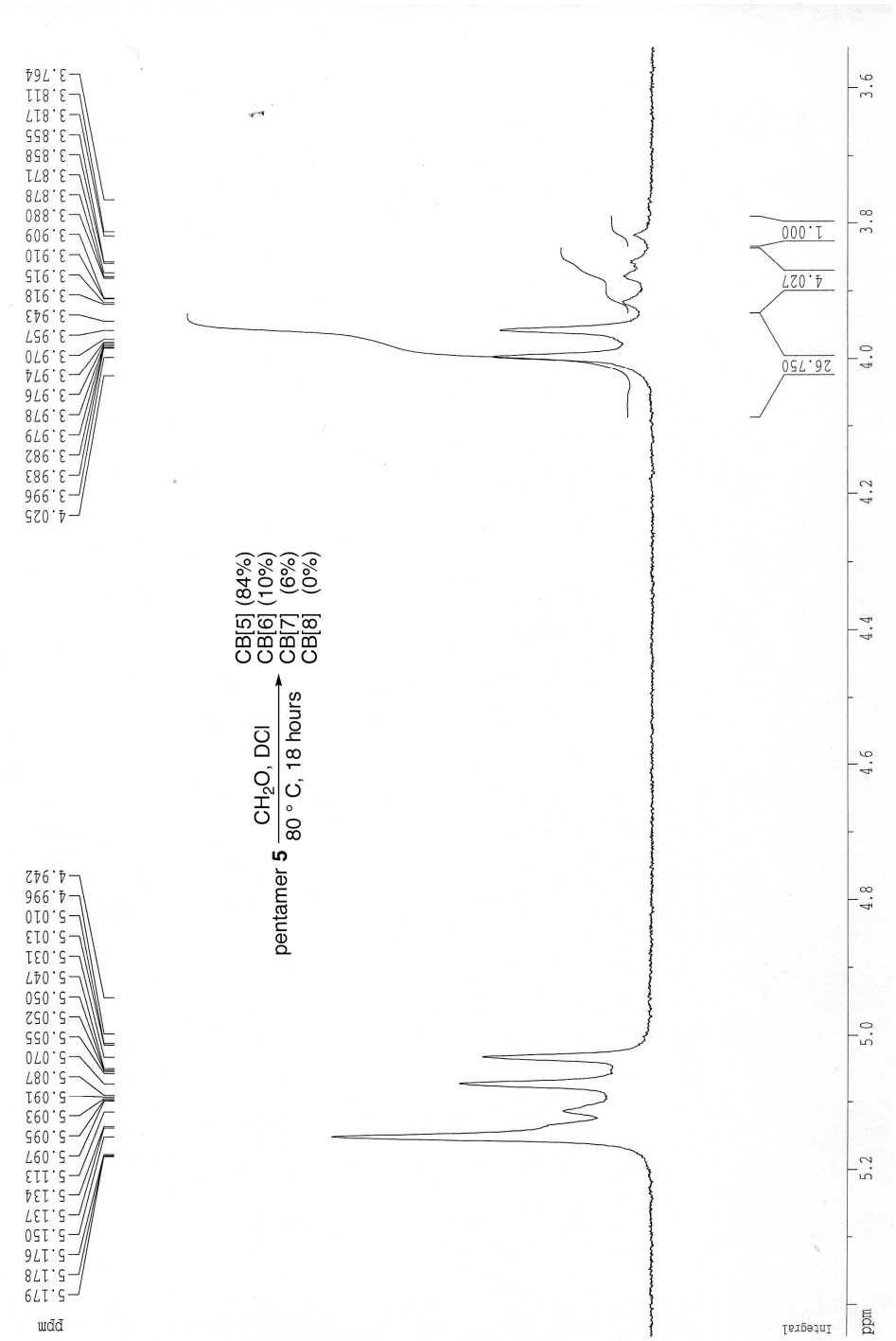

Figure S21. ^{1}H NMR spectra recorded for the reaction mixture composed of **5** and paraformaldehyde (2 eq.) upon conversion to CB[5], CB[6], CB[7], and CB[8] (400 MHz, 20% DCl / D_2O, RT).

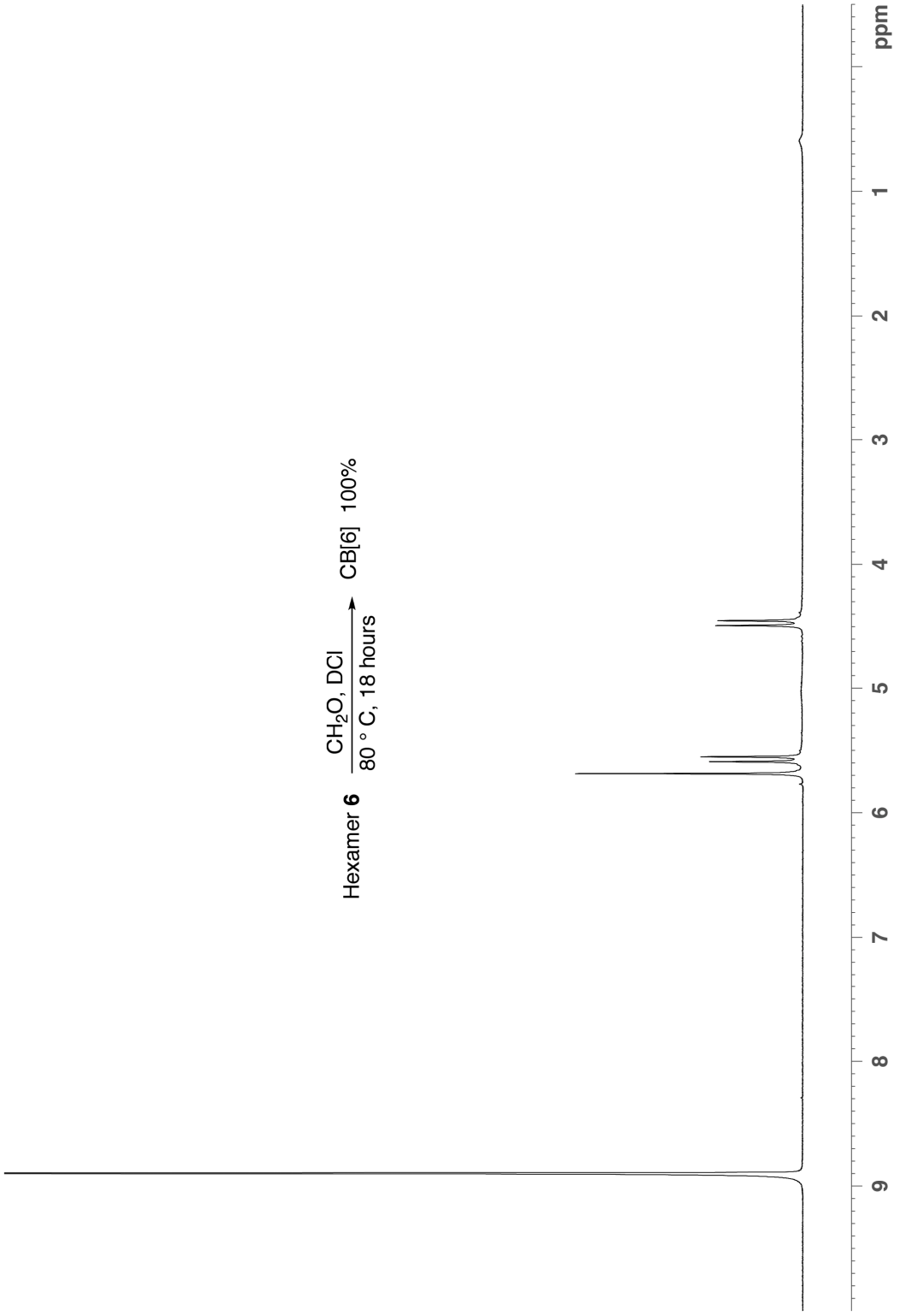

Figure S22. ^{1}H NMR spectra recorded for the reaction mixture composed of **6** and paraformaldehyde (2 eq.) upon conversion to CB[6] (400 MHz, 20% DCl / D_2O, RT).

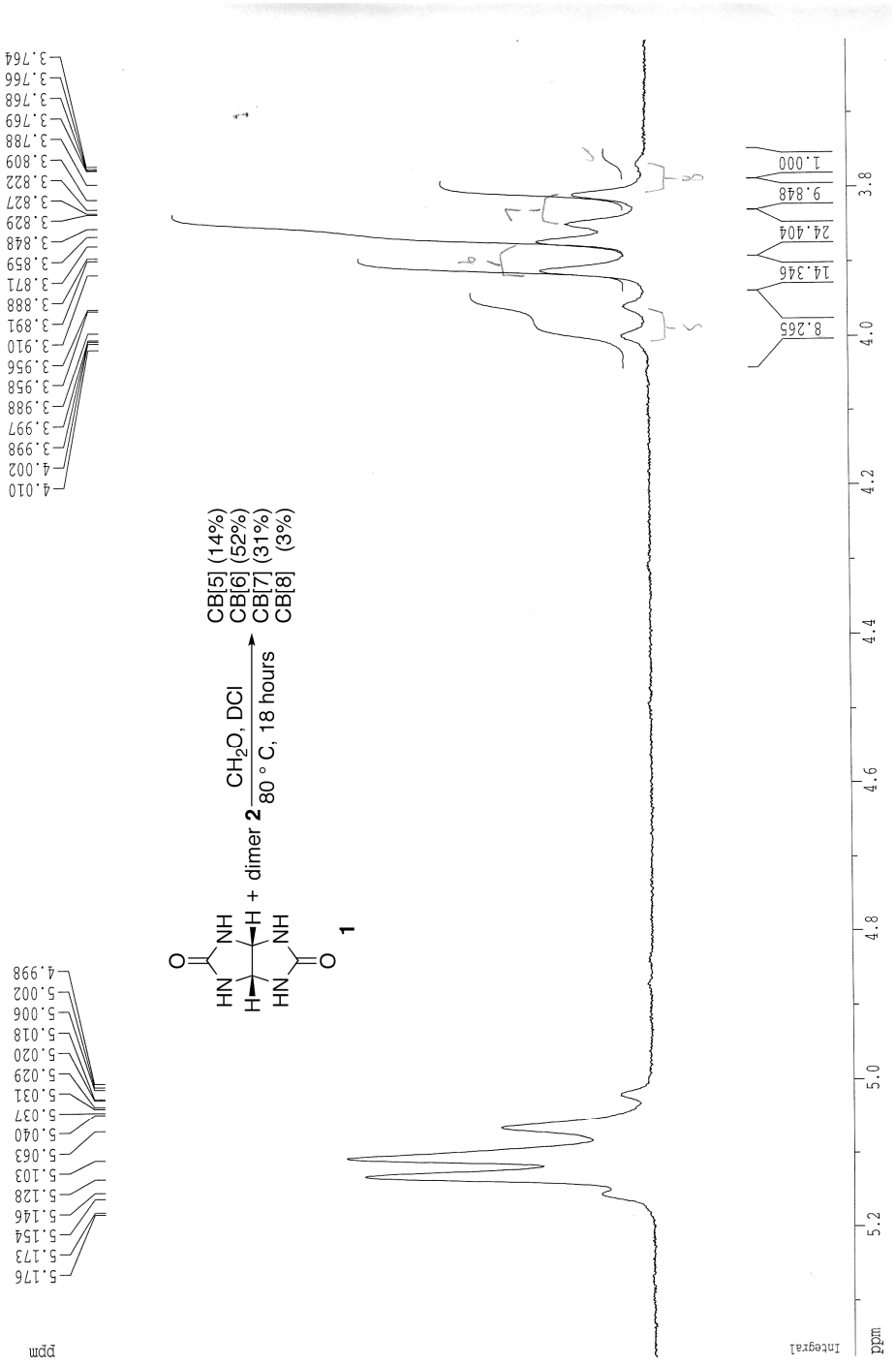

Figure S23. ^{1}H NMR spectra recorded for the reaction mixture composed of **1**, **2**, and paraformaldehyde (4 eq.) upon conversion to CB[5], CB[6], CB[7], and CB[8] (400 MHz, 20% DCl / D_2O, RT).

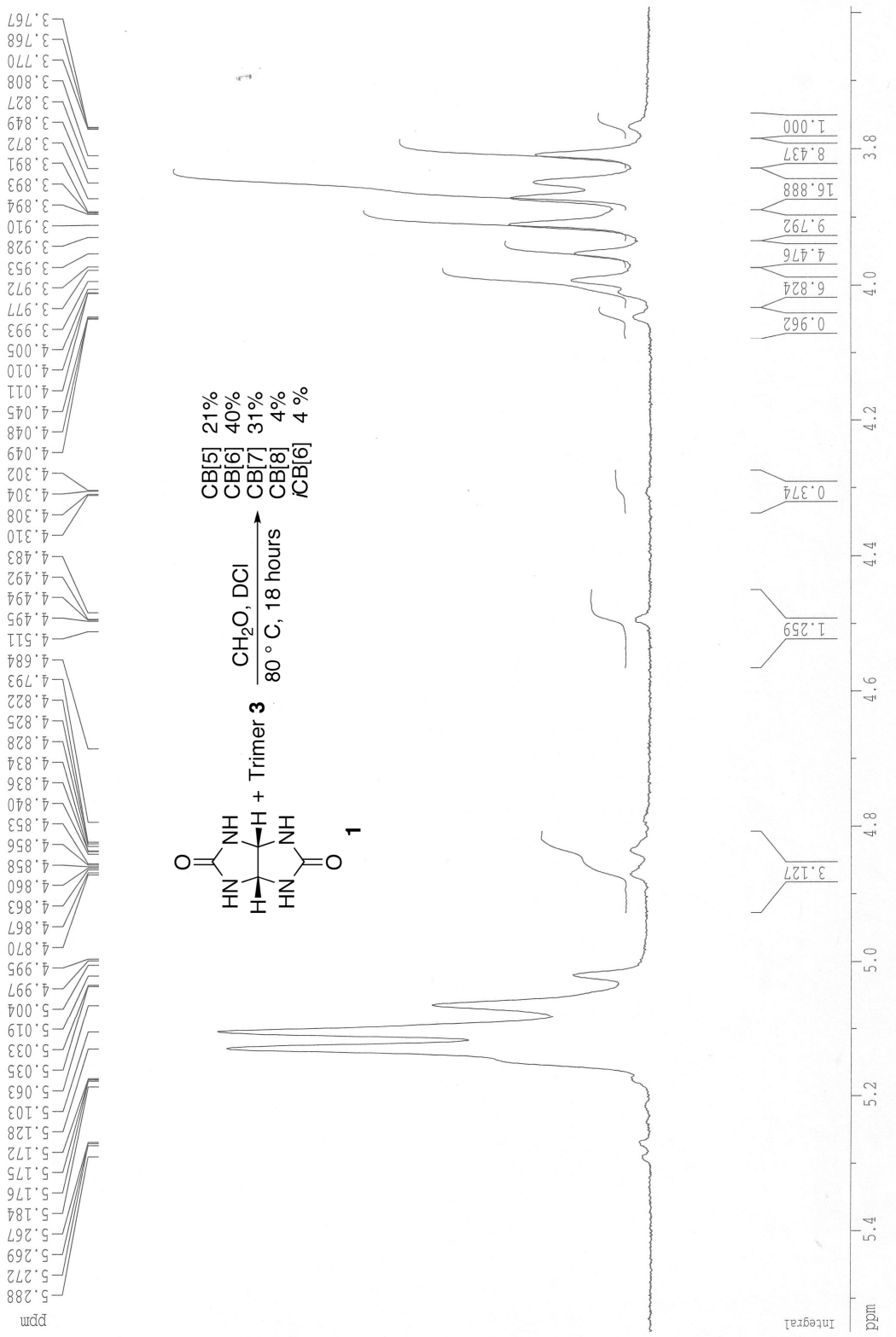

Figure S24. ^{1}H NMR spectra recorded for the reaction mixture composed of **1**, **3**, and paraformaldehyde (4 eq.) upon conversion to CB[5], CB[6], CB[7], CB[8], znd *i*CB[6] (400 MHz, 20% DCl / D_2O, RT).

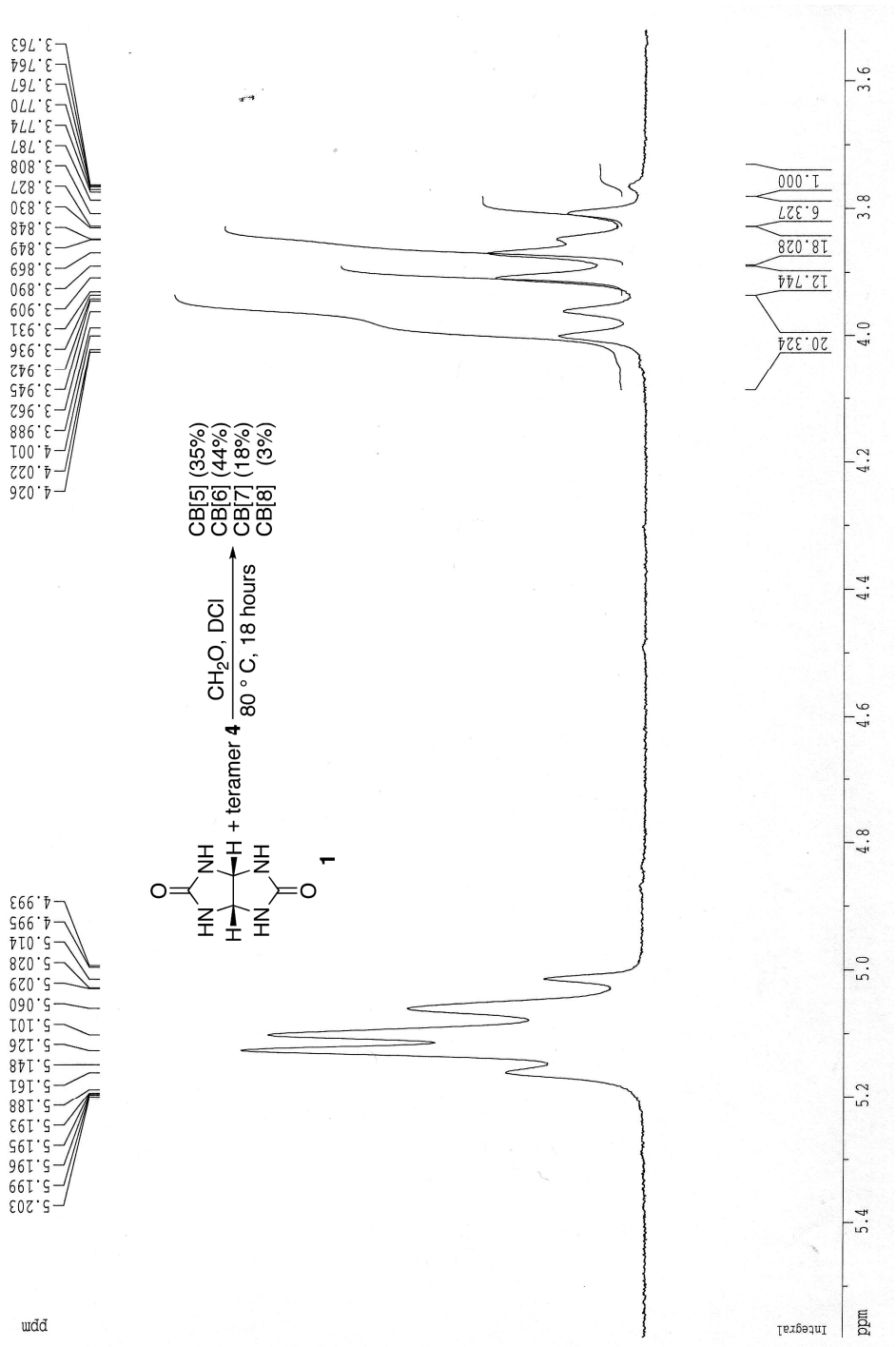

Figure S25. ^{1}H NMR spectra recorded for the reaction mixture composed of **1**, **4**, and paraformaldehyde (4 eq.) upon conversion to CB[5], CB[6], CB[7], and CB[8] (400 MHz, 20% DCl / D_2O, RT).

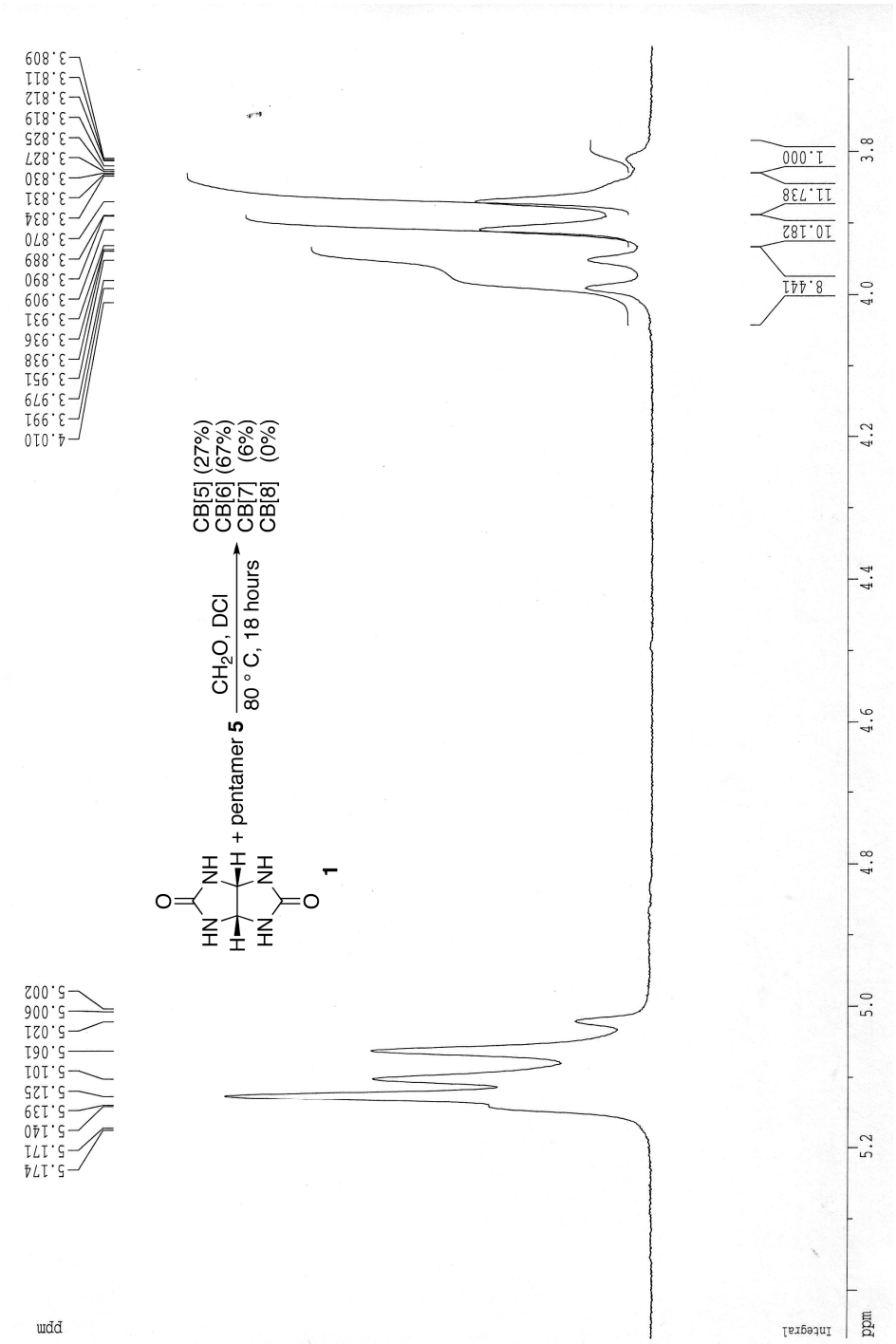

Figure S26. ^{1}H NMR spectra recorded for the reaction mixture composed of **1**, **5**, and paraformaldehyde (4 eq.) upon conversion to CB[5], CB[6], CB[7], and CB[8] (400 MHz, 20% DCl / D_2O, RT).

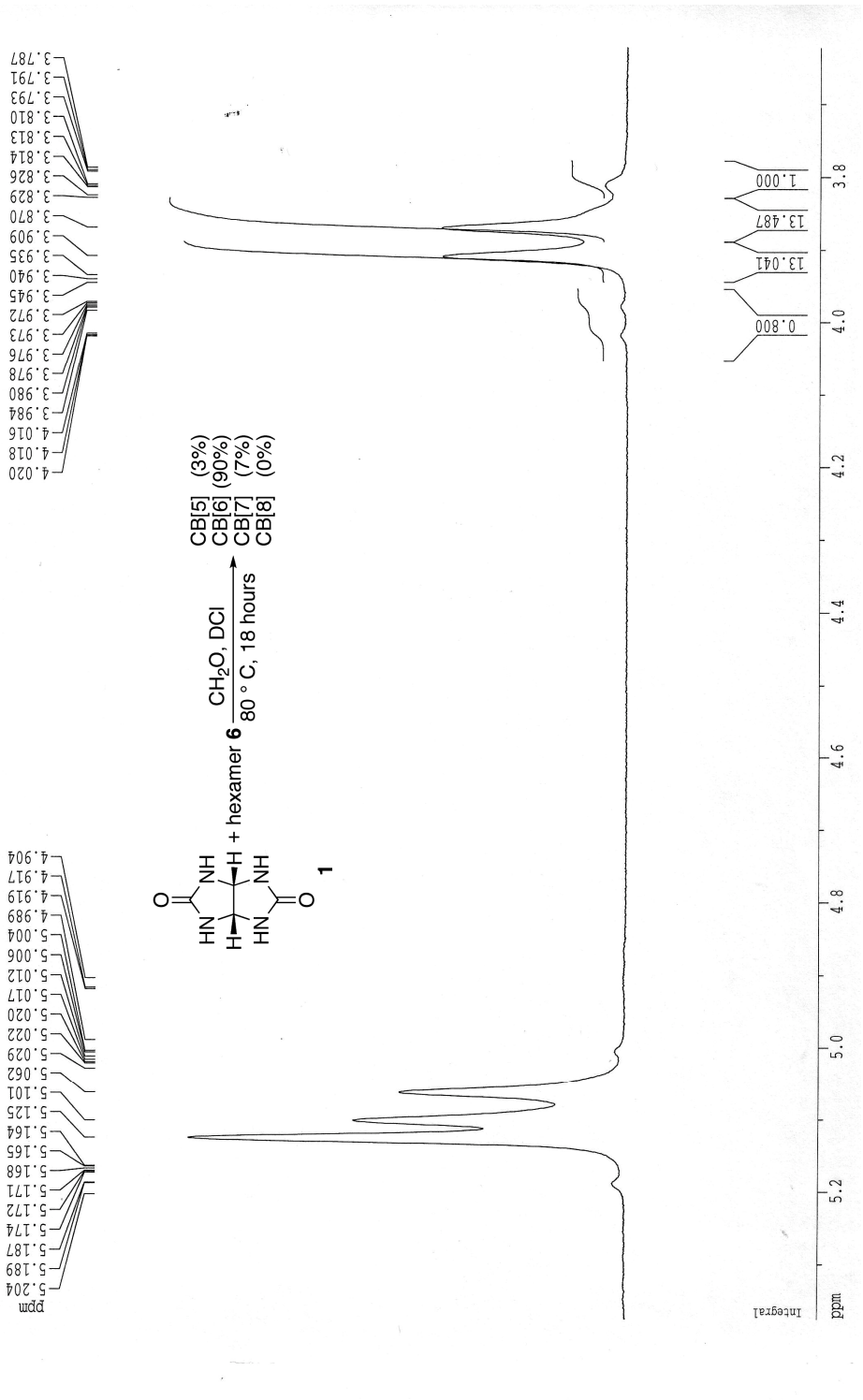

Figure S27. ^{1}H NMR spectra recorded for the reaction mixture composed of **1**, **6**, and paraformaldehyde (4 eq.) upon conversion to CB[5], CB[6], CB[7], and CB[8] (400 MHz, 20% DCl / D_2O, RT).

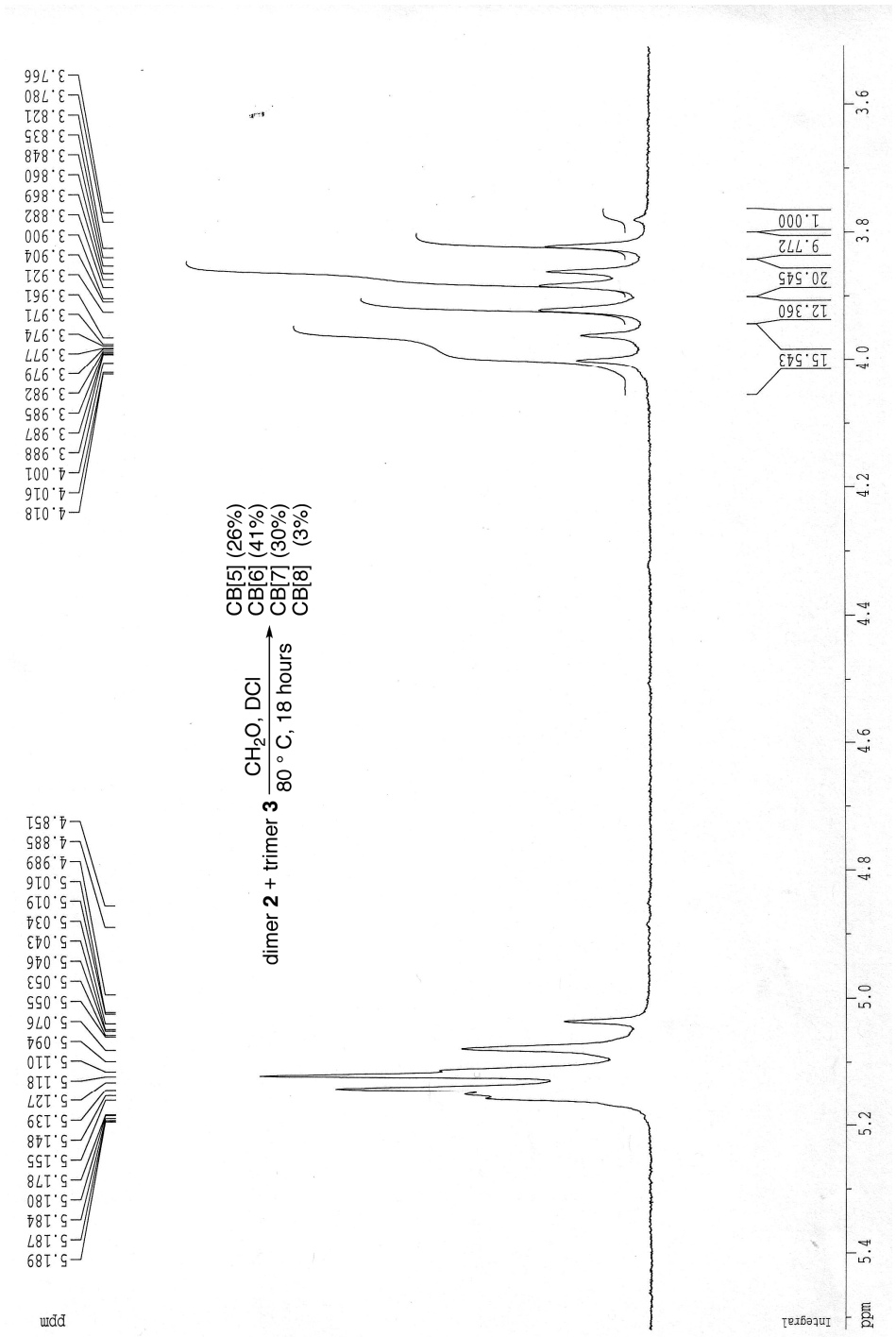

Figure S28. ^{1}H NMR spectra recorded for the reaction mixture composed of **2**, **3**, and paraformaldehyde (4 eq.) upon conversion to CB[5], CB[6], CB[7], and CB[8] (400 MHz, 20% DCl / D_2O, RT).

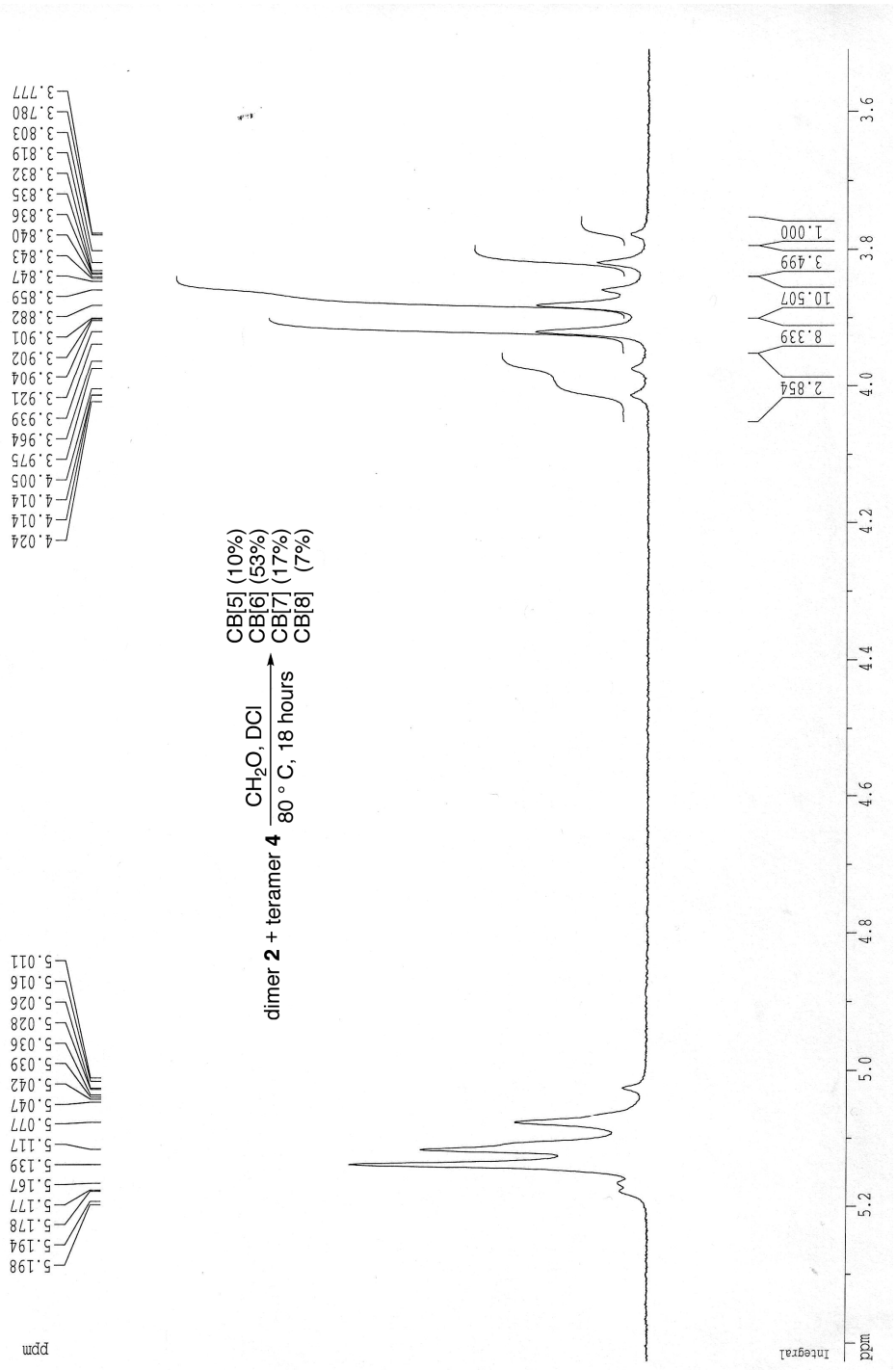

Figure S29. ^{1}H NMR spectra recorded for the reaction mixture composed of **2**, **4**, and paraformaldehyde (4 eq.) upon conversion to CB[5], CB[6], CB[7], and CB[8] (400 MHz, 20% DCl / D_2O, RT).

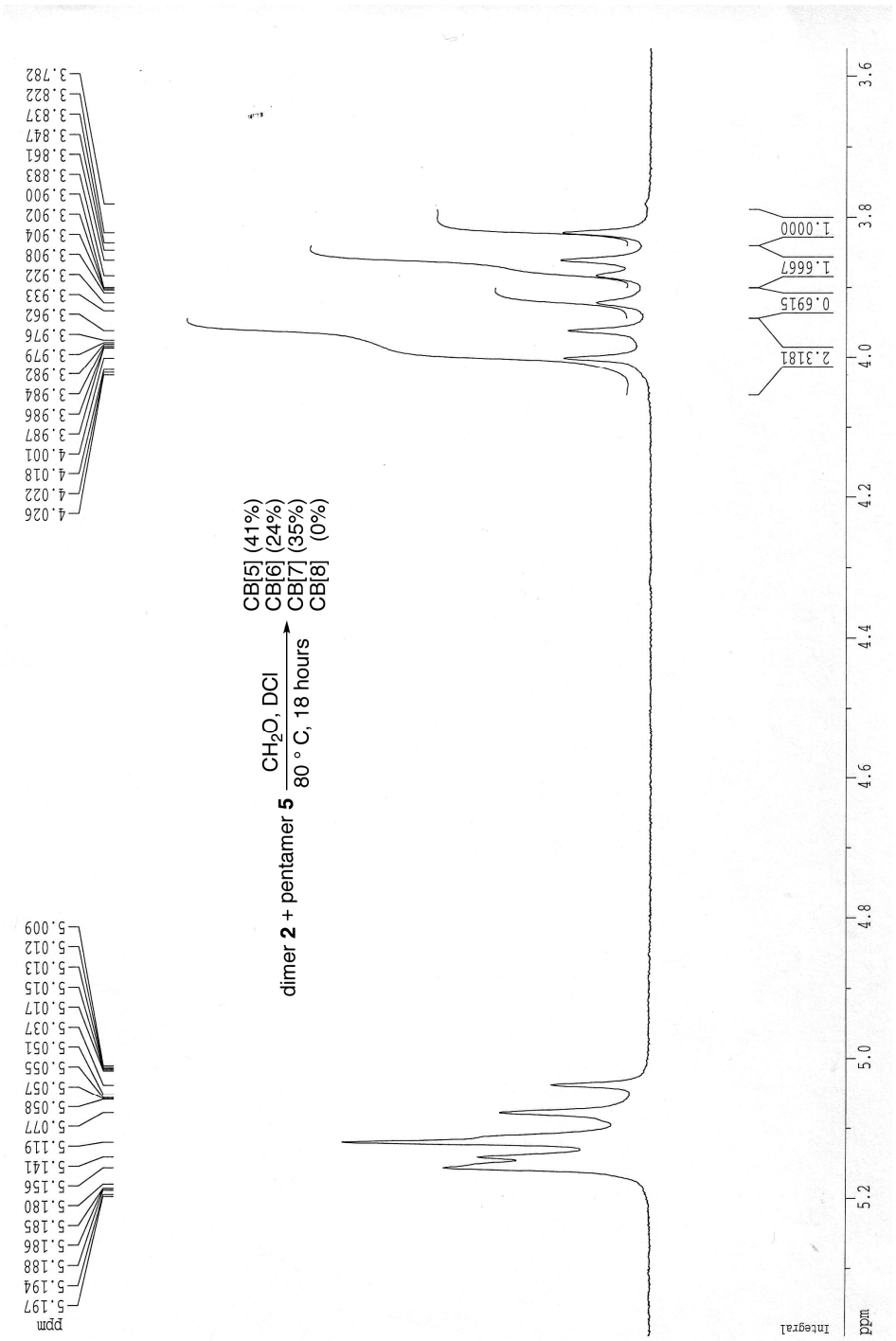

Figure S30. ^{1}H NMR spectra recorded for the reaction mixture composed of **2**, **5**, and paraformaldehyde (4 eq.) upon conversion to CB[5], CB[6], CB[7], and CB[8] (400 MHz, 20% DCl / D_2O, RT).

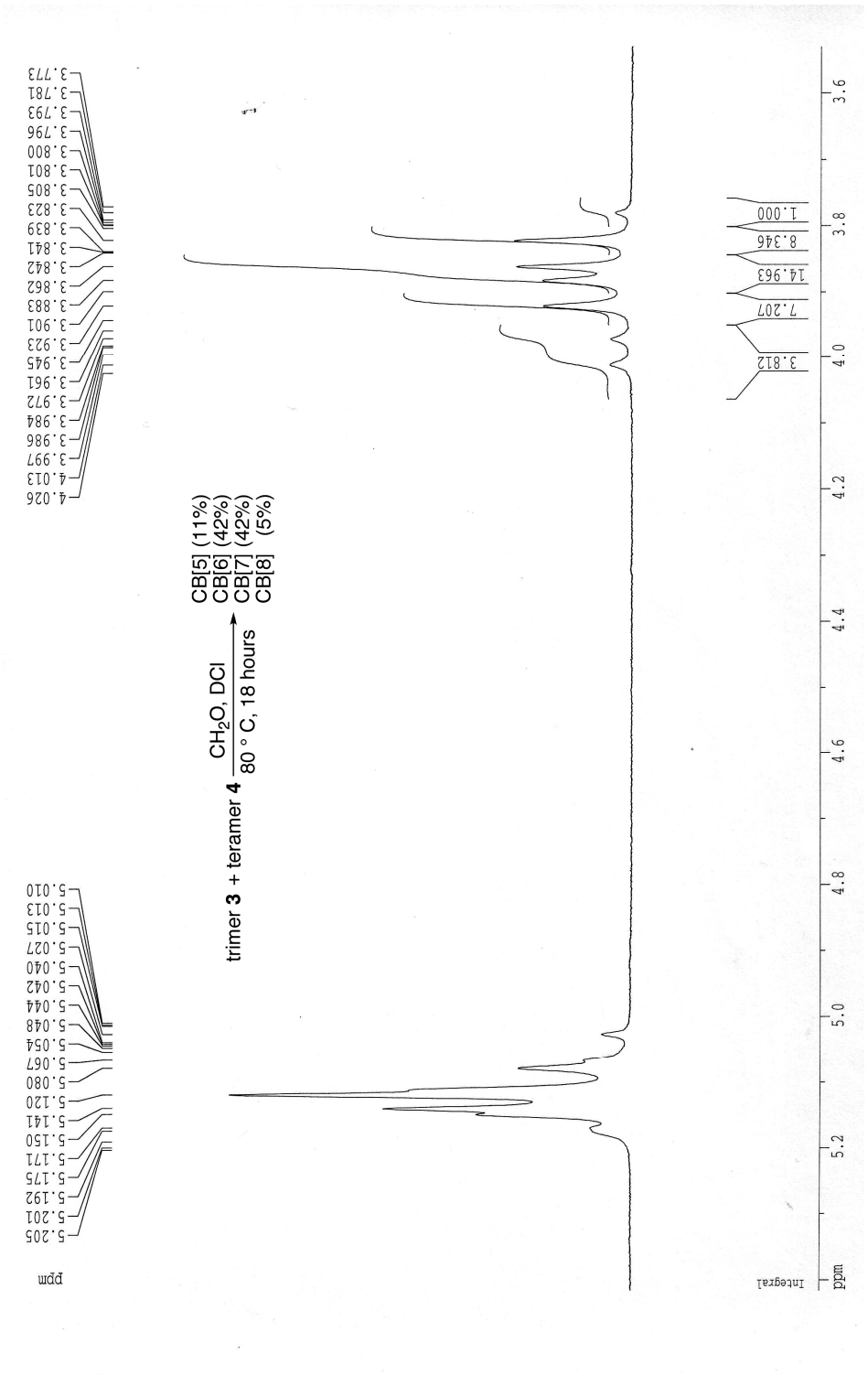

Figure S31. ^{1}H NMR spectra recorded for the reaction mixture composed of **3**, **4**, and paraformaldehyde (4 eq.) upon conversion to CB[5], CB[6], CB[7], and CB[8] (400 MHz, 20% DCl / D_2O, RT).

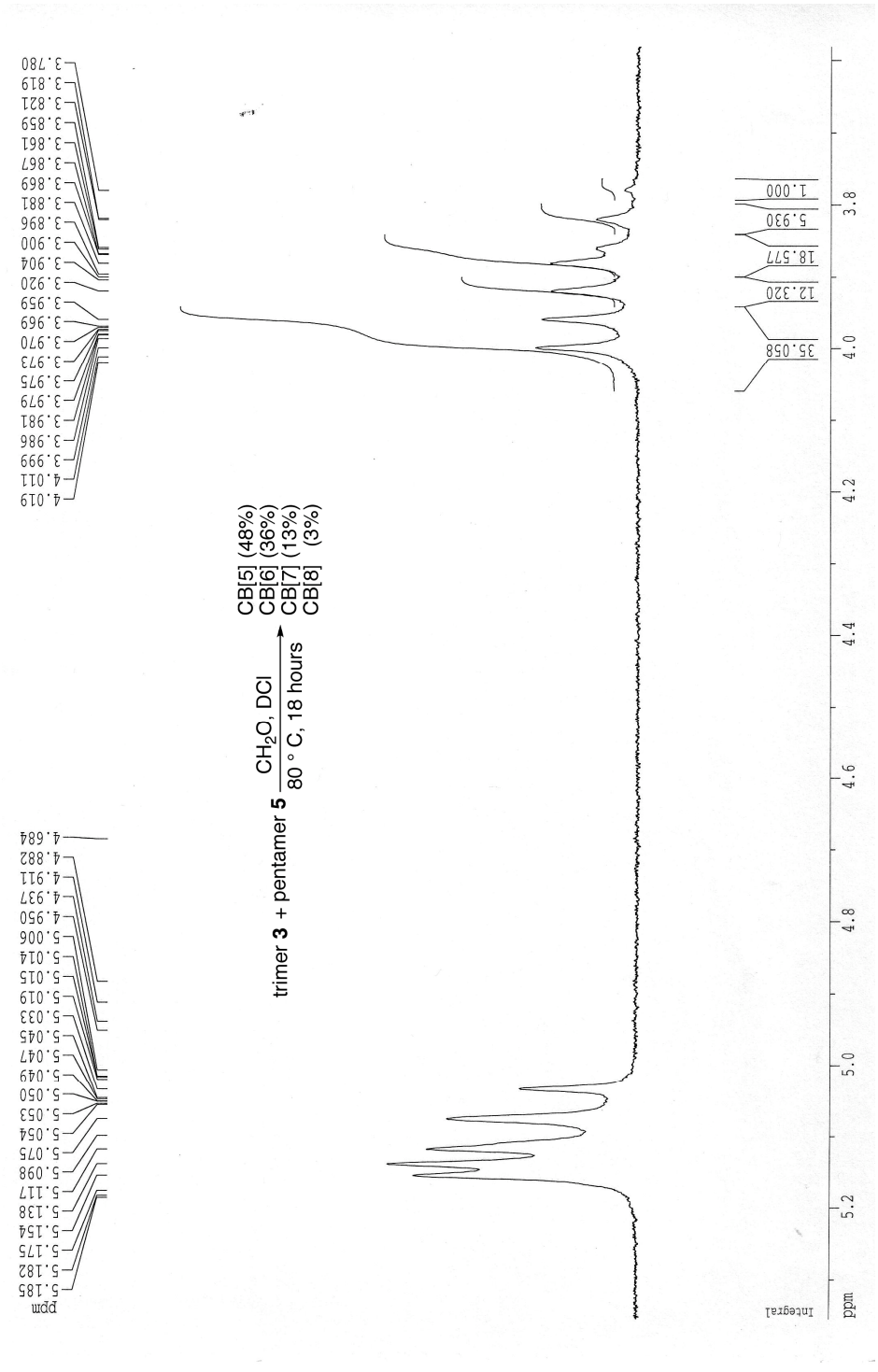

Figure S32. ^{1}H NMR spectra recorded for the reaction mixture composed of **3**, **5**, and paraformaldehyde (4 eq.) upon conversion to CB[5], CB[6], CB[7], and CB[8] (400 MHz, 20% DCl / D_2O, RT).

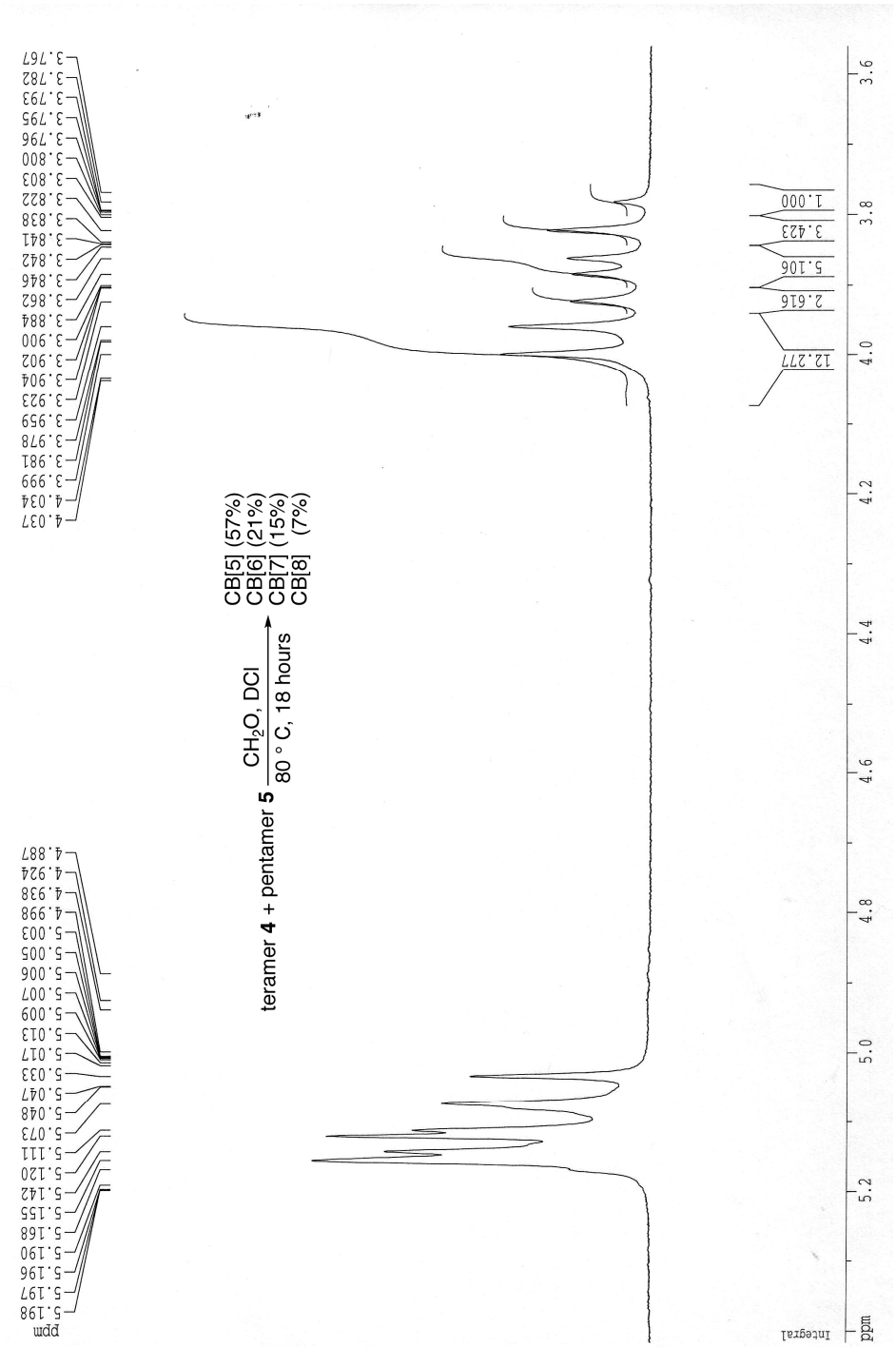

Figure S33. ^{1}H NMR spectra recorded for the reaction mixture composed of **4**, **5**, and paraformaldehyde (4 eq.) upon conversion to CB[5], CB[6], CB[7], and CB[8] (400 MHz, 20% DCl / D_2O, RT).

Crystal Structure Information for UM # 1306

Issues by: Peter Y. Zavalij

Crystal No. & ID	:	**1306**: Isaacs/Huang - dimer CB2
Compound name	:	CB2·5CF_3COOH
Chemical formula	:	$C_{10}H_{12}N_8O_4$·5(CF_3COOH)
Final R_1 [I>2σ(I)]	:	**3.84 %**

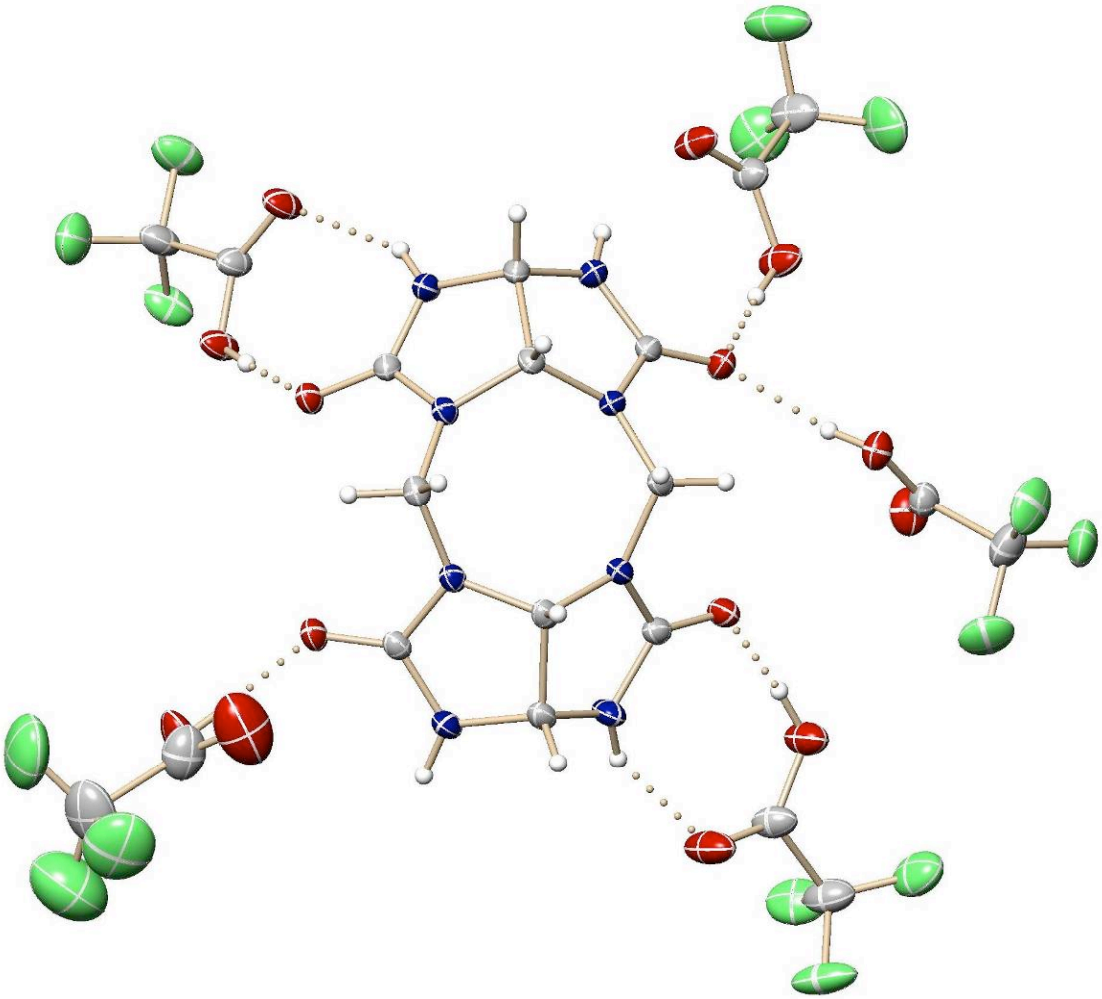

Figure S34. A view of CB2·5CF_3COOH showing the numbering scheme employed. Anisotropic atomic displacement ellipsoids for the non-hydrogen atoms are shown at the 25% probability level. Hydrogen atoms are displayed with an arbitrarily small radius.

A colorless prism of $C_{20}H_{17}F_{15}N_8O_{14}$, approximate dimensions 0.24 × 0.35 × 0.375 mm^3, was used for the X-ray crystallographic analysis. The X-ray intensity data were measured at 223(2) K on a three-circle diffractometer system equipped with Bruker Smart1000 CCD area detector using a graphite monochromator and a MoKα fine-focus sealed tube (λ= 0.71073 Å) operated at 50 kV and 40 mA. The detector was placed at a distance of 4.958 cm from the crystal.

A total of 1487 frames were collected with a scan width of 0.3° in ω and an exposure time of 13 sec/frame using SMART (Bruker, 1999). The total data collection time was 8.32 hours. The frames were integrated with SAINT software package using a narrow-frame integration algorithm. The integration of the data using a Orthorhombic unit cell yielded a total of 24774 reflections to a maximum θ angle of 27.50°, of which 7659 were independent (completeness = 99.4%, R_{int} = 1.75%, R_{sig} = 1.66%) and 6778 were greater than 2σ(I). The final cell dimensions of a = 8.8769(3) Å, b = 12.8191(4) Å, c = 29.5359(9) Å, α= 90°, β= 90°, γ= 90°, V = 3361.00(19) $Å^3$, are based upon the refinement of the XYZ-centroids of 5901 reflections with 2.1 < θ < 28.1° using SAINT. Analysis of the data showed 0.00 % decay during data collection. Data were corrected for absorption effects with the Semi-empirical from equivalents method using SADABS (Sheldrick, 1996). The minimum and maximum transmission coefficients were 0.849 and 0.955.

The structure was solved and refined using the SHELXS-97 (Sheldrick, 1990) and SHELXL-97 (Sheldrick, 1997) software in the space group $P2_12_12_1$ with Z = 4 for the formula unit $C_{20}H_{17}F_{15}N_8O_{14}$. The final anisotropic full-matrix least-squares refinement on F^2 with 851 variables converged at R_1 = 3.84 % for the observed data and wR_2 = 8.16 % for all data. The goodness-of-fit was 1.000. The largest peak on the final difference map was 0.235$\bar{e}/Å^3$ and the largest hole was -0.182$\bar{e}/Å^3$. On the basis of the final model, the calculated density was 1.736 g/cm^3 and F(000), 1760$\bar{e}$.

Comments:

- Data set quality: very good
- Twinning: none
- Disorder: moderate to heavy disorder of solvent CF3COOH (Table 5):
  - #1 - CF3 in 2 orientations
  - #2,3 - CF3 in 3 orientations
  - #4,5 - whole molecule in 2 orientations; in addition one orientation #5 has COOH in 3 orientations
- H-atoms refinement: constraned, Uiso refined; extensive H-bonding; all possible H-bonds are realized and make sense
- Residual density: near disordered groups
- Structure quality: very good

  Check CIF: Platon (all alerts are due to the disorder and are explainable)

  Publishable!

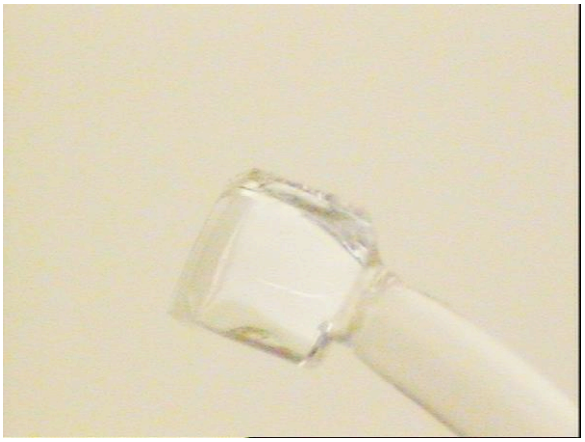

Table 1. Crystal data and structure refinement for **CB2**·5CF_3COOH.

X-ray labbook No.		1306
Crystal ID		Isaacs/Huang - dimmer CB2
Empirical formula		$C_{20}H_{17}F_{15}N_8O_{14}$
Formula weight		878.42
Temperature		223(2) K
Wavelength		0.71073 Å
Crystal size		0.375 × 0.35 × 0.24 mm^3
Crystal habit		colorless prism
Crystal system		Orthorhombic
Space group		$P2_12_12_1$
Unit cell dimensions		a = 8.8769(3) Å α = 90°
		b = 12.8191(4) Å β = 90°
		c = 29.5359(9) Å γ = 90°
Volume		3361.00(19) $Å^3$
Z		4
Density, ρ_{calc}		1.736 g/cm^3
Absorption coefficient, μ		0.193 mm^{-1}
F(000)		1760ē
Diffractometer		Bruker Smart1000 CCD area detector
Radiation source		fine-focus sealed tube, MoKα
Generator power		50 kV, 40 ma
Detector distance		4.958 cm
Detector resolution		8.33 pixels/mm
Total frames		1487
Frame size		512 pixels
Frame width		0.3 °
Exposure per frame		13 sec
Total measurement time		8.32 hours
Data collection method		ω scans
θ range for data collection		2.68 to 27.50°
Index ranges		$-10 \le h \le 11$, $-16 \le k \le 15$, $-38 \le l \le 37$
Reflections collected		24774
Independent reflections		7659
Observed reflection, I>2σ(I)		6778
Coverage of independent reflections		99.4 %
Variation in check reflections		0.00 %
Absorption correction		Semi-empirical from equivalents
		SADABS (Sheldrick, 1996)
Max. and min. transmission		0.955 and 0.849
Structure solution technique		direct
Structure solution program		SHELXS-97 (Sheldrick, 1990)
Refinement technique		Full-matrix least-squares on F^2
Refinement program		SHELXL-97 (Sheldrick, 1997)
Function minimized		$\Sigma w(F_o^2 - F_c^2)^2$
Data / restraints / parameters		7659 / 1012 / 851
Goodness-of-fit on F^2		1.000
Δ/σ_{max}		0.001
Final R indices:	R_1, I>2σ(I)	0.0384
	wR_2, all data	0.0816
	R_{int}	0.0175
	R_{sig}	0.0166
Weighting scheme		$w = 1/[\sigma^2(F_o^2) + (0.02P)^2 + 1.53P]$,
		$P = [\max(F_o^2, 0) + 2F_o^2]/3$
Absolute structure parameter		0.0(7)
Extinction coefficient		0.0035(3)
Largest diff. peak and hole		0.235 and -0.182ē/$Å^3$

$R_1 = \Sigma||F_o|-|F_c||/\Sigma|F_o|$, $wR2 = [\Sigma w(F_o^2-F_c^2)^2/\Sigma w(F_o^2)^2]^{1/2}$

Crystal Structure Information for UM # 1407

Issued by: Peter Y. Zavalij

Crystal No. & ID	:	**1407**: Isaacs tetramer CB4 none-cyclic
Compound name	:	Na*2CB4*H2O*7TFA
Chemical formula	:	$[(C_{22}H_{24}N_{16}O_8)_2 \cdot (H_2O) \cdot Na]^+ \cdot 6(CF_3COOH)(CF_3COO)^-$
Final R_1 [I>2σ(I)]	:	**7.79 %**

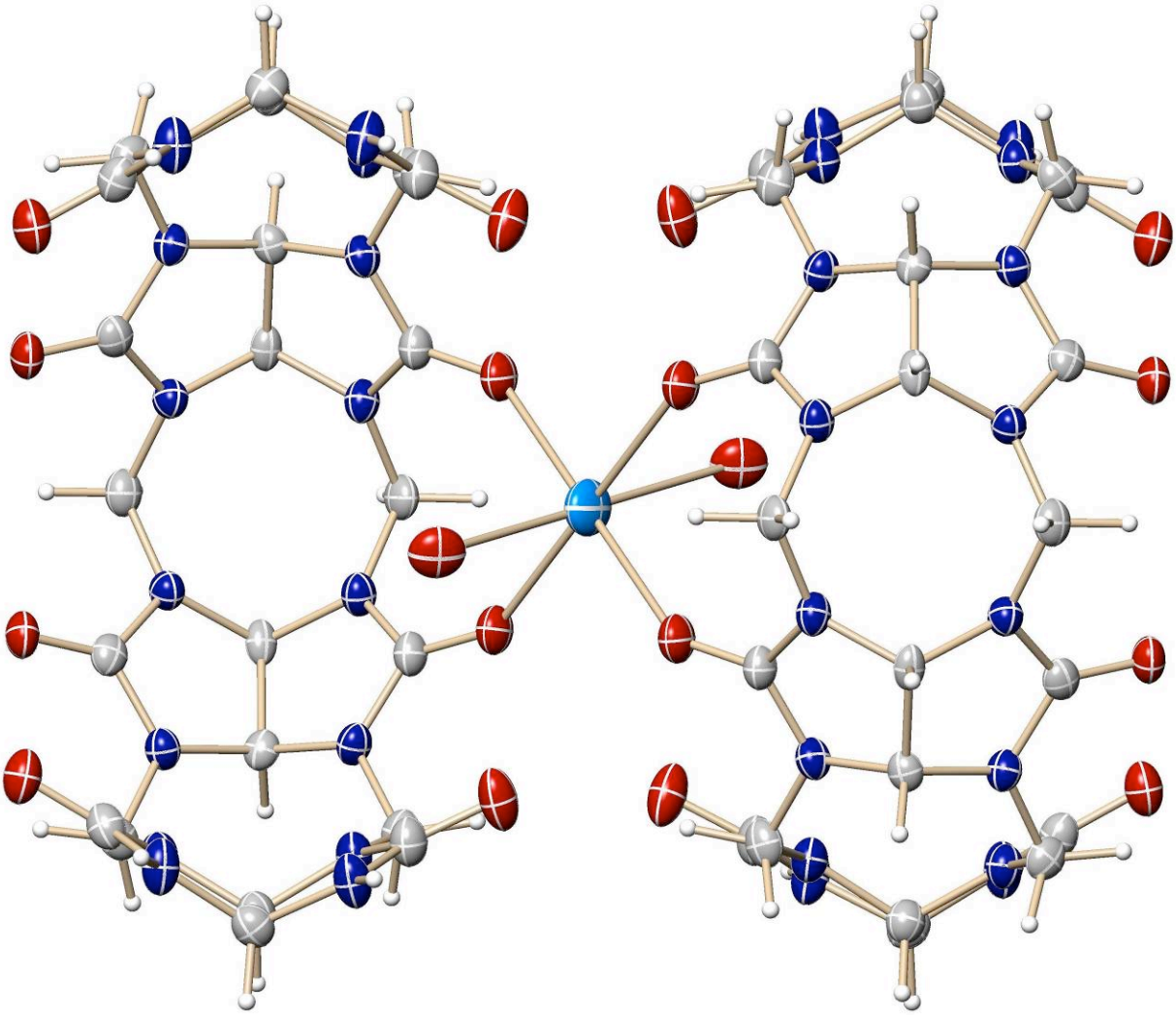

Figure S35. A view of UM#1407 showing the numbering scheme employed. Anisotropic atomic displacement ellipsoids for the non-hydrogen atoms are shown at the 30% probability level. Hydrogen atoms are displayed with an arbitrarily small radius.

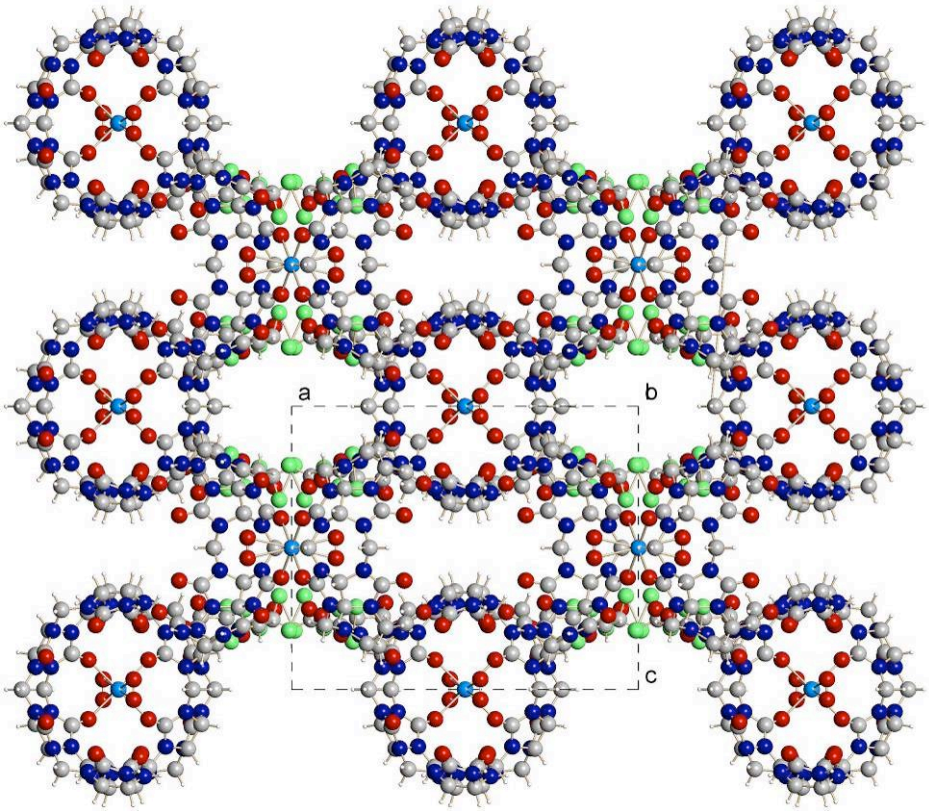

A colorless prism of $C_{58}H_{56}F_{21}N_{32}NaO_{31}$, approximate dimensions 0.09 × 0.11 × 0.26 mm^3, was used for the X-ray crystallographic analysis. The X-ray intensity data were measured at 220(2) K on a three-circle diffractometer system equipped with Bruker Smart1000 CCD area detector using a graphite monochromator and a MoKα fine-focus sealed tube (λ= 0.71073 Å) operated at 50 kV and 40 mA. The detector was placed at a distance of 4.939 cm from the crystal.

A total of 1824 frames were collected with a scan width of 0.5° in ω and an exposure time of 38 sec/frame using SMART (Bruker, 1999). The total data collection time was 22.88 hours. The frames were integrated with SAINT software package using a narrow-frame integration algorithm. The integration of the data using a Tetragonal unit cell yielded a total of 25719 reflections to a maximum θ angle of 20.00°, of which 2590 were independent (completeness = 99.6%, R_{int} = 6.86%, R_{sig} = 3.89%) and 2044 were greater than 2σ(I). The final cell dimensions of *a* = 18.6306(8) Å, *b* = 18.6306(8) Å, *c* = 15.2173(12) Å, α= 90°, β= 90°, γ= 90°, *V* = 5281.9(5) $Å^3$, are based upon the refinement of the XYZ-centroids of 4859 reflections with 2.4 < θ < 21.7° using SAINT. Analysis of the data showed ? % decay during data collection. Data were corrected for absorption effects with the Semi-empirical from equivalents method using SADABS (Sheldrick, 1996). The minimum and maximum transmission coefficients were 0.937 and 0.988.

The structure was solved and refined using the SHELXS-97 (Sheldrick, 1990) and SHELXL-97 (Sheldrick, 1997) software in the space group $P4_2/m$ with *Z* = 2 for the formula unit $C_{58}H_{56}F_{21}N_{32}NaO_{31}$. The final anisotropic full-matrix least-squares refinement on F^2 with 339 variables converged at R_1 = 7.79 % for the observed data and wR_2 = 18.67 % for all data. The goodness-of-fit was 1.001. The largest peak on the final difference map was 0.783$\bar{e}/Å^3$ and the largest hole was -0.297$\bar{e}/Å^3$. On the basis of the final model, the calculated density was 1.333 g/cm^3 and F(000), 2152$\bar{e}$.

Comments:

- Data set quality: good < 40° 2θ
- Twinning: none
- Disorder: substantial solvent removed using SQUEEZE (except 1 TFA and 1 water)
- H-atoms refinement: constrained
- Residual density: near disordered groups
- Structure quality: good
  Publishable!

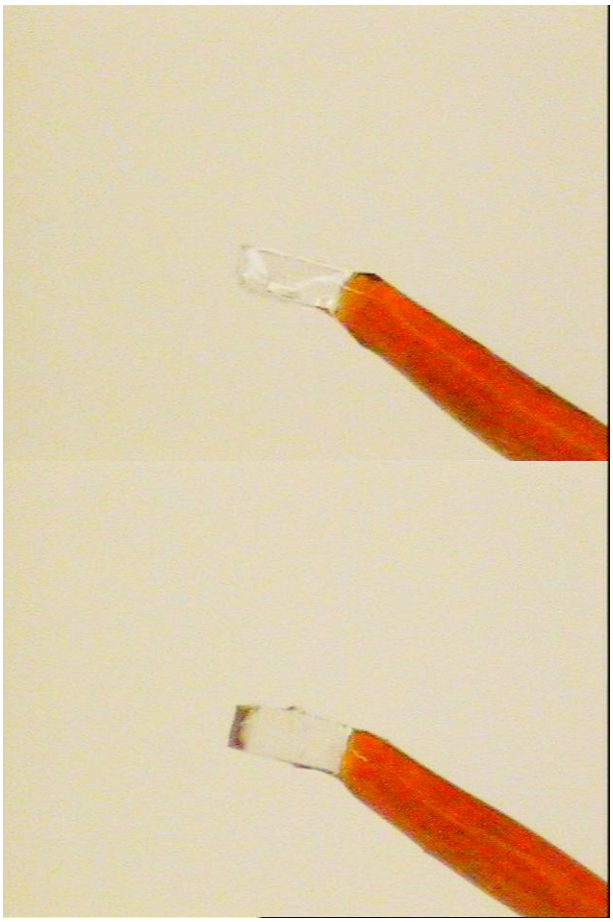

Table 1. Crystal data and structure refinement for UM#1407.

X-ray lab book No.		1407
Crystal ID		Isaacs tetramer CB4 none-cyclic
Empirical formula		$C_{58}H_{56}F_{21}N_{32}NaO_{31}$
Formula weight		2119.34
Temperature		220(2) K
Wavelength		0.71073 Å
Crystal size		0.26 × 0.11 × 0.09 mm^3
Crystal habit		colorless prism
Crystal system		Tetragonal
Space group		$P4_2/m$
Unit cell dimensions		a = 18.6306(8) Å α = 90°
		b = 18.6306(8) Å β = 90°
		c = 15.2173(12) Å γ = 90°
Volume		5281.9(5) $Å^3$
Z		2
Density, ρ_{calc}		1.333 g/cm^3
Absorption coefficient, μ		0.134 mm^{-1}
F(000)		2152ē
Diffractometer		Bruker Smart1000 CCD area detector
Radiation source		fine-focus sealed tube, Mo*K*α
Generator power		50 kV, 40 mA
Detector distance		4.939 cm
Detector resolution		8.33 pixels/mm
Total frames		1824
Frame size		512 pixels
Frame width		0.5 °
Exposure per frame		38 sec
Total measurement time		22.88 hours
Data collection method		ω and φ scans
θ range for data collection		1.09 to 20.00°
Index ranges		$-17 \le h \le 17, -17 \le k \le 17, -14 \le l \le 14$
Reflections collected		25719
Independent reflections		2590
Observed reflection, I>2σ(I)		2044
Coverage of independent reflections		99.6 %
Variation in check reflections		? %
Absorption correction		Semi-empirical from equivalents
		SADABS (Sheldrick, 1996)
Max. and min. transmission		0.988 and 0.937
Structure solution technique		direct
Structure solution program		SHELXS-97 (Sheldrick, 1990)
Refinement technique		Full-matrix least-squares on F^2
Refinement program		SHELXL-97 (Sheldrick, 1997)
Function minimized		$\Sigma w(F_o^2 - F_c^2)^2$
Data / restraints / parameters		2590 / 129 / 339
Goodness-of-fit on F^2		1.020
Δ/σ_{max}		0.000
Final R indices:	R_1, I>2σ(I)	0.0779
	wR_2, all data	0.1867
	R_{int}	0.0686
	R_{sig}	0.0389
Weighting scheme		$w = 1/[\sigma^2(F_o^2) + (0.02P)^2 + 29.5P]$,
		$P = [\max(F_o^2, 0) + 2F_o^2]/3$
Largest diff. peak and hole		0.783 and -0.297ē/$Å^3$

$R_1 = \Sigma||F_o|-|F_c||/\Sigma|F_o|$, $wR2 = [\Sigma w(F_o^2-F_c^2)^2/\Sigma w(F_o^2)^2]^{1/2}$

Crystal Structure Information for UM # 1426b

Issued by: Peter Y. Zavalij

Crystal No. & ID	:	**1426b**: Isaacs/Huang Ser from T/H in T xtal-2 - b
Compound name	:	[CB5<0.85TFA]*4.6TFA*4H_2O
Chemical formula	:	$C_{28}H_{30}N_{20}O_{10}\cdot 5.45CF_3COOH\cdot 4H_2O$
Final R_1 [I>2σ(I)]	:	**8.54 %**

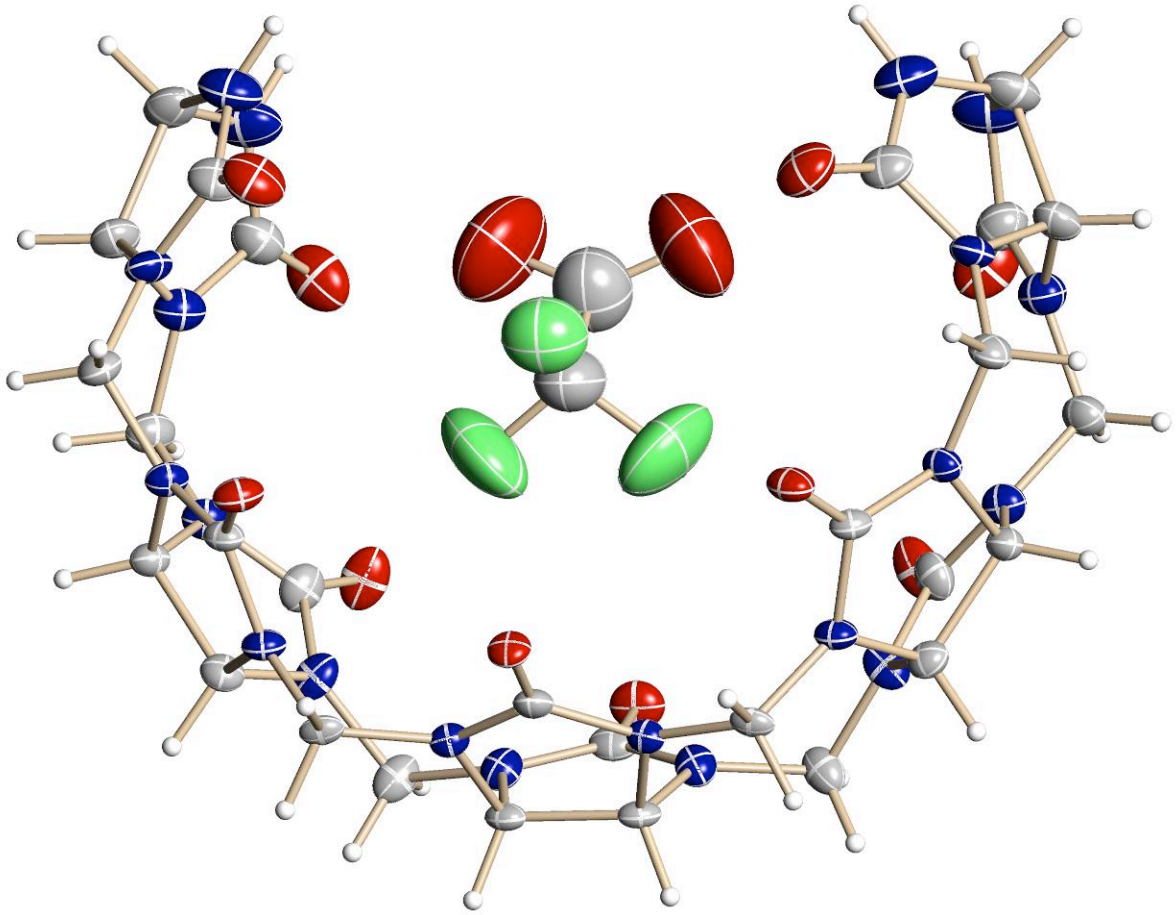

Figure S36. A view of UM#1426 showing the numbering scheme employed. Anisotropic atomic displacement ellipsoids for the non-hydrogen atoms are shown at the 30% probability level. Hydrogen atoms are displayed with an arbitrarily small radius.

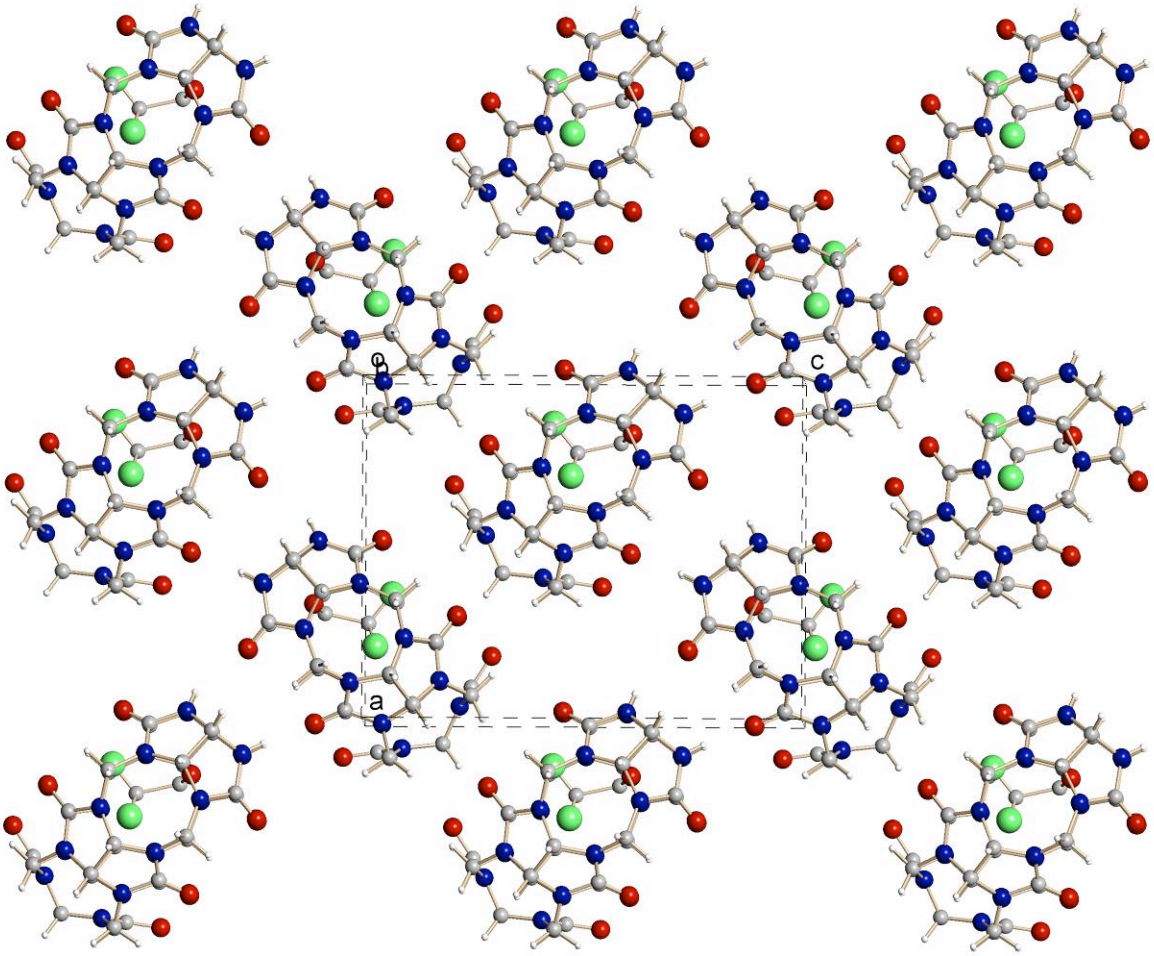

Figure 1. Packing of UM#1426 along **b**-axis revealing chains of H-bonded pentamer.

A colorless prism of $C_{28}H_{30}N_{20}O_{10}\cdot 5.45CF_3COOH\cdot 4H_2O$, approximate dimensions 0.14 × 0.18 × 0.34 mm^3, was used for the X-ray crystallographic analysis. The X-ray intensity data were measured at 220(2) K on a three-circle diffractometer system equipped with Bruker Smart1000 CCD area detector using a graphite monochromator and a MoKα fine-focus sealed tube (λ= 0.71073 Å) operated at 50 kV and 30 mA. The detector was placed at a distance of 4.939 cm from the crystal.

A total of 1818 frames were collected with a scan width of 0.3° in ω and an exposure time of 38 sec/frame using SMART (Bruker, 1999). The total data collection time was 22.80 hours. The frames were integrated with SAINT software package using a narrow-frame integration algorithm. The integration of the data using a Orthorhombic unit cell yielded a total of 28204 reflections to a maximum θ angle of 22.50°, of which 3824 were independent (completeness = 99.4%, R_{int} = 10.58%, R_{sig} = 7.41%) and 2830 were greater than 2σ(I). The final cell dimensions of a = 11.662(4) Å, b = 33.042(11) Å, c = 14.952(5) Å, α= 90°, β= 90°, γ= 90°, V = 5762(3) $Å^3$, are based upon the refinement of the XYZ-centroids of 9031 reflections with 2.2 < θ < 22.3° using SAINT. Analysis of the data showed 0.00 % decay during data collection. Data were corrected for absorption effects with the Semi-empirical from equivalents method using SADABS (Sheldrick, 1996). The minimum and maximum transmission coefficients were 0.917 and 0.976.

The structure was solved and refined using the SHELXS-97 (Sheldrick, 1990) and SHELXL-97 (Sheldrick, 1997) software in the space group *Pnma* with Z = 4 for the formula unit $C_{28}H_{30}N_{20}O_{10}\cdot 5.45CF_3COOH\cdot 4H_2O$. The final anisotropic full-matrix least-squares refinement on F^2 with 326 variables converged at R_1 = 8.54 % for the observed data and wR_2 = 17.91 % for all data. The goodness-of-fit was 1.000. The largest peak on the final difference map was 0.325$\bar{e}/Å^3$ and the largest hole was -0.294$\bar{e}/Å^3$. On the basis of the final model, the calculated density was 1.723 g/cm^3 and F(000), 3031$\bar{e}$.

Comments:

- Data set quality: average
- Twinning: none
- Disorder: substantially disordered solvent – removed using squeeze except guest TFA
- H-atoms refinement: constrained
- Residual density: near disordered groups
- Structure quality: good to average
  Publishable!

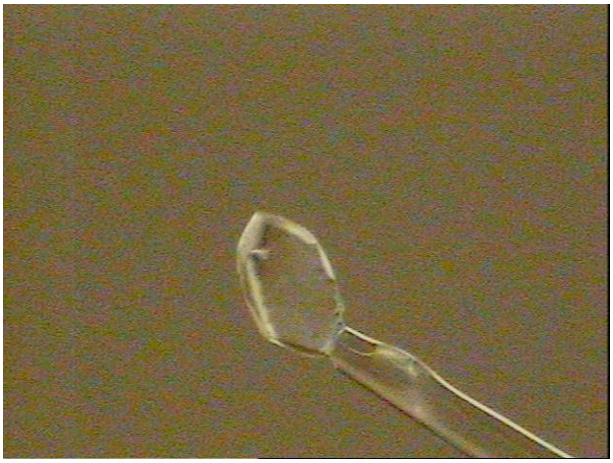

Table 1. Crystal data and structure refinement for UM#1426.

X-ray lab book No.		1426b
Crystal ID		Isaacs/Huang Ser from T/H in T xtal-2 - b
Empirical formula		$C_{28}H_{30}N_{20}O_{10}\cdot 5.45CF_3COOH\cdot 4H_2O$
Formula weight		1494.74
Temperature		220(2) K
Wavelength		0.71073 Å
Crystal size		0.34 × 0.18 × 0.14 mm^3
Crystal habit		colorless prism
Crystal system		Orthorhombic
Space group		Pnma
Unit cell dimensions		a = 11.662(4) Å α = 90°
		b = 33.042(11) Å β = 90°
		c = 14.952(5) Å γ = 90°
Volume		5762(3) $Å^3$
Z		4
Density, ρ_{calc}		1.723 g/cm^3
Absorption coefficient, μ		0.175 mm^{-1}
F(000)		3031ē
Diffractometer		Bruker Smart1000 CCD area detector
Radiation source		fine-focus sealed tube, Mo*K*α
Generator power		50 kV, 30 mA
Detector distance		4.939 cm
Detector resolution		8.33 pixels/mm
Total frames		1818
Frame size		512 pixels
Frame width		0.3 °
Exposure per frame		38 sec
Total measurement time		22.80 hours
Data collection method		ω scans
θ range for data collection		2.72 to 22.50°
Index ranges		$-12 \le h \le 12$, $-35 \le k \le 35$, $-15 \le l \le 15$
Reflections collected		28204
Independent reflections		3824
Observed reflection, I>2σ(I)		2830
Coverage of independent reflections		99.4 %
Variation in check reflections		0.00 %
Absorption correction		Semi-empirical from equivalents
		SADABS (Sheldrick, 1996)
Max. and min. transmission		0.976 and 0.917
Structure solution technique		direct
Structure solution program		SHELXS-97 (Sheldrick, 1990)
Refinement technique		Full-matrix least-squares on F^2
Refinement program		SHELXL-97 (Sheldrick, 1997)
Function minimized		$\Sigma w(F_o^2 - F_c^2)^2$
Data / restraints / parameters		3824 / 84 / 326
Goodness-of-fit on F^2		1.003
Δ/σ_{max}		0.000
Final R indices:	R_1, I>2σ(I)	0.0854
	wR_2, all data	0.1791
	R_{int}	0.1058
	R_{sig}	0.0741
Weighting scheme		$w = 1/[\sigma^2(F_o^2) + (0.002P)^2 + 18.7P]$,
		$P = [\max(F_o^2, 0) + 2F_o^2]/3$
Largest diff. peak and hole		0.325 and -0.294ē/$Å^3$

$R_1 = \Sigma||F_o|-|F_c||/\Sigma|F_o|$, $wR2 = [\Sigma w(F_o^2-F_c^2)^2/\Sigma w(F_o^2)^2]^{1/2}$

Crystal Structure Information for UM # 1513

Issued by: Peter Y. Zavalij

Crystal No. & ID	:	**1513**: Isaacs/WHHuang CB_6 not-cycle in H_2O, MeOH
Compound name	:	CB_6 hydrate
Chemical formula	:	$(C_{34}H_{36}N_{24}O_{12})\cdot 11H_2O\cdot 2HCl$
Final R_1 [I>2σ(I)]	:	**5.65 %**

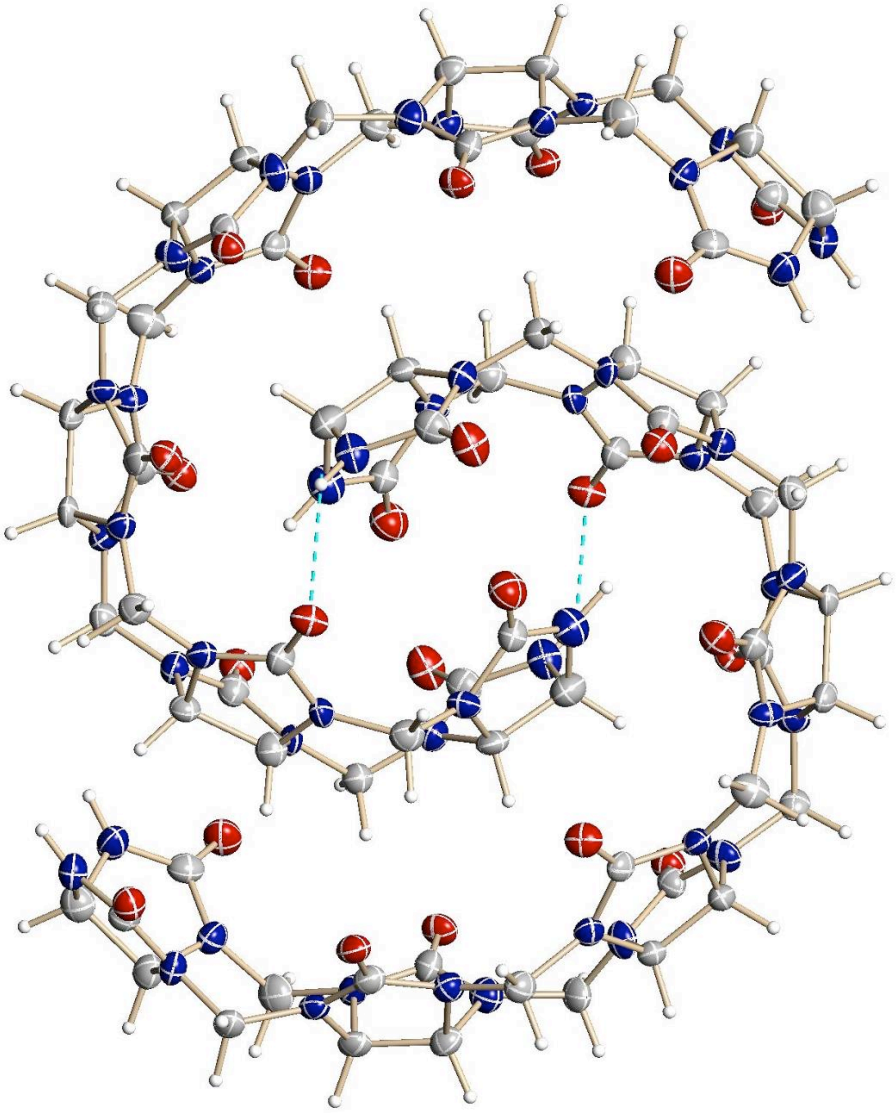

Figure S37. A view of UM#1513 showing the numbering scheme employed. Anisotropic atomic displacement ellipsoids for the non-hydrogen atoms are shown at the 30% probability level. Hydrogen atoms are displayed with an arbitrarily small radius.

A colorless ball of $(C_{34}H_{36}N_{24}O_{12})\cdot 11H_2O\cdot 2HCl$, approximate dimensions 0.08 × 0.225 × 0.25 mm^3, was used for the X-ray crystallographic analysis. The X-ray intensity data were measured at 220(2) K on a three-circle diffractometer system equipped with Bruker Smart1000 CCD area detector using a graphite monochromator and a MoKα fine-focus sealed tube (λ= 0.71073 Å) operated at 50 kV and 30 mA. The detector was placed at a distance of 4.950 cm from the crystal.

A total of 1381 frames were collected with a scan width of 0.3° in ω and an exposure time of 38 sec/frame using SMART (Bruker, 1999). The total data collection time was 17.3 hours. The frames were integrated with SAINT software package using a narrow-frame integration algorithm. The integration of the data using a Orthorhombic unit cell yielded a total of 51174 reflections to a maximum θ angle of 22.50°, of which 6402 were independent (completeness = 99.5%, R_{int} = 8.22%, R_{sig} = 6.71%) and 3874 were greater than 2σ(I). The final cell dimensions of a = 24.119(2) Å, b = 12.8676(13) Å, c = 31.795(3) Å, α= 90°, β= 90°, γ= 90°, V = 9867.6(17) $Å^3$, are based upon the refinement of the XYZ-centroids of 6864 reflections with 2.1 < θ < 20.3° using SAINT. Analysis of the data showed 0 % decay during data collection. Data were corrected for absorption effects with the Semi-empirical from equivalents method using SADABS (Sheldrick, 1996). The minimum and maximum transmission coefficients were 0.932 and 0.981.

The structure was solved and refined using the SHELXS-97 (Sheldrick, 1990) and SHELXL-97 (Sheldrick, 1997) software in the space group *Pbca* with Z = 8 for the formula unit $(C_{34}H_{36}N_{24}O_{12})\cdot 11H_2O\cdot 2HCl$. The final anisotropic full-matrix least-squares refinement on F^2 with 631 variables converged at R_1 = 5.65 % for the observed data and wR_2 = 12.50 % for all data. The goodness-of-fit was 1.000. The largest peak on the final difference map was 0.297$\bar{e}/Å^3$ and the largest hole was -0.269$\bar{e}/Å^3$. On the basis of the final model, the calculated density was 1.675 g/cm^3 and F(000), 5200$\bar{e}$.

Overall structure quality considerations:

1. Strong data set, no disorder, R_1 4% maximum. Publishable quality.
2. **Good data set, perhaps some minor disorder, R_1 6% maximum. Publishable quality.**
3. Average data set and/or easily modeled disorder or twinning. Publishable with care.
4. Weak data and/or major disorder or twinning that is not easily modeled. Publishable in some cases.
5. Very weak data and/or unexplained features of data or model. Not of publishable quality.

A structure with a quality factor of 4 or 5 should not be used for a regulatory document without prior consultation.

Comments:

- Data quality:	good (barely diffract to 45° 2θ)
- Twinning:	none
- Disorder:	solvent – squeezed out using Platon
- H-atoms:	constrained geometry as riding on attached atom (A) Uiso(H)=1.5*U_{iso}(A) for CH_3 and 1.2*U_{iso}(A) for other groups
- Residual density:	near heavy atoms & in the middle of the bonds
- Structure quality:	good to average
Publishable	Yes

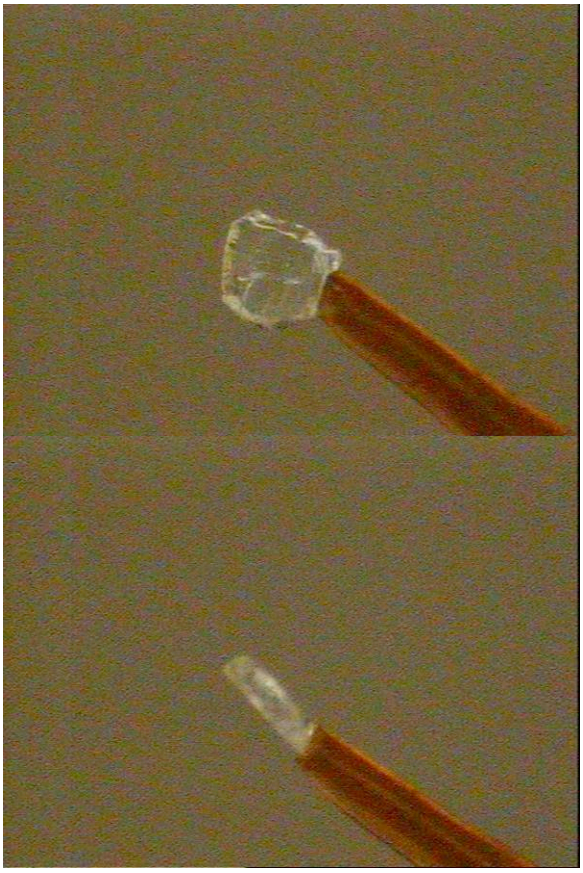

Table 1. Crystal data and structure refinement for UM#1513.

X-ray lab book No.		1513
Crystal ID		Isaacs/WHHuang CB6 not-cycle in H2O, MeOH
Empirical formula		$(C_{34}H_{36}N_{24}O_{12})\cdot 11H_2O\cdot 2HCl$
Formula weight		1243.96
Temperature		220(2) K
Wavelength		0.71073 Å
Crystal size		0.25 × 0.225 × 0.08 mm^3
Crystal habit		colorless ball
Crystal system		Orthorhombic
Space group		*Pbca*
Unit cell dimensions		a = 24.119(2) Å α = 90°
		b = 12.8676(13) Å β = 90°
		c = 31.795(3) Å γ = 90°
Volume		9867.6(17) $Å^3$
Z		8
Density, ρ_{calc}		1.675 g/cm^3
Absorption coefficient, μ		0.243 mm^{-1}
F(000)		5200ē
Diffractometer		Bruker Smart1000 CCD area detector
Radiation source		fine-focus sealed tube, MoKα
Generator power		50 kV, 30 mA
Detector distance		4.950 cm
Detector resolution		8.33 pixels/mm
Total frames		1381
Frame size		512 pixels
Frame width		0.3 °
Exposure per frame		38 sec
Total measurement time		17.3 hours
Data collection method		ω and φ scans
θ range for data collection		2.56 to 22.50°
Index ranges		$-24 \le h \le 25$, $-13 \le k \le 13$, $-34 \le l \le 34$
Reflections collected		51174
Independent reflections		6402
Observed reflection, I>2σ(I)		3874
Coverage of independent reflections		99.5 %
Variation in check reflections		0 %
Absorption correction		Semi-empirical from equivalents
		SADABS (Sheldrick, 1996)
Max. and min. transmission		0.981 and 0.932
Structure solution technique		direct
Structure solution program		SHELXS-97 (Sheldrick, 1990)
Refinement technique		Full-matrix least-squares on F^2
Refinement program		SHELXL-97 (Sheldrick, 1997)
Function minimized		$\Sigma w(F_o^2 - F_c^2)^2$
Data / restraints / parameters		6402 / 3 / 631
Goodness-of-fit on F^2		1.000
Δ/σ_{max}		0.000
Final R indices:	R_1, I>2σ(I)	0.0565
	wR_2, all data	0.1250
	R_{int}	0.0822
	R_{sig}	0.0671
Weighting scheme		$w = 1/[\sigma^2(F_o^2) + (0.02P)^2 + 13.15P]$,
		$P = [\max(F_o^2, 0) + 2F_o^2]/3$
Largest diff. peak and hole		0.297 and -0.269ē/$Å^3$

$R_1 = \Sigma||F_o|-|F_c||/\Sigma|F_o|$, $wR2 = [\Sigma w(F_o^2-F_c^2)^2/\Sigma w(F_o^2)^2]^{1/2}$

Chapter5: Nor-Seco-Cucurbit[6]uril Functions as an Aldehyde Reactive Cucurbituril Synthon – Supporting Information

Angew. Chem.

by *Wei-Hao Huang, Peter Y. Zavalij, and Lyle Isaacs**

Department of Chemistry and Biochemistry, University of Maryland, College Park, MD 20742

Table of Contents **Pages**

Experimental Section.

General. The guests used in this study were purchased from commercial suppliers and were used as their HCl salts. Melting points were measured on a Meltemp apparatus in open capillary tubes and are uncorrected. IR spectra were recorded on Thermo Nicolet IR200 spectrometer and are reported in cm^{-1}. NMR spectra were measured on spectrometers operating at 400, 500, or 600 MHz for ^{1}H and 100 or 125 MHz for ^{13}C. Mass spectrometry was performed using a VG 7070E magnetic sector instrument by fast atom bombardment (FAB) using the indicated matrix or on a JEOL AccuTOF electrospray instrument. Computational results were obtained using Spartan 02 running on a Macintosh personal computer.

Preparation, Purification and Characterization of ns-CB[6]. A mixture of glycoluril (1.42 g, 9.99 mmol), paraformaldehyde (0.50 g, 16.69 mmol), and conc. HCl (4 mL) was heated at 50 ºC for 3 days. The resulting solution was separated by centrifugation and precipated by pouring into MeOH to yield a crude solid (1300 mg). Purification of the mixture was achieved by chromatography on a Dowex 50WX2 column equilibrated with 1:1 formic acid:water. The sample was loaded onto the column as a solution in the eluent (88% HCOOH: (0.2M HCl/H_2O), 1:1, v:v). The fractions of the column were collected and the solvent was removed by rotary evaporation. The resulting solid was washed with MeOH to remove soluble impurities. The CB[6]:*ns*-CB[6] ratio in this crude solid can vary depending on column efficiency. It is possible to decrease the amount of CB[6] by recrystallization

from TFA. Final purification of samples containing mainly *ns*-CB[6] can be achieved by suspending in water containing enough hexanediammonium ion to complex the CB[6] impurity. The heterogenous mixture was then centrifuged and the solid obtained by decanting the supernatant. The solid was washed with several portions of water and dried at high vacuum overnight (47 mg, 3%). M.p. > 300 ºC. IR (KBr, cm^{-1}): 3271w, 1726s, 1466s, 1414s, 1375s, 1326s, 1149s, 964s, 667s, 617s, 796s. ^{1}H NMR (400 MHz, 35% DCl): 5.69 (d, J = 8.8, 2H), 5.64 (d, J = 8.8, 2H), 5.55-5.35 (m, 18H), 5.17 (d, J = 16.0, 1H), 4.44 (d, J = 16.0, 1H), 4.40-4.20 (m, 10H). ^{13}C NMR (100 MHz, 35% DCl, ext. dioxane reference): 159.3, 159.0, 155.9, 155.8, 155.6, 73.2, 69.9, 69.8, 69.7, 69.6, 67.6, 53.6, 51.3, 51.2, 50.9, 50.7. (only 16 of the 19 expected resonances were observed). MS (ES): *m/z* 562 (100, [M + *p*-xylenediamine + 2H]$^{2+}$, *m/z* spacing = 0.5 confirmed for molecular ion).

Compound **2**. Compound **1** (100 mg, 0.10 mmol) was dissolved in HCl (0.2 mL) and *o*-phthaldialdehyde (13.4 mg, 0.10 mmol) was added to the mixture. The reaction mixture was stirred at room temperature for two days. The reaction mixture was poured into MeOH (5 mL), the solid isolated by filtration, and dried overnight at high vacuum. The crude solid (80 mg), was recrystallized from TFA (2.6 mL) to yield **2** (64 mg, 57%) as a white solid. IR (neat, cm^{-1}): 3474w, 3014s, 2926s, 1726s, 1463s, 1416s, 1376s, 1326s, 1293s, 1225s, 1175s, 962s, 795s, 755s, 671s, 628s. ^{1}H NMR (400 MHz, D_2O): 7.35 (br, 2H), 7.29 (br, 2H), 6.70 (s, 2H), 5.65-5.35 (m, 22H), 4.25-4.00 (d, 10H), 2.34 (d, J = 12.0, 1H). ^{13}C NMR (125 MHz, D_2O): 163.4, 160.6, 157.8, 157.0, 135.3, 131.0, 125.4, 118.2, 115.9, 85.0, 71.5, 71.4, 71.2, 71.0, 69.7, 53.1, 52.7,

52.2, 51.8. (not all of the 23 expected resonances were observed). ES-MS: *m*/*z* 1101 (100, $[M + H]^+$: ($[M + H]^+$, $C_{43}H_{40}N_{24}$, calcd 1100.32). X-ray crystal structure (from TFA).

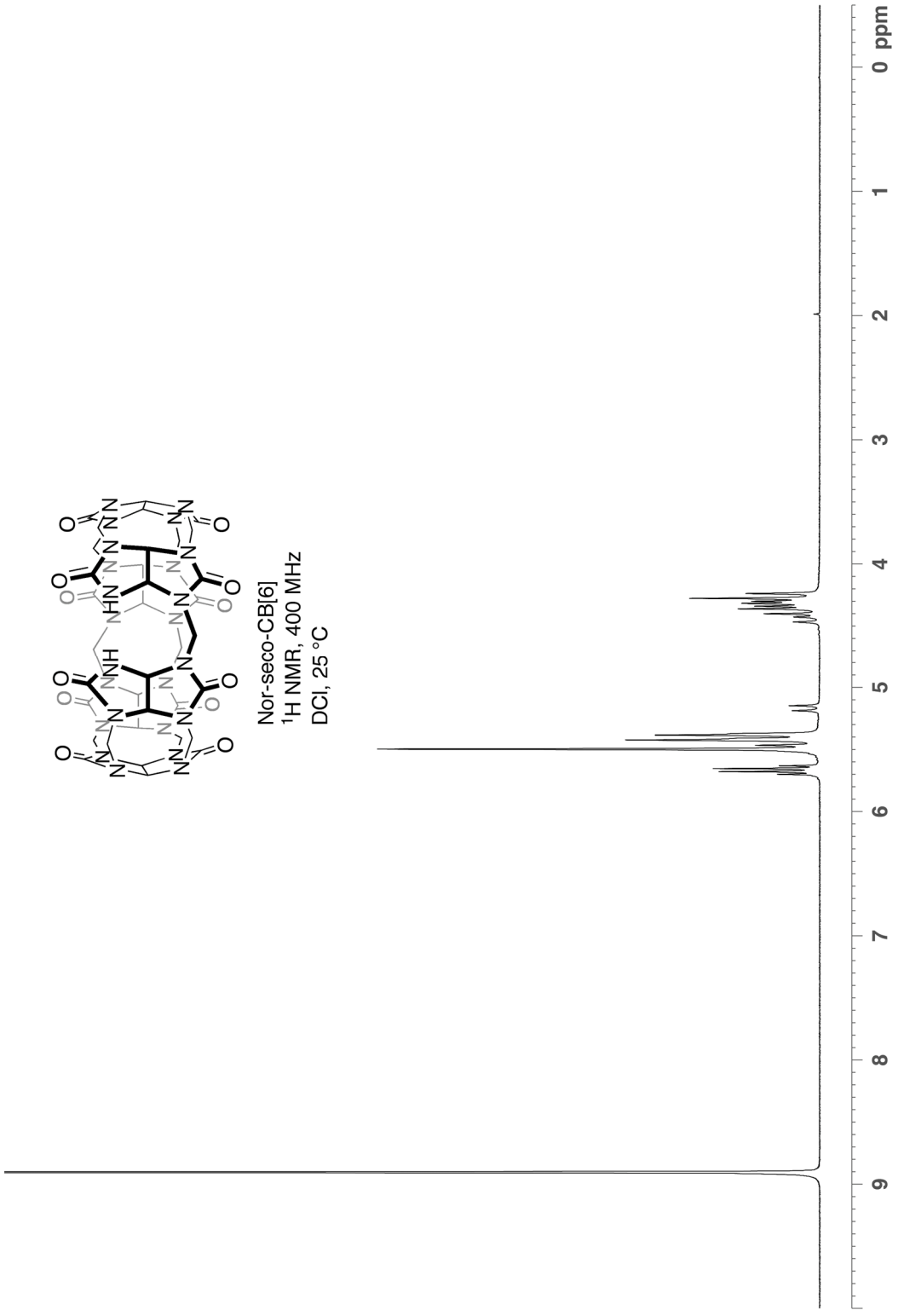

Figure S1. ^{1}H NMR spectrum recorded for *ns*-CB[6] (400 MHz, 35% DCl, 25 ºC).

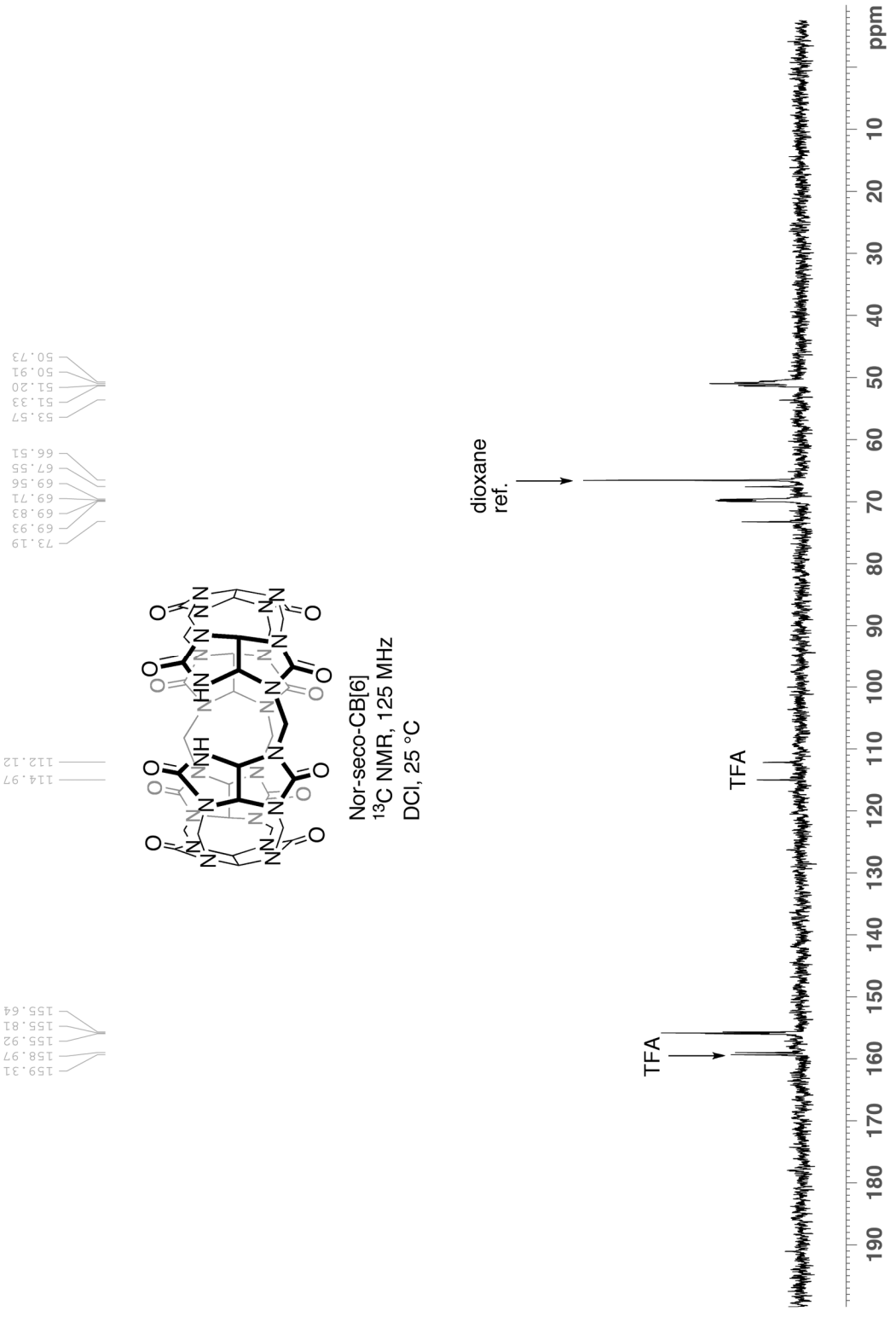

Figure S2. ^{13}C NMR spectrum recorded for *ns*-CB[6] (125 MHz, 35% DCl, 25 ºC).

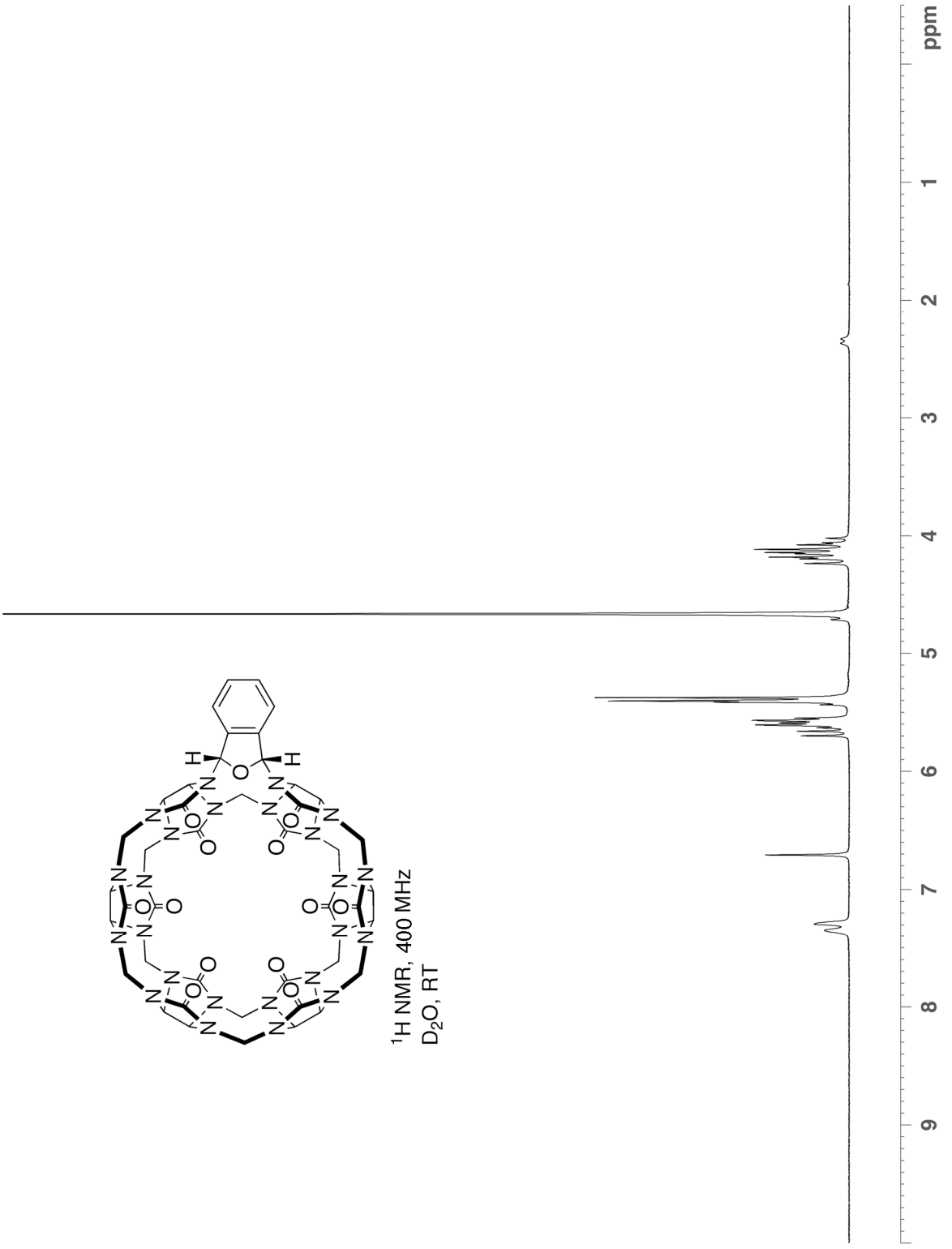

Figure S3. ^{1}H NMR spectrum recorded for **2** (400 MHz, D_2O, 25 ºC).

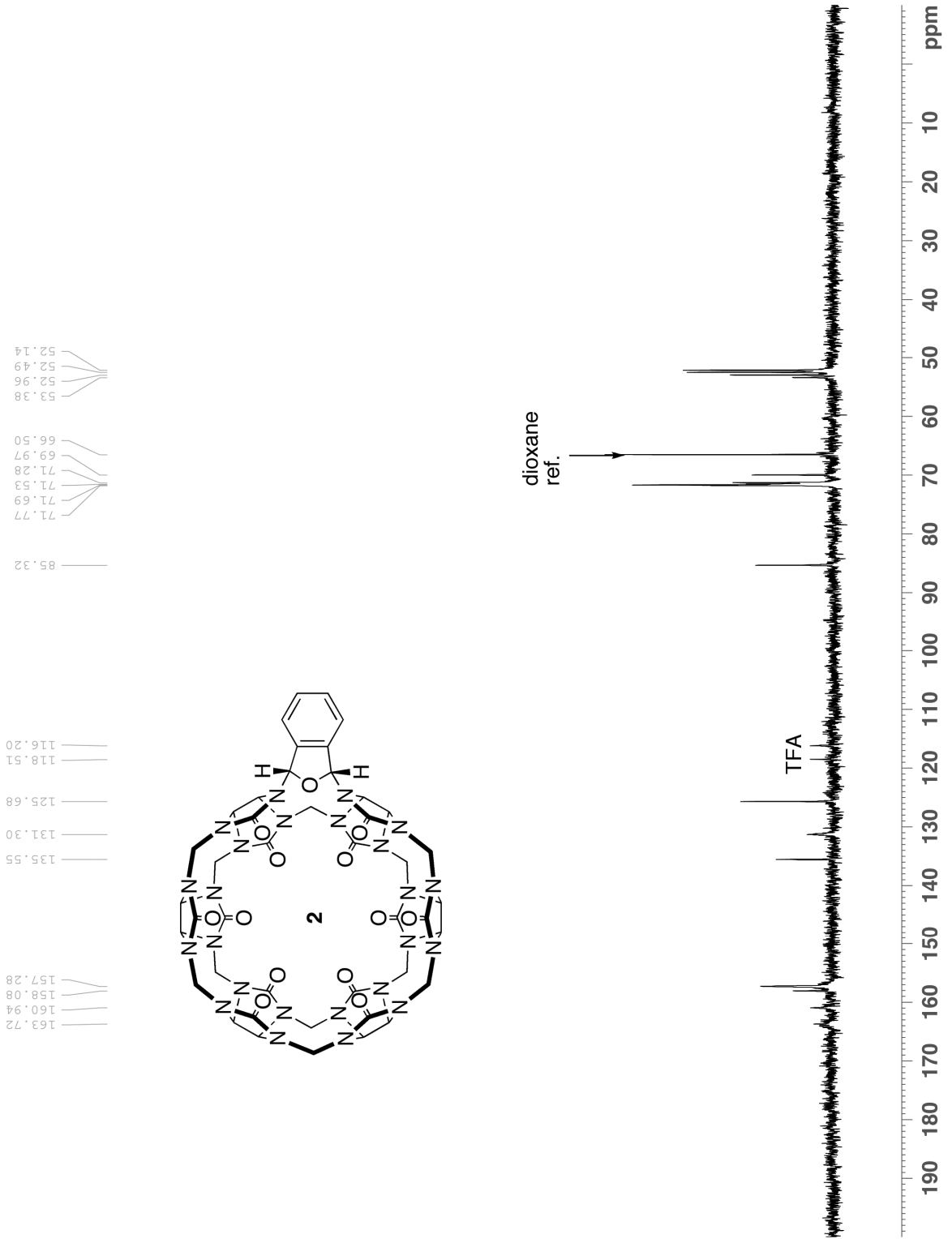

Figure S4. ^{13}C NMR spectrum recorded for **2** (125 MHz, D_2O, 25 ºC).

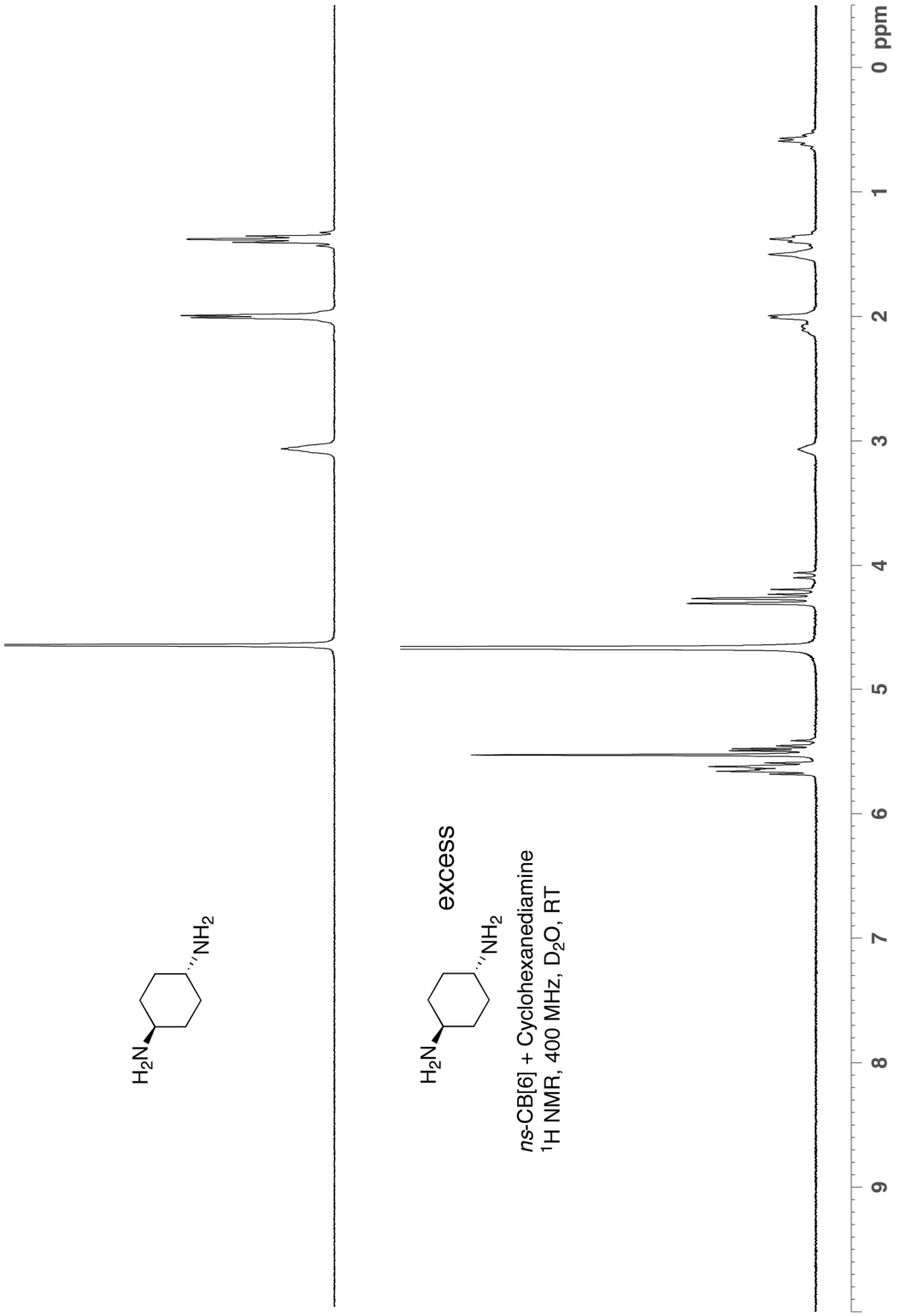

Figure S5. ^{1}H NMR spectra recorded for cyclohexanediamine and its complex with *ns*-CB[6] (400 MHz, D_2O, 25 ºC).

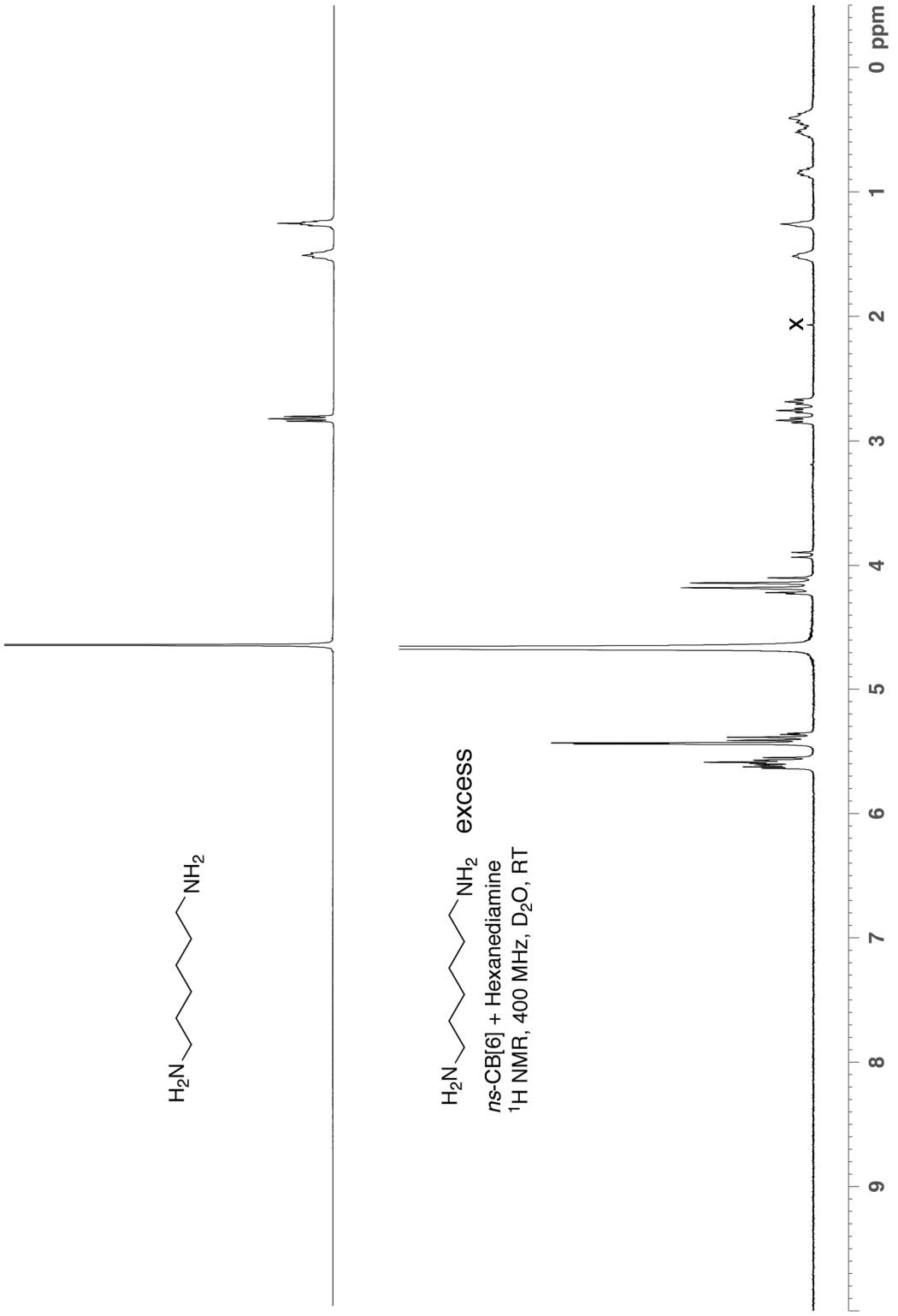

Figure S6. ^{1}H NMR spectra recorded for hexanediamine and its complex with *ns*-CB[6] (400 MHz, D_2O, RT, x = trace acetone impurity).

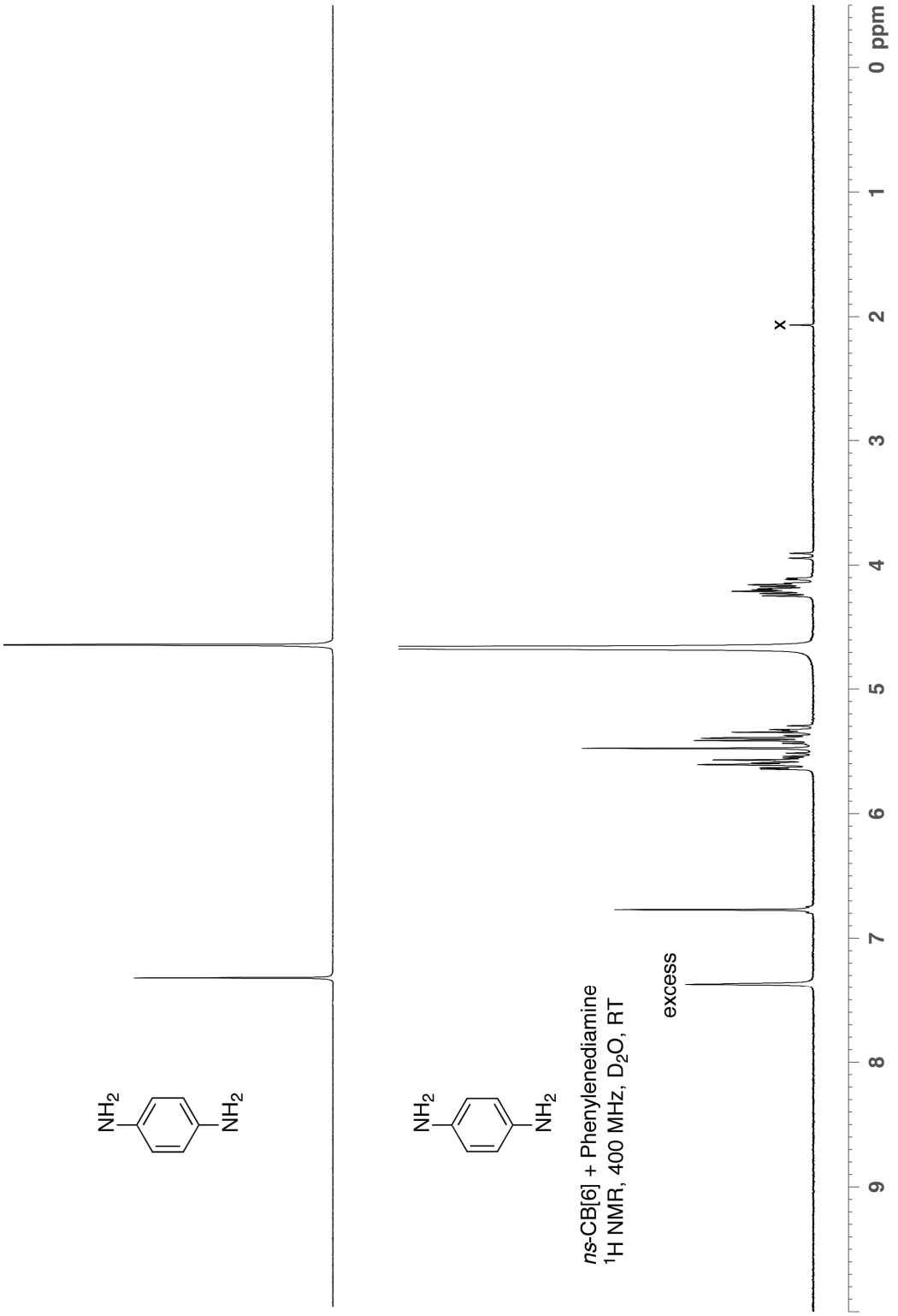

Figure S7. ^{1}H NMR spectra recorded for phenylenediamine and its complex with *ns*-CB[6] (400 MHz, D_2O, RT, x = trace acetone impurity).

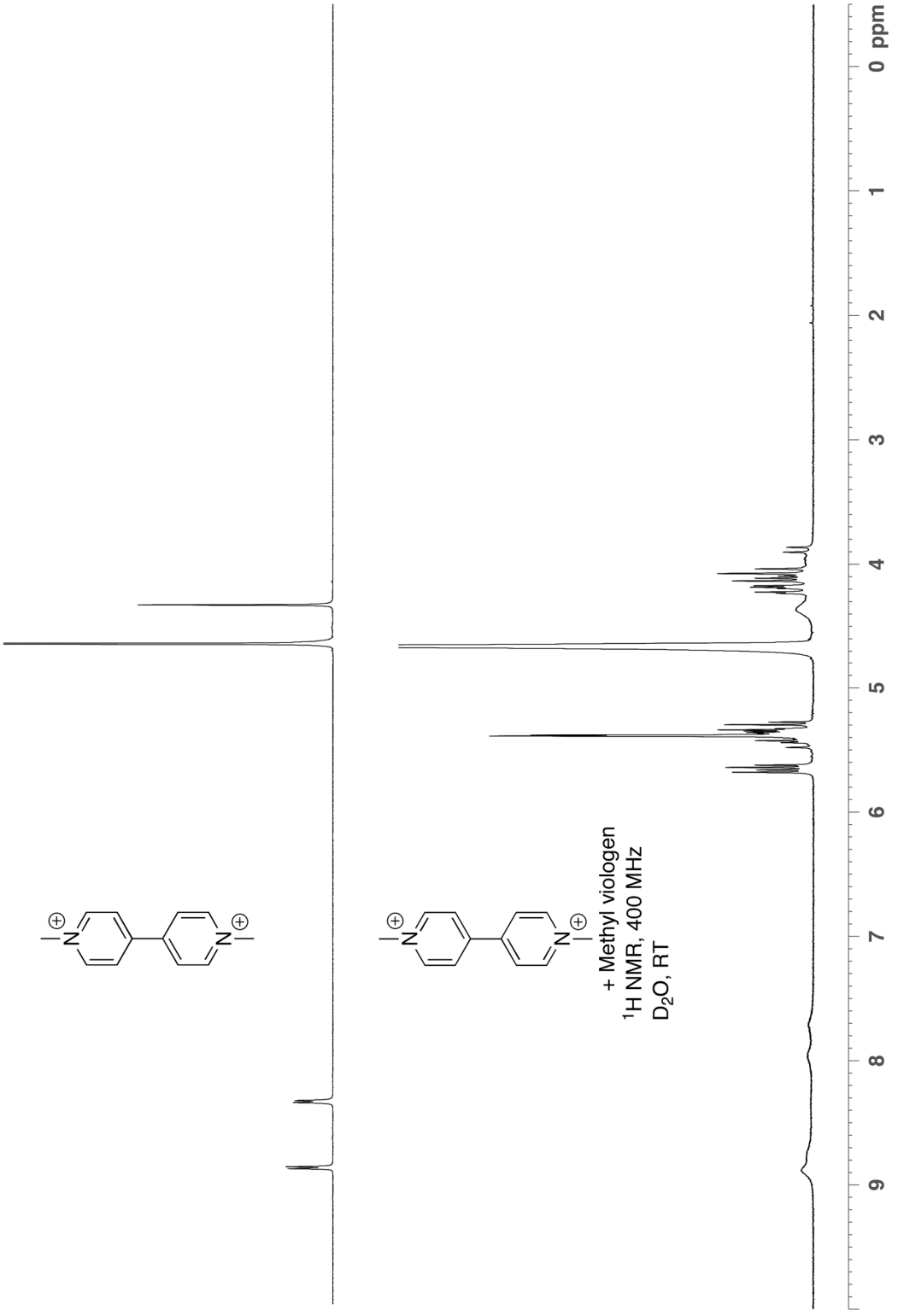

Figure S8. ^{1}H NMR spectra recorded for methyl viologen and its complex with *ns*-CB[6] (400 MHz, D_2O, RT).

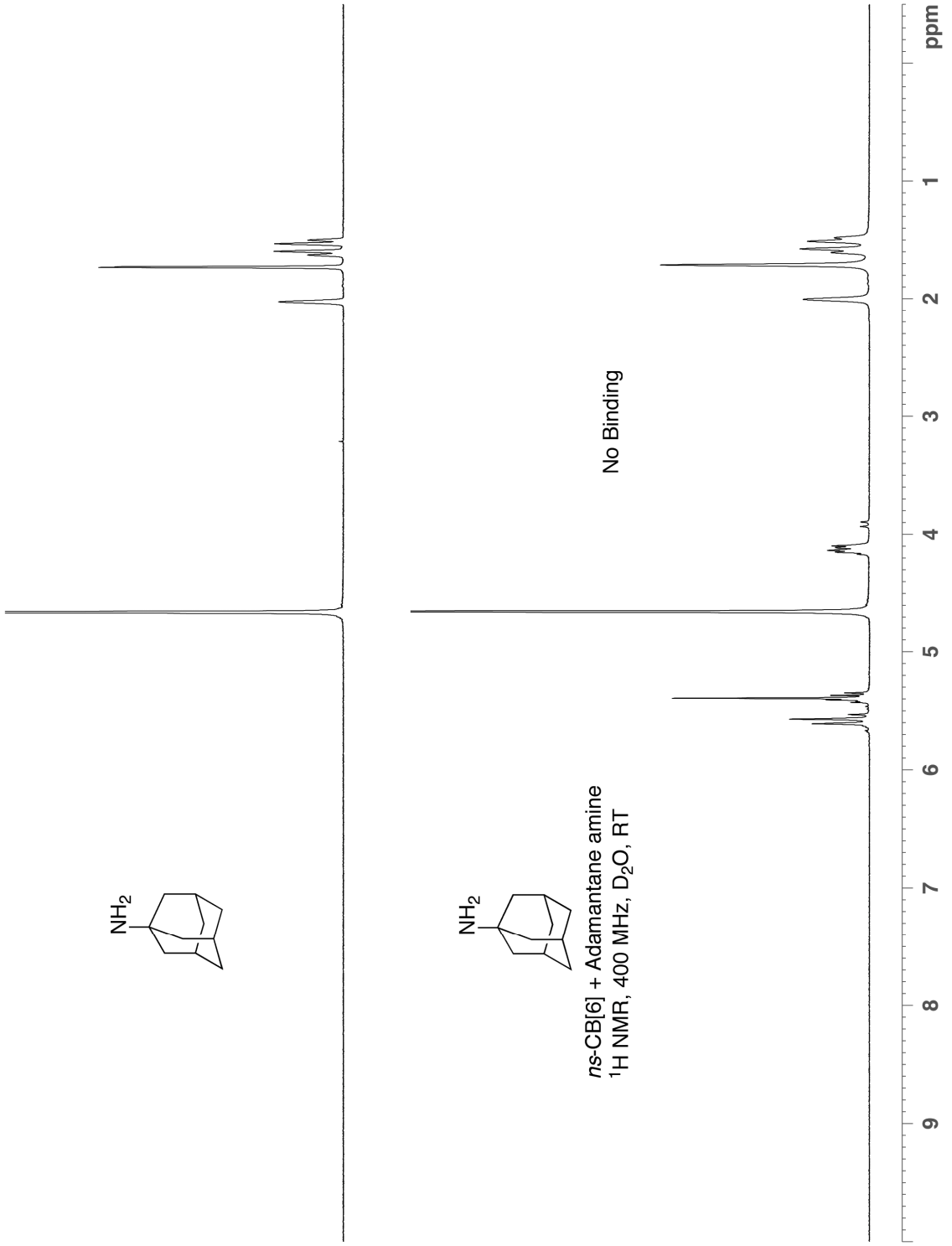

Figure S9. ^{1}H NMR spectra recorded for 1-aminoadamantane and its non-binding mixture with *ns*-CB[6] (400 MHz, D_2O, RT).

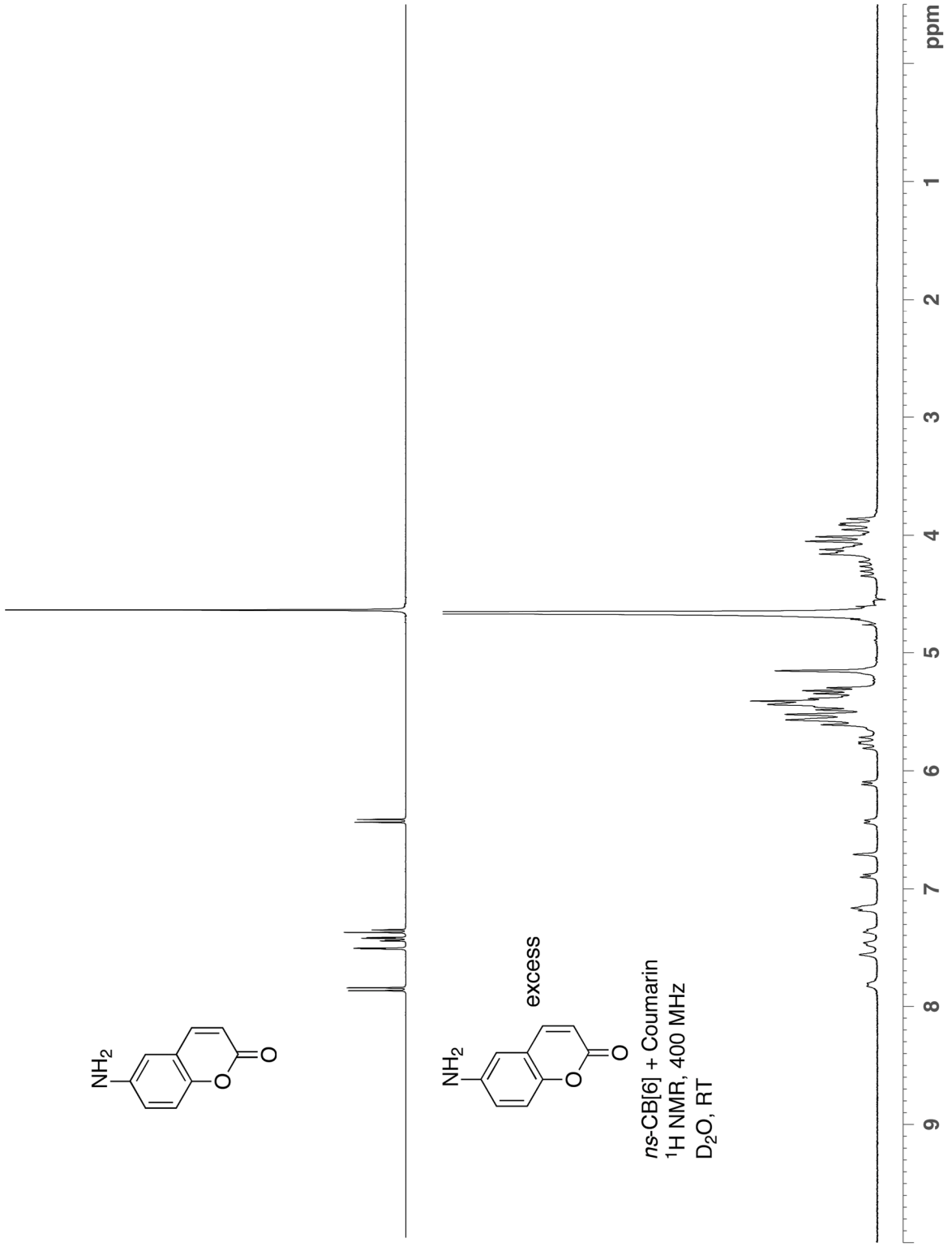

Figure S10. ^{1}H NMR spectra recorded for aminocoumarin and its complex with *ns*-CB[6] (400 MHz, D_2O, RT).

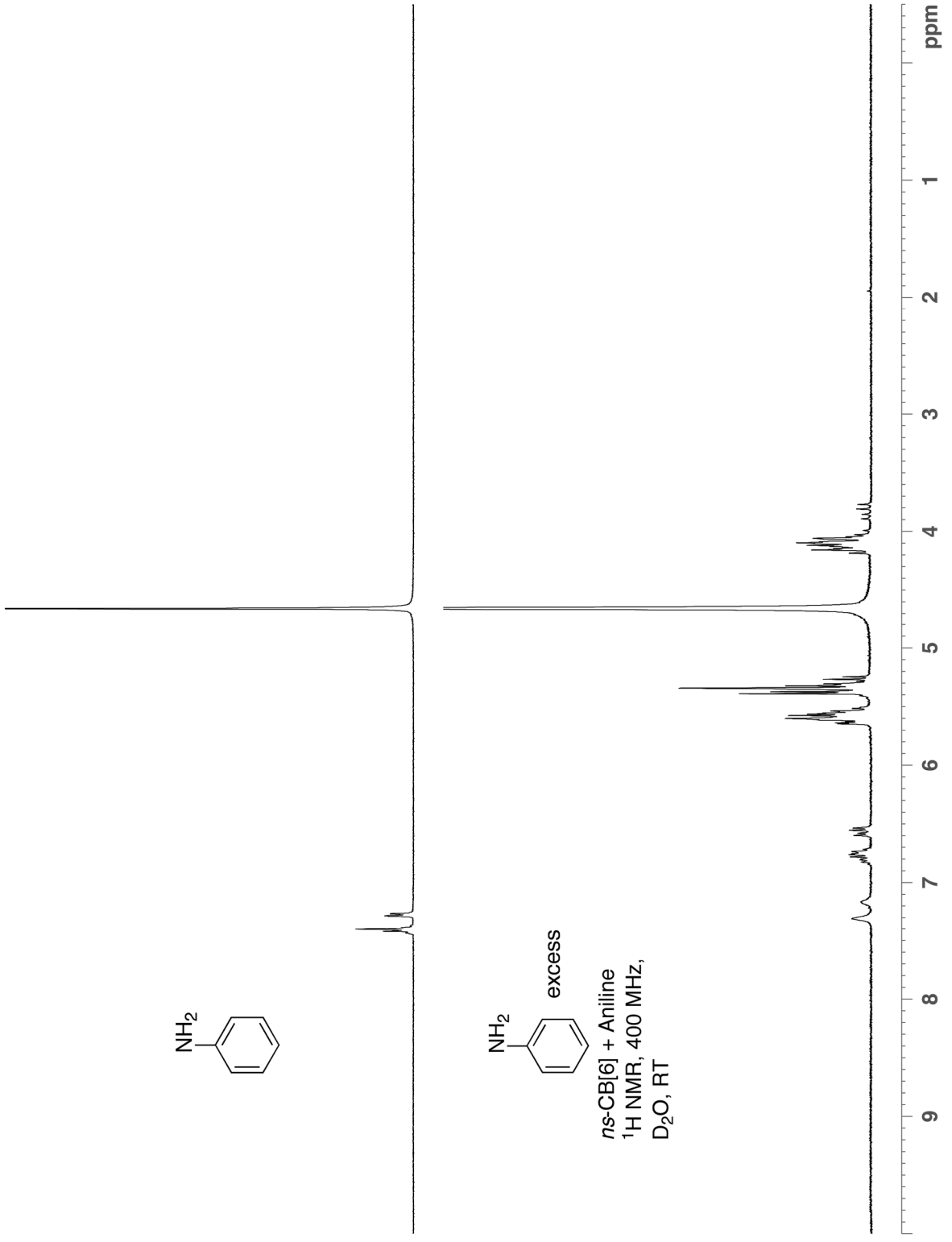

Figure S11. ^{1}H NMR spectra recorded for aniline and its complex with *ns*-CB[6] (400 MHz, D_2O, RT). The ratio of the two diastereomers is 67:33.

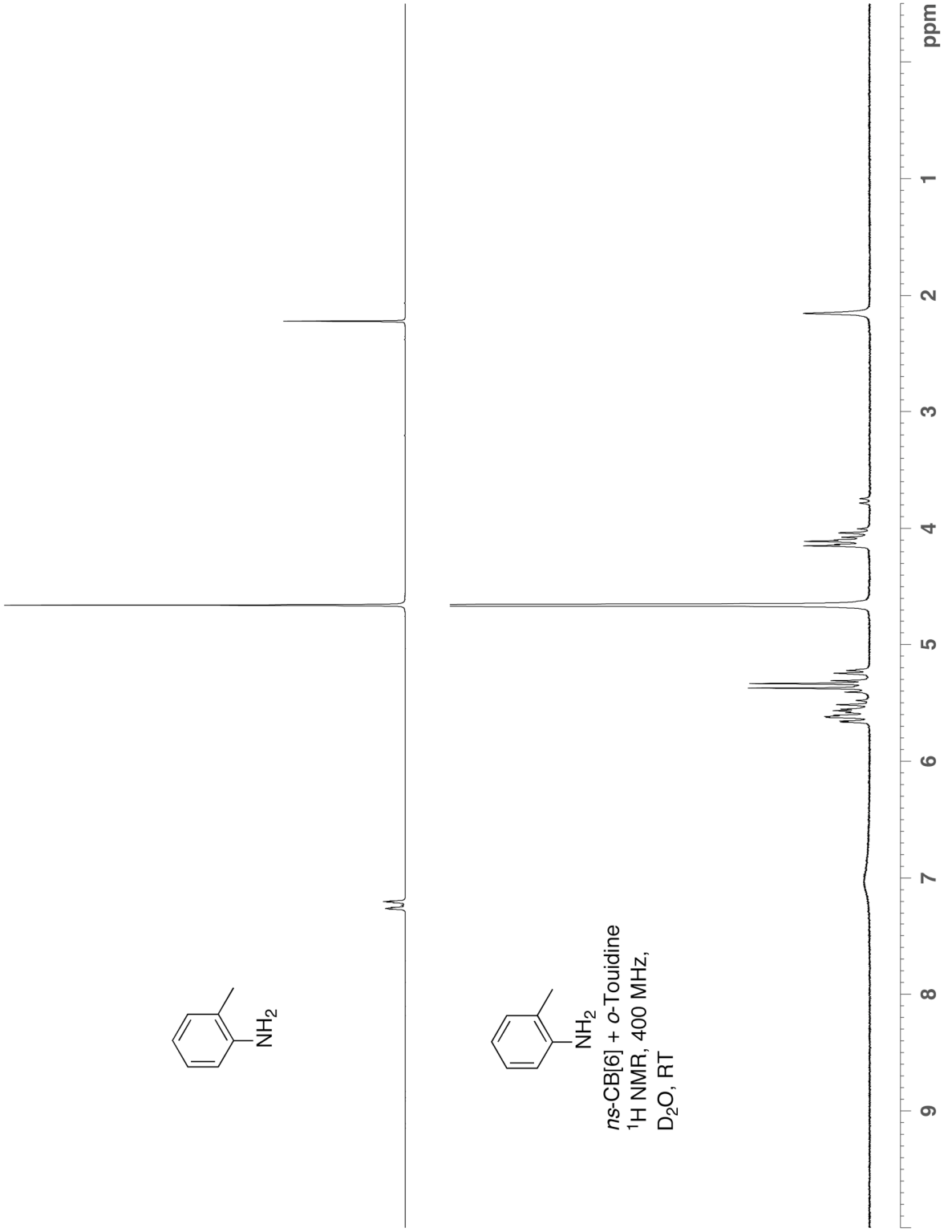

Figure S12. ^{1}H NMR spectra for *o*-toluidine and its mixture with *ns*-CB[6] (400 MHz, D_2O, RT).

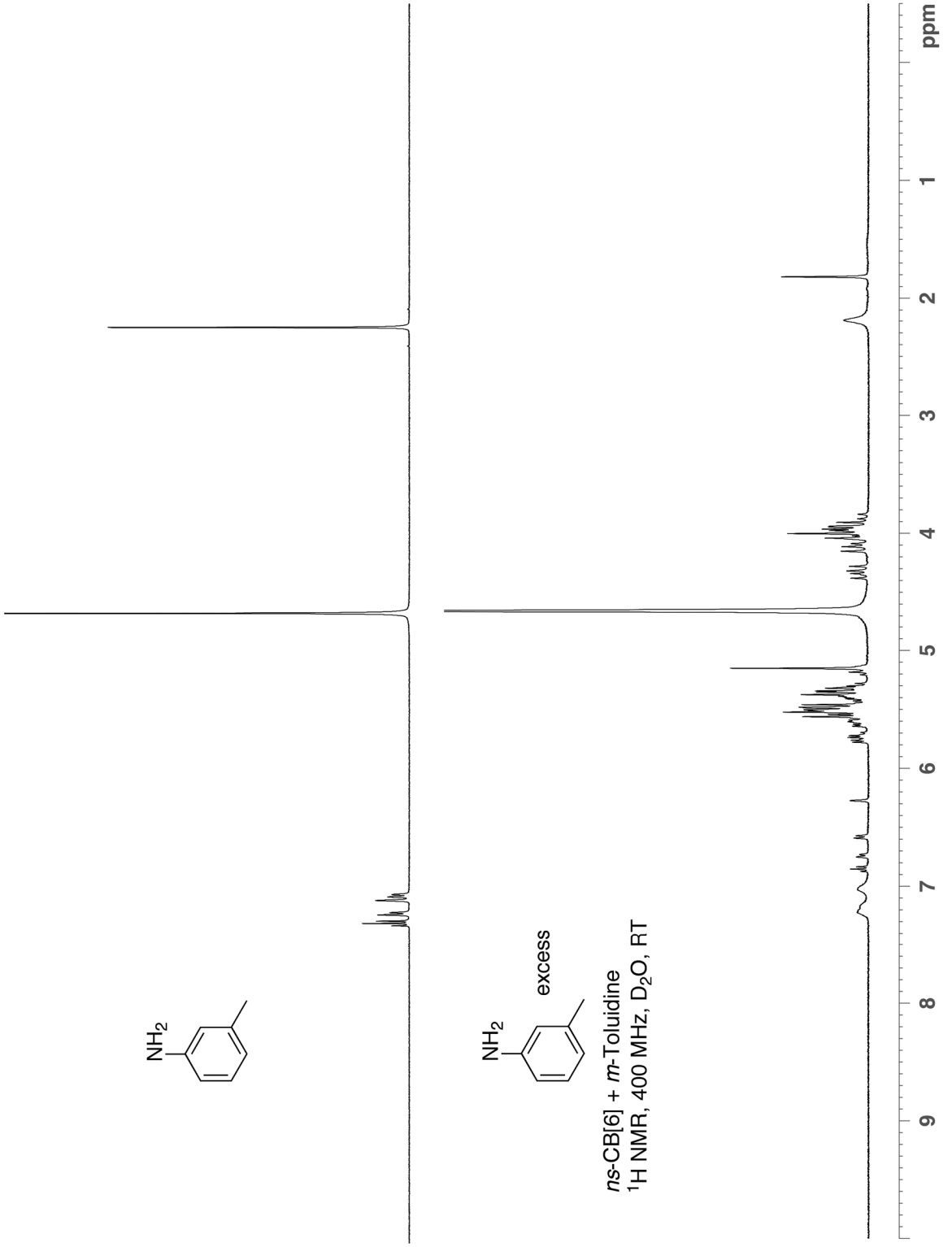

Figure S13. ^{1}H NMR spectra recorded for *m*-toluidine and its complex with *ns*-CB[6] (400 MHz, D_2O, RT).

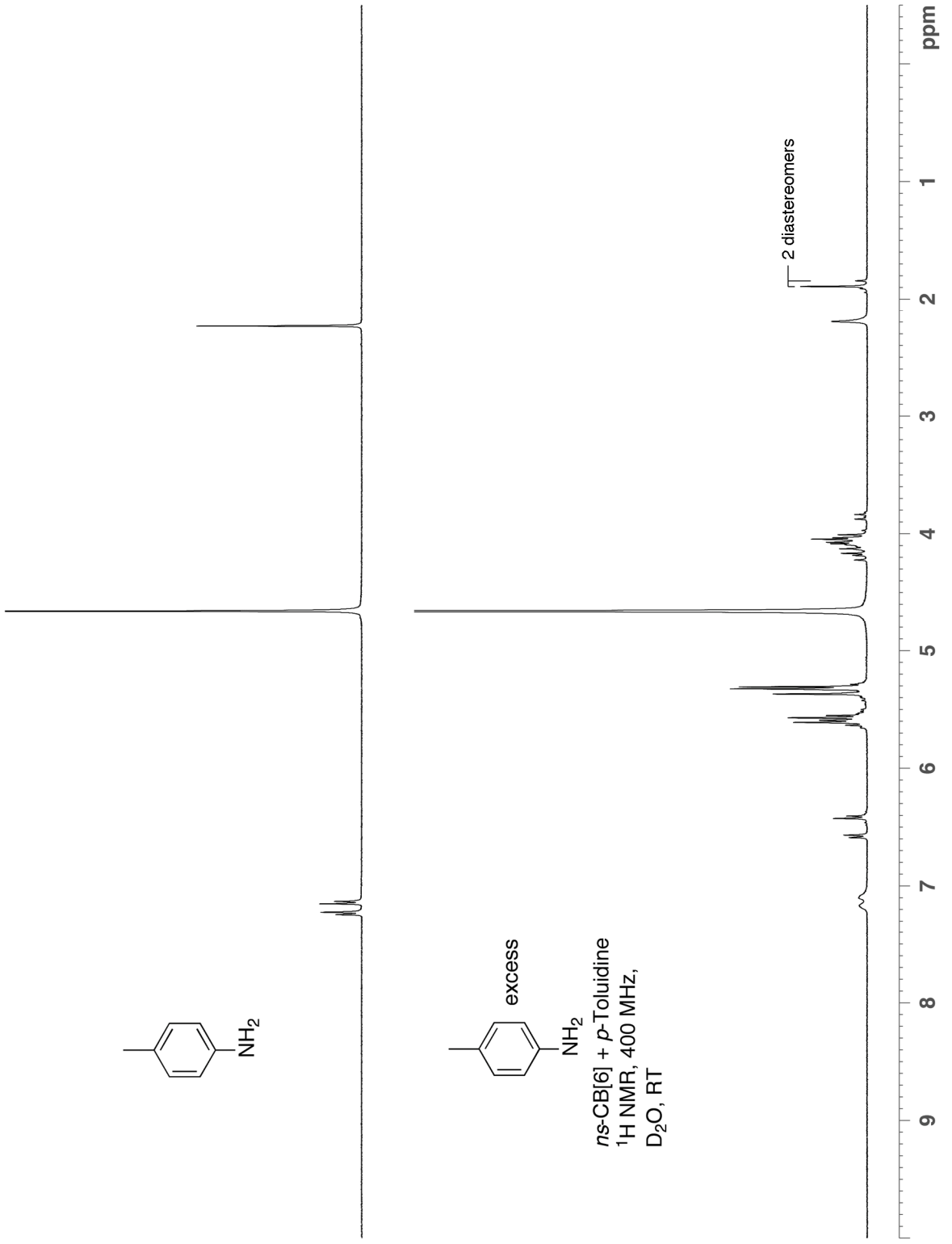

Figure S14. ^{1}H NMR spectra recorded for *p*-toluidine and its complex with *ns*-CB[6] (400 MHz, D_2O, RT). The ratio of the two diastereomers is 76:24.

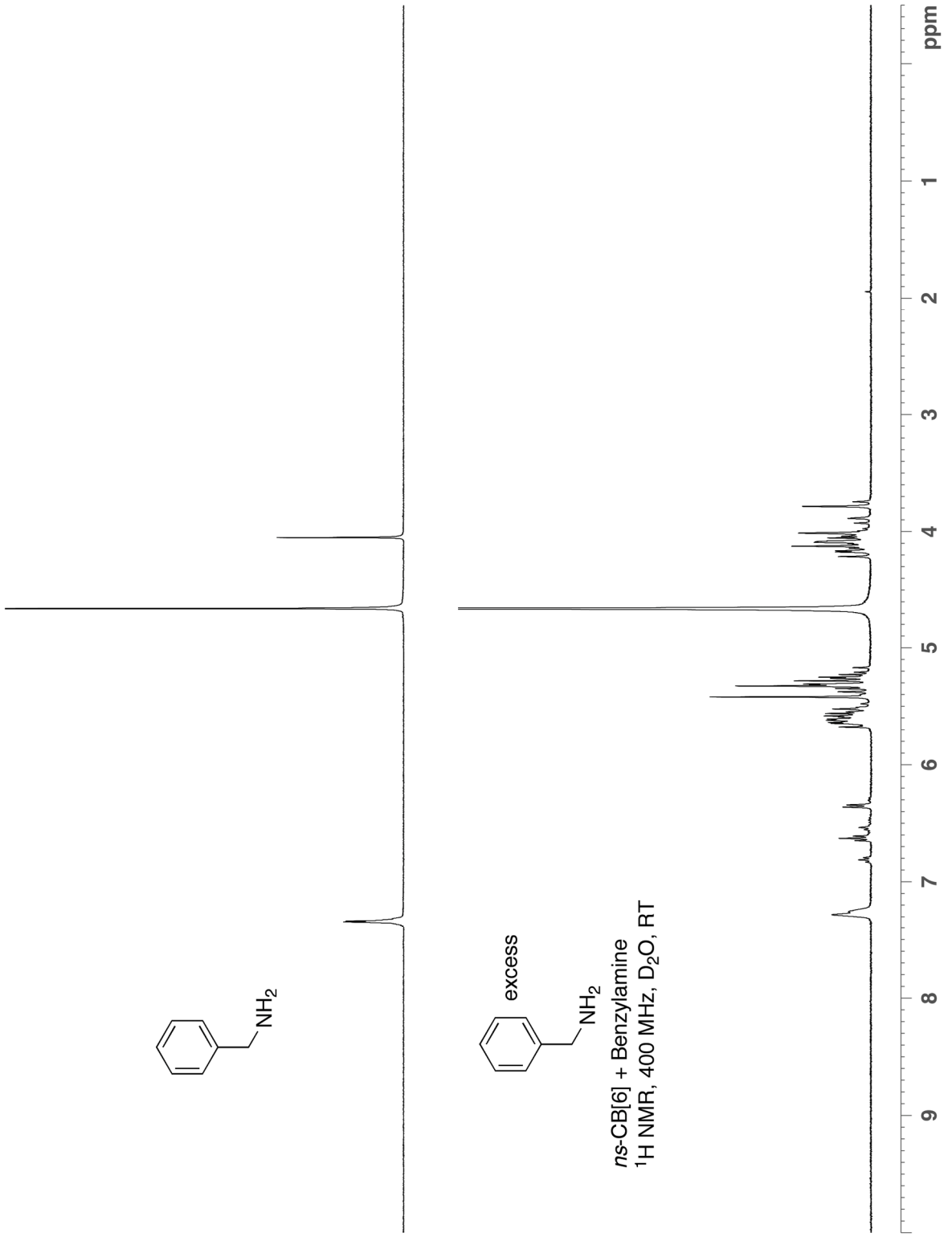

Figure S15. ^{1}H NMR spectra recorded for benzylamine and its complex with *ns*-CB[6] (400 MHz, D_2O, RT).

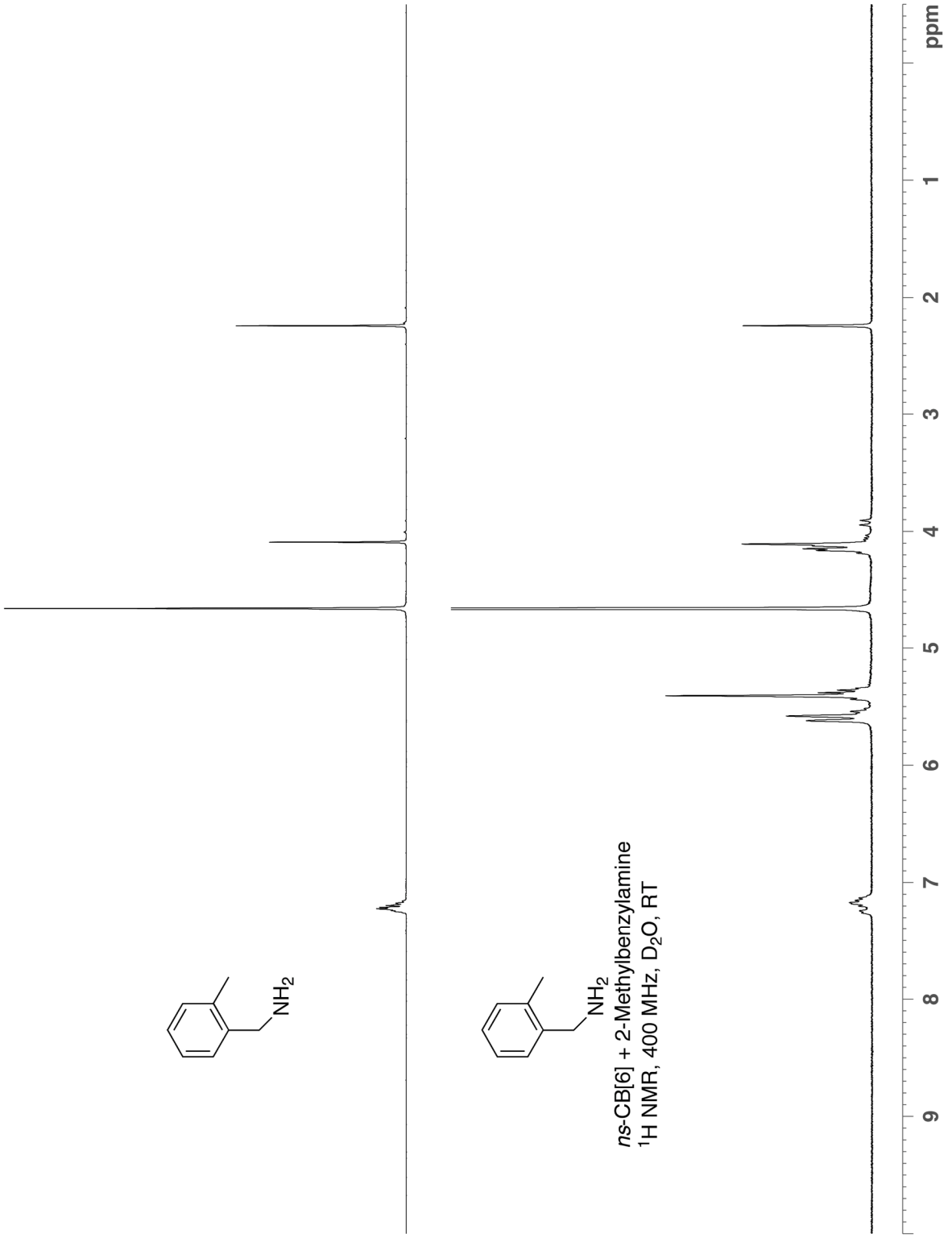

Figure S16. ^{1}H NMR spectrum recorded for 2-methylbenzylamine and when mixed with *ns*-CB[6] (400 MHz, D_2O, RT).

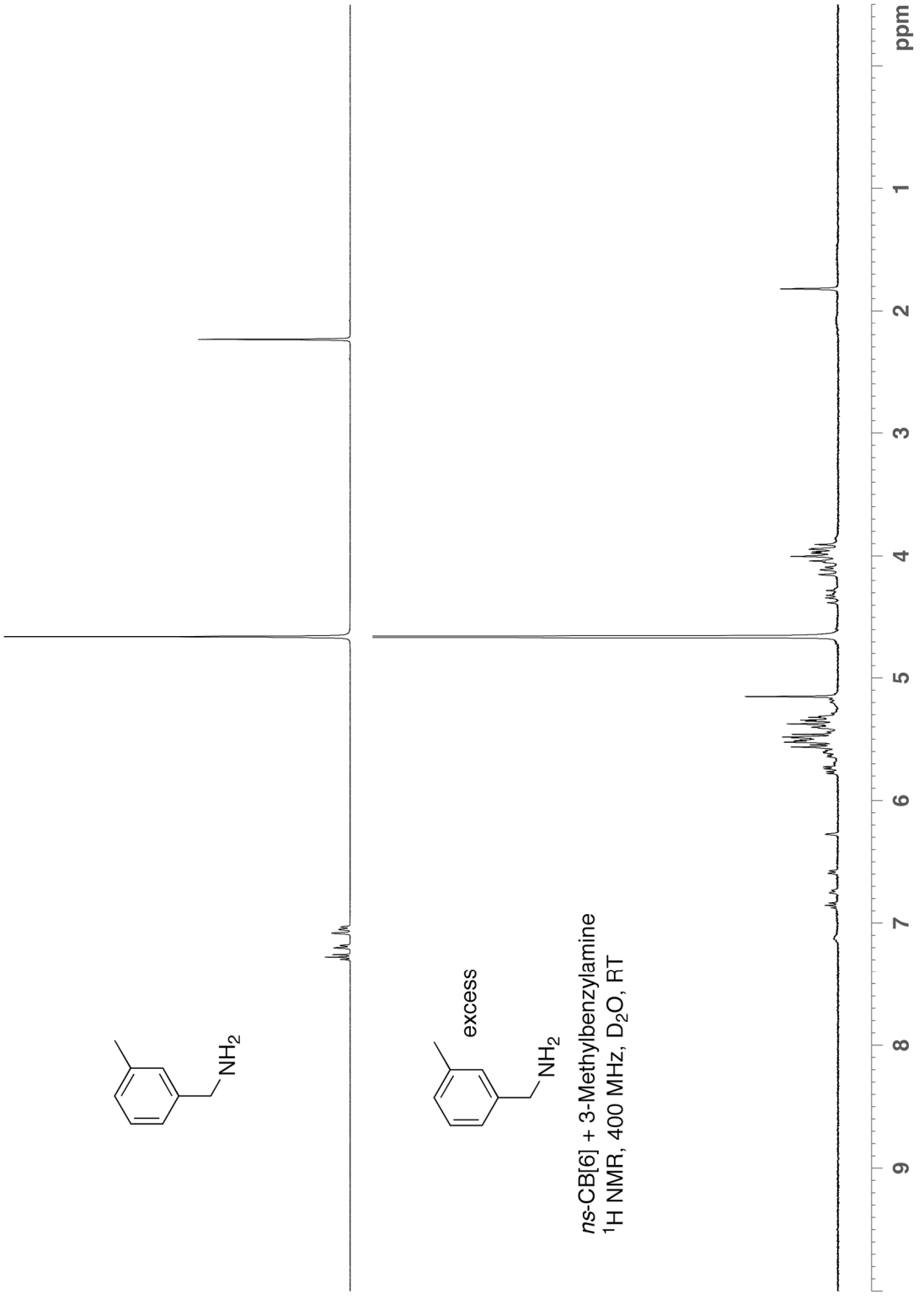

Figure S17. ^{1}H NMR spectra recorded for 3-methylbenzylamine and its complex with *ns*-CB[6] (400 MHz, D_2O, RT).

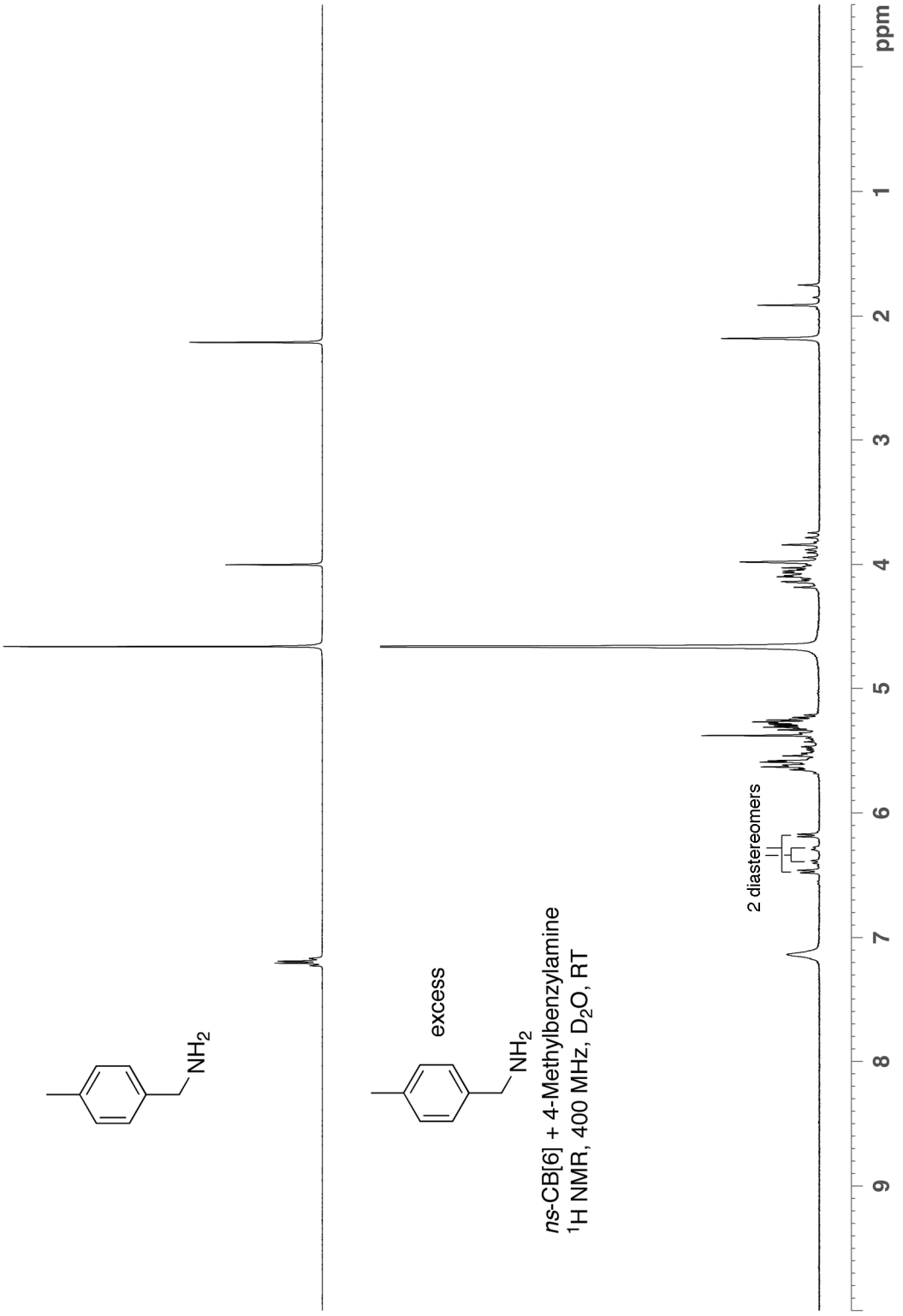

Figure S18. ^{1}H NMR spectra recorded for 4-methylbenzylamine and its complex with *ns*-CB[6] (400 MHz, D_2O, RT). The ratio of the two diastereomers is 71:29.

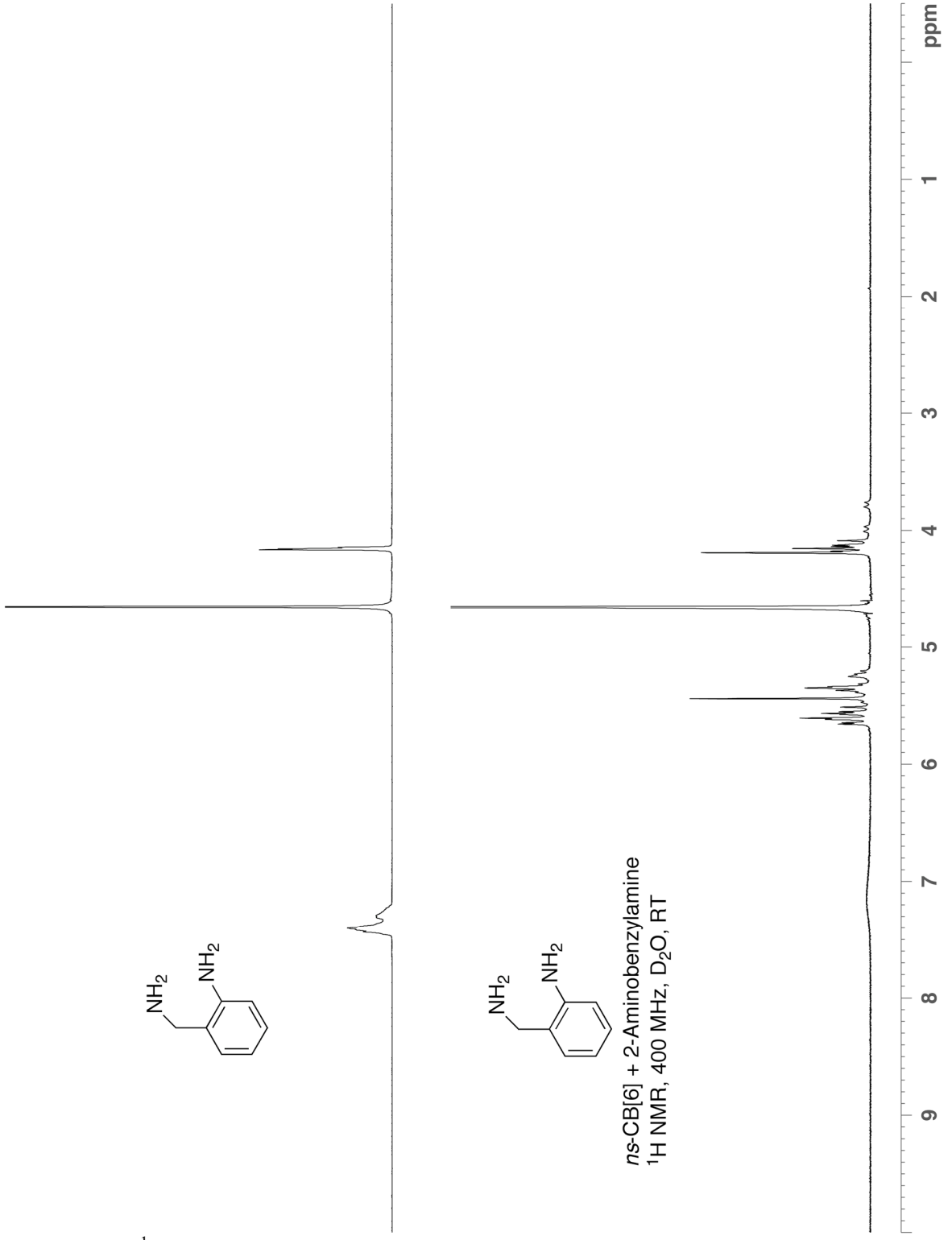

Figure S19. ^{1}H NMR spectrum recorded for 2-aminobenzylamine and its complex with *ns*-CB[6] (400 MHz, D_2O, RT).

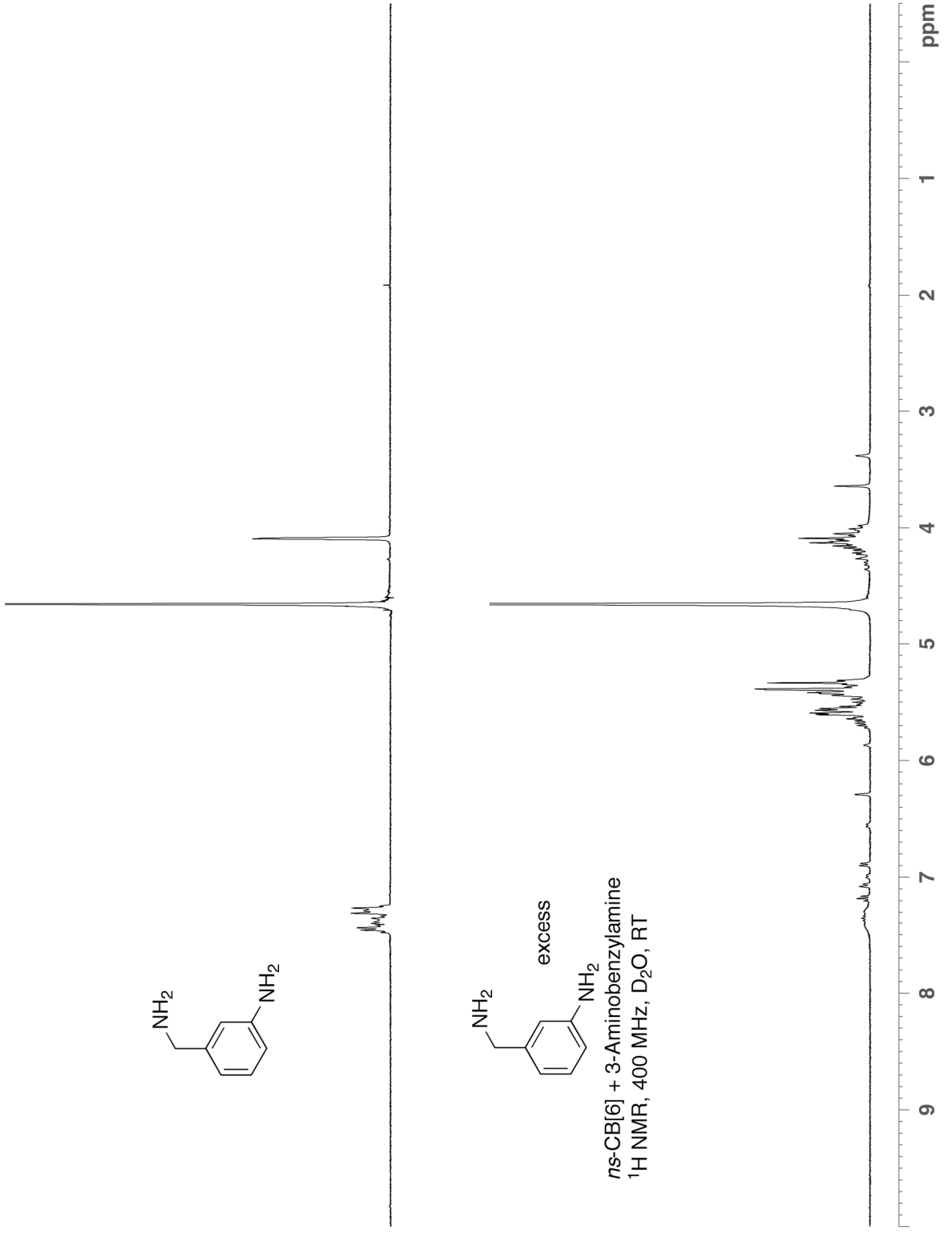

Figure S20. ^{1}H NMR spectrum recorded for 3-aminobenzylamine and its complex with *ns*-CB[6] (400 MHz, D_2O, RT). The ratio of the two diastereomers is 58:42.

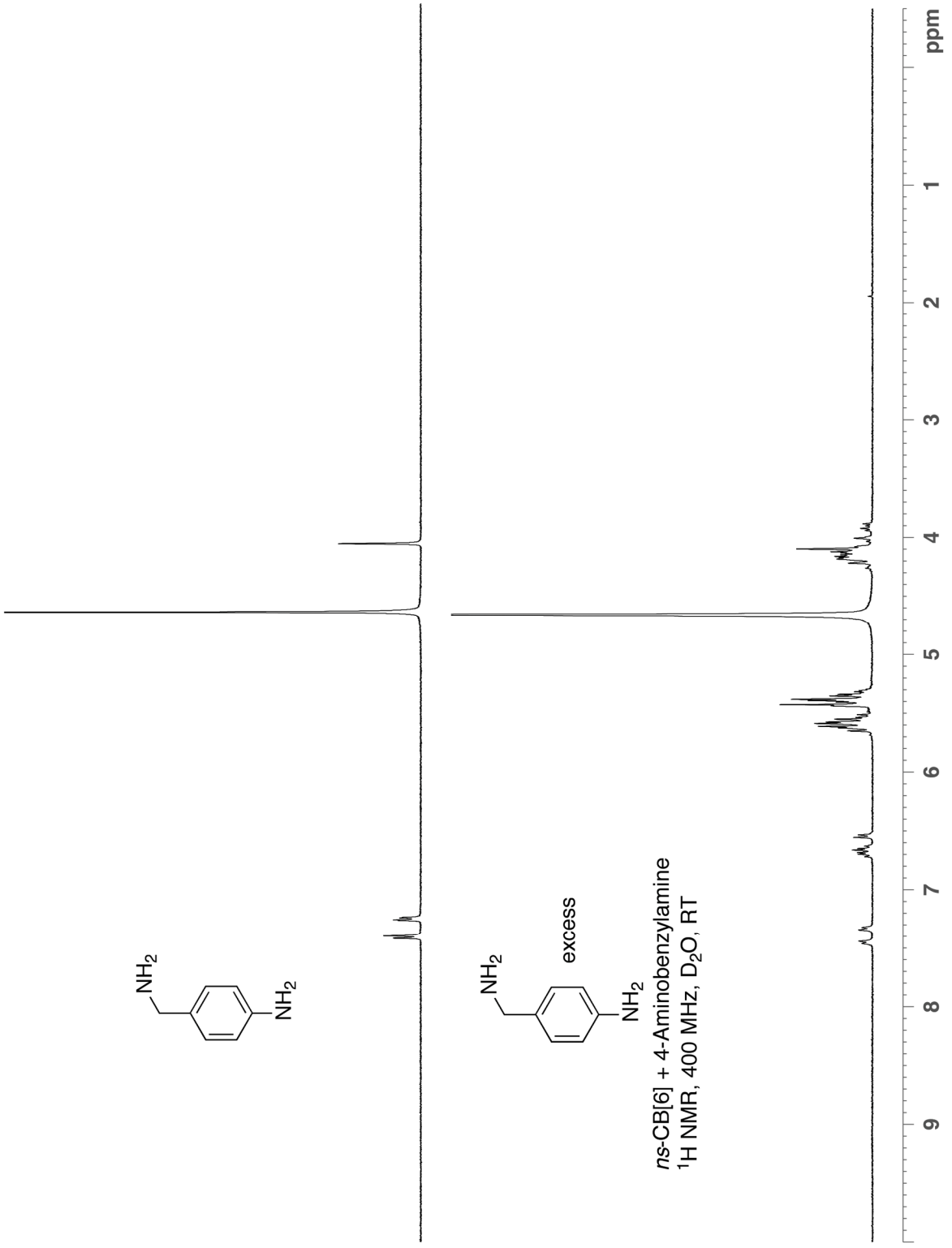

Figure S21. ^{1}H NMR spectra recorded for 4-aminobenzylamine and its complex with *ns*-CB[6] (400 MHz, D_2O, RT). The ratio of the two diastereomers is 72:28.

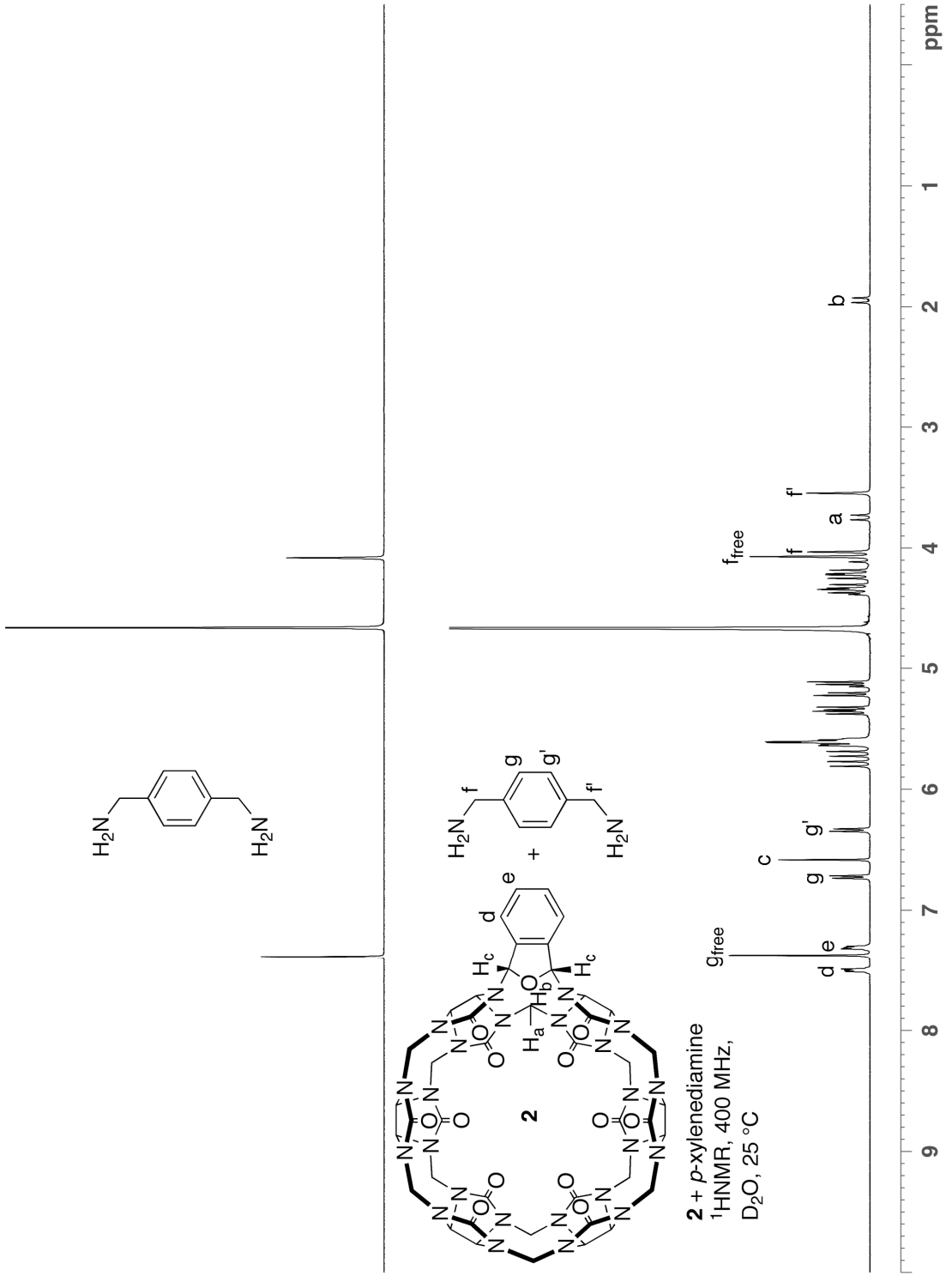

Figure S22. ^{1}H NMR spectra recorded for *p*-xylenediamine and its complex with **2** (400 MHz, D_2O, RT).

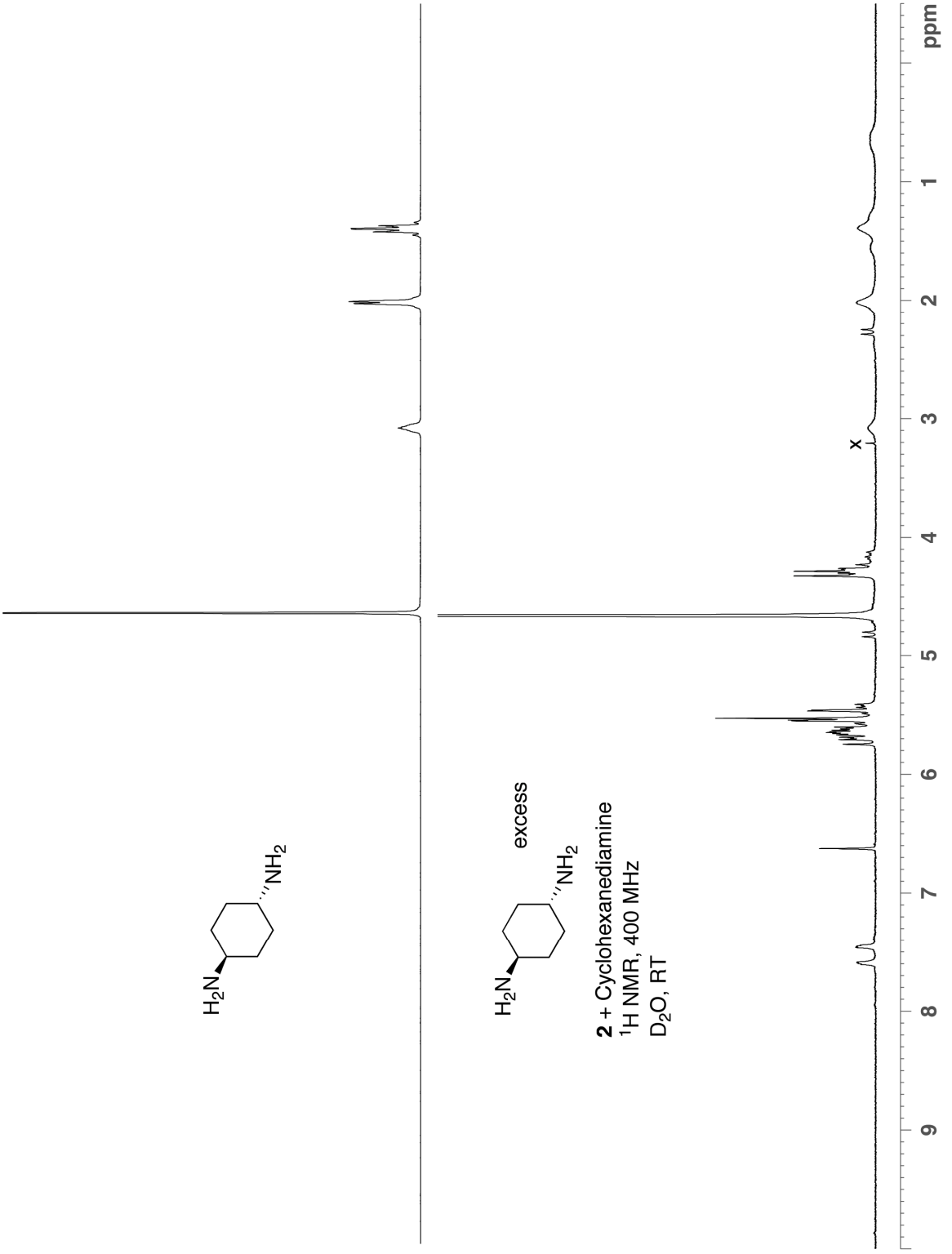

Figure S23. ^{1}H NMR spectra recorded for cyclohexanediamine and its complex with **2** (400 MHz, D_2O, RT, x = trace MeOH impurity).

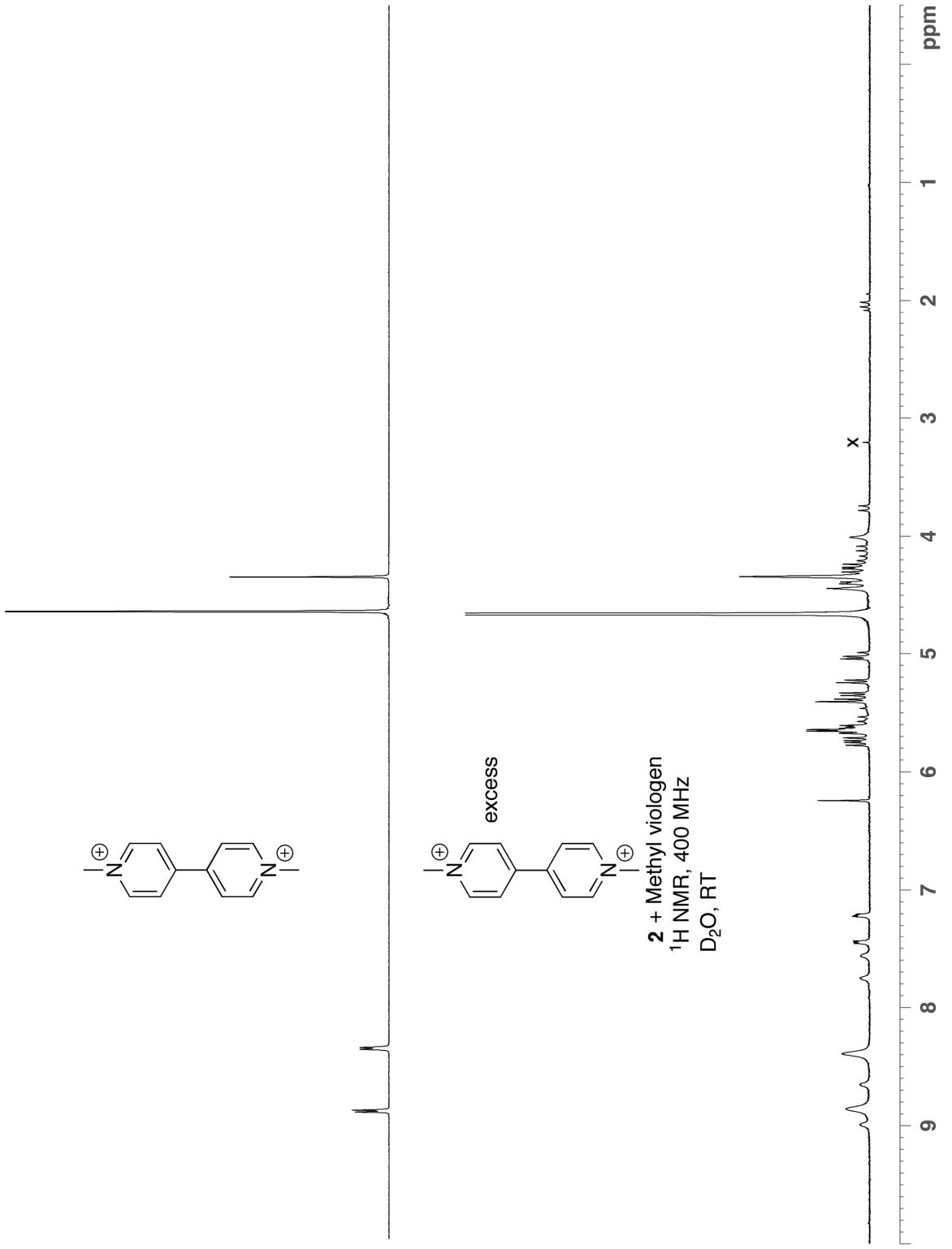

Figure S24. ^{1}H NMR spectra recorded for methyl viologen and its complex with **2** (400 MHz, D_2O, RT, x = trace MeOH impurity).

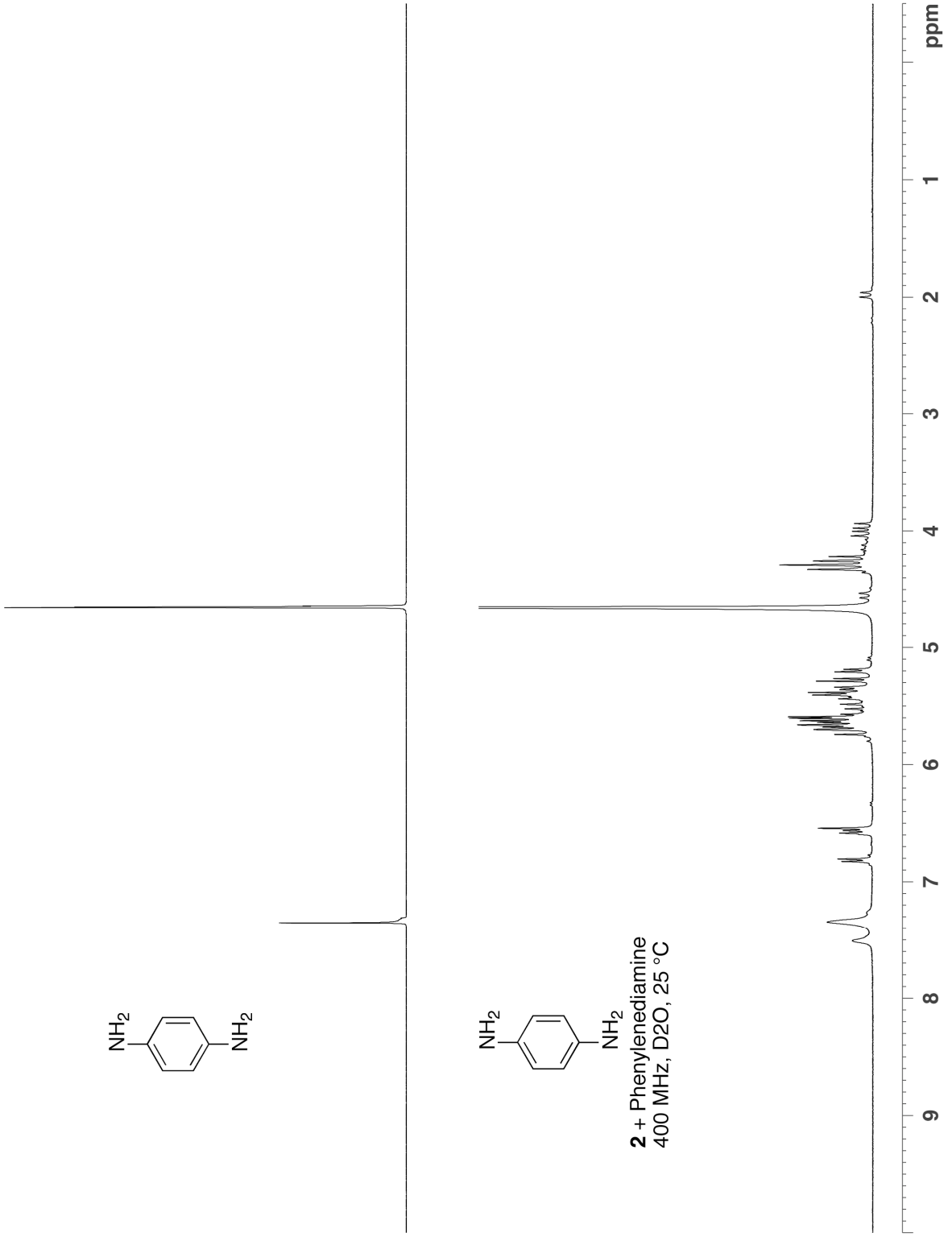

Figure S25. ^{1}H NMR spectra recorded for phenylenediamine and its complex with **2** (400 MHz, D_2O, RT).

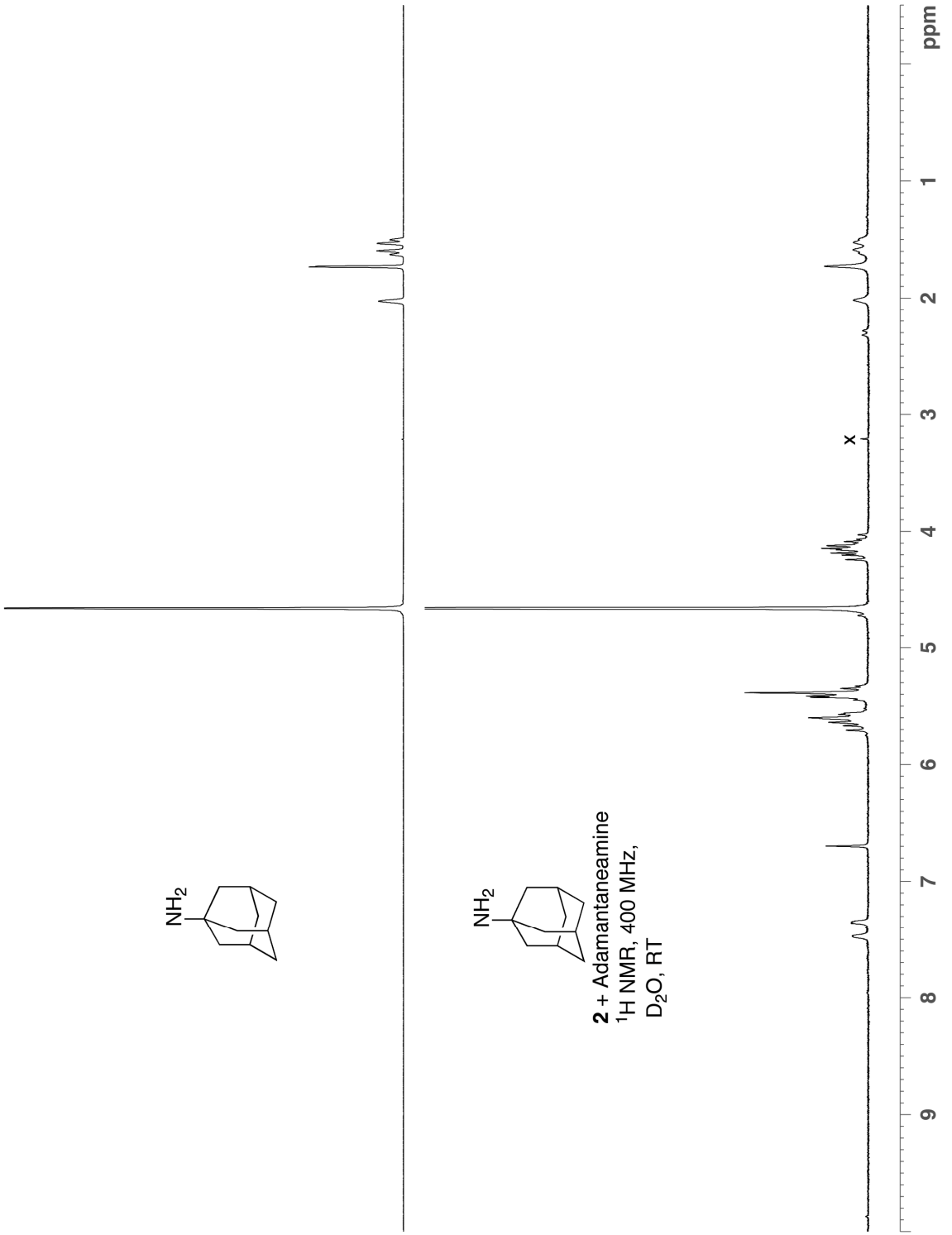

Figure S26. ^{1}H NMR spectra recorded for adamantaneamine and as a mixture with **2** (400 MHz, D_2O, RT, x = trace MeOH impurity).

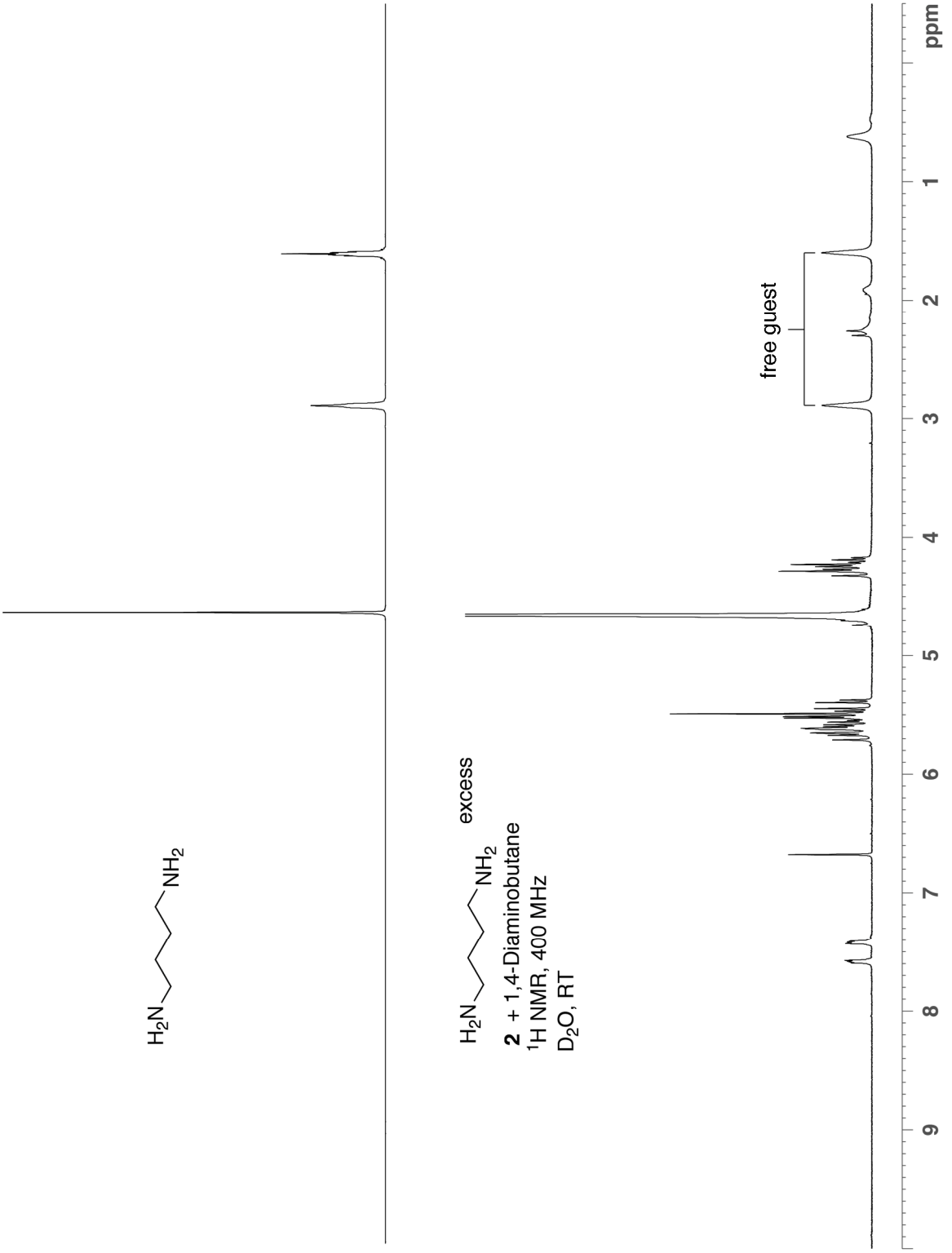

Figure S27. ^{1}H NMR spectra recorded for 1,4-diaminobutane and its complex with **2** (400 MHz, D_2O, RT).

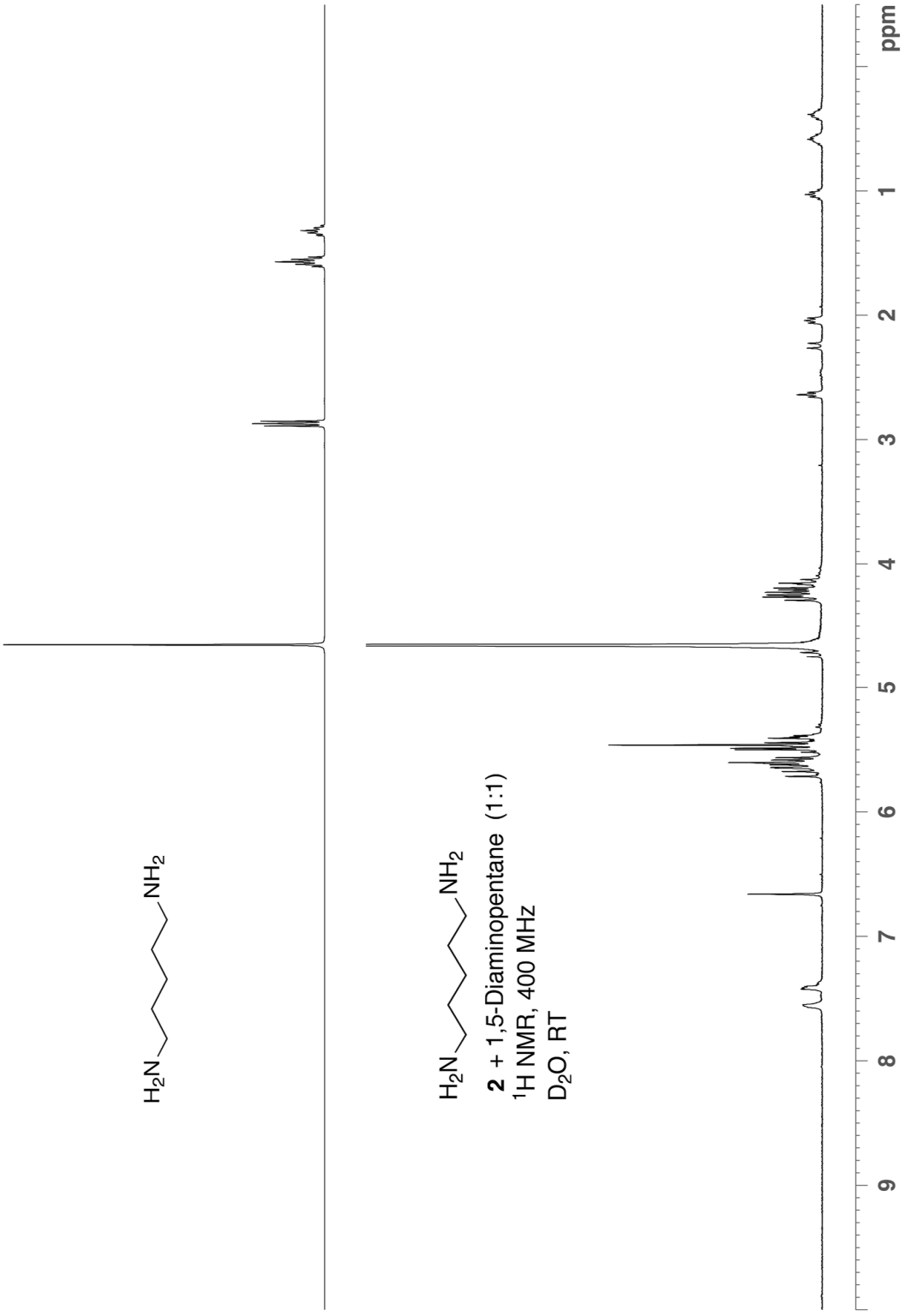

Figure S28. ^{1}H NMR spectra recorded for 1,5-diaminopentane and its complex with **2** (400 MHz, D_2O, RT).

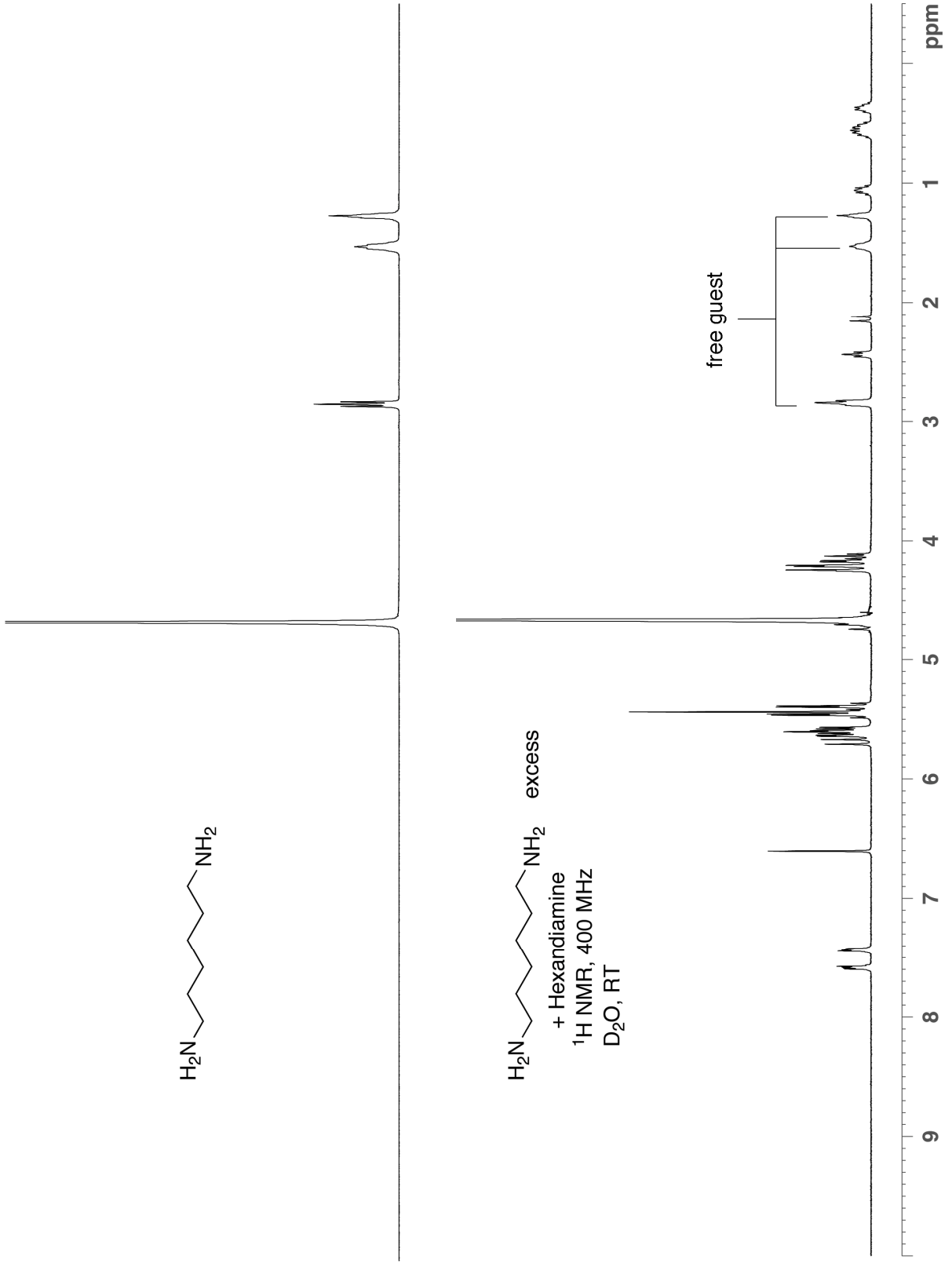

Figure S29. ^{1}H NMR spectra recorded for hexanediamine and its complex with **2** (400 MHz, D_2O, RT).

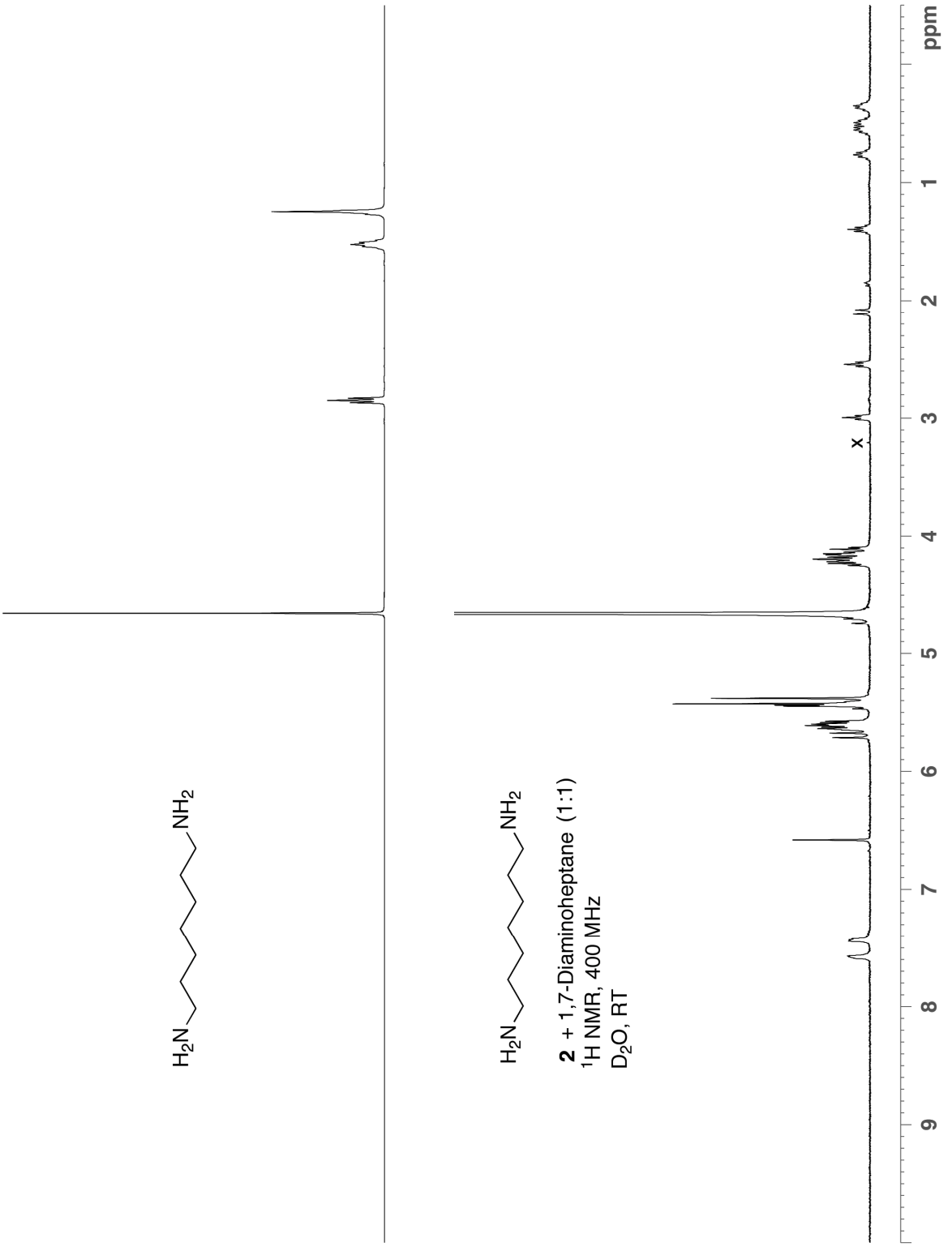

Figure S30. ^{1}H NMR spectra recorded for 1,7-diaminoheptane and its complex with **2** (400 MHz, D_2O, RT, x = trace MeOH impurity).

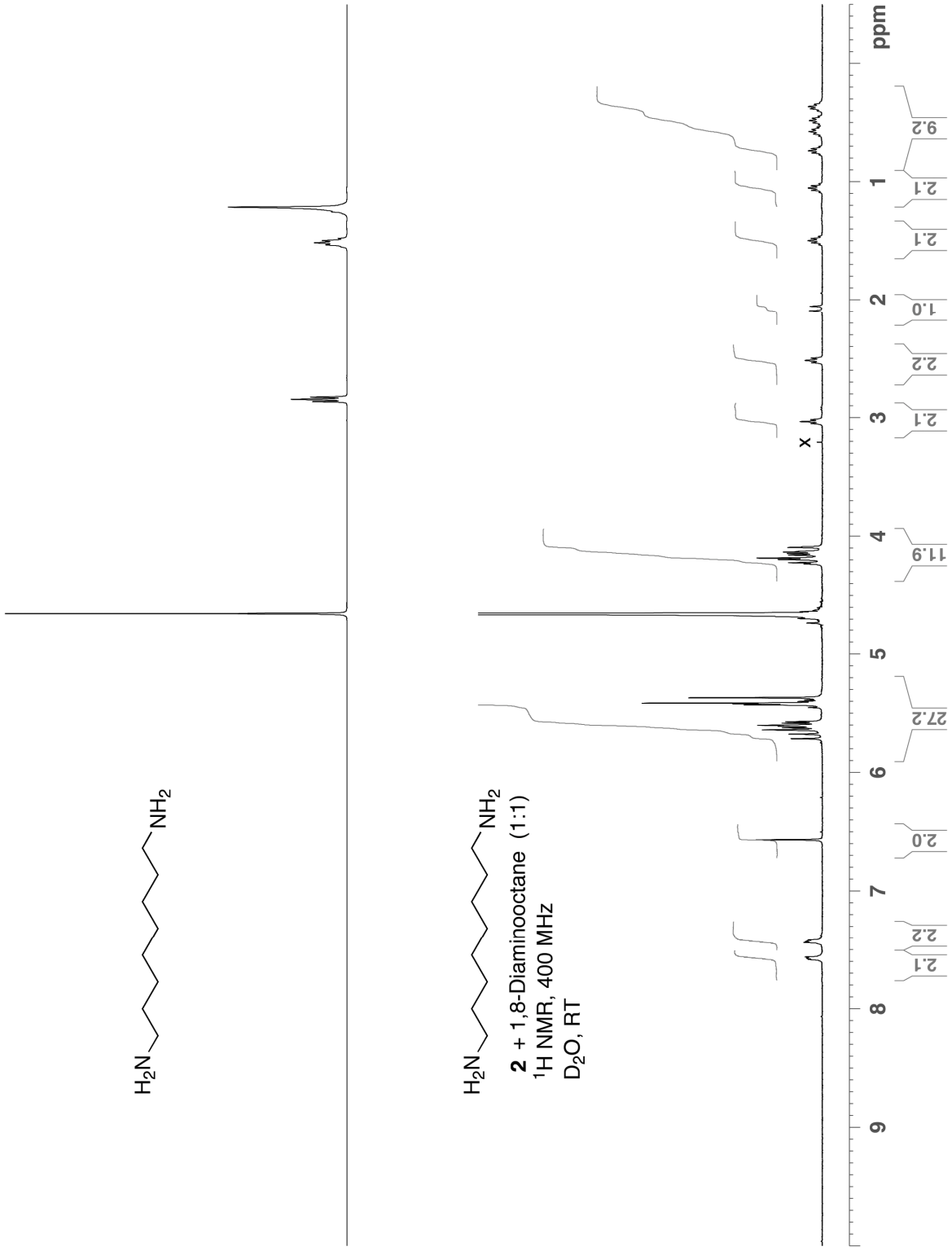

Figure S31. ^{1}H NMR spectra recorded for 1,8-diaminooctane and its complex with **2** (400 MHz, D_2O, RT, x = trace MeOH impurity).

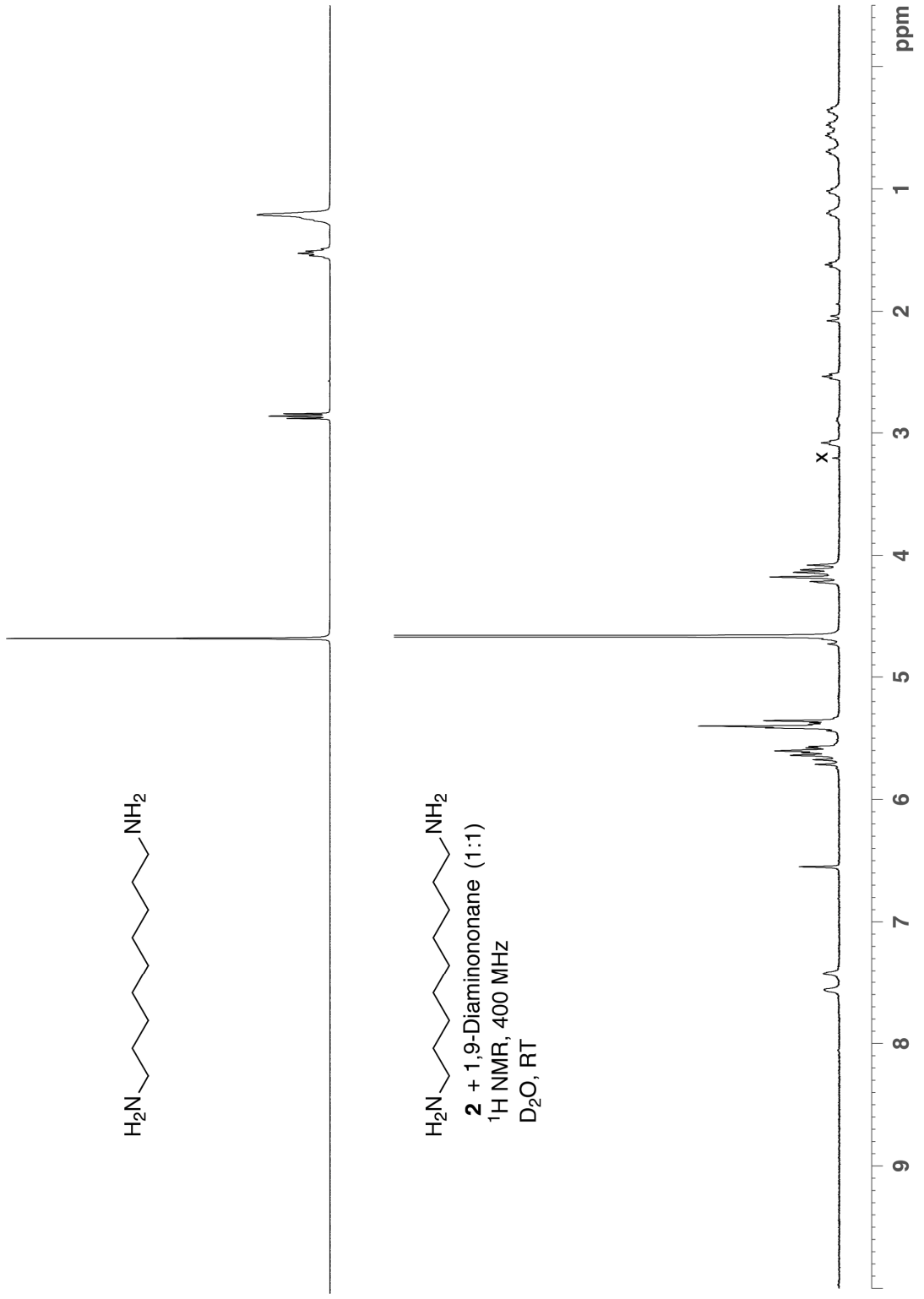

Figure S32. ^{1}H NMR spectra recorded for 1,9-diaminononane and its complex with **2** (400 MHz, D_2O, RT, x = trace MeOH impurity).

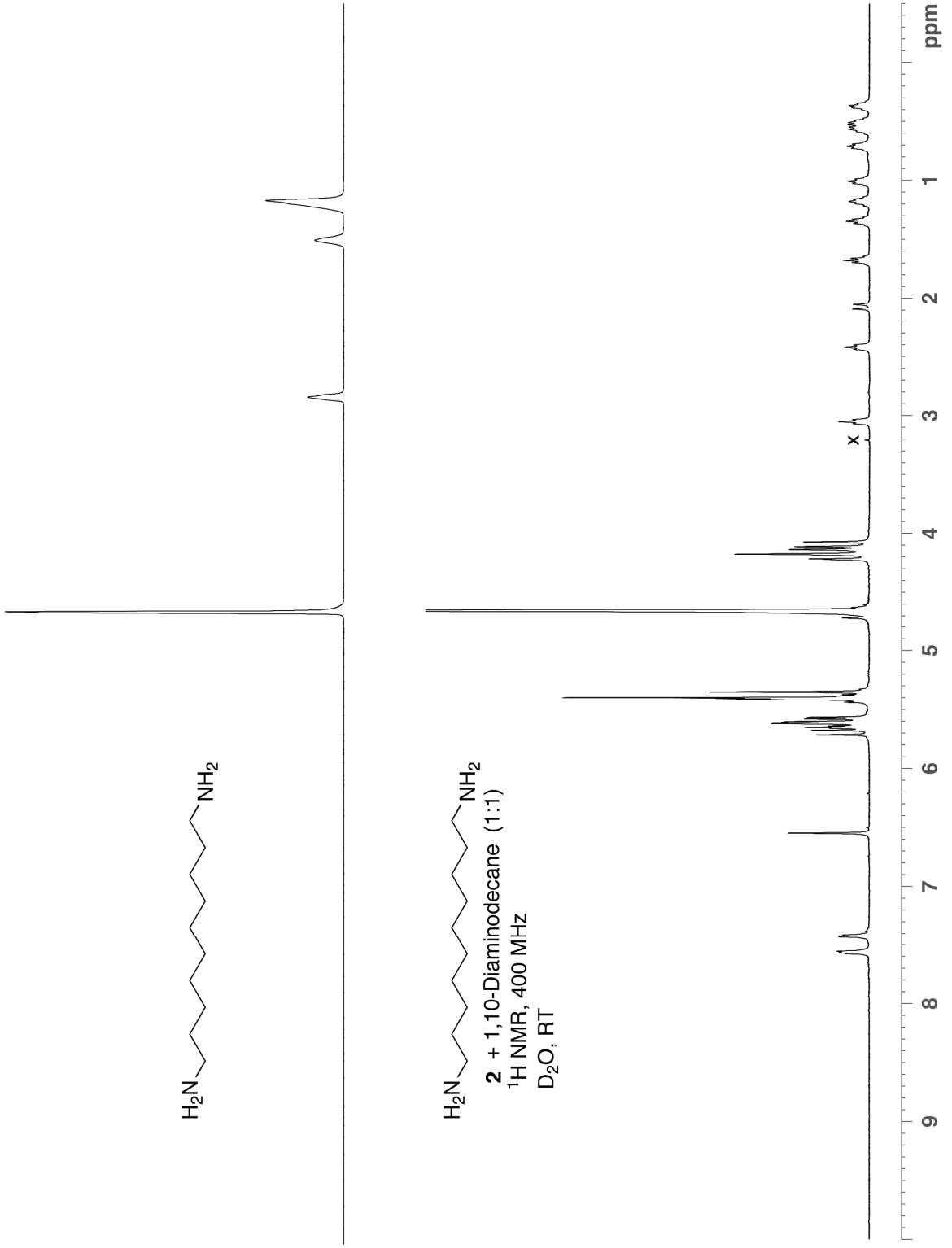

Figure S33. ^{1}H NMR spectra recorded 1,10-diaminodecane and its complex with **2** (400 MHz, D_2O, RT, x = trace MeOH impurity).

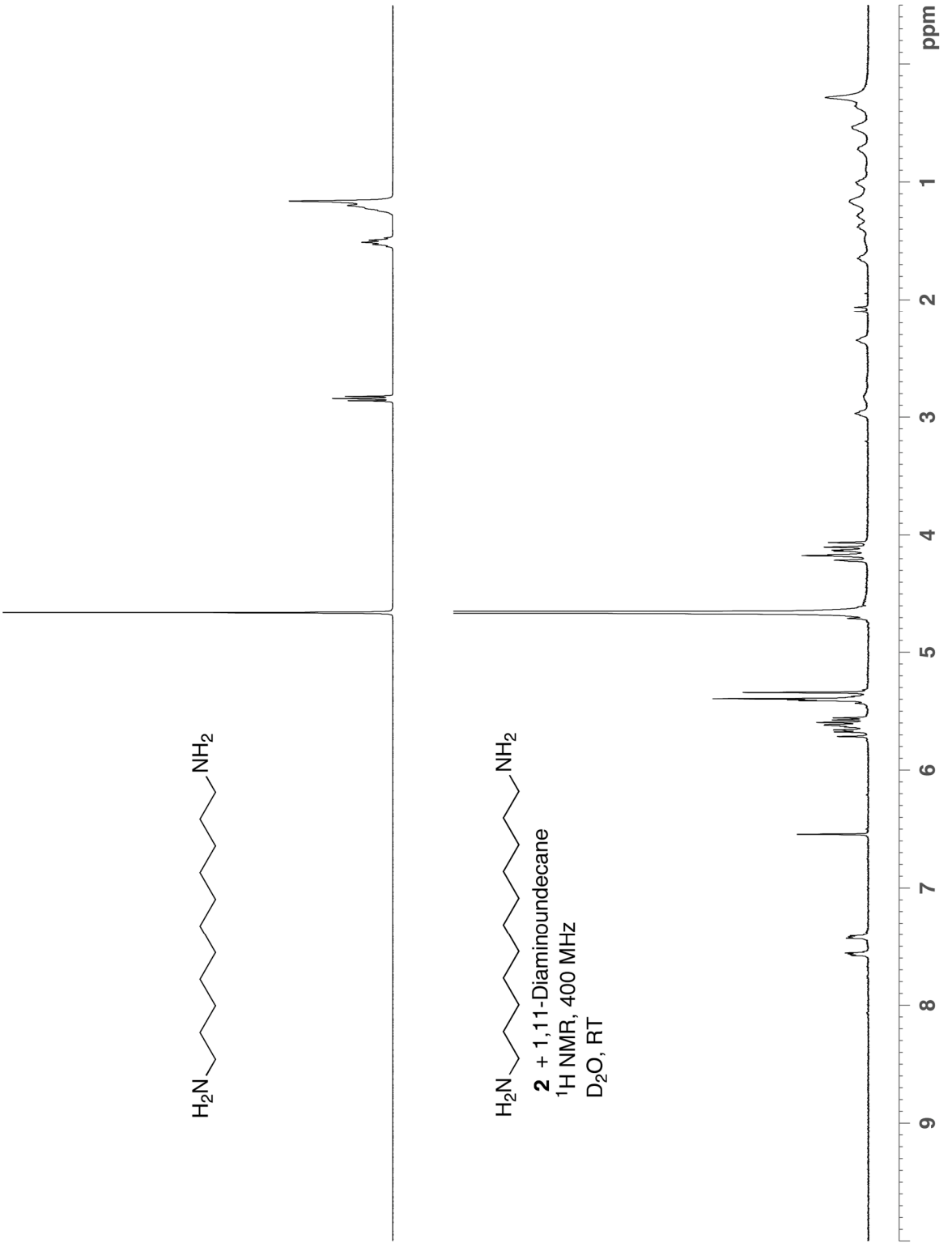

Figure S34. ^{1}H NMR spectra recorded 1,11-diaminoundecane and its complex with **2** (400 MHz, D_2O, RT).

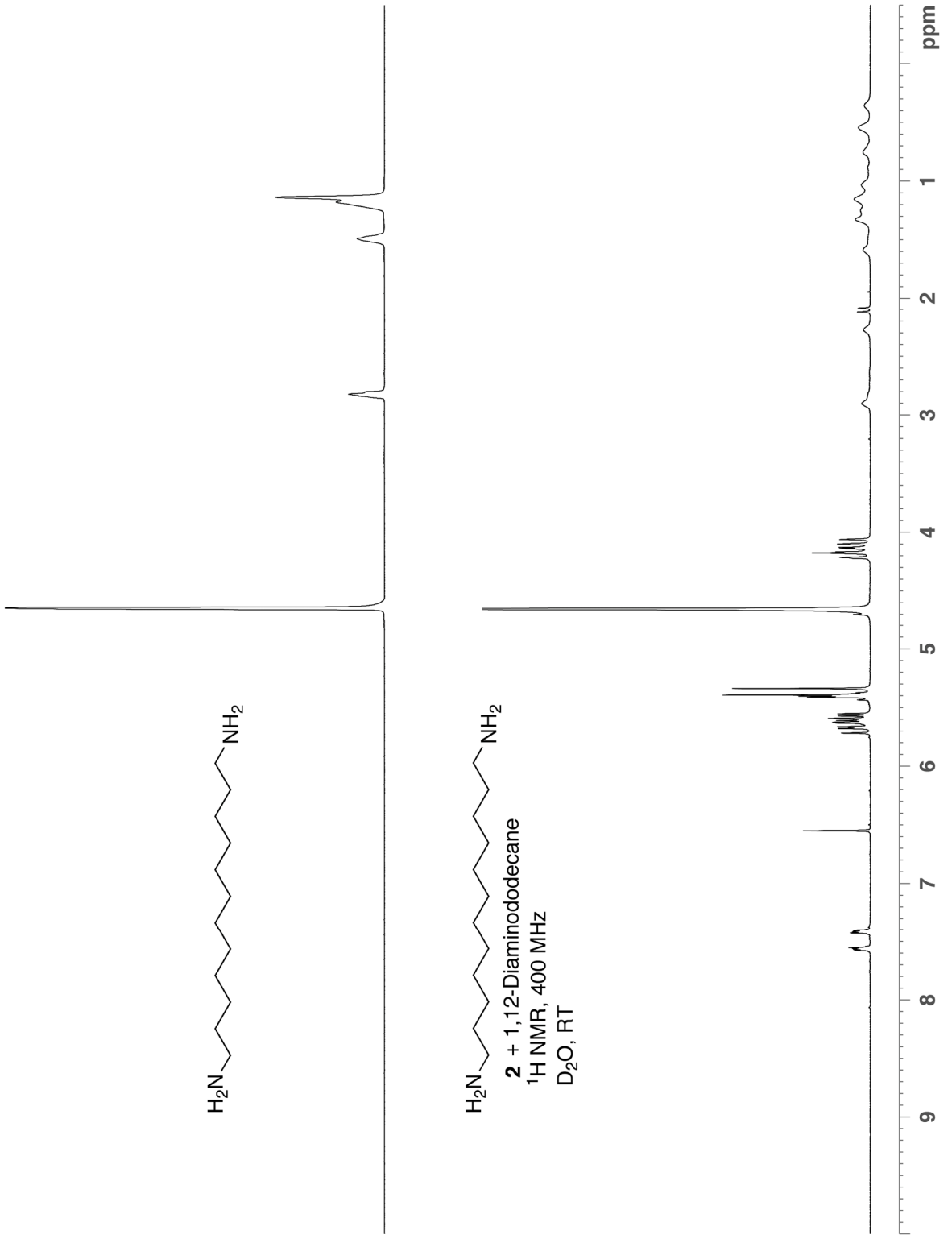

Figure S35. ^{1}H NMR spectra recorded for 1,12-diaminododecane and its complex with **2** (400 MHz, D_2O, RT).

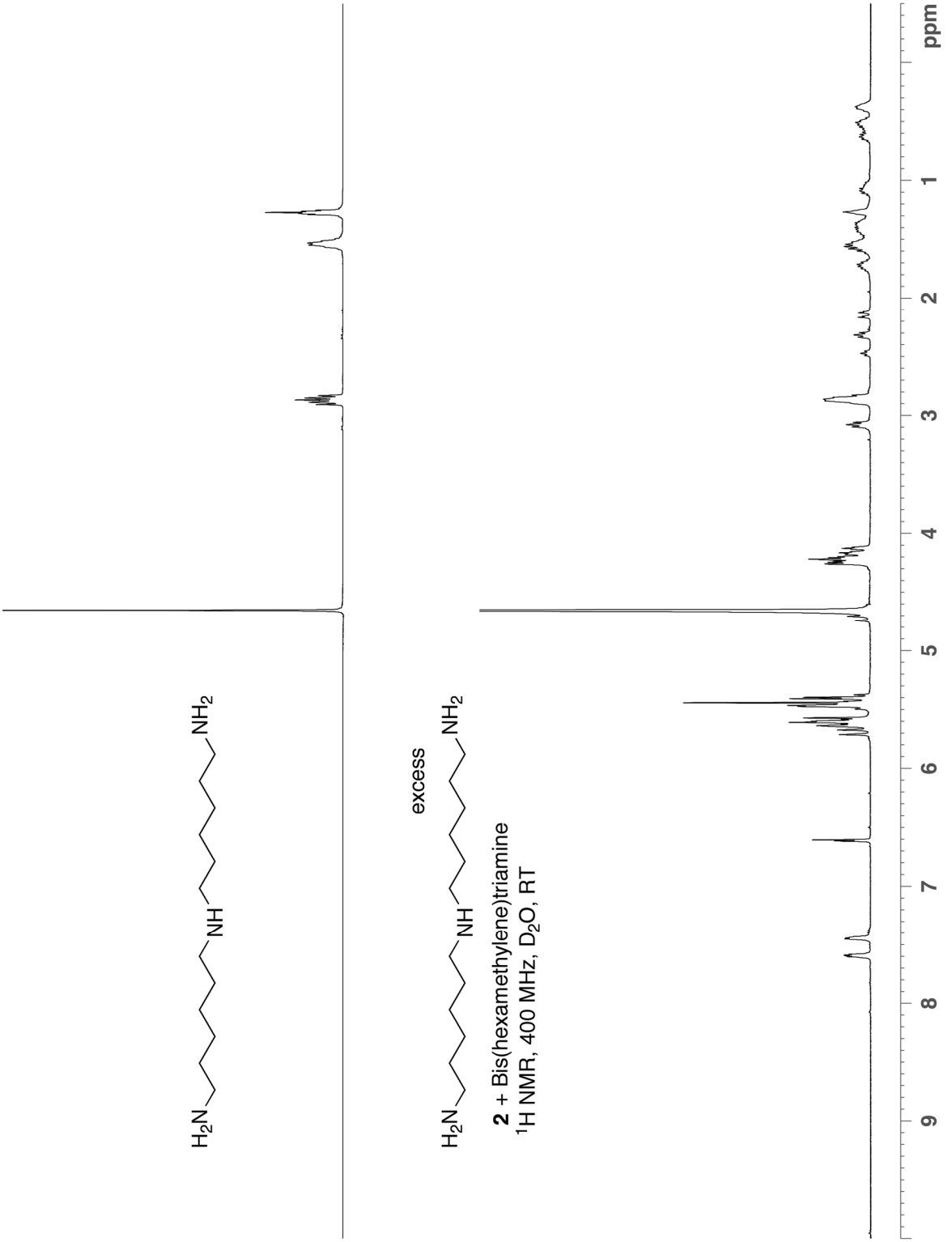

Figure S36. ^{1}H NMR spectra recorded for bis(hexamethylene)triamine and its complex with **2** (400 MHz, D_2O, RT).

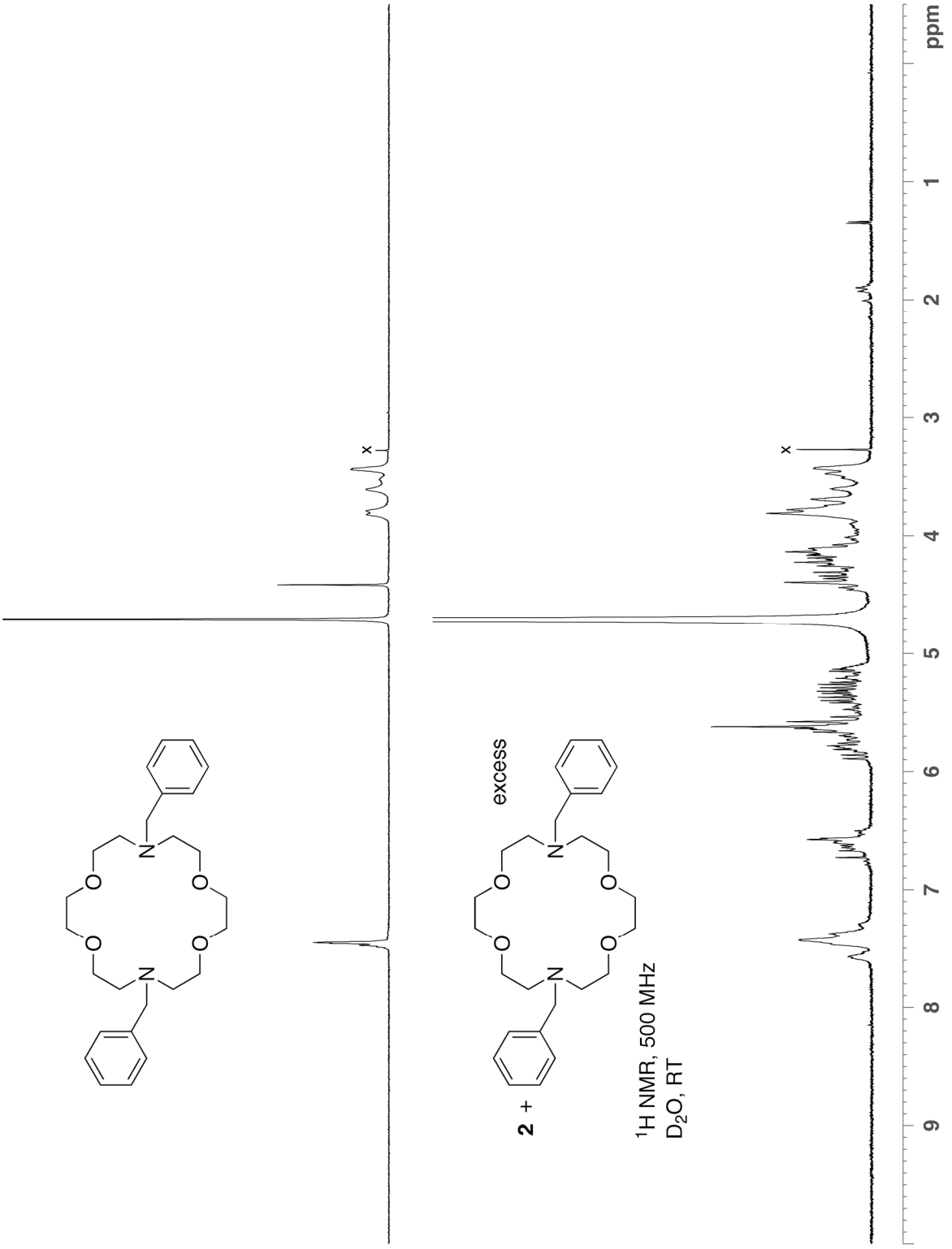

Figure S37. ^{1}H NMR spectra recorded for 1,10-dibenzyl-1,10-diaza-18-crown-6 and its complex with **2** (400 MHz, D_2O, RT, x = trace MeOH impurity).

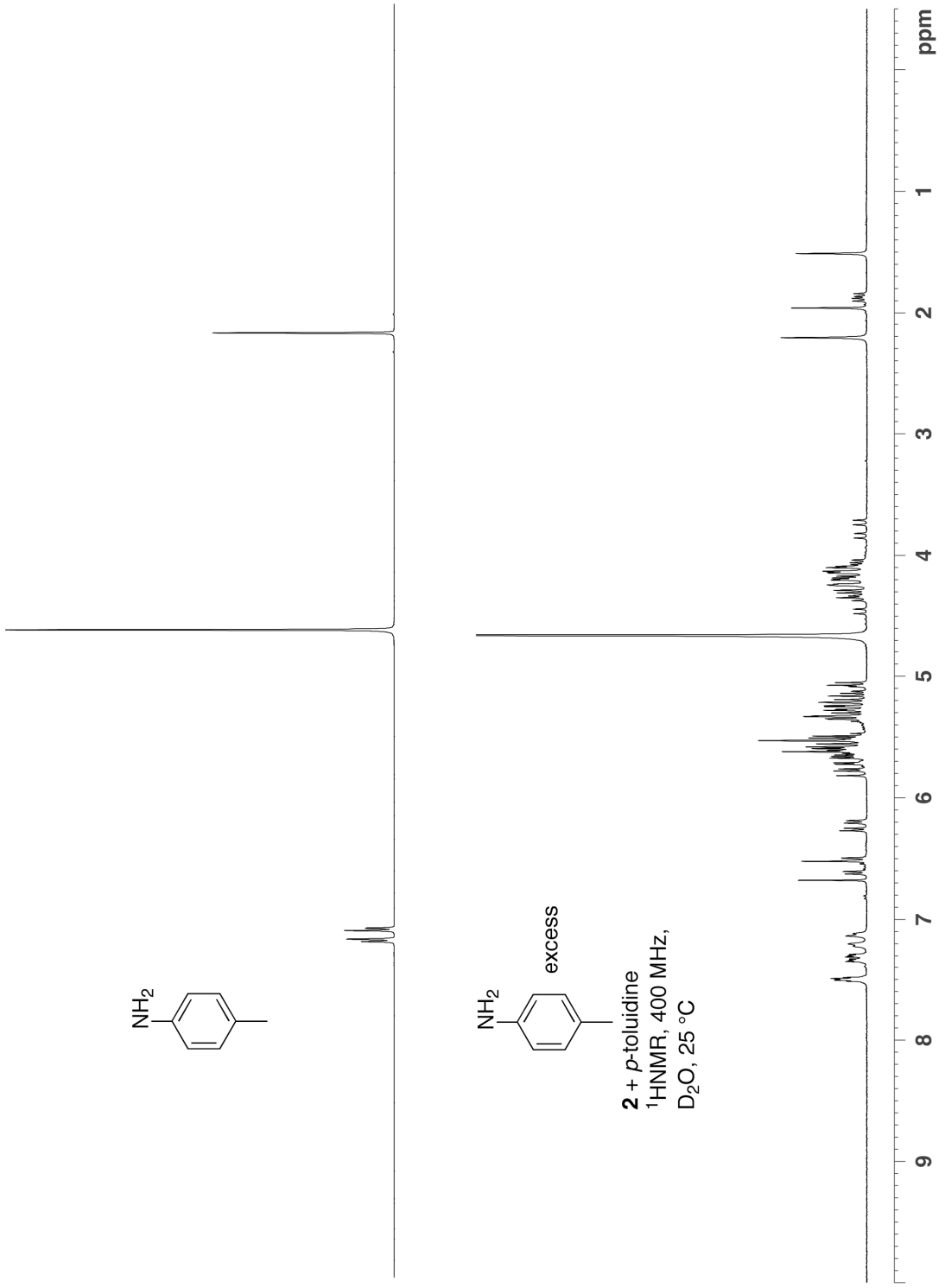

Figure S38. ^{1}H NMR spectra recorded for *p*-toluidine and its complex **2** (400 MHz, D_2O, RT).

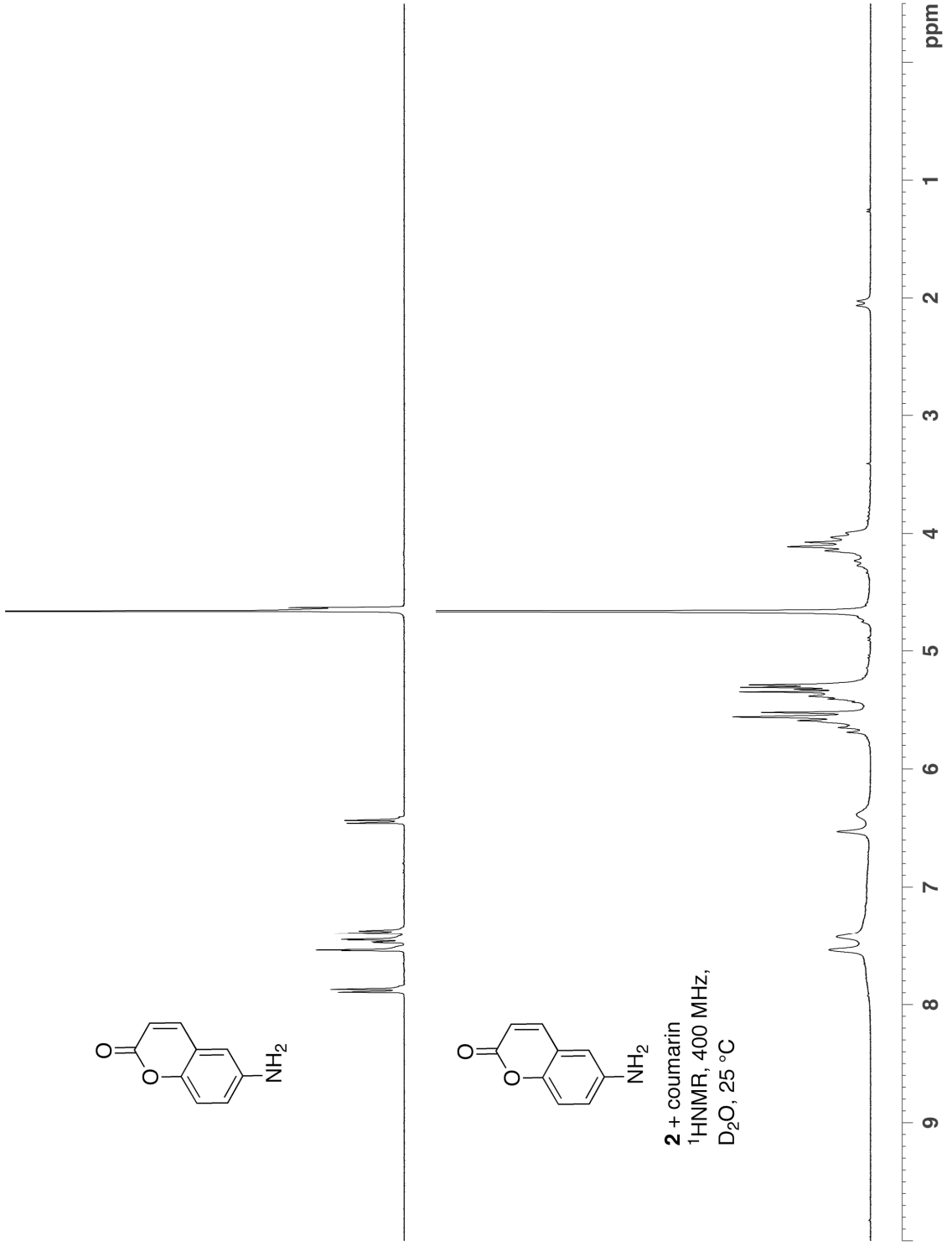

Figure S39. ^{1}H NMR spectra recorded for coumarin and its complex **2** (400 MHz, D_2O, RT).

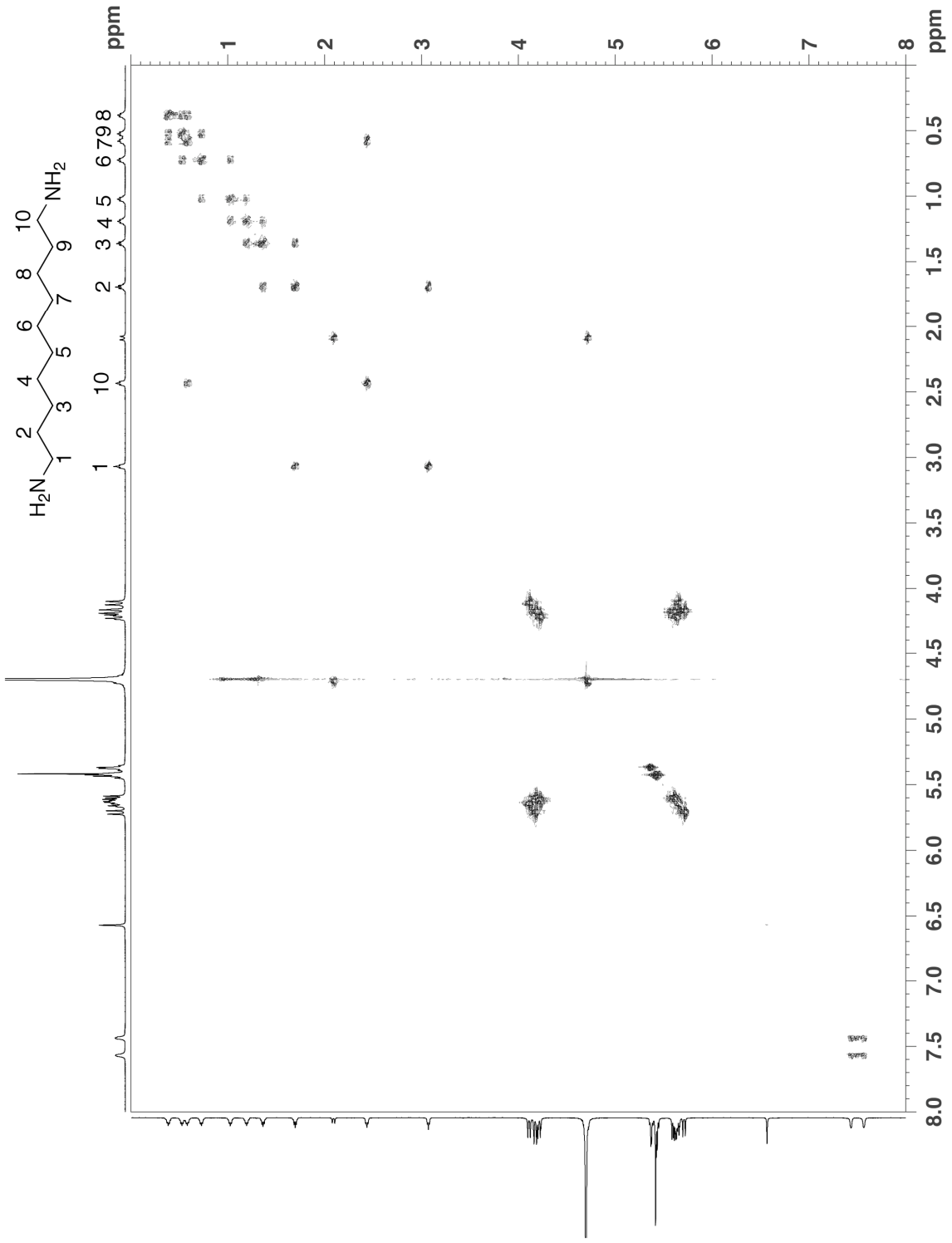

Figure S40. ^{1}H-^{1}H COSY NMR spectrum recorded for **2**•1,10-diaminodecane (600 MHz, D_2O, RT).

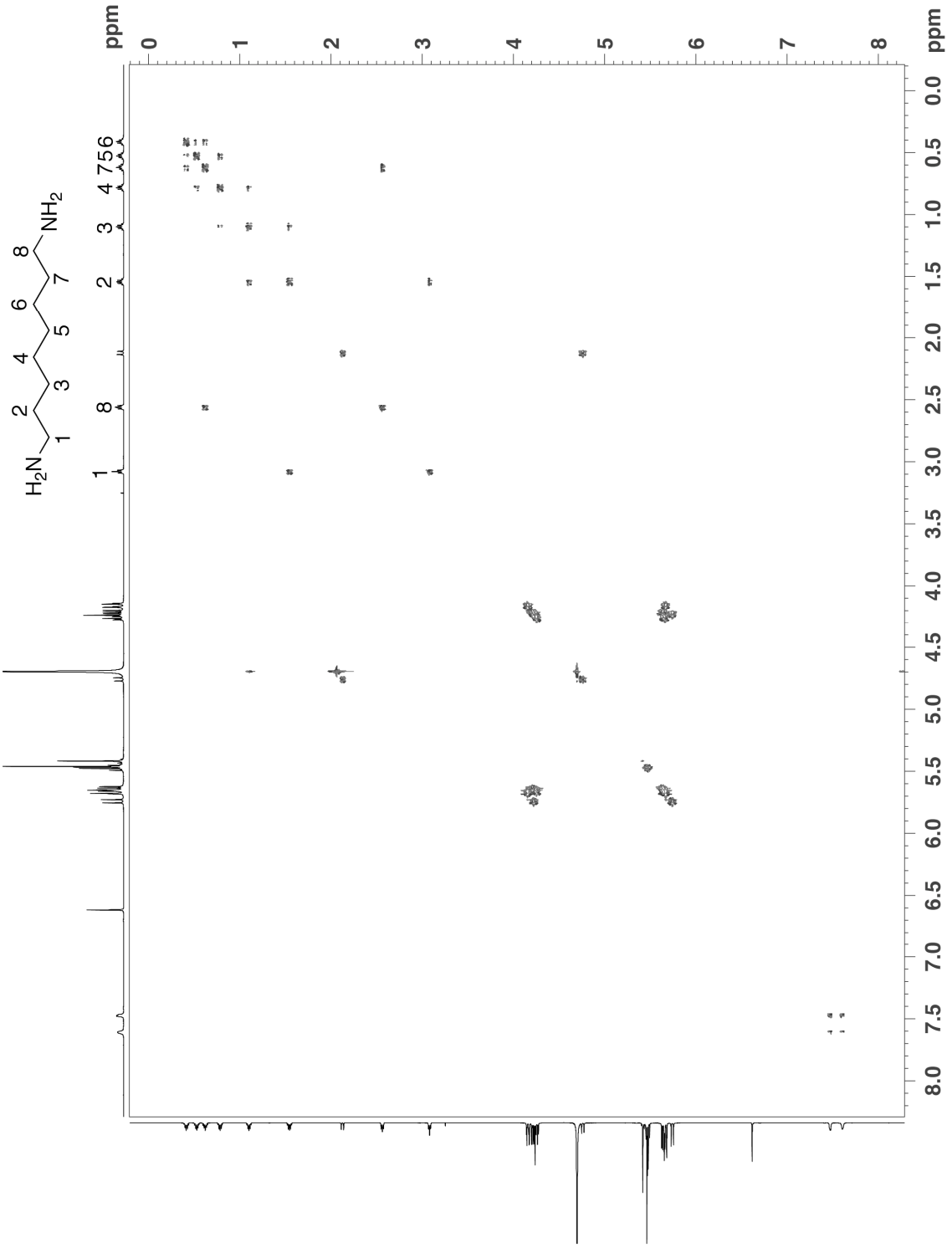

Figure S41. ^{1}H-^{1}H COSY NMR spectrum recorded for **2**•1,8-diaminooctane (600 MHz, D_2O, RT).

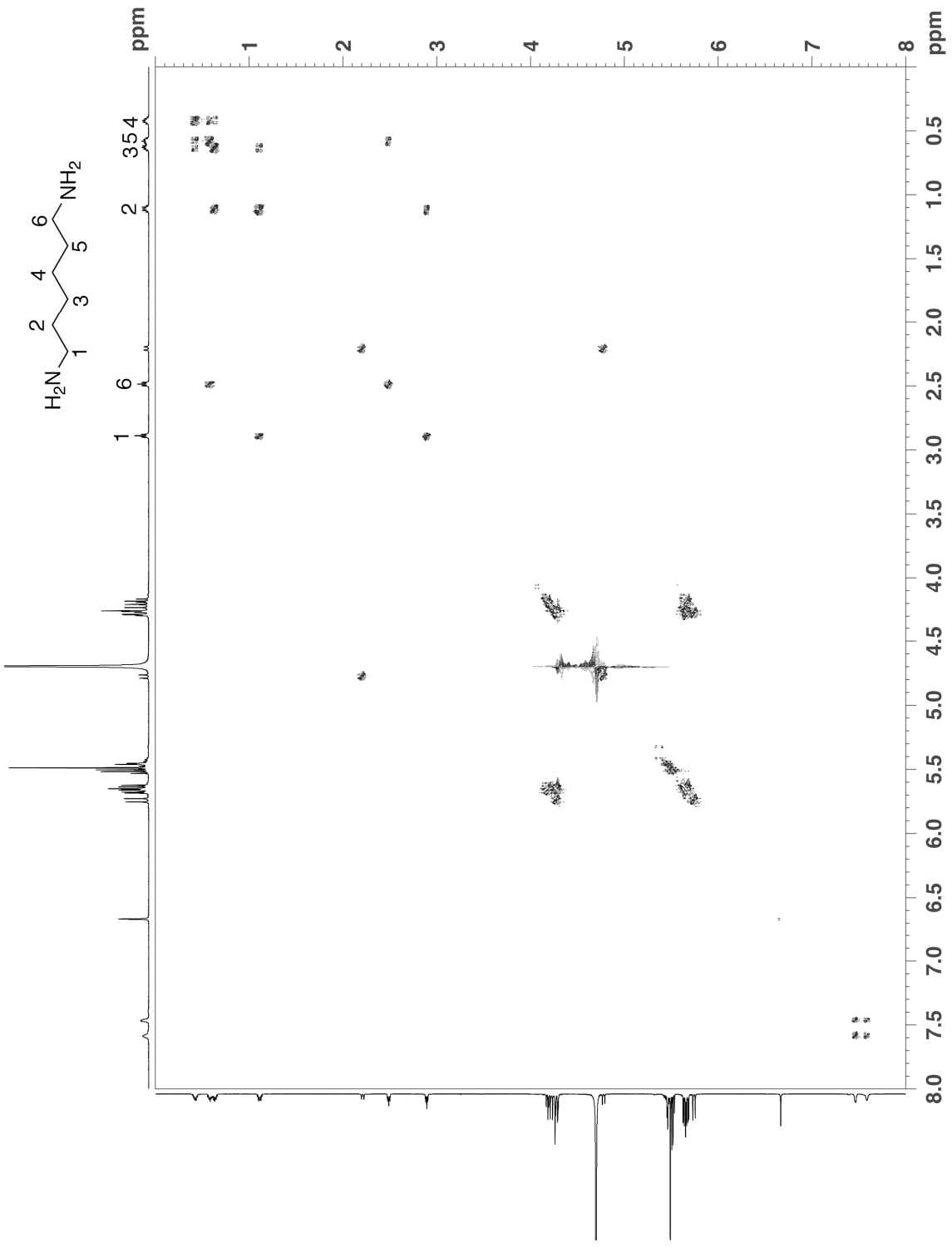

Figure S42. ^{1}H-^{1}H COSY NMR spectrum recorded for **2**•1,6-diaminohexane (600 MHz, D_2O, RT).

Crystal Structure Information for UM # 1574

Issued by: Peter Y. Zavalij

Crystal No. & ID	:	**1574**: Isaacs/Wei-Hao Huang
Compound name	:	$[K(H_2O)_2(CB6')_2 \cdot 2TFAH](TFA) \cdot \sim 4TFAH \cdot \sim 13H_2O$
Chemical formula	:	$KC_{100}H_{116}F_{21}N_{48}O_{55}$
Final R_1 [I>2σ(I)]	:	**5.37 %**

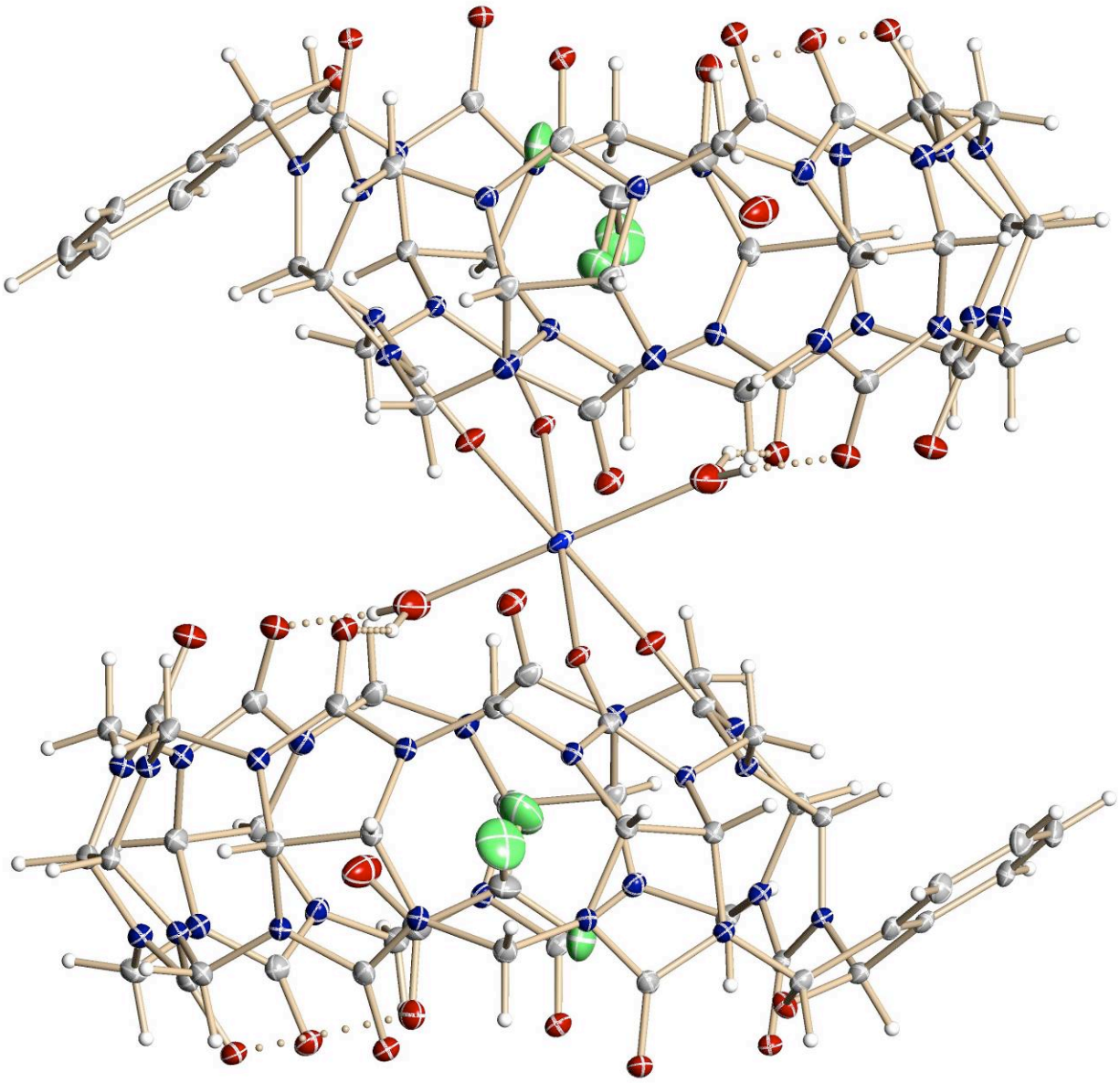

Figure S43. A view of UM#1574 showing the numbering scheme employed. Anisotropic atomic displacement ellipsoids for the non-hydrogen atoms are shown at the 30% probability level. Hydrogen atoms are displayed with an arbitrarily small radius.

A colorless prism of $KC_{100}H_{116}F_{21}N_{48}O_{55}$, approximate dimensions 0.095×0.15×0.40 mm^3, was used for the X-ray crystallographic analysis. The X-ray intensity data were measured at 150(2) K on a three-circle diffractometer system equipped with Bruker Smart Apex II CCD area detector using a graphite monochromator and a MoKα fine-focus sealed tube (λ= 0.71073 Å) . The detector was placed at a distance of 5.8 cm from the crystal.

A total of 2491 frames were collected with a scan width of 0.3° an exposure time of 20 sec/frame using Apex2 (Bruker, 2005). The total data collection time was 18 hours. The frames were integrated with Apex2 software package using a narrow-frame integration algorithm. The integration of the data using a Monoclinic unit cell yielded a total of 66732 reflections to a maximum θ angle of 25.00°, of which 12908 were independent (completeness = 99.9%, R_{int} = 3.86%, R_{sig} = 3.22%) and 9287 were greater than 2σ(I). The final cell dimensions of a = 31.0746(11) Å, b = 16.9744(6) Å, c = 28.0904(10) Å, α = 90°, β = 97.9680(10)°, γ = 90°, V = 14673.9(9) $Å^3$, are based upon the refinement of the XYZ-centroids of 16943 reflections with 2.3 < θ < 28.0° using Apex2 software. Analysis of the data showed 0 % decay during data collection. Data were corrected for absorption effects with the Semi-empirical from equivalents method using SADABS (Sheldrick, 1996). The minimum and maximum transmission coefficients were 0.917 and 0.984.

The structure was solved and refined using the SHELXS-97 (Sheldrick, 1990) and SHELXL-97 (Sheldrick, 1997) software in the space group *C2/c* with Z = 4 for the formula unit $KC_{100}H_{116}F_{21}N_{48}O_{55}5$. The final anisotropic full-matrix least-squares refinement on F^2 with 925 variables converged at R_1 = 5.37 % for the observed data and wR_2 = 10.48 % for all data. The goodness-of-fit was 1.000. The largest peak on the final difference map was 0.618$\bar{e}/Å^3$ and the largest hole was -0.697$\bar{e}/Å^3$. On the basis of the final model, the calculated density was 1.498 g/cm^3 and F(000), 6800$\bar{e}$.

Overall structure quality considerations:

1. Strong data set, no disorder, R_1 4% maximum. Publishable quality.
2. **Good data set, perhaps some minor disorder, R_1 6% maximum. Publishable quality.**
3. Average data set and/or easily modeled disorder or twinning. Publishable with care.
4. Weak data and/or major disorder or twinning that is not easily modeled. Publishable in some cases.
5. Very weak data and/or unexplained features of data or model. Not of publishable quality.

A structure with a quality factor of 4 or 5 should not be used for a regulatory document without prior consultation.

Comments:

- Data quality:	very good
- Twinning:	none
- Disorder:	solvent TFA and water, removed using Squeeze from Platon
- H-atoms:	constrained geometry as riding on attached atom (A)
	$U_{iso}(H)=1.5U_{iso}(A)$ for CH_3 and $1.2U_{iso}(A)$ for other groups
- Residual density:	near disordered groups
- Structure quality:	good
Publishable	Yes

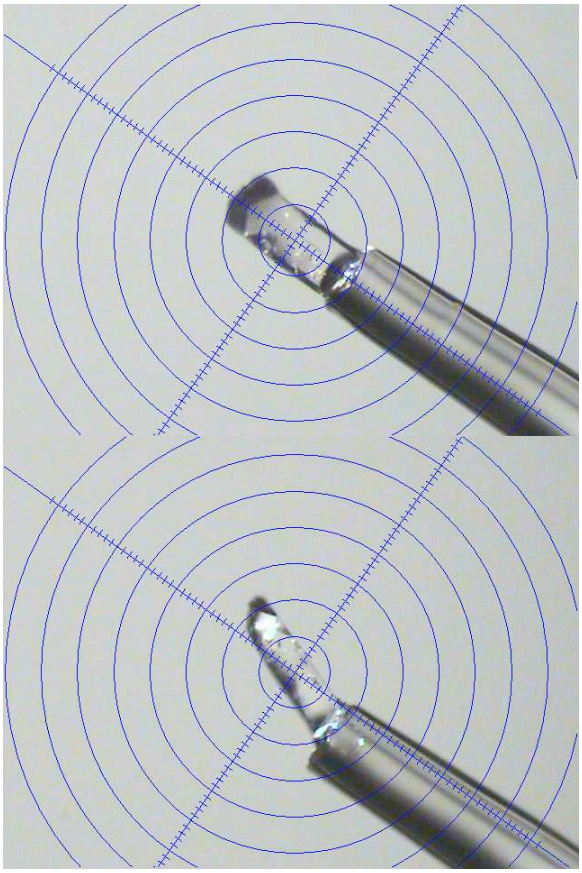

Table S1. Crystal data and structure refinement for UM#1574.

X-ray lab book No.		1574
Crystal ID		Isaacs/Wei-Hao Huang
Empirical formula		$KC_{100}H_{116}F_{21}N_{48}O_{55}$
Formula weight		3308.51
Temperature		150(2) K
Wavelength		0.71073 Å
Crystal size		0.40×0.15×0.095 mm^3
Crystal habit		colourless prism
Crystal system		Monoclinic
Space group		C2/c
Unit cell dimensions		a = 31.0746(11) Å α = 90°
		b = 16.9744(6) Å β = 97.9680(10)°
		c = 28.0904(10) Å γ = 90°
Volume		14673.9(9) $Å^3$
Z		4
Density, ρ_{calc}		1.498 g/cm^3
Absorption coefficient, μ		0.166 mm^{-1}
F(000)		6800ē
Diffractometer		Bruker Smart Apex II CCD area detector
Radiation source		fine-focus sealed tube, MoKα
Detector distance		5.8 cm
Data collection method		ω and scans
Total frames		2491
Frame size		1024 pixels
Frame width		0.3°
Exposure per frame		20 sec
Total measurement time		18 hours
θ range for data collection		1.32 to 25.00°
Index ranges		$-33 \le h \le 36$, $-20 \le k \le 20$, $-33 \le l \le 33$
Reflections collected		66732
Independent reflections		12908
Observed reflection, I>2σ(I)		9287
Coverage of independent reflections		99.9 %
Variation in check reflections		0 %
Absorption correction		Semi-empirical from equivalents SADABS (Sheldrick, 1996)
Max. and min. transmission		0.984 and 0.917
Structure solution technique		direct
Structure solution program		SHELXS-97 (Sheldrick, 1990)
Refinement technique		Full-matrix least-squares on F^2
Refinement program		SHELXL-97 (Sheldrick, 1997)
Function minimized		$\Sigma w(F_o^2 - F_c^2)^2$
Data / restraints / parameters		12908 / 256 / 925
Goodness-of-fit on F^2		1.067
Δ/σ_{max}		0.000
Final R indices:	R_1, I>2σ(I)	0.0537
	wR_2, all data	0.1048
	R_{int}	0.0386
	R_{sig}	0.0322
Weighting scheme		$w = 1/[\sigma^2(F_o^2)+ (0.002P)^2 + 46.6P]$, $P = [\max(F_o^2 ,0) + 2F_o^2]/3$
Largest diff. peak and hole		0.618 and -0.697ē/$Å^3$

$R_1 = \Sigma||F_o|-|F_c||/\Sigma|F_o|$, $wR_2 = [\Sigma w(F_o^2-F_c^2)^2/\Sigma w(F_o^2)^2]^{1/2}$

Crystal Structure Information for UM # 1597

Issued by: Peter Y. Zavalij

Crystal No. & ID	:	**1597**: Isaacs/Wei-Hao Huang 1,9 @150K
Compound name	:	CBPh diamine diiodide
Chemical formula	:	$[(C_{43}H_{40}N_{24}O_{13})<(C_9H_{24}N_2)]I_2 \cdot 15H_2O$
Final R_1 [I>2σ(I)]	:	**7.23 %**

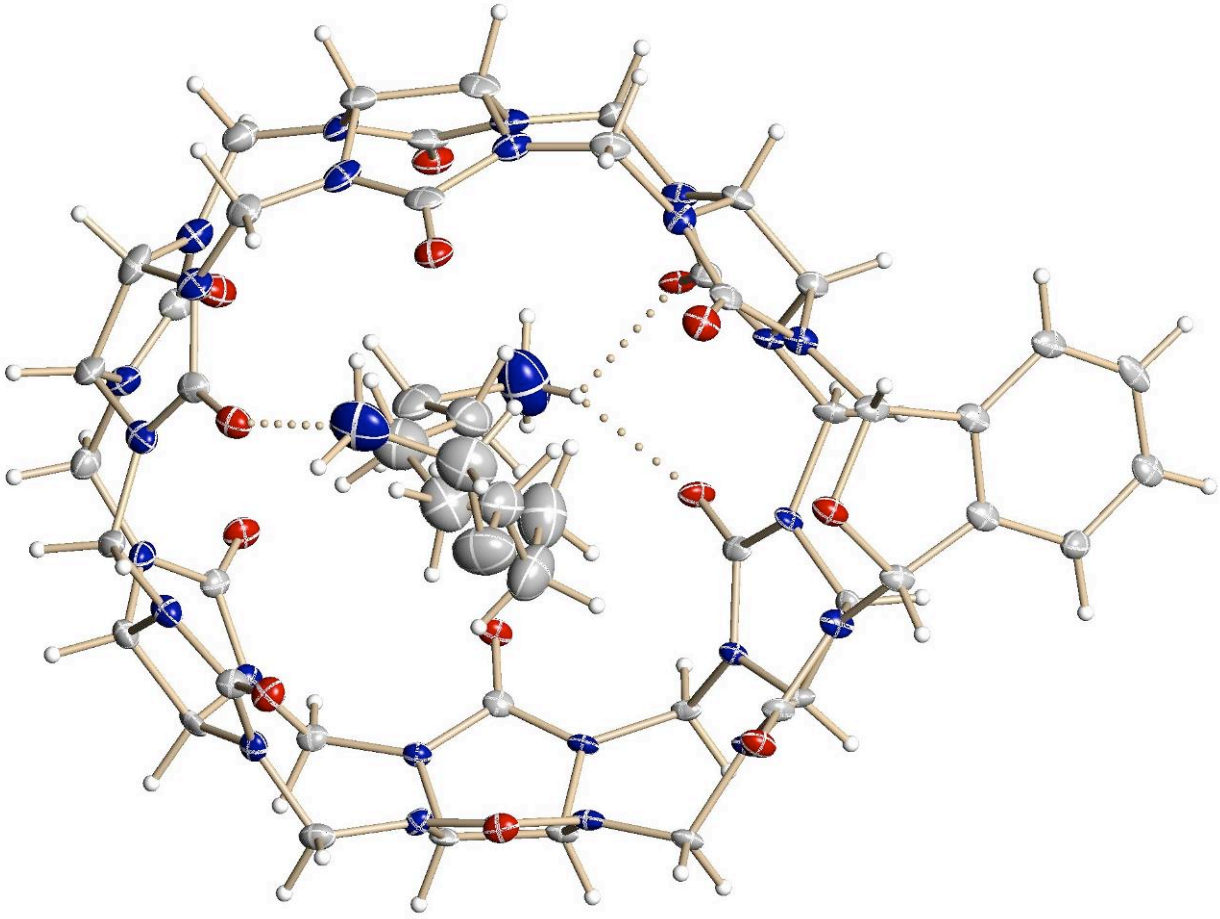

Figure S44. A view of UM#1597. Anisotropic atomic displacement ellipsoids for the non-hydrogen atoms are shown at the 30% probability level. Hydrogen atoms are displayed with an arbitrarily small radius.

A yellow prism of $[(C_{43}H_{40}N_{24}O_{13})<(C_9H_{24}N_2)]I_2 \cdot 15H_2O$, approximate dimensions 0.195× 0.35× 0.39 mm^3, was used for the X-ray crystallographic analysis. The X-ray intensity data were measured at 150(2) K on a three-circle diffractometer system equipped with Bruker Smart Apex II CCD area detector using a graphite monochromator and a MoKα fine-focus sealed tube (λ= 0.71073 Å). The detector was placed at a distance of 6.00 cm from the crystal.

A total of 2035 frames were collected with a scan width of 0.3° in ω and an exposure time of 30 sec/frame using Apex2 (Bruker, 2005). The total data collection time was 20.1 hours. The frames were integrated with Apex2 software package using a narrow-frame integration algorithm. The integration of the data using a Cubic unit cell yielded a total of 134638 reflections to a maximum θ angle of 22.50°, of which 9175 were independent (completeness = 99.8%, R_{int} = 5.31%, R_{sig} = 2.37%) and 8432 were greater than 2σ(I). The final cell dimensions of a = 27.6038(2) Å, b = 27.6038(2) Å, c = 27.6038(2) Å, α= 90°, β= 90°, γ= 90°, V = 21033.3(3) $Å^3$, are based upon the refinement of the XYZ-centroids of 37157 reflections with 2.2 < θ < 21.0° using Apex2. Analysis of the data showed 0 % decay during data collection. Data were corrected for absorption effects with the Semi-empirical from equivalents method using SADABS (Sheldrick, 1996). The minimum and maximum transmission coefficients were 0.734 and 0.823.

The structure was solved and refined using the SHELXS-97 (Sheldrick, 1990) and SHELXL-97 (Sheldrick, 1997) software in the space group $P2_13$ with Z = 12 for the formula unit $C_{52}H_{94}I_2N_{26}O_{28}$. The final anisotropic full-matrix least-squares refinement on F^2 with 862 variables converged at R_1=7.23 % for the observed data and wR_2=18.35 % for all data. The goodness-of-fit was 1.000. The largest peak on the final difference map was 0.576$\bar{e}$/$Å^3$ and the largest hole was -0.852$\bar{e}$/$Å^3$. On the basis of the final model, the calculated density was 1.691 g/cm^3 and F(000), 11016$\bar{e}$.

Overall structure quality considerations:

1. Strong data set, no disorder, R_1 4% maximum. Publishable quality.
2. Good data set, perhaps some minor disorder, $R_1$6% maximum. Publishable quality.
3. **Average data set and/or easily modeled disorder or twinning. Publishable with care.**
4. Weak data and/or major disorder or twinning that is not easily modeled. Publishable in some cases.
5. Very weak data and/or unexplained features of data or model. Not of publishable quality.

A structure with a quality factor of 4 or 5 should not be used for a regulatory document without prior consultation.

Comments:

- Data quality:	good
- Twinning:	merohedral, refined using twin/basf to 7:1 ratio
- Disorder:	substantial disorder of water and iodine ions; accounted for using squeeze (see CIF for details);
	guest molecule disordered in two orientations in about 1:1 ratio
- H-atoms:	constrained geometry as riding on attached atom (A)
	Uiso(H)=1.5*U_{iso}(A) for CH_3 and 1.2*U_{iso}(A) for other groups
- Residual density:	near heavy atoms &near disordered groups
- Structure quality:	good & average because of strong disorder and significantly elevated thermal motion of guest
Publishable	Yes with care

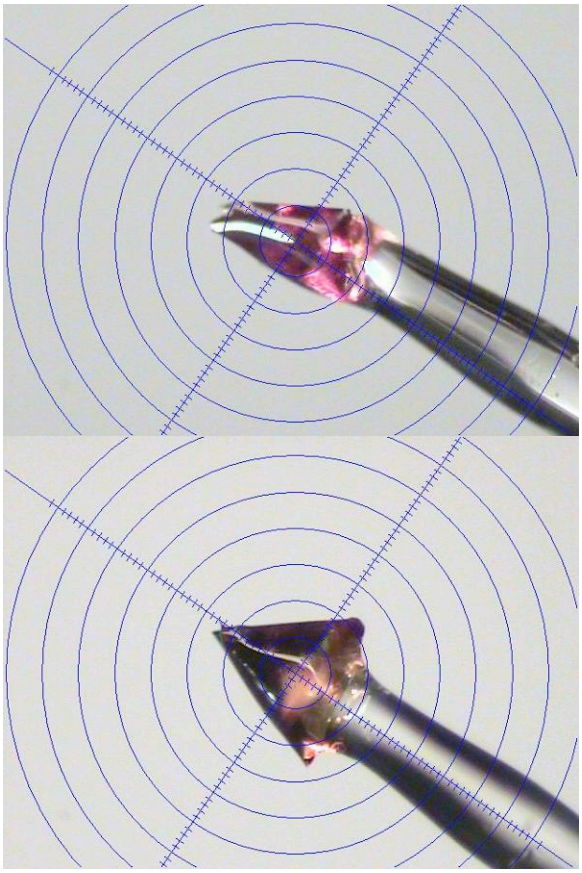

Table S2. Crystal data and structure refinement for UM#1597.

X-ray lab book No.		1597
Crystal ID		Isaacs/Wei-Hao Huang 1,9 @150K
Empirical formula		$C_{52}H_{94}I_2N_{26}O_{28}$
Formula weight		1785.33
Temperature		150(2) K
Wavelength		0.71073 Å
Crystal size		0.39 × 0.35 × 0.195 mm^3
Crystal habit		yellow prism
Crystal system		Cubic
Space group		$P2_13$
Unit cell dimensions		a = 27.6038(2) Å α = 90°
		b = 27.6038(2) Å β = 90°
		c = 27.6038(2) Å γ = 90°
Volume		21033.3(3) $Å^3$
Z		12
Density, ρ_{calc}		1.691 g/cm^3
Absorption coefficient, μ		1.000 mm^{-1}
F(000)		11016$\bar{e}$
Diffractometer		Bruker Smart Apex II CCD area detector
Radiation source		fine-focus sealed tube, MoKα
Detector distance		6.00 cm
Detector resolution		83.33 pixels/mm
Total frames		2035
Frame size		512 pixels
Frame width		0.3°
Exposure per frame		30 sec
Total measurement time		20.1 hours
Data collection method		ω and φ scans
□ range for data collection		1.81 to 22.49°
Index ranges		$-29 \le h \le 29$, $-29 \le k \le 27$, $-29 \le l \le 29$
Reflections collected		134638
Independent reflections		9175
Observed reflection, I>2□(I)		8432
Coverage of independent reflections		99.8 %
Variation in check reflections		0 %
Absorption correction		Semi-empirical from equivalents
		SADABS (Sheldrick, 1996)
Max. and min. transmission		0.823 and 0.734
Structure solution technique		direct
Structure solution program		SHELXS-97 (Sheldrick, 1990)
Refinement technique		Full-matrix least-squares on F^2
Refinement program		SHELXL-97 (Sheldrick, 1997)
Function minimized		$\Delta w(F_o^2 - F_c^2)^2$
Data / restraints / parameters		9175 / 189 / 862
Goodness-of-fit on F^2		1.003
□/□$_{max}$		0.001
Final R indices:	R_1, I>2□(I)	0.0723
	wR_2, all data	0.1835
	R_{int}	0.0531
	R_{sig}	0.0237
Weighting scheme		$w = 1/[\sigma^2(F_o^2)+(0.09P)^2+87P]$, $P = [max(F_o^2,0)+2F_o^2]/3$
Absolute structure parameter		0.13(3)
Largest diff. peak and hole		0.576 and -0.852$\bar{e}$ /$Å^3$

$R_1 = \Sigma||F_o|-|F_c||/\Sigma|F_o|$, $wR2 = [\Sigma w(F_o^2 - F_c^2)^2/\Sigma w(F_o^2)^2]^{1/2}$

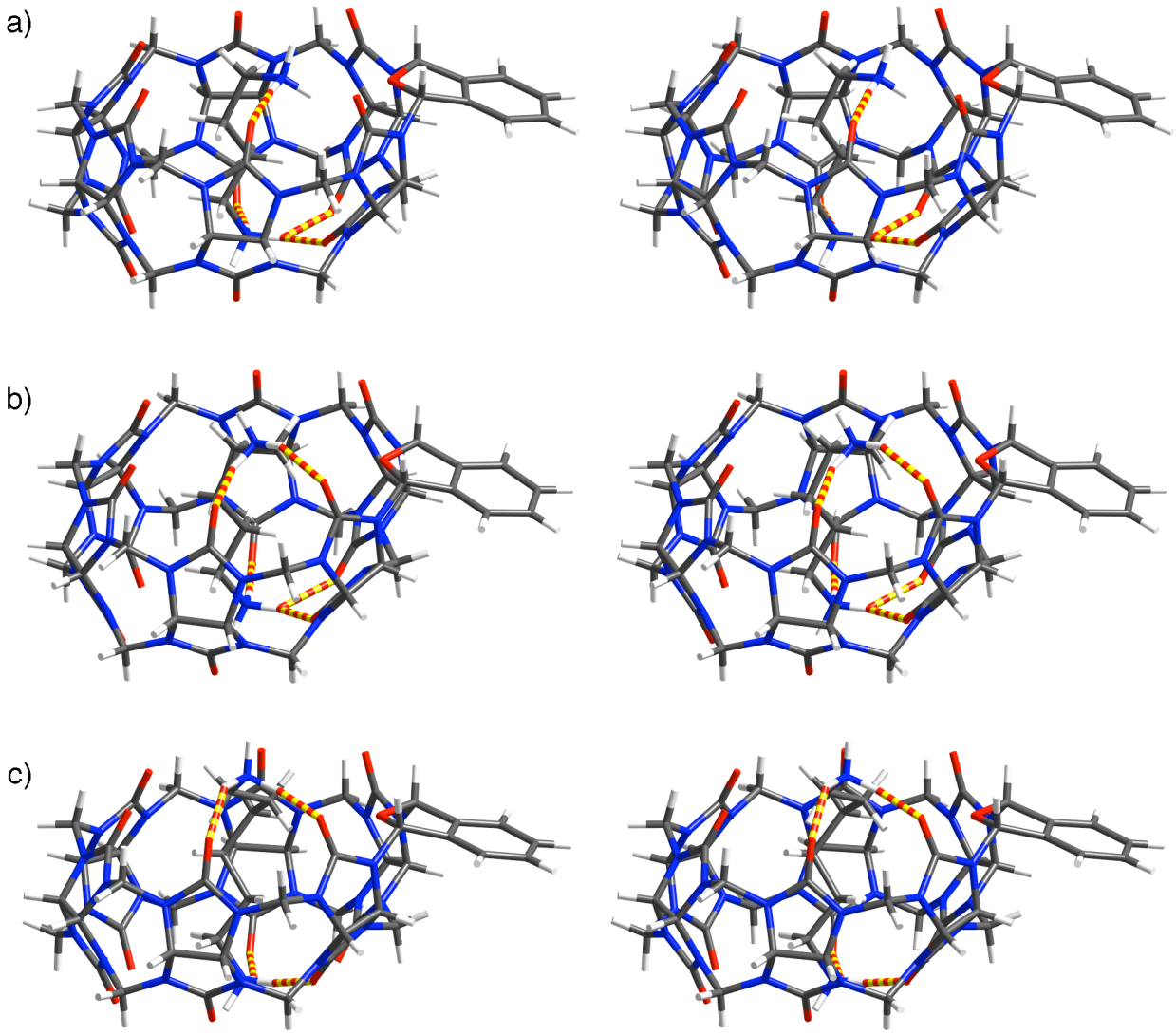

Figure S45. Cross-eyed stereoviews of MMFF minimized geometries of: a) **2•3a**, b) **2•3b**, c) **2•3c**. Color code: C, grey; H, white; N, blue; O, red; H-bonds, red-yellow striped.

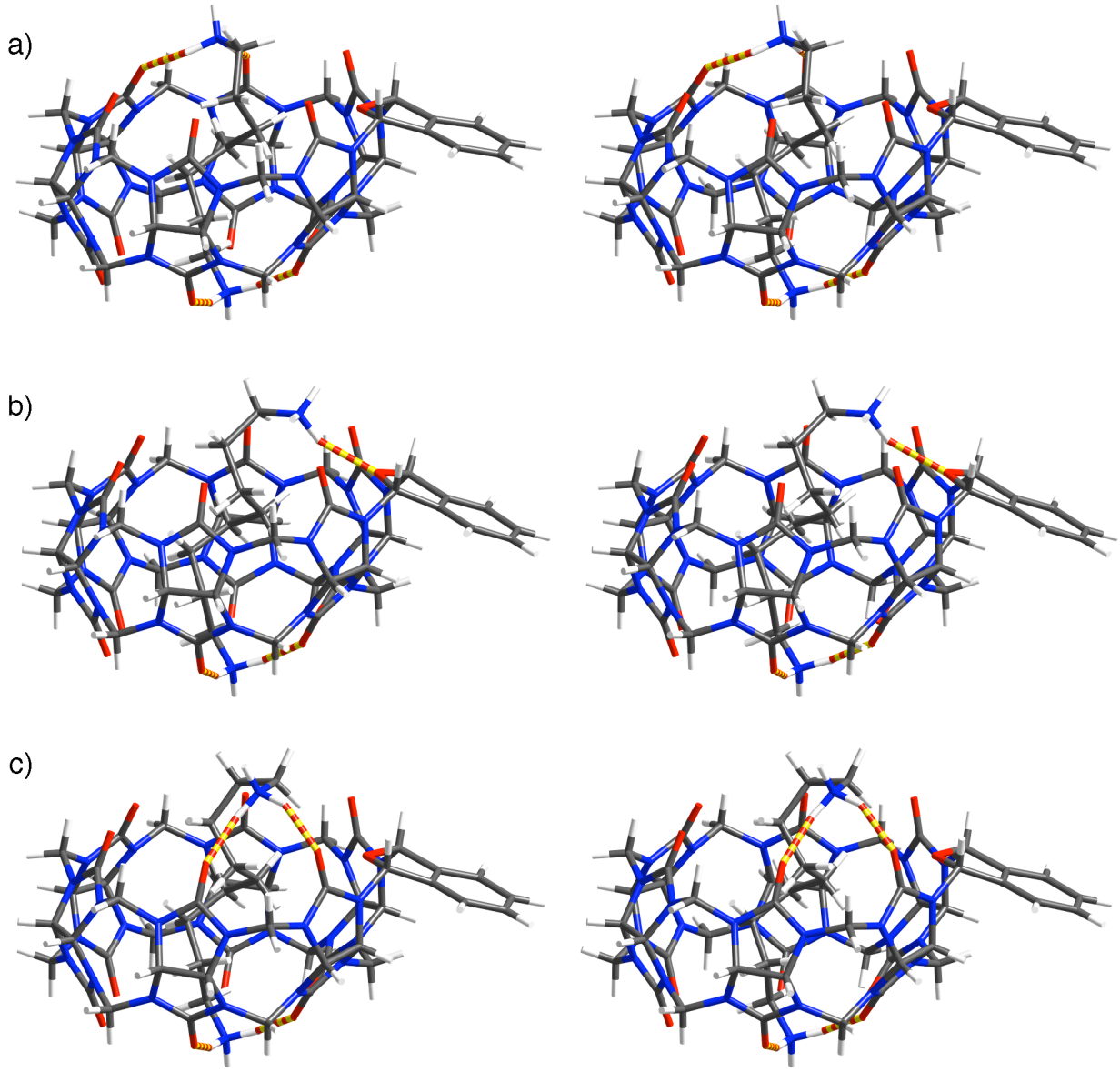

Figure S46. Cross-eyed stereoviews of MMFF minimized geometries of: a) **2•3d**, b) **2•3e**, c) **2•3f**. Color code: C, grey; H, white; N, blue; O, red; H-bonds, red-yellow striped.

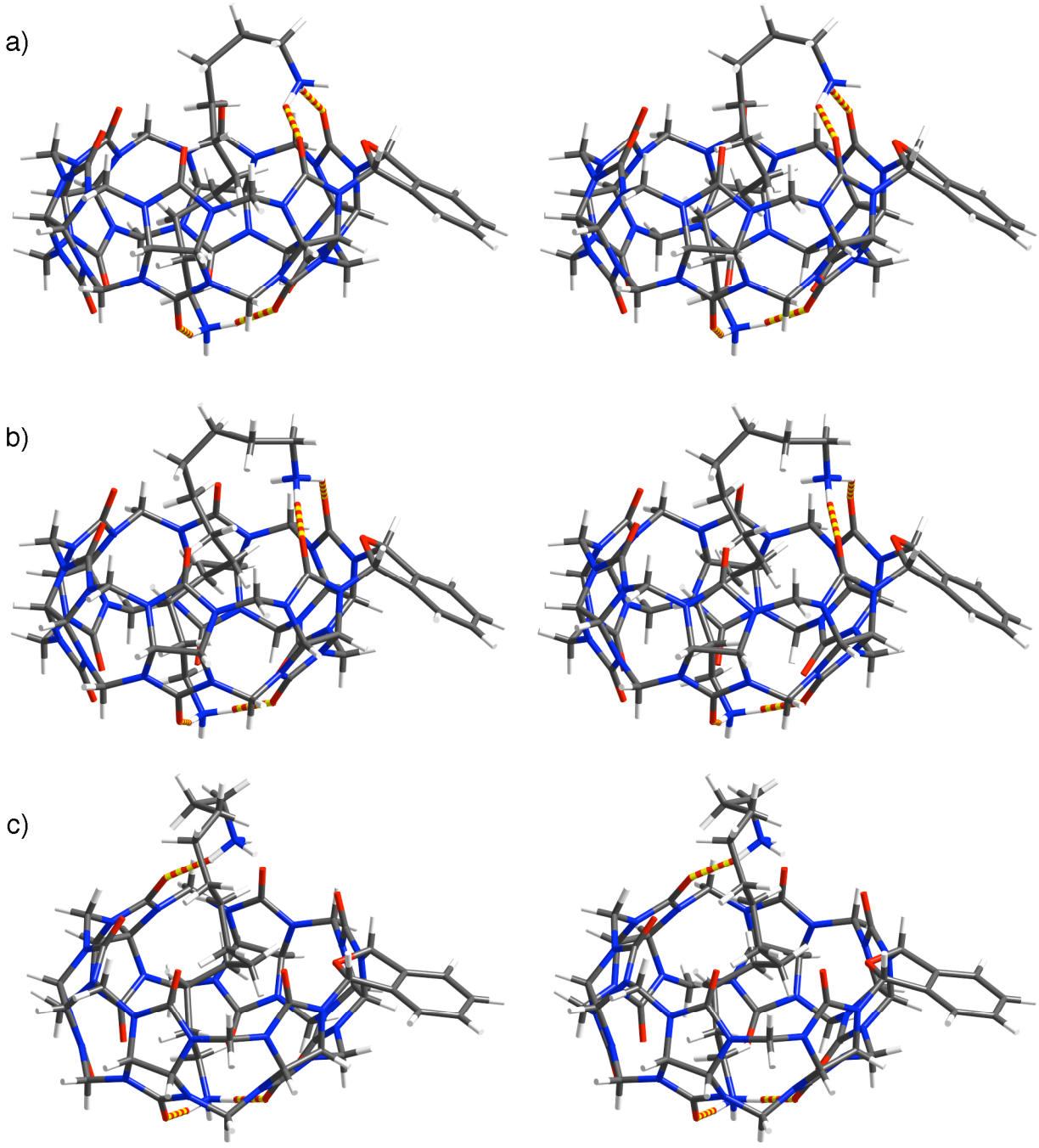

Figure S47. Cross-eyed stereoviews of MMFF minimized geometries of: a) **2•3g**, b) **2•3h**, c) **2•3i**. Color code: C, grey; H, white; N, blue; O, red; H-bonds, red-yellow striped.

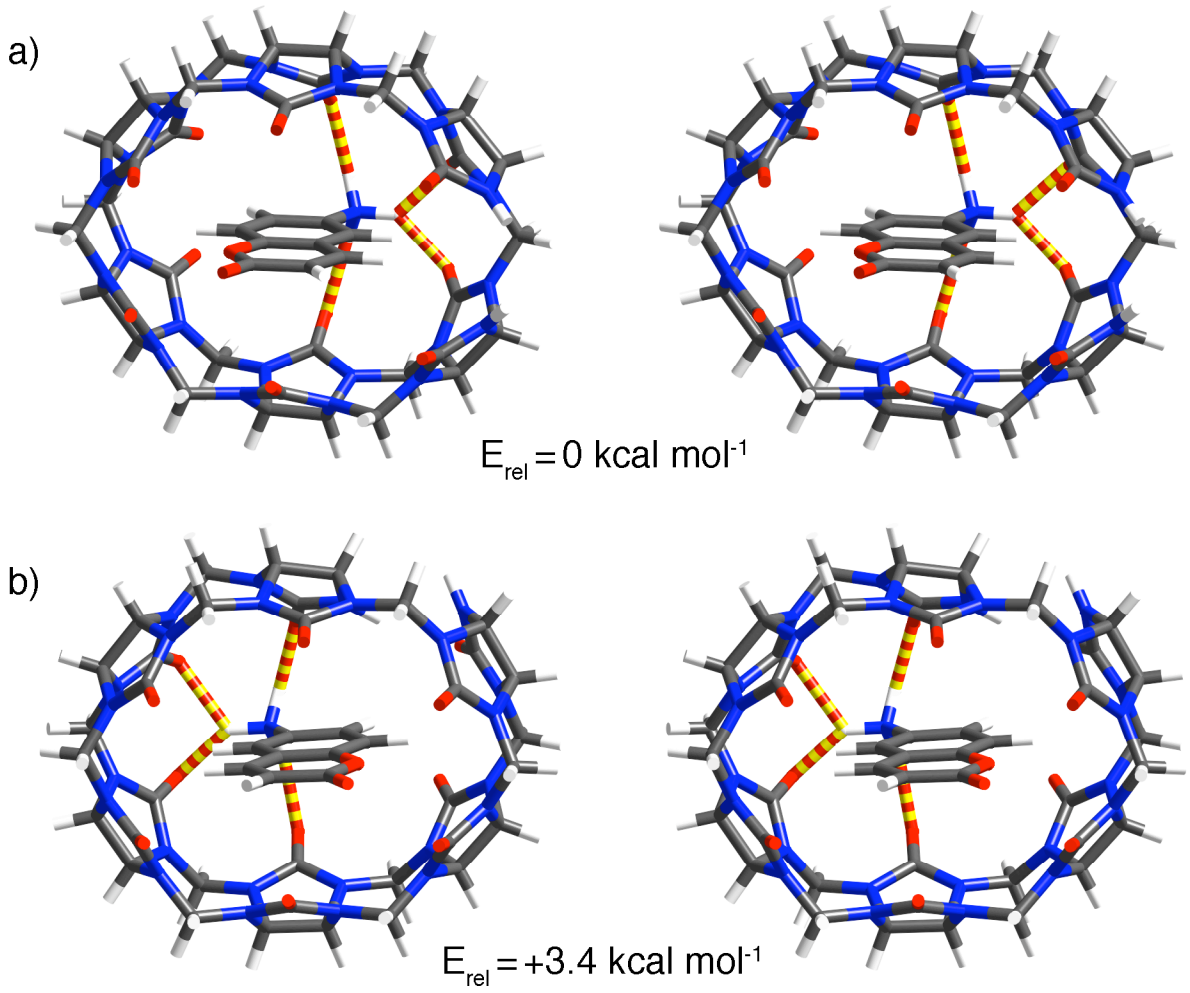

Figure S48. Cross-eyed stereoviews of MMFF minimized geometries and heats of formation for: a) bottom-*ns*-CB[6]•**9**, and b) top-*ns*-CB[6]•**9**. Color code: C, grey; H, white; N, blue; O, red; H-bonds, red-yellow striped.

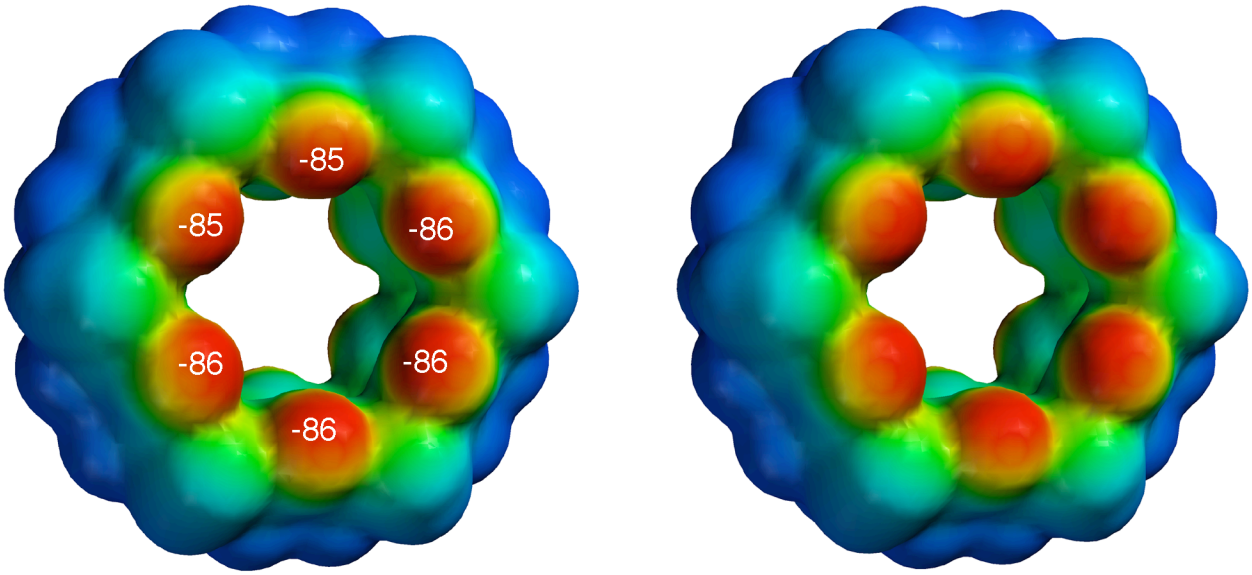

Figure S49. Stereoscopic representation of the electrostatic surface potential (PM3) plot for CB[6]. The red to blue color range spans –85 to +35 kcal mol^{-1}.

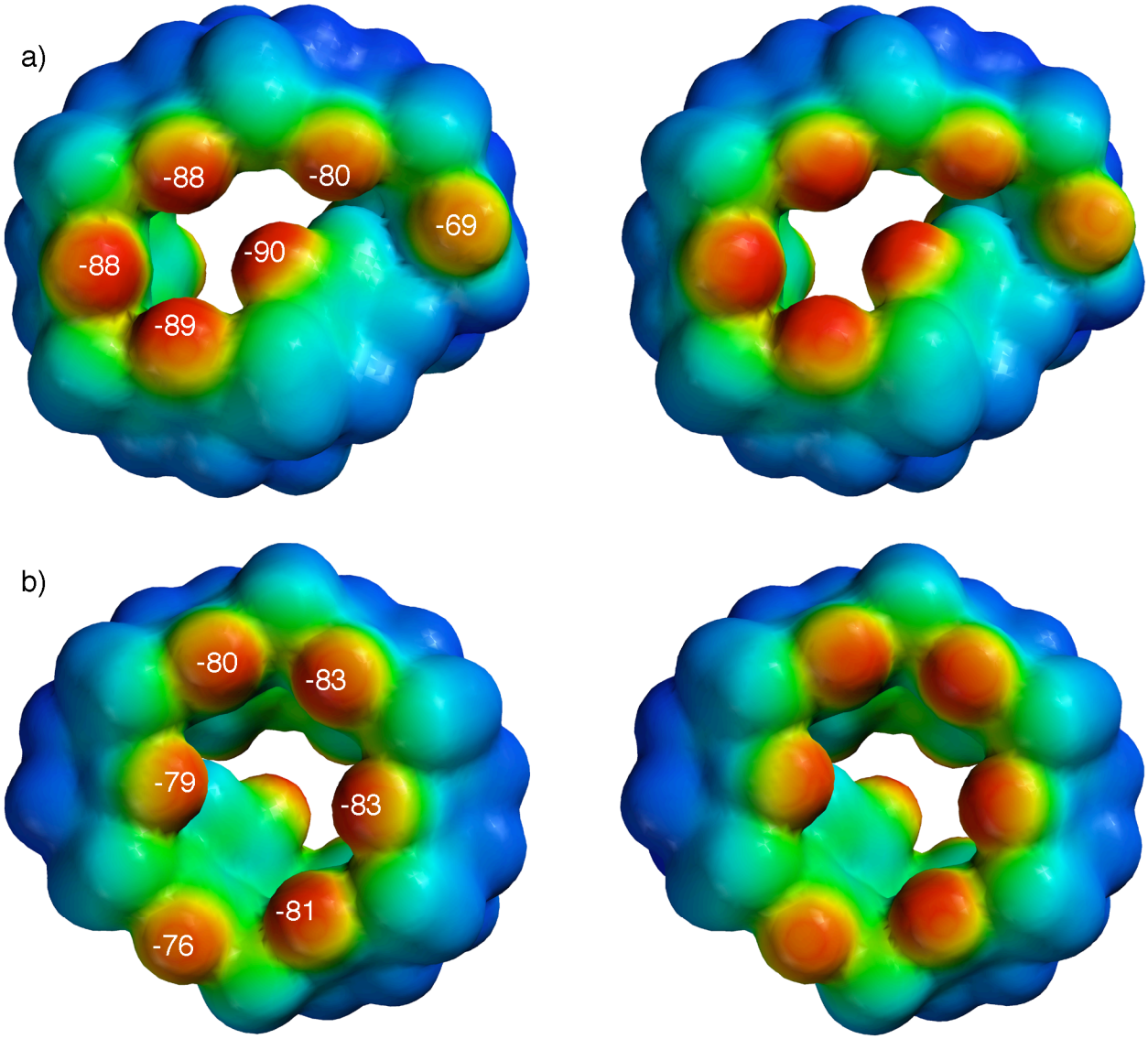

Figure S50. Stereoscopic representations of the electrostatic surface potential (PM3) plot for the MMFF minimized geometry of *ns*-CB[6]: a) top view, and b) bottom view. The red to blue color range spans –85 to +35 kcal mol^{-1}.

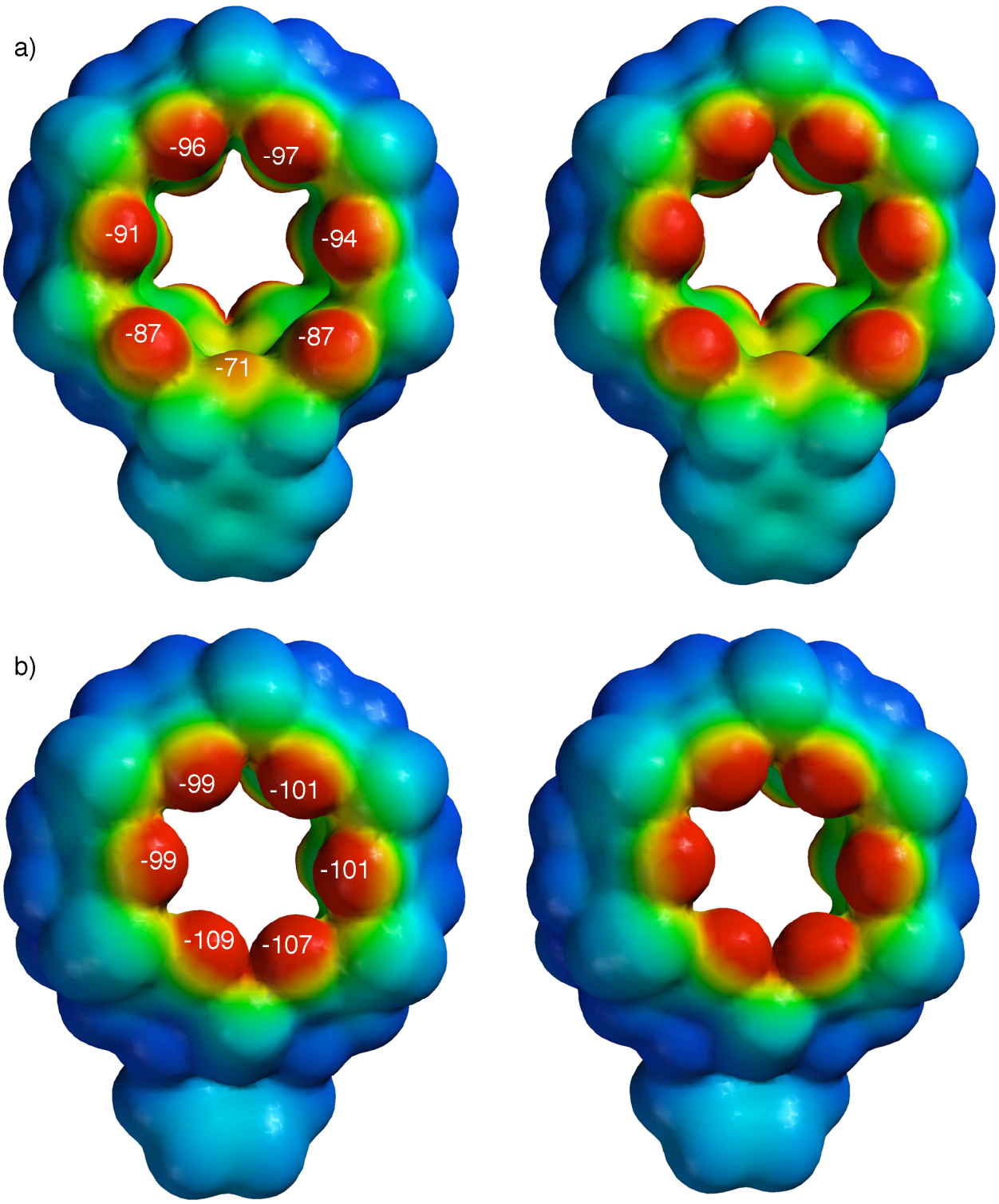

Figure S51. Stereoscopic representation of the electrostatic surface potential (PM3) plot for **2**: a) top view, and b) bottom view. The red to blue color range spans –85 to +35 kcal mol^{-1}.

References

(1) Behrend, R.; Meyer, E.; Rusche, F. *Liebigs Ann. Chem.* **1905**, *339*, 1-37.

(2) Freeman, W. A.; Mock, W. L.; Shih, N. Y. *J. Am. Chem. Soc.* **1981**, *103*, 7367-7368.

(3) Flinn, A.; Hough, G. C.; Stoddart, J. F.; Williams, D. J. *Angew. Chem., Int. Ed.* **1992**, *31*, 1475-1477.

(4) Wu, A.; Chakraborty, A.; Witt, D.; Lagona, J.; Damkaci, F.; Ofori, M. A.; Chiles, J. K.; Fettinger, J. C.; Isaacs, L. *J. Org. Chem.* **2002**, *67*, 5817-5830.

(5) Chakraborty, A.; Wu, A.; Witt, D.; Lagona, J.; Fettinger, J. C.; Isaacs, L. *J. Am. Chem. Soc.* **2002**, *124*, 8297-8306.

(6) Witt, D.; Lagona, J.; Damkaci, F.; Fettinger, J. C.; Isaacs, L. *Org. Lett.* **2000**, *2*, 755-758.

(7) Mock, W. L.; Shih, N. Y. *J. Org. Chem.* **1983**, *48*, 3618-3619; Mock, W. L.; Shih, N. Y. *J. Am. Chem. Soc.* **1988**, *110*, 4706-4710.

(8) Mock, W. L.; Shih, N. Y. *J. Org. Chem.* **1986**, *51*, 4440-4446.

(9) Mock, W. L.; Shih, N. Y. *J. Am. Chem. Soc.* **1989**, *111*, 2697-2699.

(10) Mock, W. L.; Irra, T. A.; Wepsiec, J. P.; Manimaran, T. L. *J. Org. Chem.* **1983**, *48*, 3619-3620; Mock, W. L.; Irra, T. A.; Wepsiec, J. P.; Adhya, M. *J. Org. Chem.* **1989**, *54*, 5302-5308.

(11) Mock, W. L.; Pierpont, J. *J. Chem. Soc., Chem. Commun.* **1990**, 1509-1511.

(12) Day, A. I.; Arnold, A. P.; Blanch, R. J.; Snushall, B. *J. Org. Chem.* **2001**, *66*, 8094-8100.

(13) Isaacs, L.; Park, S.-K.; Liu, S.; Ko, Y. H.; Selvapalam, N.; Kim, K.; Lik, H.; Zavalij, P. Y.; Kim, G.-H.; Lee, H.-S.; Kim, K. *J. Am. Chem. Soc.* **2005**, *127*, 18000-18001.

(14) Huang, W.-H.; Liu, S.; Zavalij, P. Y.; Isaacs, L. *J. Am. Chem. Soc.* **2006**, *128*, 14744-114745.

(15) Kim, J.; Jung, I.-S.; Kim, S.-Y.; Lee, E.; Kang, J.-K.; Sakamoto, S.; Yamaguchi, K.; Kim, K. *J. Am. Chem. Soc.* **2000**, *122*, 540-541.

(16) Lee, J. W.; Samal, S.; Selvapalam, N.; Kim, H.-J.; Kim, K. *Acc. Chem. Res.* **2003**, *36*, 621-630.

(17) Day, A. I.; Blanch, R. J.; Arnold, A. P.; Lorenzo, S.; Lewis, G. R.; Dance, I. *Angew. Chem., Int. Ed.* **2002**, *41*, 275-277.

(18) Liu, S.; Zavalij, P. Y.; Isaacs, L. *J. Am. Chem. Soc.* **2005**, *127*, 16798-16799.

(19) Liu, S.; Ruspic, C.; Mukhopadhyay, P.; Chakrabarti, S.; Zavalij, P. Y.; Isaacs, L. *J. Am. Chem. Soc.* **2005**, *127*, 15959-15967.

(20) Mukhopadhyay, P.; Wu, A.; Isaacs, L. *J. Org. Chem.* **2004**, *69*, 6157-6164.

(21) Mukhopadhyay, P.; Zavalij, P. Y.; Isaacs, L. *J. Am. Chem. Soc.* **2006**, *128*, 14093-14102.

(22) Jun, S. I.; Lee, J. W.; Sakamoto, S.; Yamaguchi, K.; Kim, K. *Tetrahedron Lett.* **2000**, *41*, 471-475.

(23) Moon, K.; Grindstaff, J.; Sobransingh, D.; Kaifer, A. E. *Angew. Chem., Int. Ed.* **2004**, *43*, 5496-5499.

(24) Ong, W.; Kaifer, A. E. *Angew. Chem., Int. Ed.* **2003**, *42*, 2164-2167.

(25) Lim, Y.-B.; Kim, T.; Lee, J. W.; Kim, S.-M.; Kim, H.-J.; Kim, K.; Park, J.-S. *Bioconjugate Chem.* **2002**, *13*, 1181-1185; Lee, J. W.; Ko, Y. H.; Park, S.-H.; Yamaguchi, K.; Kim, K. *Angew. Chem., Int. Ed.* **2001**, *40*, 746-749.

(26) Jeon, W. S.; Ziganshina, A. Y.; Lee, J. W.; Ko, Y. H.; Kang, J.-K.; Lee, C.; Kim, K. *Angew. Chem. Int. Ed.* **2003**, *42*, 4097-4100; Ko, Y. H.; Kim, K.; Kang, J.-K.; Chun, H.; Lee, J. W.; Sakamoto, S.; Yamaguchi, K.; Fettinger, J. C.; Kim, K. *J. Am. Chem. Soc.* **2004**, *126*, 1932-1933.

(27) Jeon, W. S.; Kim, E.; Ko, Y. H.; Hwang, I.; Lee, J. W.; Kim, S.-Y.; Kim, H. J.; Kim, K. *Angew. Chem. Int. Ed.* **2005**, *44*, 87-91.

(28) Marquez, C.; Nau, W. M. *Angew. Chem., Int. Ed.* **2001**, *40*, 3155-3160.

(29) Jeon, Y. J.; Kim, S.-Y.; Ko, Y. H.; Sakamoto, S.; Yamaguchi, K.; Kim, K. *Org. Biomol. Chem.* **2005**, *3*, 2122-2125.

(30) Wheate, N. J.; Day, A. I.; Blanch, R.; Arnold, A.; Cullinane, C.; Collins, J. G. *Chem. Commun.* **2004**, 1424-1425; Wheate, N. J.; Buck, D. P.; Day, A. I.; Collins, J. G. *Dalton Trans.* **2006**, 451-458.

(31) Rowan, A. E.; Elemans, J. A. A. W.; Nolte, R. J. M. *Acc. Chem. Res.* **1999**, *32*, 995-1006; Rebek, J. J. *Acc. Chem. Res.* **1999**, *32*, 278-286.

(32) Eliel, E. L.; Wilen, S. H. *Stereochemistry of Organic Compounds*; J. Wiley and Sons: New York, 1994.

(33) Buschmann, H.-J.; Fink, H.; Schollmeyer, E. "Preparation of cucurbituril" *Ger. Offen.* (Germany): DE 19603377, **1997** [*Chem. Abstr.* **1997**, *127*, 205599].

(34) Lagona, J.; Fettinger, J. C.; Isaacs, L. *Org. Lett.* **2003**, *5*, 3745-3747.

(35) Lagona, J.; Fettinger, J. C.; Isaacs, L. *J. Org. Chem.* **2005**, *70*, 10381-10392.

(36) Lagona, J.; Wagner, B. D.; Isaacs, L. *J. Org. Chem.* **2006**, *71*, 1181-1190.

(37) Day, A. I.; Arnold, A. P.; Blanch, R. J. *Molecules* **2003**, *8*, 74-84.

(38) Zhao, Y.; Xue, S.; Zhu, Q.; Tao, Z.; Zhang, J.; Wei, Z.; L., L.; Hu, M.; Xiao, H.; Day, A. I. *Chin. Science Bull.* **2004**, *49*, 1111-1116.

(39) Jon, S. Y.; Selvapalam, N.; Oh, D. H.; Kang, J.-K.; Kim, S.-Y.; Jeon, Y. J.; Lee, J. W.; Kim, K. *J. Am. Chem. Soc.* **2003**, *125*, 10186-10187.

(40) Lee, H.-K.; Park, K. M.; Jeon, Y. J.; Kim, D.; Oh, D. H.; Kim, H. S.; Park, C. K.; Kim, K. *J. Am. Chem. Soc.* **2005**, *127*, 5006-5007.

(41) Jeon, Y. J.; Kim, H. J.; Jon, S.; Selvapalam, N.; Oh, D. H.; Seo, I.; Park, C.-S.; Jung, S. R.; Koh, D.-S.; Kim, K. *J. Am. Chem. Soc.* **2004**, *126*, 15944-15945.

(42) Petersen, H. *Synthesis* **1973**, 243-292.

(43) Butler, A. R.; Leitch, E. *J. Chem. Soc., Perkin Trans. 2* **1980**, 103-109.

(44) Rudkevich, D. M. *Angew. Chem., Int. Ed.* **2004**, *43*, 558-571.

(45) Rekharsky, M.; Yamamura, H.; Inoue, C.; Kawai, M.; Osaka, I.; Arakawa, R.; Shiba, K.; Sato, A.; Ko, Y. H.; Selvapalam, N.; Kim, K.; Inoue, Y. *J. Am. Chem. Soc.* **2006**, *128*, 14871-14880.

(46) Ling, Y.; Kaifer, A. E. *Chem. Mater.* **2006**, *18*, 5944-5949.

(47) Jeon, W. S.; Moon, K.; Park, S. H.; Chun, H.; Ko, Y. H.; Lee, J. Y.; Lee, E. S.; Samal, S.; Selvapalam, N.; Rekharsky, M. V.; Sindelar, V.; Sobransingh, D.; Inoue, Y.; Kaifer, A. E.; Kim, K. *J. Am. Chem. Soc.* **2005**, *127*, 12984-12989.

(48) Rekharsky, M. V.; Mori, T.; Yang, C.; Ko, Y. H.; Selvapalam, N.; Kim, H.; Sobransingh, D.; Kaifer, A. E.; Liu, S.; Isaacs, L.; Chen, W.; Moghaddam, S.;

Gilson, M. K.; Kim, K.; Inoue, Y. *Proc. Natl. Acad. Sci. U. S. A.* **2007**, *104*, 20737-20742.

(49) Lagona, J.; Mukhopadhyay, P.; Chakrabarti, S.; Isaacs, L. *Angew. Chem., Int. Ed.* **2005**, *44*, 4844-4870.

(50) Kim, K.; Selvapalam, N.; Ko, Y. H.; Park, K. M.; Kim, D.; Kim, J. *Chem. Soc. Rev.* **2007**, *36*, 267-279.

(51) Mohanty, J.; Pal, H.; Ray, A. K.; Kumar, S.; Nau, W. M. *ChemPhysChem* **2007**, *8*, 54-56.

(52) Bali, M. S.; Buck, D. P.; Coe, A. J.; Day, A. I.; Collins, J. G. *Dalton Trans.* **2006**, 5337-5344.

(53) Jon, S. Y.; Ko, Y. H.; Park, S. H.; Kim, H.-J.; Kim, K. *Chem. Commun.* **2001**, 1938-1939; Choi, S.; Park, S. H.; Ziganshina, A. Y.; Ko, Y. H.; Lee, J. W.; Kim, K. *Chem. Commun.* **2003**, 2176-2177; Pattabiraman, M.; Natarajan, A.; Kaliappan, R.; Mague, J. T.; Ramamurthy, V. *Chem. Commun.* **2005**, 4542-4544; Wang, R.; Yuan, L.; Macartney, D. H. *J. Org. Chem.* **2006**, *71*, 1237-1239.

(54) Bush, M. E.; Bouley, N. D.; Urbach, A. R. *J. Am. Chem. Soc.* **2005**, *127*, 14511-14517; Heitmann, L. M.; Taylor, A. B.; Hart, P. J.; Urbach, A. R. *J. Am. Chem. Soc.* **2006**, *128*, 12574-12581; Rekharsky, M. V.; Yamamura, H.; Ko, Y. H.; Kim, K.; Inoue, Y. *Peptide Sci.* **2006**, *43*, 393-394.

(55) Sindelar, V.; Cejas, M. A.; Raymo, F. M.; Chen, W.; Parker, S. E.; Kaifer, A. E. *Chem. Eur. J.* **2005**, *11*, 7054-7059; Ling, Y.; Wang, W.; Kaifer, A. E. *Chem. Commun.* **2007**, 610-612.

(56) Ooya, T.; Inoue, D.; Choi, H. S.; Kobayashi, Y.; Loethen, S.; Thompson, D. H.; Ko, Y. H.; Kim, K.; Yui, N. *Org. Lett.* **2006**, *8*, 3159-3162; Sobransingh, D.; Kaifer, A. E. *Org. Lett.* **2006**, *8*, 3247-3250; Sindelar, V.; Silvi, S.; Kaifer, A. E. *Chem. Commun.* **2006**, 2185-2187; Liu, Y.; Li, X.-Y.; Zhang, H.-Y.; Li, C.-J.; Ding, F. *J. Org. Chem.* **2007**, *72*, 3640-3645; Tuncel, D.; Özsar, Ö.; Tiftik, H. B.; Salih, B. *Chem. Commun.* **2007**, 1369-1371; Ko, Y. H.; Kim, E.; Hwang, I.; Kim, K. *Chem. Commun.* **2007**, 1305-1315.

(57) Liu, S.; Zavalij, P. Y.; Lam, Y.-F.; Isaacs, L. *J. Am. Chem. Soc.* **2007**, *129*, 11232-11241; Liu, S.; Shukla, A. D.; Gadde, S.; Wagner, B. D.; Kaifer, A. E.; Isaacs, L. *Angew. Chem., Int. Ed.* **2008**, *47*, ASAP.

(58) Liu, S.; Kim, K.; Isaacs, L. *J. Org. Chem.* **2007**, *72*, 6840-6847.

(59) Wu, A.; Chakraborty, A.; Witt, D.; Lagona, J.; Damkaci, F.; Ofori, M. A.; Chiles, J. K.; Fettinger, J. C.; Isaacs, L. *J. Org. Chem.* **2002**, *67*, 5817-5830.

(60) So, Y.-H. *Acc. Chem. Res.* **2001**, *34*, 753-758; Flory, P. J. *Chem. Rev.* **1946**, *39*, 137-197.

(61) Day, A. I.; Blanch, R. J.; Coe, A.; Arnold, A. P. *J. Inclusion Phenom. Macrocyclic Chem.* **2002**, *43*, 247-250.

(62) The influence of glycoluril concentration, acid identity and concentration and temperature have also been studied by Day and co-workers. The point in the mechanistic pathway where these variable exert their influence remains unclear.

(63) Huang, W.-H.; Zavalij, P. Y.; Isaacs, L. *Angew. Chem., Int. Ed.* **2007**, *46*, 7425-7427.

(64) Huang, W.-H.; Zavalij, P. Y.; Isaacs, L. *Angew. Chem., Int. Ed.* **2008**, *48*, submitted.

(65) Rebek, J. J. *Acc. Chem. Res.* **1999**, *32*, 278-286; Rowan, A. E.; Elemans, J. A. A. W.; Nolte, R. J. M. *Acc. Chem. Res.* **1999**, *32*, 995-1006; Wu, A.; Chakraborty, A.; Fettinger, J. C.; Flowers, R. A., II; Isaacs, L. *Angew. Chem., Int. Ed.* **2002**, *41*, 4028-4031; Isaacs, L.; Witt, D. *Angew. Chem., Int. Ed.* **2002**, *41*, 1905-1907.

(66) Compounds **13**(m,n) and **17**(m,n) are chiral when $m \neq n$.

(67) If the reaction is run to completion we observe a more complex mixture whose analysis by ^{1}H NMR spectroscopy is challenging.

(68) This analysis is theoretically based and ignores the potential influence of strain and intramolecular NH•••O H-bonds that are known to impact the stability and geometry of CB[n] and (±)-bis-ns-CB[6].

(69) Blanch, R. J.; Sleeman, A. J.; White, T. J.; Arnold, A. P.; Day, A. I. *Nano Lett.* **2002**, *2*, 147-149.

(70) In none of these reactions did we observe the formation of CB[10]•CB[5] which suggests that the formation of this aggregate is probably more complex than the reaction of two molecules of **5** to give CB[10] followed by stabilization with CB[5].

(71) Day has previously shown that CB[n] forming reactions when conducted at high dilution lead mainly to CB[5]. At high dilution intermolecular reactions are slowed and chain-growth rather than step-growth processes tend to dominate.

(72) Ong, W.; Kaifer, A. E. *Organometallics* **2003**, *22*, 4181-4183.

(73) Mock, W. L. *Top. Curr. Chem.* **1995**, *175*, 1-24.

(74) Mohanty, J.; Nau, W. M. *Angew. Chem., Int. Ed.* **2005**, *44*, 3750-3754.

(75) a) Miyahara, Y.; Abe, K.; Inazu, T. *Angew. Chem. Int. Ed.* **2002**, *41*, 3020-3023. (b) Kellersberger, K. A.; Anderson, J. D.; Ward, S. M.; Krakowiak, K. E.; Dearden, D. V. *J. Am. Chem. Soc.* **2001**, *123*, 11316-11317.

(76) Zhao, J.; Kim, H.-J.; Oh, J.; Kim, S.-Y.; Kim, J. W.; Sakamoto, S.; Yamaguchi, K.; Kim, K. *Angew. Chem., Int. Ed.* **2001**, *40*, 4233-4235.

(77) Wu, A.; Isaacs, L. *J. Am. Chem. Soc.* **2003**, *125*, 4831-4835.

(78) Timmerman, P.; Verboom, W.; van Veggel, F. C. J. M.; van Duynhoven, J. P. M.; Reinhoudt, D. N. *Angew. Chem., Int. Ed. Engl.* **1994**, *33*, 2345-2348.

(79) Shinkai, S.; Ikeda, M.; Sugasaki, A.; Takeuchi, M. *Acc. Chem. Res.* **2001**, *6*, 494-503.

(80) Nagarajan, E. R.; Oh, D. H.; Selvapalam, N.; Ko, Y. H.; Park, K. M.; Kim, K. *Tetrahedron Lett.* **2006**, *47*, 2073-2075.

(81) Kellersberger, K. A.; Anderson, J. D.; Ward, S. M.; Krakowiak, K. E.; Dearden, D. V. *J. Am. Chem. Soc.* **2001**, *123*, 11316-11317.

(82) Lee, J. Y.; Lee, E. S.; Samal, S.; Selvapalam, N.; Rekharsky, M. V.; Sindelar, V.; Sobransingh, D.; Inoue, Y.; Kaifer, A. E.; Kim, K. *J. Am. Chem. Soc.* **2005**, *127*, 12984-12989.

(83) Rekharsky, M. V.; Yamamura, H.; Inoue, C.; Kawai, M.; Osaka, I.; Arakawa, R.; Shiba, K.; Sato, A.; Ko, Y. H.; Selvapalam, N.; Kim, K.; Inoue, Y. *J. Am. Chem. Soc.* **2006**, *128*, 14871-14880.

(84) CCDC-647412 (**1**), CCDC-647413 ((±)-bis-*ns*-CB[6]•**3**), and CCDC-647414 ((±)-bis-*ns*-CB[6]•TFA) contains the supplementary crystallographic data for this paper. These data can be obtained free of charge via www.ccdc.cam.ac.uk/conts/retrieving.html (or from the Cambridge Crystallographic Data Centre, 12, Union Road, Cambridge CB21EZ, UK; fax: (+44) 1223-336-033; or deposit@ccdc.cam.ac.uk). (85) The ROESY spectrum of the mixture of diastereomers did not provide information that would allow us to assign the major and minor resonances to a specific diastereomer. To resolve this issue will require the resolution of (±)-bis-*ns*-CB[6].

(85) (±)-Bis-*ns*-CB[6] features connections between two pairs of homotopic NH groups of identical topicity whereas bis-*ns*-CB[10] previously isolated has connections between two pairs of homotopic NH groups of opposite topicity.

(86) The ROESY spectrum of the mixture of diastereomers did not provide information that would allow us to assign the major and minor resonances to a specific diastereomer. We are in the process of resolving this issue by separating the enantiomers of (±)-bis-*ns*-CB[6] by chromatography on a chiral stationary phase.

(87) Compound **12** and (±)-bis-*ns*-CB[6] form a 1:1 inclusion complex rather than a supramolecular polymeric exclusion complex.

(88) Product resubmission experiments confirm that trimer **1** is converted to (±)-bis-*ns*-CB[6] by condensation with CH_2O under acidic conditions.

(89) Several constitutional isomers of (±)-bis-*ns*-CB[*n*] are possible depending on the length of the glycoluril oligomer fragments that condense (e.g. (±)-bis-*ns*-CB[7] can be formed from tetramer and trimer fragments or from dimer and pentamer fragments).

(90) A. Henning, H. Bakirci, W. M. Nau, *Nature Methods* **2007**, *4*, 629-632.

(91) K. Kim, N. Selvapalam, Y. H. Ko, K. M. Park, D. Kim, J. Kim, *Chem. Soc. Rev.* **2007**, *36*, 267-279.

(92) J. Kim, Y. Ahn, K. M. Park, Y. Kim, Y. H. Ko, D. H. Oh, and K. Kim *Angew. Chem. Int. Ed.* **2007**, *46*, 7393 –7395.

(93) I. Hwang, K. Baek, M. Jung, Y. Kim, K. M. Park, D.-W. Lee, N. Selvapalam, K. Kim, *J. Am. Chem. Soc.* **2007**, *129*, 4170-4171.

(94) The reaction between *ns*-CB[6] and (substituted) benzaldehydes was also conducted. These reactions as less clean than between *ns*-CB[6] and *o*-phthalaldehyde which we attribute to the potential for two diastereomeric orientations of the pendant Ar group.

(95) CCDC-676703 (**2**) and CCDC-676704 (**V-2•V-3f**) contains the supplementary crystallographic data for this paper. These data can be obtained free of charge via www.ccdc.cam.ac.uk/conts/retrieving.html (or from the Cambridge Crystallographic Data Centre, 12 Union Road, Cambridge CB21EZ, UK; fax: (+44) 1223-336-033; or deposit@ccdc.cam.ac.uk).

(96) We did not observe intra-complex ROESY cross-peaks that would allow us to assign these complexes as a specific diastereomer. MMFF calculations

(Supporting Information) suggest that the complex between *ns*-CB[6] and **V-9** is best formulated as bottom-*ns*-CB[6]•**V-9**.

(97) Mock previously showed that CB[6] binds to **V-11** but rejects isomeric **V-12** and **V-13** because only the geometry of **V-11** allows both substituents to pass through the C=O lined portals. See: Mock, W. L.; Shih, N. Y. *J. Org. Chem.* **1986**, *51*, 4440-4446. Interestingly, *meta*-substituted **V-19** forms a mixture of top- and bottom-diastereomers with *ns*-CB[6] because both portals are satisfied by ion-dipole interactions.

(98) H.-J. Buschmann, A. Wego, A. Zielesny, E. Schollmeyer, *J. Incl. Phenom. Macrocyclic Chem.* **2006**, *54*, 241-246.

(99) A related phenomenon has been observed by Kim and co-workers for the complex of CB[8] with long chain alkyltrimethylammonium ions. K. Kim, personal communication.

(100) Rebek and co-workers have shown that *n*-alkanes exhibit helical conformations inside self-assembled capsules to maximize non-covalent interactions between host and guest. For a review, see: J. Rebek, Jr. *Chem. Commun.* **2007**, 2777-2789.